A Novel Capillary Polymerase Chain Reaction Machine

by

Jeffrey Tsungshuan Chiou

Submitted to the Department of Mechanical Engineering
in partial fulfillment of the requirements for the degree of
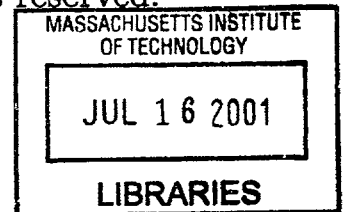
Doctor of Philosophy

at the

MASSACHUSETTS INSTITUTE OF TECHNOLOGY

October 2000
[February 2001]

ARCHIVES

Author ....
Department of Mechanical Engineering
October 27, 2000

Certified by....
....
Daniel J. Ehrlich
Director, BioMEMs Laboratory, Whitehead Institute
Thesis Supervisor

Accepted by ....
....
Ain A. Sonin
Chairman, Department Committee on Graduate Students

A Novel Capillary Polymerase Chain Reaction Machine

by

Jeffrey Tsungshuan Chiou

Abstract

I built a novel prototype capillary polymerase chain reaction machine. The purpose was to perform a single reaction as fast as possible with a reaction volume ~ 100 nl. The PCR mix is in the form of a 1 μl droplet that moves between three heat zones inside of a 1 mm I.D. capillary filled with mineral oil via pneumatic actuation. A laser beam waveguides down the capillary until it strikes the drop, at which point it scatters. The scatter is picked up by a series of photodiodes to provide position feedback. Due to the efficient heat transfer arrangement, the drop can transition between different temperature steps in $\sim$2 seconds, which includes both drop motion and temperature equilibration. It was extensively tested in both 10-cycle and 30-cycle PCR, including nearly 200 successful 30-cycle runs. The 30-cycle PCR was typically 74% (as high as 78%) efficient, and took only 23 minutes. This compares well with existing machines in the literature.

Acknowledgments

I would like to thank my advisor, Dr. Dan Ehrlich, for making this project possible. The concept of a small sample volume, 3-heat-zone reciprocating-motion PCR machine was originally his vision. Dan is an exceptionally easy person to work with, and made sure that I had all the resources I needed to complete this work.

I would also like to thank the members of my committee, Prof. Paul Matsudaira and Prof. Ain Sonin. Their advice and guidance was very useful.

I received a great deal of informal guidance from the members of various labs that I have worked in, whose members are too numerous to mention. Thanks to the members of the Ehrlich Lab (both the Lincoln Lab and Whitehead Institute groups), Matsudaira Lab, Fluid Dynamics Lab, and Newman Lab for Biomechanics. Special thanks go to Steve Palmacci and Matt Footer, who fielded endless questions when I started at Lincoln Lab and Whitehead Institute, respectively.

Many thanks go to my family, who had faith that I could reach this point even before I was old enough to know what a "Ph.D" was. I would not be able to accomplish anything without their years of support and guidance.

My friends made this *long* journey not only bearable, but fun. Of special note (roughly chronological order): Joe "The Man" Doeringer; Justin "Juiceman" Won; Benjie "That Prick" Sun; Ya-Hui "Ellie" Ku; Linus Sun, the "Trent" to my "Mikey"; and Caroline "Big C" Chang. You guys are the best.

And finally, I would like to thank God, through which all things are possible— including the completion of this seemingly neverending task.

Contents

Chapter 1

Introduction

Polymerase chain reaction (PCR) is arguably the single most widely used technique in molecular biology today. It is used to produce many copies of a specified portion of initial template DNA Large quantities of DNA are typically required for determination of strand size by electrophoresis, a common diagnostic technique. PCR is also widely used to precisely alter DNA by site-specific mutagenesis.

PCR is usually performed in a 100 μl aliquot. The aliquot is put into a disposable plastic tube, which is placed in a computer-controlled heat block. The heat block goes up and down in temperature to perform the reaction, which is complete 1–2 hours later. Much of this time is spent heating and cooling the block.

The purpose of this thesis was to produce a proof of concept for a fast polymerase chain reaction machine capable of handling sample volumes on the order of 100 nl. Instead of 1–2 hours, the current machine can finish the reaction in about 20 minutes. While admittedly not yet in a commercial form, the device demonstrates that PCR will be executed much more quickly in the future, increasing productivity. The
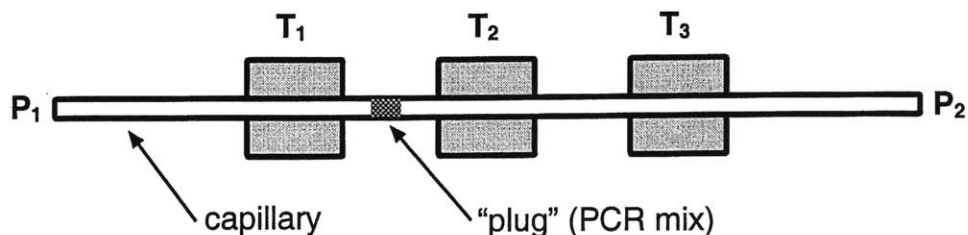
Figure 1-1: Basic capillary PCR machine concept.

machine uses a 1 μl aliquot. This saves on expensive reagent costs.

The basic concept is shown in Fig. 1-1. A 1μl drop, or "plug", of PCR sample mix is placed inside of an oil-filled capillary. PCR is performed by manipulating pressures P_1 and P_2 to move the plug to heat zones at the three PCR step temperatures T_1, T_2, and T_3, established by heat blocks. Since there is one heat block for each PCR step, there is no time spent changing a heat block temperature. The plug volume is small, and heats quickly. The machine was successfully used to perform about 200 PCR reactions, and required about 20 minutes to perform 30 cycles of a 500 base-pair target.

This work opens with an explanation of the polymerase chain reaction in Chapter 2. This is followed by a review of current fast PCR machines in Chapter 3. Chapter 4 provides a detailed description of a novel fast PCR machine. Chapters 5 and 6 detail PCR experiments using this device. Chapters 7, 8, and 9 are detailed engineering analyses of the device, especially pertaining to its speed limits. The work concludes with recommendations for future work in Chapter 10.

Due to the large number of symbols used in this work, each chapter has its own nomenclature, listed at the end of the chapter. The usage of symbols may be different from those of other chapters.

1.1 Nomenclature

P_1, P_2 Pressures at the capillary ends.

T_1, T_2, T_3 Heat block temperatures.

Chapter 2

The Polymerase Chain Reaction

The polymerase chain reaction, or "PCR," is a common technique in molecular biology. It is used to produce many copies of a portion of DNA. While it attempts to mimic *in vivo* DNA replication, it is not identical. To understand how PCR works, we must look at the basic structure of DNA.

2.1   DNA Structure

DNA is made up of nucleotides. Each *nucleotide* consists of a nitrogen-containing base and three phosphate groups are attached attached to a pentose sugar. There are only four different types of nucleotides found in DNA: deoxyadenosine triphosphate (dATP, referred to as 'A' for sequencing purposes), deoxycytidine triphosphate (dCTP; 'C'), deoxyguanosine triphosphate (dGTP; 'G'), and deoxythymine triphosphate (dTTP; 'T'). They are collectively referred to as dNTPs, and are also called *bases*. The nucleotides can form a chain (Fig. 2-1). The phosphate group at the 5' position of
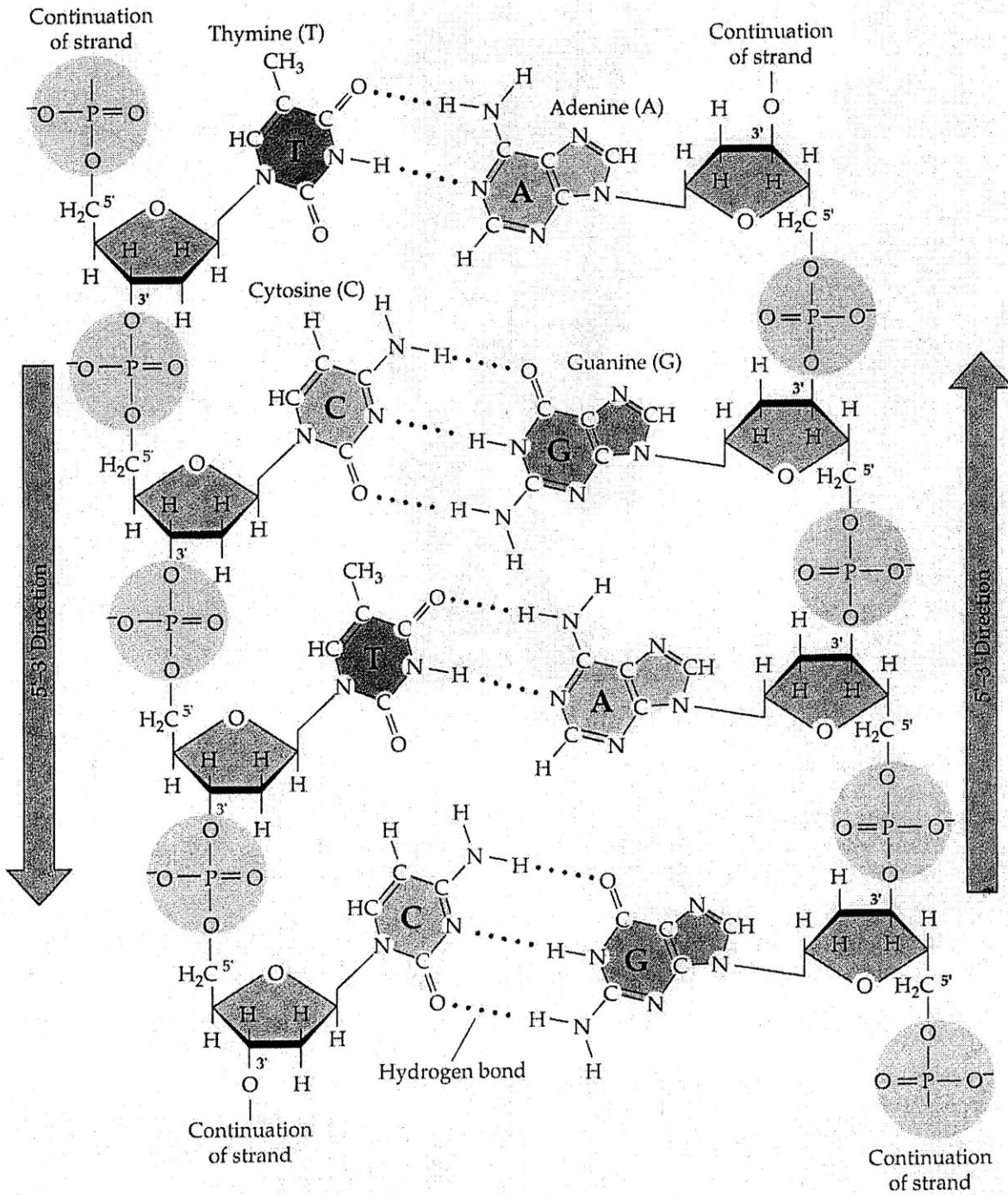
Figure 2-1: The chemical structure of DNA. From [70, page 247].

one nucleotide links with the 3' hydroxyl group of the next nucleotide. The remaining two phosphate groups are clipped off by DNA polymerase, the enzyme catalyzing the reaction. Additional nucleotides are added in the same manner, always at the end of the existing chain with the free hydroxyl group at the 3' position. This is referred to as the *3' end*. The other end with the free phosphate group at the 5' position is called the *5' end*. The chain itself is a *single stranded DNA* (ssDNA) strand which is said to go in the 5' to 3' direction. The length of DNA is expressed in bases: a strand 1000 bases long would be expressed as 1.0 kb (kilobases), for example.

Two single stranded DNA strands can combine to form a *double stranded* DNA (dsDNA) strand. The two strands run alongside each other, forming a ladder-like structure. The 5' end of one strand is at the 3' end of the other strand, so the ssDNA strands are said to run *antiparallel* to each other. Each base on one strand hydrogen bonds to its corresponding base on the other strand (Fig. 2-2). An 'A' will only bond with a 'T', and a 'G' will only bond with a 'C'. For two ssDNA to form a dsDNA, the two ssDNA sequences must match up according to these rules[1]. They are said to be *complementary*. For example, if one ssDNA is 5'-ATGC-3', then the other must be 3'-TACG-5'. The actual shape of dsDNA results from twisting the "ladder" into a spiral. This produces the familiar double helix structure.

---

[1]A small percentage of bases can be mismatched under some circumstances.

16
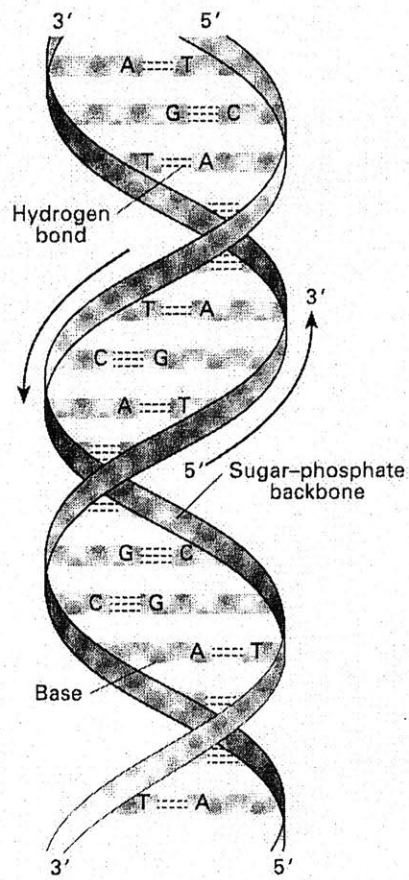
Figure 2-2: A's pair with T's, and C's pair with G's. From [58, page 1].

Denature (94 C)

Anneal (50-60 C)

Extend (70-80 C)

DNA

primer 1   primer 2
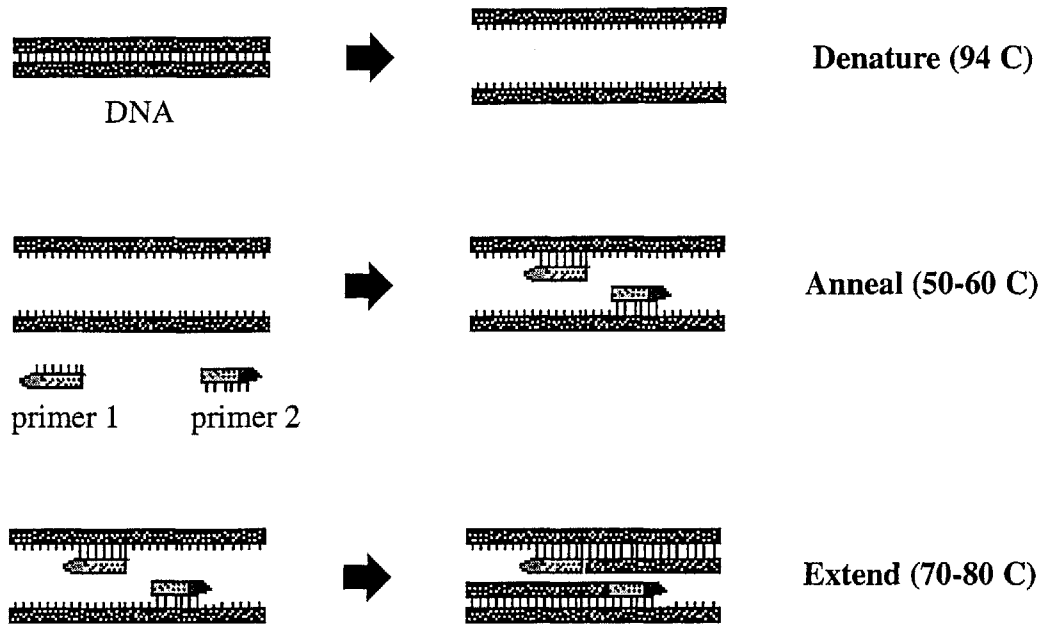
Figure 2-3: Denaturing, annealing and extension steps for one cycle.

2.2 PCR Overview

In vivo DNA replication is very complex, and involves the concerted effort of many different proteins [70]. PCR is comparatively simple, and involves only one protein: DNA Polymerase. PCR was invented in 1985 by Kary Mullis [54, 56, 74]. He received the 1993 Nobel Prize in chemistry for this contribution. PCR is performed by subjecting a specific fluid mix to a cyclic heating process. The mix includes copies of the initial *template* DNA, free nucleotides, short ssDNA sequences called *primers*, and a thermostable DNA polymerase—usually *Thermus aquaticus* DNA Polymerase (*Taq*).

The first step in PCR is *denaturating* (see Fig. 2-3). This takes place around[2] 94–96°C. At this temperature, the hydrogen bonds between bases are not strong

---

[2]The optimal time and temperature for each step depends on the particular DNA, primers, polymerase, etc.

enough to hold the dsDNA together. The dsDNA dissociates into ssDNA.

The next step is *annealing*. The temperature of the aliquot is brought to 50–60°C to optimize the binding (annealing) of the primers to the ssDNA. At this temperature, the ssDNA strands can recombine. Therefore, the aliquot contains much greater numbers of primers than DNA in order to favor primer-ssDNA hybridization. A primer is a short sequence of DNA, typically 20–30 bases long, that is complementary to the desired start point of DNA replication. There are two types of primers present—one that binds to each of the two ssDNA strands. These are called the *forward* and *reverse* primers. DNA polymerase cannot act on a ssDNA that does not have a primer.

The third step is *extension*. This is the actual synthesis of new DNA. To facilitate this process, the temperature is brought to 70–80°C. A DNA polymerase molecule that recognizes a ssDNA-primer pair will start attaching free nucleotides to construct the ssDNA's complement. The forward and reverse primers usually do not anneal at the ends of the template DNA, so the new DNA is almost always shorter than the template.

The denaturing, annealing, and extension steps are repeated. Each sequence of these steps is termed a *cycle*. PCR usually has 20–45 cycles [58]. Extension produces new DNA beginning at the primers (see Fig. 2-4). After the initial few extension steps, the vast majority of new dsDNA that is produced is the region between and including the two primers. By specifying the primers, researchers can search for and amplify specific portions of template DNA.

Theoretically, each cycle can double the number of existing DNA strands. In
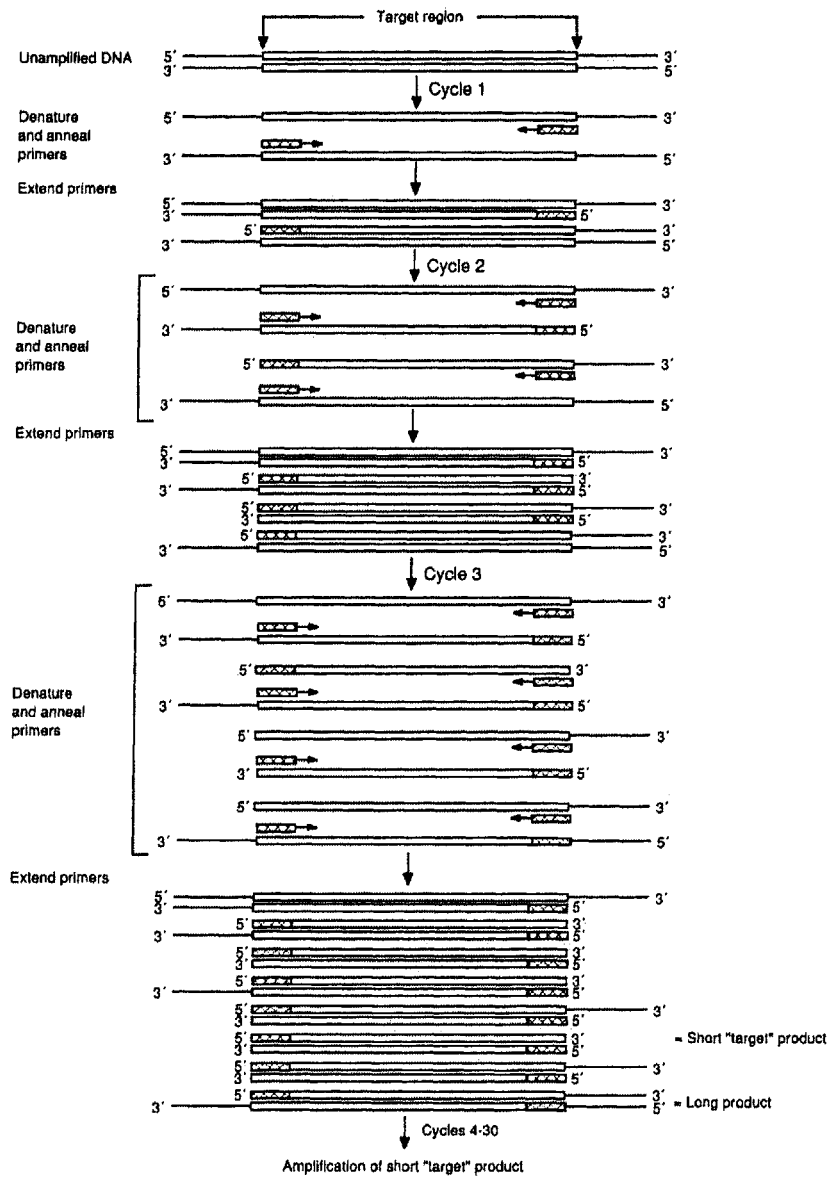
Figure 2-4: Accumulation of product as PCR proceeds. From [58, page 4].

Amount	Constituent
1 μg	mammalian DNA
0.5 μM	forward primer
0.5 μM	reverse primer
0.2 mM	dATP
0.2 mM	dCTP
0.2 mM	dGTP
0.2 mM	dTTP
2.5 units	*Taq* DNA polymerase
1.5 mM	MgCl$_2$
50 mM	KCl
10 mM	Tris·HCl (pH 9.0 at 25°C)
0.01%	Triton X-100

Table 2.1: A typical 100 μl PCR mix. From [43].

reality, the process is not 100% efficient. Its efficiency, Y, is defined as follows [13]:

$$\frac{\text{concentration of product}}{\text{concentration of template}} = (1 + Y)^n \qquad (2.1)$$

where n is the number of cycles. A typical PCR reaction is 70% efficient [13].

2.3 The PCR Mix

PCR mixes vary. A mix must be adjusted to find the optimal constituents to go along with a given set of template and primers [13]. A typical PCR mix is shown in Table 2.1. The constituents are mixed together in distilled water to a total volume of 100 μl. A description of each constituent follows.

Mammalian DNA length varies, but is typically 3.0×10^9 bp long [88, page 621].

dsDNA is[3] 660 g/bp·mole. Therefore, the DNA concentration in Table 2.1 is 5×10^{-15}

M. If plasmid rather than mammalian DNA is used, only 0.1 ng is required [43]. Since

plasmid length is around 1.2–3 kb [46], this is a concentration of about 10^{-12} M.

In general, PCR efficiency is greater for smaller sized template DNA [13]. The

minimum amount of starting mammalian template DNA is around 100 copies per 100

μl reaction (1.7×10^{-18}M) [73], though under very special conditions, even a single

DNA molecule may be amplified[4]. Concentrations greater than 10 μg template per

100 μl reaction (5×10^{-14} M) hurts the reproducibility of the reaction [13]. At this

concentration, contaminants from DNA preparation may also decrease the efficiency

of the reaction [43].

The primers are short pieces of DNA, each $\approx$20–30 bp in length [43, 58]. Each

should have a sequence complementary to the end of one of the expected product

strands. The 20 bp minimum length is to ensure that each primer is complementary

to a unique position of the template DNA. Beyond this minimum, primer length

is kept short to minimize costs—primer synthesis is usually priced per base. Each

primer should be chosen so that its 3' end sequence is neither complementary to itself

nor the other primer [58]. Primer concentration should be at least 10 times that of the

expected product concentration [13] so that ssDNA-primer complexes are formed in

favor of dsDNA complexes during annealing. However, if primer concentration is too

---

[3]Therefore, ssDNA is 330 g/bp·mol. These are average numbers, assuming equal numbers of A,
C, G and T bases. A more precise equation for the molecular weight of ssDNA is [45]:

$$(\#A \times 313.2) + (\#C \times 289.2) + (\#G \times 329.2) + (\#T \times 304.2) - 62 + [(\text{total } \# \text{ of bases}) - 1] \times 17$$

[4]For example, [34, 53].

high, they can anneal to incorrect, *nearly* complementary locations [13]. This results in erroneous product and decreased efficiency. The product specified by primers can be up to 10 kb long if *Taq* is used. However, products greater than 3 kb in length cause the reaction to be very inefficient [43, 65]. Different polymerases and protocols must be used to amplify longer targets [5].

The dNTPs are the building blocks from which the product DNA is built. The optimal concentration is around 50-200 μM for each of the four dNTPs. Too large of a concentration increases the rate at which DNA polymerase incorporates erroneous dNTP[6] [73]. A dNTP concentration of 4–6 mM actually *decreases* the *Taq* extension rate [24].

DNA polymerase is the enzyme that constructs the product DNA from the dNTPs. There are a variety of DNA polymerases available [4]. They vary in their fidelity (the chance that they will incorporate an erroneous dNTP), thermostability (how much activity they maintain after being heated), maximum product length, etc. However, they all have enough heat resistance to withstand multiple denature cycles. The quantity of DNA polymerase is usually specified in units of activity. One *unit* is defined [69] as the amount of enzyme that will build 10 nanomoles of ssDNA product in 30 minutes at 74°C. The reason why the enzymes are not specified in terms of molar concentration is because their activity per mole varies from purification to purification.

---

[5]For example, Kainz et al. [36] were able to amplify a 15.6 kb target using the *Tub* DNA polymerase and nonstandard PCR protocol.

[6]For example, under normal circumstances, *Taq* incorporates one wrong base every 4800 bases [38].

Of all the DNA polymerases available, the one most commonly used in PCR is that purified from *Thermus aquaticus*. It is referred to as *Taq*, for short. It was originally isolated from a hot spring in Yellowstone National Park [24]. The reason for its popularity is that it was the first DNA polymerase used for PCR [55]. It is still one of the fastest polymerases. Its speed is estimated at 60–120 bases/second (see Section 2.5.5). *Taq* will slowly lose activity at denaturing temperatures. In a standard PCR mix, its half life is 130 min at 92.5°C, 40 min at 95°C, and 5–6 min at 97.5°C [24]. Estimates of the optimal temperature for extension vary, but fall within the 70–80°C range [4, 13, 24, 31, 43, 55]. Concentration of *Taq* is 0.5-5 units per 100 μl PCR mix [31]. While greater concentrations of the enzyme can increase efficiency (up to a point), concentrations greater than 2.5 units per 100 μl can increase the amount of erroneous product [43].

$MgCl_2$ is necessary for the polymerase to work. The dNTPs bind to the Mg^{++} ions [73]. This does not affect the dNTPs: when the free dNTP concentration becomes low enough, they unbind. However, 0.5–2.5 mM free (not bound to dNTP) Mg^{++} is required by the polymerase [31]. The optimal concentration of $MgCl_2$ varies from mix to mix. While all constituent concentrations may be optimized for PCR, optimization of $MgCl_2$ concentration is critical [13, 43]. Too much $MgCl_2$ results in erroneous products. Too little results in low product yield.

KCl is often included to aid annealing. Each phosphate group in ssDNA is negatively charged, so the whole strand has a negative charge [70, page 320]. This makes the DNA strands repel each other. Fortunately, K^+ ions cluster around the negative

charges, neutralizing them and permitting annealing[7]. 50–55 mM of KCl should used [4]. Larger amounts inhibit *Taq* [31].

Tris·HCl is a buffer whose presence ensures the optimal pH for the polymerase. This range is 7.8–9.4 for *Taq* [4]. The manufacturer often specifies (and provides buffer of) the optimal pH for its polymerase.

The Triton X-100 is present to stabilize the DNA polymerase. Gelatin or bovine serum albumin ("BSA") are sometimes used instead [13]. BSA also serves as a blocking agent—it sticks to the walls of the tube holding the mix so less *Taq* gets stuck on the walls.

Other additives, such as glycerol, dimethylsulfoxide, or formamide , are sometimes included in the mix. These help the reaction by lowering the denaturing temperature [13]. Annealing will also take place at a lower temperature, but this can be an advantage if the current annealing temperature is low enough for the primers to anneal at incorrect locations.

2.4   PCR Time Schedule

A conventional PCR machine[8] is shown in Fig. 2-5. The ~100 μl PCR mix is pipetted into a small disposable plastic "Eppendorf" tube[9]. A thin layer of mineral oil is sometimes placed on top of the mix to prevent evaporation[10]. The tube is placed

---

[7]While KCl is the most commonly used to provide monovalent cations, sometimes other salts are used, such as NaCl [43].

[8]For example, a Techne PHC-3 (Princeton, NJ).

[9]Eppendorf is a brand name. The generic term is microfuge tube, which denotes a tube suitable for use in a small centrifuge.

[10]Newer machines often have a heated cover for the heat block which eliminates the need for mineral oil.

Aliquot in tube

Heater block
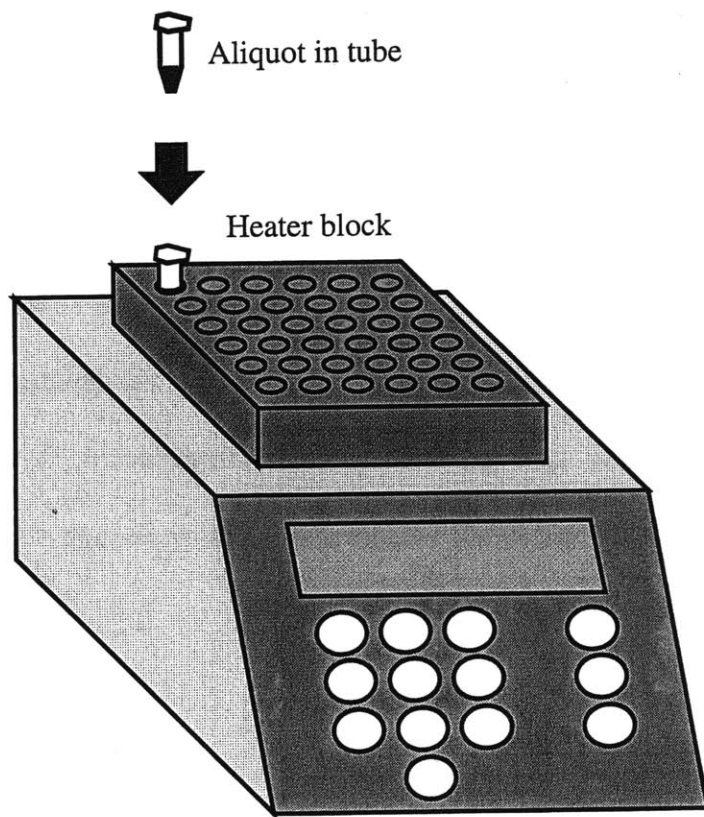
Figure 2-5: A standard PCR machine.

Cycle	Denature	Anneal	Extend
1	94°C, 5 min.	50°C, 2 min.	72°C, 3 min.
2–29	94°C, 1 min.	50°C, 2 min.	72°C, 3 min.
30	94°C, 1 min.	50°C, 2 min.	72°C, 10 min.

Table 2.2: A typical PCR heating schedule. From [75, Chap. 14].

inside of a computer-controlled heat block.

A typical heating schedule is shown in Table 2.2. The cycle is run 30 times. If there is a large amount of initial template, fewer cycles may be run. If there is very little initial template, up to 45 cycles may be run. More cycles are extremely unlikely to produce additional product (see Section 2.5.5).

The denature step in cycle 1 is longer than in subsequent cycles. In cycle 1, all the DNA is template. Template is usually much longer than the product, so it requires a longer time to denature. In subsequent cycles, product is present. Since product is usually shorter than template, shorter denature times are required.

The extension step in the last cycle is also longer than in other cycles. This is to ensure that all product extension is complete.

While the extension time is fixed at 3 min in Table 2.2, the amount of time used is usually varied according to product length. A common rule of thumb is 1 min per kb of product [73].

Like the PCR mix, PCR cycle times vary. While the schedule shown in Table 2.2 serves as a starting point, the researcher must tweak it to optimize a particular mix. The annealing temperature, in particular, is often optimized for the specific primers used.

100
95
90
85
80
75
70
65
60
55
50

0 10 20 30 40 50 60 70 80 90 100 110 120 130 140 150 160 170 180 190 200

Time (secs)
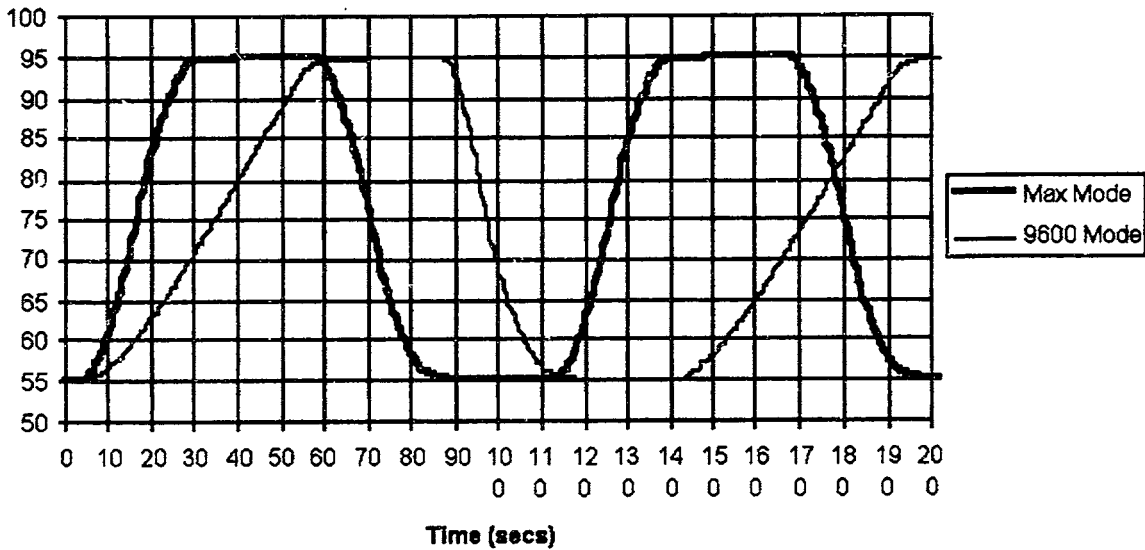
Max Mode
9600 Mode

Figure 2-6: Fastest temperature transitions of two state-of-the-art conventional PCR machines: the Perkin Elmer GeneAmp 9700 (recently introduced as of Feb 2000) and the slightly older GeneAmp 9600. The heavier "MAX Mode" line indicates the fastest temperature transitions available to the 9700 ($\Delta 40°$ C in ≈ 20 sec). The lighter "9600 Mode" indicates the fastest temperature transition available to the 9600 ($\Delta 40°$ C heating in ≈ 50 sec, and cooling in ≈ 20 seconds). Taken directly from the manufacturer product literature [64].

2.5 PCR Theory

The time schedule presented in Table 2.2 is conservative. It was developed for the conventional type of PCR machine shown in Fig. 2-5. This type of machine can only change temperature at ≈ 1–$2°$C/second due to the large thermal mass of the heater block (see Fig. 2-6).

Since the objective of this thesis was to make a machine to perform PCR as fast as possible, it is important to review the reaction theory.

28

2.5.1 The Melting Temperature T_m

T_m is defined as the temperature at which 50% of a dsDNA's base pairs are dissociated [91]. For short DNA such as primers, this means that half of the dsDNA have split into ssDNA. For long DNA such as template, this can mean that the dsDNA is partially dissociated. T_m is neither the annealing or denaturing temperature, although it is closely related to both. The annealing temperature is lower than T_m, because it is the temperature at which all the complementary ssDNA bind. The denaturing temperature should be higher than T_m, since it is the temperature at which dsDNA completely dissociates.

T_m is usually calculated with a simple empirical formula. One such formula [58] is:

$$T_m = 2(\# \text{ A} + \text{T}) + 4(\# \text{ C} + \text{G}) \qquad \text{for 1M salt, } L \leq 20 \qquad (2.2)$$

where T_m is in °C. "# A + T" is the total number of A and T bases in the DNA, and "# C + G" is the total number of C and G bases in the DNA. L is the length, in bases. When an A pairs with a T, it forms 2 hydrogen bonds. When a C pairs with a G, it forms 3 hydrogen bonds. Therefore, a C-G bond is stronger than an A-T bond. This is reflected in T_m.

The most common formula used to calculate T_m includes the following variations:

from [58], for $14 \leq L \leq 70$:

$$T_m = 81.5 + 16.6 \log_{10}[J^+] + 0.41(\%GC) - \frac{600}{L} - 0.63(\%FA) \qquad (2.3)$$

From [3, 45], for $L \geq 10$:

$$T_m = 81.5 + 16.6 \log_{10}[J^+] + 0.41(\%GC) - \frac{675}{L} - 0.65(\%FA) - (\%mismatch) \qquad (2.4)$$

From [91], for large L:

$$T_m = 81.5 + 16.6 \log_{10} \left(\frac{[Na^+]}{1.0 + 0.7[Na^+]} \right) + 0.41(\%GC) - \frac{500}{L} - (\%mismatch)$$

$$(2.5)$$

In Eqs. (2.3), (2.4), and (2.5), T_m is in °C; $[J^+]$ is the molar concentration of the generic monovalent salt ion J^+; L is length in bases; $\%GC$ is the percentage of bases in the DNA that are G or C; $\%FA$ is the percentage of formamide in the PCR mix (see page 25); and $\%mismatch$ is the percentage of bases in the binding region that are not complementary[11]. For standard PCR mixes, J^+ is the potassium ion K^+ from KCl. However, in Eq. (2.5), $[K^+]$ should *not* be substituted for $[Na^+]$. Rather, the reference [91] states that a standard PCR buffer containing 1.5 mM $MgCl_2$ and 50 mM KCl behaves like a 0.20M Na^+ solution.

Breslauer et al. [10] developed a more complex, accurate method for determining T_m for short DNA, building upon the earlier RNA work of Borer et al. [7]. They

---

[11]It is possible for annealing occur if a small portion of the bases are not complementary.

Interaction	ΔH^0, kcal/mol	ΔS^0, cal/(mol·K)	ΔG^0, kcal/mol
AA/TT	-9.1	-24.0	-1.9
AT/TA	-8.6	-23.9	-1.5
TA/AT	-6.0	-16.9	-0.9
CA/GT	-5.8	-12.9	-1.9
GT/CA	-6.5	-17.3	-1.3
CT/GA	-7.8	-20.8	-1.6
GA/CT	-5.6	-13.5	-1.6
CG/GC	-11.9	-27.8	-3.6
GC/CG	-11.1	-26.7	-3.1
GG/CC	-11.0	-26.6	-3.1

Table 2.3: Thermodynamic values of Breslauer et al. [10] for short dsDNA strands at 1M NaCl, 25°C, and pH 7.

$$\Delta H_{total} = \Delta H_i + \sum_n \Delta H_n^0$$

-11.0   -9.1   -9.1   -11.0

5′-G-G-A-A-T-T-C-C-3′
* * * * * * * * *
3′-C-C-T-T-A-A-G-G-5′

-5.6   -8.6   -5.6
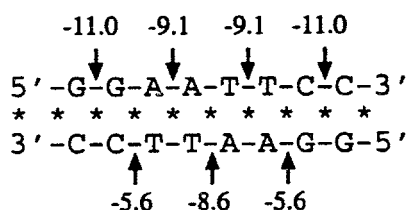
For the above dsDNA,

$\Delta H_{total} = [0 + (2 \times -11.0) + (2 \times -9.1) + (2 \times -5.6) + 8.6]$ kcal/mol = -60.0 kcal/mol

Figure 2-7: Sample calculation of H_{total} for method of Breslauer et al. [10]. H_{total} is the sum of the ΔH^0 values of adjacent base pairs from Table 2.3 and ΔH_i, the initiation enthalpy. Breslauer et al. chose $\Delta H_i = 0$.

analyzed 28 different DNA fragments, ranging in size from 6–20 bases, to get the thermodynamic data presented in Table 2.3. These values are used to calculate the values of ΔH_{total}, ΔS_{total}, and ΔG_{total}. Fig. 2-7 shows an example calculation of ΔH_{total}. ΔS_{total} and ΔG_{total} are calculated similarly from values of ΔS^0 and ΔG^0, respectively. While the helix initiation enthalphy is taken as zero,

$$\Delta H_i = 0 \qquad (2.6)$$

there is a more complex expression for ΔG_i:

$$\Delta G_i = \Delta G_{i1} + \Delta G_{sym} \qquad (2.7)$$

Normally, ΔG_{i1} is 5 kcal/mol and ΔG_{sym} is zero. If the dsDNA is made up exclusively of A·T base pairs, ΔG_{i1} is 6 kcal/mol. If the dsDNA is made up of two identical (self-complementary) ssDNA, ΔG_{sym} is 0.4 kcal/mol. The value of ΔS_i was found by Borer et al. [7] to be

$$\Delta S_i = -16.8 \text{ cal/(mol·K)} \qquad (2.8)$$

From the definition of Gibbs free energy[12],

$$\Delta G = \Delta H - T\Delta S \qquad (2.9)$$

where T is absolute temperature. If $\Delta G = 0$, the reaction is in equilibrium; if $\Delta G < 0$, the reaction is spontaneous. Hence, T_m can be found from Eq. (2.9) by setting $\Delta G = 0$.

Borer et al. [7] present the following equation, which accounts for DNA concentration:

$$T_m = \frac{\Delta H}{R \ln[c/4] + \Delta S} \qquad (2.10)$$

---

[12]For example, see [11, page 706].

c is the total concentration of both complementary DNA strands, in molar; and $R = 1.987 \times 10^{-3}$ kcal/mol·K, the universal gas constant. Note that T_m is expressed in Kelvins. The equation applies to the case in which both ssDNA are at the same concentration. In PCR, the concentration of primers is much greater than the concentration of product[13].

The ΔG, ΔH, and ΔS values were found at 25°C. They are most accurate for predicting T_m if $(0°C < T_m < 40°C)$ [7]. The studies of Breslauer and Borer were conducted in 1 M NaCl at pH 7.0. PCR is typically performed in 50 mM KCl at pH 9.

Wetmur modified Eq. (2.10) to account for varying salt concentration [91]:

$$T_m = \frac{\Delta H}{R \ln[c] + \Delta S} + 16.6 \log_{10} \left(\frac{[Na^+]}{1.0 + 0.7[Na^+]} \right) + 3.83 \qquad (2.11)$$

where T_m is in K; R is the universal gas constant; $[Na^+]$ is the concentration of Na^+ in molar; and $[c]$ is the concentration of primer, in molar. As with Eq. (2.5), Wetmur notes that a standard PCR buffer with 1.5 mM $MgCl_2$ and 50 mM KCl is equivalent to a Na^+ concentration of 0.20 M. Eq. (2.11) assumes that the concentration of primers is much greater than the concentration of product. If it is used for equal amounts of complementary DNA, then $[c]$ is replaced by $[c/4]$, as in Eq. (2.10).

---

[13]Unless so many cycles are run that product concentration approaches primer concentration. Notice there are two reactions going on: the forward primer annealing to one product ssDNA, and the reverse primer annealing to the other product ssDNA. Each reaction can be considered separately. However, the primer T_m's are usually similar and their concentrations are usually identical. Template is not considered since its concentration is much lower than that of product

2.5.2 Denaturing

Matthew Meselson and Franklin Stahl were the first to observe heat denaturation of DNA [47] while verifying Watson and Crick's semiconservative model of DNA replication [70, page 250]. According to the model, when dsDNA doubles, the resulting dsDNA each contain one DNA strand from the original DNA, and one DNA strand built from new bases. Meselson and Stahl grew *E. Coli* cells for 17 generations in a medium where the sole nitrogen source was heavy ^{15}N rather than ordinary ^{14}N. Subsequently, all the cell DNA was heavy. The cells were then transferred into a medium containing ordinary ^{14}N. After one cell division cycle, they examined the DNA. It had an intermediate density, between those of normal and heavy DNA. After two cell division cycles, some of the DNA was normal density, and some was intermediate density. This proved that DNA replication was semiconservative, rather than completely conservative (where new DNA is formed entirely from new dNTPs, in which case there would be no intermediate density DNA) or dispersive (where all DNA strands would have identical density).

Meselson and Stahl heated some of the intermediate density DNA at 100°C for 30 minutes. Two different density DNA were produced. The heating had dissociated intermediate density dsDNA into normal and heavy density ssDNA.

The literature on denaturation is sparse. Wetmur [91] presents a method for calculating denaturing time for a given temperature, but it only applies to short lengths of DNA. Golo and Kats presented a complex mathematical model of denaturation [25]. However, they do not provide the coefficient values necessary to determine

temperature or rate.

As mentioned previously[14], denaturing is typically at 94–96°C. This narrow range is used for almost all PCRs. If the temperature is too high, the DNA polymerase will degrade. If the temperature is too low, most dsDNA will not dissociate into ssDNA. Primers cannot anneal to dsDNA, so product yield will be low. Complete dissociation is especially important during the first denaturing cycle. Template DNA is almost always much longer than the product DNA, and requires a longer time to denature. For this reason, the first denature cycle is usually longer than subsequent cycles.

2.5.3 Annealing Temperature

DNA renaturation was discovered in 1961 by Marmur and Doty [47]. They found that when denatured *D. pneumoniae* DNA was cooled gradually, its transforming activity[15] was partially restored. Further investigation proved that the ssDNA was recombining into dsDNA.

The optimal annealing temperature is around 25°C below the primer T_m, though the rate changes very little in the range of 15–30°C below[16] T_m [92]. Primers anneal fastest at this temperature. If the annealing temperature is too low, the primers can anneal to regions of the DNA that are not perfectly complementary. Incorrect products are made. If the annealing temperature is too high, the primers will not bind to the DNA quickly. This can result in low yield.

---

[14]See page 18.

[15]Transformation is the process in which raw bacterial DNA in the proximity of a bacterial cell is incorporated into the cell's own DNA [70].

[16]Newton and Graham [58] note that in some cases, the optimal annealing temperature may actually be 3–12°C *higher* than the calculated T_m.

The optimal annealing temperature for a given primer, template, and mix must be determined experimentally. Denaturing and extension temperatures do not vary as much. Many modern PCR machines[17] have heat blocks with temperatures that vary from one end to the other, specifically to test a range of annealing temperatures simultaneously.

Several equations have been published to determine the annealing temperature T_{ANN}. They serve as a starting point from which to fine tune T_{ANN}. If the reaction does not have to be highly optimized, they may be used as is.

One method would be calculate to T_m using one of the formulae in section 2.5.1, and set $T_{\text{ANN}} = T_m - 25°C$. There are also empirical equations for calculating T_{ANN}, such as the following [58]:

$$T_{\text{ANN}} = 22 + 1.46\,[\,2 \times (\#G + C) + (\#A + C)]$$ (2.12)

where T_{ANN} is in °C.

Rychlik et al. [72] tested 11 different primer pairs on 2 different template DNA to produce PCR products 135–10,881 bases long using a Perkin-Elmer/Cetus Thermal Cycler. They came up with the following formula for the T_{ANN}:

$$T_{\text{ANN}} = 0.3T_m^{\text{primer}} + 0.7T_m^{\text{product}} - 14.9\text{K}$$ (2.13)

---

[17]For example, the Robocycler Gradient 96. Stratagene, La Jolla, CA.

T_m^{primer} is a variant of Eq. (2.10):

$$T_m^{\text{primer}} = \frac{\Delta H}{R \ln(c/4\text{M}) + \Delta S} + (16.6\text{K}) \log[\text{K}^+] \qquad (2.14)$$

where ΔH and ΔS are as specified in Section 2.5.1; R is the universal gas constant; c is the sum concentration of a primer and its complementary ssDNA; and $[\text{K}^+]$ is the molar concentration of K^+. Since product concentration changes several thousandfold over the course of PCR, they determined that a value of $c = 250$ pM should be used in Eq. (2.14). For T_m^{product} they used Eq. (2.4), since Eq. (2.14) is not applicable to long molecules.

2.5.4 Annealing Rate

The annealing rate is explored DNA hybridization studies. DNA hybridization is a general term for complementary ssDNA combining into dsDNA. It applies to both equal and unequal length complementary DNA. Annealing is a more specific term used to describe the attachment of primers to product or template ssDNA during PCR.

Hybridization takes place in two stages. First, there is an initiation stage where two complementary DNA come into contact. This is followed by the two ssDNA "zipping up" to become dsDNA. The hybridization process is second order with respect to strand concentration. This shows that the process is dominated by the initiation stage. The subsequent base pairing process is much faster by comparison [90, 92].

The kinetics of DNA hybridization were laid out by Wetmur and Davidson in 1968 [92], and have changed little since. For the following reaction, where ssDNA species A and B combine to form dsDNA species D:

$$A + B \xrightarrow{k} D \qquad (2.15)$$

The concentration of A is described as:

$$-\frac{dA}{dt} = kAB \qquad (2.16)$$

k in Eqs. (2.15) and (2.16) is a rate constant.

Initially, DNA hybridization studies were performed with equal numbers of identical-length complementary ssDNA. In this case, $A = B$, and Eq. (2.16) becomes

$$-\frac{dA}{dt} = kA^2 \qquad (2.17)$$

Let C indicate the total strand concentration:

$$C = A + B \qquad (2.18)$$

Following the terminology of Wetmur, k is k_2 if the species concentrations are specified in *base pairs* per volume[18]. If the concentrations and lengths of A and B are the same, $C = 2A$ and $C_b = 2A_b$, where the subscript b denotes a concentration in bases per

---

[18]Strand concentration $\times$ (strand length in bases).

volume (rather than strands per volume). Eq. (2.17) becomes

$$-\frac{dC_b}{dt} = \frac{k_2}{2}C_b^2 \tag{2.19}$$

Integrating,

$$\frac{1}{C_{b,f}} - \frac{1}{C_{b,i}} = \frac{k_2}{2}t \quad \text{OR} \quad \frac{C_{b,i}}{C_{b,f}} = 1 + \frac{k_2}{2}C_{b,i}t \tag{2.20}$$

In Eq. (2.20), the i and f subscripts refer to initial (at time $t = 0$) and final (at time t) states.

In the case of PCR, there should always be many more primers than product DNA[19]. Therefore, the primer concentration can be regarded as constant. We must return to Eq. (2.16), expressing concentrations in terms of bases per volume:

$$-\frac{dA_b}{dt} = k_2 A_b B_b \tag{2.21}$$

Here, A is one of the two types of single-stranded product DNA, and B is the corresponding free primer. Integrating, we get

$$\frac{A_f}{A_i} = e^{-k_2 B_b t} \tag{2.22}$$

Which allows us to calculate how fast annealing can take place.

---

[19]Template DNA concentration is constant and, except for the first few cycles, negligible relative to product DNA concentration.

The rate constant is calculated as follows [90, 91, 92]:

$$k_2 = \frac{k_N' \sqrt{L}}{N}$$

(2.23)

L and N are the length and complexity, respectively, of the shorter of the two ssDNA (the primer, for PCR). Normally, the two are identical[20]. The dependency of k_2 on $\sqrt{L}$ has been explained by Wetmur's "excluded volume effect" theory, which considers the fact that strands that come into contact do not necessarily have all their bases in close enough proximity to anneal. A detailed explanation and derivation may be found in [89, 92].

The length-independent rate constant k_N' is:

$$k_N' = (4.35 \log_{10}[\text{Na}^+] + 3.5) \times 10^5 \text{M}^{-1}\text{s}^{-1}$$

(2.24)

for $0.2 \leq [\text{Na}^+] \leq 4.0$ and $5 \leq \text{pH} \leq 9$ [91]. $[\text{Na}^+]$ is the concentration of Na^+, in M. KCl is usually used in PCR rather than NaCl. Wetmur [91] states that, for hybridization, a standard PCR buffer that contains 1.5 mM MgCl_2 and 50 mM KCl is equivalent to 0.20 M NaCl. In this case, Eq. (2.24) becomes

$$k_N' = 4.6 \times 10^4 \text{M}^{-1}\text{s}^{-1}$$

(2.25)

Eqs. (2.22), (2.23), and (2.25) can be used to find the theoretical annealing time.

---

[20]The two are not the same for hybridizations along sequences that have repeating sequences of DNA. The bases belonging to redundant sequences do not contribute to N.

Temperature	Extension Rate, bases/second
70°C	$> 60, < 120$
55°C	24
37°C	1.5
22°C	0.25

Table 2.4: *Taq* extension rates. From Innis et al. [32]

2.5.5 Extension

The rate of extension depends upon the particular DNA polymerase being used. The most widely used polymerase is *Taq* (see page 24). The speed of *Taq* was studied by Innis et al. [32]. They used a mix[21] of 25 nM radiolabelled primer, 50 nM M13mp18 ssDNA template, 200 μM each dNTP, 0.05% Tween 20, 0.05% Nonidet P-40, 10 mM Tris·HCl (pH 8.0), 50 mM KCl, and 2.5 mM MgCl$_2$. They annealed primer and template, added dNTPs, heated the mix to the desired extension temperature, and then added *Taq*. Small aliquots were removed at various time intervals, and EDTA[22] was put into each aliquot to halt the reaction. *Taq* was found to extend at the rates shown in Table 2.4.

A more precise rate characterization was performed by Brandis et al. [9]. They actually found the extension rate for each particular dNTP by checking the time in took to add a single nucleotide to a primer-template complex. A special apparatus was used to rapidly mix and stop reactions. Reactions were carried out at 60°C with 500 nM *Taq*, 100 nM primer-template, 2 mM Mg^{++}, and varying concentrations of the appropriate dNTP. Results are shown in Table 2.5. The data in Table 2.5 can

---

[21]The Tween 20 and Nonidet P-40 are used to stabilize the polymerase. They serve the same function as Triton X-100 in the mix described in Section 2.3.

[22]Short for ethylenediaminetetraacetic acid.

Nucleotide	k_{pol}, bases/s	K_d, μM
dATP	38 ± 2	52 ± 7
dCTP	21 ± 4	35 ± 2
dGTP	52 ± 1	36 ± 3
dTTP	31 ± 3	57 ± 20

Table 2.5: Single nucleotide *Taq* rates at 60°C. From Brandis et al. [9].

be used to calculate a reaction rate at a given dNTP concentration:

$$k_{Taq} = \frac{k_{pol}[\text{dNTP}]}{[\text{dNTP}] + K_d} \qquad (2.26)$$

where k_{Taq} is the reaction rate, and [dNTP] is the concentration of the particular dNTP. Unfortunately, this data is for 60°C , and PCR extension takes place at 70–80°C .

Since the data of Brandis et al. is only applicable at 60°C, and the data of Innis et al. only specifies a range of *Taq* extension rates, we must turn to manufacturer data for the most precise extension rate. Promega Corporation [69] reports a typical specific activity of 200,000 units/mg for their *Taq*[23]. One unit is defined as the amount of *Taq* required to extend 10 nM of bases in 30 minutes at 74°C. The 50 μl mix used by Promega to assay *Taq* activity contains 200 μM each dNTP, 50 mM NaCl, 10 mM MgCl$_2$, 50 mM Tris·HCl (pH 9.0), and 12.5 μg activated calf thymus DNA (primer-template complex). Since the DNA is 94 kDa in size, the extension rate is calculated

---

[23]This is a standard value for *Taq*. A value of 200,000 units/mg was reported by Innis et al. [32], and a slightly higher value of 250,000 units/mg was reported by Mullis [55].

at approximately 100 bases per second:

$$\left(\frac{200,000 \text{ units}}{10^{-3}\text{g } Taq}\right)\left(\frac{94,000\text{g } Taq}{\text{mol } Taq}\right)\left(\frac{10 \times 10^{-9} \text{ mol dNTP}}{(30 \cdot 60\text{s})(\text{unit})}\right) = \frac{104 \text{ mol dNTP}}{(\text{mol } Taq)(\text{s})}$$

$$(2.27)$$

Therefore, one molecule of Taq can extend 104 bases per second. Since specific activity of each batch varies, this value is somewhat variable.

Ideally, extension should result in an exponential increase in product each cycle. This is true during the initial cycles, which are termed the *exponential phase* of PCR. However, after a number of cycles, the number of ssDNA may exceed the number of DNA polymerase molecules. Only a fixed amount of new DNA can be produced each cycle. In this case, PCR has reached the *linear phase*. If even more cycles are run, the reaction will eventually stop producing more product because (1) the product concentration approaches the remaining primer concentration, and/or (2) the mix runs out of dNTPs. When the product concentration approaches the primer concentration, primer annealing does not occur preferentially to DNA reannealing. For this reason, the maximum product concentration in most PCR reactions is about 10^{10} copies per μl [13].

2.6   Nomenclature

A   dATP. See page 14.

A Generic ssDNA species. See Section 2.5.4.

A_b A, expressed in bases per volume.

43

A_f	A, after time t. See Eq. (2.22).
A_i	A, at time $t = 0$. See Eq. (2.22).
B	Generic ssDNA species. See Section 2.5.4.
B_b	B, expressed in bases per volume.
c	Total concentration of both complementary ssDNA in Eq. (2.10) and (2.14), and of primer in Eq. (2.11).
C	dCTP. See page 14.
C	$A + B$. See Section 2.5.4.
C_b	C, expressed in bases per volume.
$C_{b,f}$	C_b after time t. See Eq. (2.20)
$C_{b,i}$	C_b at time $t = 0$. See Eq. (2.20)
D	Generic dsDNA species made from A and B. See Section 2.5.4.
%FA	Percentage of formamide in the PCR mix.
G	dGTP. See page 14.
ΔG^0	One nearest neighbor pair contribution to Gibbs free energy. See Table 2.3.
ΔG_i	Helix initiation Gibbs free energy. See Eq. (2.7).
ΔG_{i1}	Term making up ΔG_i. See Eq. (2.7).
ΔG_{sym}	Term making up ΔG_i. See Eq. (2.7).
ΔG, ΔG_{total}	Total Gibbs free energy of a dsDNA strand.
%GC	Percentage of bases in the DNA that are either G or C.
ΔH^0	One nearest neighbor pair contribution to enthalpy. See Table 2.3.

ΔH_i Helix initiation enthalpy. See Fig. 2-7.

ΔH, ΔH_{total} Total enthalpy of a dsDNA strand.

J^+ Generic positive ion. See Eqs. (2.3) and (2.4).

k Rate constant of association. See Section 2.5.4.

k_2 k, if species are specified in bases per volume. See Section 2.5.4.

K_d Equilibrium association constant for *Taq*. See Table 2.5.

k'_N Length-independent rate constant. See Eqs. (2.24), (2.25).

k_{pol} Maximum *Taq* rate of phosphodiester bond formation. See Table 2.5.

k_{Taq} Equilibrium association constant for *Taq*. See Table 2.5.

L Length of the DNA, in bases.

%mismatch   % of bases in dsDNA that are not complementary.

n Number of PCR cycles (page 21).

N DNA complexity. See Eq. (2.23).

R The universal gas constant (1.987×10^{-3} kcal/mol·K).

ΔS^0 One nearest neighbor pair contribution to entropy. See Table 2.3.

ΔS_i Helix initiation entropy. See Eq. (2.8).

ΔS, ΔS_{total} Total entropy of a dsDNA strand.

t Time.

T   dTTP. See page 14.

T Absolute temperature.

T_{ANN} Optimal annealing temperature. See Section 2.5.3.

T_m — Melting temperature. See Section 2.5.1.

T_m^{primer} — Primer melting temperature. See Eqs. (2.13) and (2.14).

T_m^{product} — Product melting temperature. See Eqs. (2.13) and (2.4).

Y — PCR efficiency. See Eq. (2.1).

Chapter 3

Fast PCR Machines

Section 2.4 detailed a conventional PCR machine. It consists of a computer-controlled heater block with wells. PCR mixes are aliquotted into disposable plastic tubes, which are then placed into the wells. The heat block can change temperature at a rate of 1–2°C/second. This temperature transition time is a significant component of the overall process time, which is about 1–2 hours.

PCR is a ubiquitous and critical procedure in molecular biology. Therefore, many efforts have been made to produce faster PCR machines. This chapter details some of them.

3.1 Notes

Some of the PCR reactions detailed in this chapter use specialized methods and reagents. These include the following:

3.1.1 AmpliTaq® DNA Polymerase

AmpliTaq® DNA polymerase is a proprietary version of Taq manufactured by Applied
Biosystems (formerly PE Applied Biosystems) in Foster City, CA). It is practically
identical to ordinary Taq.

3.1.2 Hot Start PCR

Hot start PCR is conducted in such a way that the DNA polymerase is prevented
from acting until thermal cycling begins. When a standard PCR mix is formulated,
the polymerase can manufacture erroneous product as soon as it is introduced. While
the polymerase is not nearly as efficient at room temperature, it can extend slowly
nevertheless. Below the denaturation temperature, portions of DNA molecules can
exist in a denatured state[1]. Since the PCR mix is usually prepared at lower than
the annealling temperature, primers can anneal to incorrect locations, resulting in a
some amount of erroneous product. In addition, primers can have regions of comple-
mentation and form *primer dimer* complexes that can be extended. These problems
are mitigated if the polymerase cannot extend prior to thermal cycling, minimizing
the amount of initial erroneous product. Hot start PCR is more efficient and specific
than ordinary PCR [58, p. 36].

Hot start PCR requires a modified protocol. In the beginning, the polymerase
was not added until the rest of the mix reached the denaturation temperature. More
recently, wax was used in the following procedure: the mix is prepared sans DNA

---

[1]In addition, template is sometimes single-stranded.

polymerase. A wax bead is put into the tube, and the tube is heated to melt the wax. When it cools, it forms a layer on top of the mix. Next, a solution containing the DNA polymerase is pipetted on top of the wax, the tube is closed, and thermal cycling initiated. During the initial denature cycle, the wax melts, allowing the DNA polymerase to enter the mix.

Both of the above procedures requires at least one additional step. To overcome this inconvenience, the AmpliTaq Gold® DNA polymerase[2] and TaqStart™ antibody[3] have been developed. AmpliTaq Gold® is identical to AmpliTaq®, except that it requires an initial period of 10 min at 95°C to activate it. TaqStart™ is an antibody which attaches to Taq, rendering it inert when the two are together. When it is heated to > 70°C., it detaches from the Taq and becomes inactive.

3.1.3 Fluorescent Detection and TaqMan™

PCR product yield is generally quantified using fluorescence. Fluorescent techniques vary in sensitivity, and are generally only quantitative if also applied to a control of known DNA concentration. Unless mentioned otherwise, the PCR yields in this chapter are quantified via agarose gel electrophoresis. The sample is manually loaded into one end of the agarose gel. A voltage is applied across the gel, such that the DNA migrates through the gel, with shorter DNA fragments migrating faster than longer ones. The gel is permeated with fluorescent intercalcating dye, typically ethidium bromide or SYBR, which gets stuck in the DNA. The dye is excited by UV light and

---

[2]Applied Biosystems (formerly PE Applied Biosystems). Foster City, CA.
[3]Clontech. Palo Alto, CA.

visualized by eye.

Fluorescent based detection techniques are generally much more ($\sim$ 1000) times more sensitive than agarose gel electrophoresis. While ethidium bromide and SYBR are fluorescent, the intercalcating dye in the gel and the thickness of the gel provide background that interferes with sensitive detection. In addition, fluorescence in agarose gels is visualized by eye. Most other fluorescent detection uses photodiodes, photomultipliers, etc. that provide much greater optical sensitivity. The greater overall sensitivity of fluorescent methods allows detection of product at an earlier cycle than via agarose gel electrophoresis. The linear (rather than exponential) extension range can be avoided (see 2.5.5), resulting in a report of higher reaction efficiency.

Recently, the fluorescent detection scheme of choice is based on the TaqMan^{TM} system[4] [28]. It uses a DNA probe that has two fluorescent molecules attached to it, one on either end: a reporter and a quencher. When the probe is intact, the quencher suppresses the reporter fluorescence. During annealing, the probe hybridizes to a location in the target region downstream of one of the primers. During extension, when the DNA polymerase reaches the probe, it chews it up into pieces, which break away from the target. The reporter, now free of the quencher, is free to fluoresce. Hence, fluorescence is proportion to the amount of PCR product made, which can be tracked as the reaction proceeds in real time.

---

[4]Applied Biosystems (formerly PE Applied Biosystems). Foster City, CA.
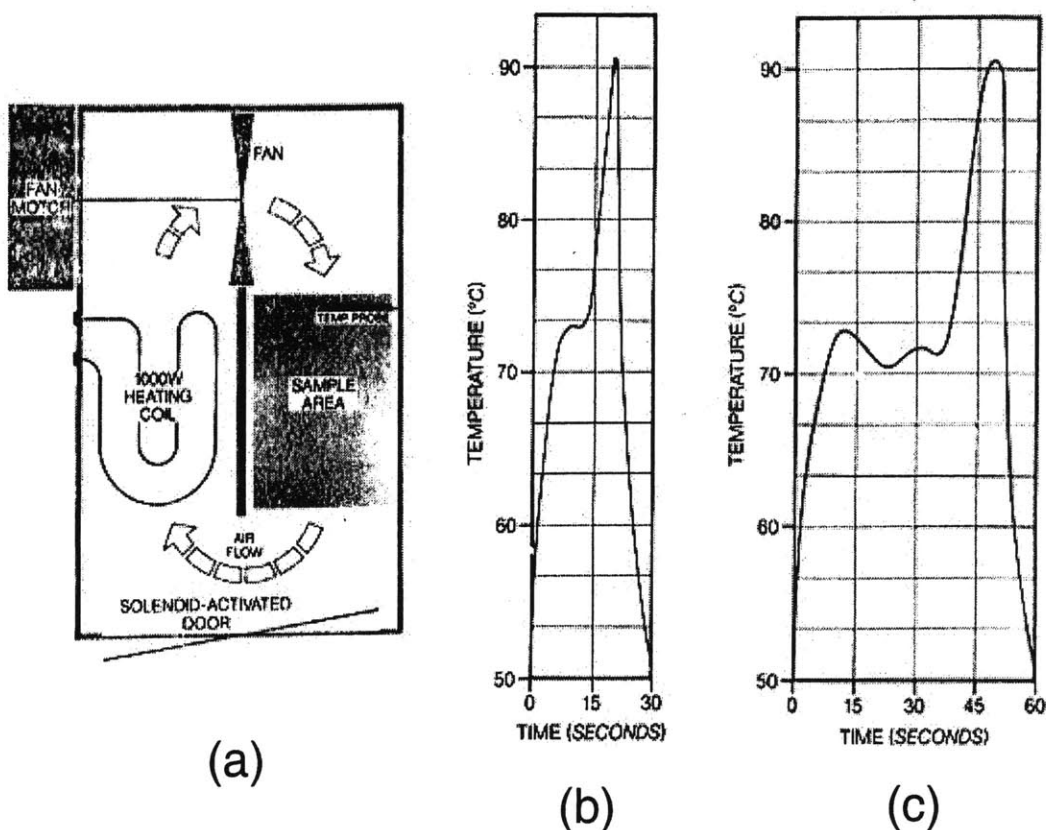
Figure 3-1: The air cycler: (a) schematic; (b) temperature history for one 30 second cycle; (c) temperature history for one 60 second cycle. From [98]. Note that the device spikes to the denature and annealing temperatures, without holding them there.

3.2 Air Cycler

Carl T. Wittwer et al. at the University of Utah Medical School developed a thermal cycler based on hot air [96, 98, 99] (see Fig. 3-1). To overcome the need for heating and cooling a heat block, they did away with one altogether. Instead, capillary action is used to inject 10 μl PCR mix into each 0.52mm I. D., 8 cm long glass capillary. The tubes are flame sealed and placed into a chamber inside of the machine. To heat the capillaries, a blow-dryer type arrangement involving a fan and 1000W heater coil is used. To cool the capillaries, a door in the chamber is opened to let out the hot air, and the fan blows ambient air over the tubes.

In their third work [99], Wittwer et al. examined the effect of individual annealing, denaturing, and extension times on product yield. Their PCR mix contained 5 ng/μl (1.9 × 10^{-15} M) human genomic DNA, 0.5 μM of each primer (536 bp target), 0.04 units/μl Taq, 50 mM Tris-HCl (pH 8.5 at 25°C), 3 mM MgCl$_2$, 20 mM KCl, 500 ng/μl bovine serum albumin, 0.5 mM each dNTP, and 2.5% (wt/vol) Ficoll 400. The template DNA was denatured by boiling prior to PCR.

The following default thermal schedule was used: 30 cycles of denaturation at (92–94°C, 1 s); 9 s transition to annealing; annealing at (54–56°C, 1 s); 4 s transition to extension; extension at (75–79°C, 10 s); and 5 s transition back to denaturing. They varied the time and temperature of each step about the default to optimize yield. Optimal temperature conditions were as follows—denaturing: 91–97°C at ≤ 1 s denaturing; annealing: 55°C at < 1 s; extension: 75–79°C at 40 s. Optimal time conditions were as follows—denaturing: < 1 to 8 s at 92–94°C; annealing: < 1 s at 54–56°C, at a ramp time from denaturing to annealing of 9 s (the fastest tested); extension: ≥ 40 s at 75–79°C.

Wittwer et al. concluded that denaturing and annealing occur almost instantaneously. In fact, they achieved good results spiking down to the annealing temperature and up to the denaturing temperature, with no dwell time at all (see Fig. 3-1 b, c). Faster temperature transitions were found to reduce overall PCR time without lessening yield. Fast annealing to extension transition actually improved yield. Yield, however, still benefits from longer extension times. 30 cycles in 15 minutes yielded product visible on an agarose gel. However, the yield was not nearly as high as a run that took 40 minutes for 30 cycles, which was comparable to that from a commercial

Perkin-Elmer Cetus DNA Thermal Cycler.

The device was made into a commercial product, the Air Thermo-Cycler[5]. Later, Wittwer et al. developed the LightCycler[TM] [97], which adds an optical detection system[6]. If fluorescent probe is added to the PCR mix, the amount of PCR product can be tracked as the reaction progresses, down to ~1 pM.

Idaho technology's air cyclers have been incorporated with other detection and preparation devices. Swerdlow et al. [84] used an HPLC pump to push PCR mix through a line of interconnected PEEK and Teflon tubing. 7 cm of tubing holding 17 μl of mix is coiled inside of a model 1605 air cycler and can be sealed from the rest of the line with HPLC valves. First PCR is performed on 17 μl of the mix, and then the fluid is pumped into a capillary electrophoresis unit to detect product. The PCR mix contained 2 pg/μl (4.2×10^{-13} M) M13mp18 DNA template (7.2 kb), 0.5 μM each primer (20 and 21 bases, fluorescently labelled, defining a 303 bp target), 0.2 mM each dNTP, 51 mM Tris-HCl (pH 8.3), 2 mM $MgCl_2$, 0.48 mg/ml bovine serum albumin, and 0.04 units/μl AmpliTaq[®] DNA polymerase. The thermal cycling consisted of 25 cycles of 92°C for 0 s, 62°C for 0 s, and 74°C for 0 s, with a final extension of 74°C for 30 s. 0 s means that the cycler was programmed to go to the desired temperature, and then immediately go to the next temperature without waiting. This took a total of 8 min. The end product was barely detectable by CE, and was not quantified.

Meldrum et al. [50] used a RapidCycler air cycler to amplify samples processed by their ACAPELLA-1K system. ACAPELLA-1K automates the process of transferring

---

[5]Idaho Technology, Idaho Falls, ID.
[6]Idaho Technology, Idaho Falls, ID.

samples from 96 well microtitre plates into capillaries, adding PCR reagents, and placing the capillaries into cassettes. The cassettes must be manually loaded into the RapidCycler for thermal cycling, though. The ACAPELLA-1K system can process fifteen hundred 2 μl samples in 8 hours.

3.3 PCR in Silicon

Initial developments in the area of micromechanics utilized lithographic techniques to etch miniature gears and motors out of silicon, and to pattern supporting electronics directly onto the surface. It is no wonder that microfluidics explored the same approach, constructing pumps, valves, and even PCR machines out of silicon.

3.3.1 Wilding et al.: PCRChip

Wilding et al. [15, 16, 80, 93, 94] applied lithographic techniques to etch a 14mm × 17mm well into silicon 115 μm deep. The well was coated with 2000 Å of SiO_2 for biocompatibility. A Pyrex cover was bonded onto the top of the well, creating a 12 μl PCR chamber (see Fig. 3-2). The structure, dubbed the "PCRChip" by its developers, was mounted on a 40 mm × 40 mm copper block fused to a Peltier heater-cooler. 40 l/min of air was directed over the block to help dissipate heat.

The PCRChip has several advantages. Since it has a small thermal mass, it is easier to heat and cool than conventional heat block-based PCR machines. The large surface to volume ratio ensures quick, uniform sample heating. Small aliquot size saves on reagent costs. The silicon structure can be mass produced cheaply.
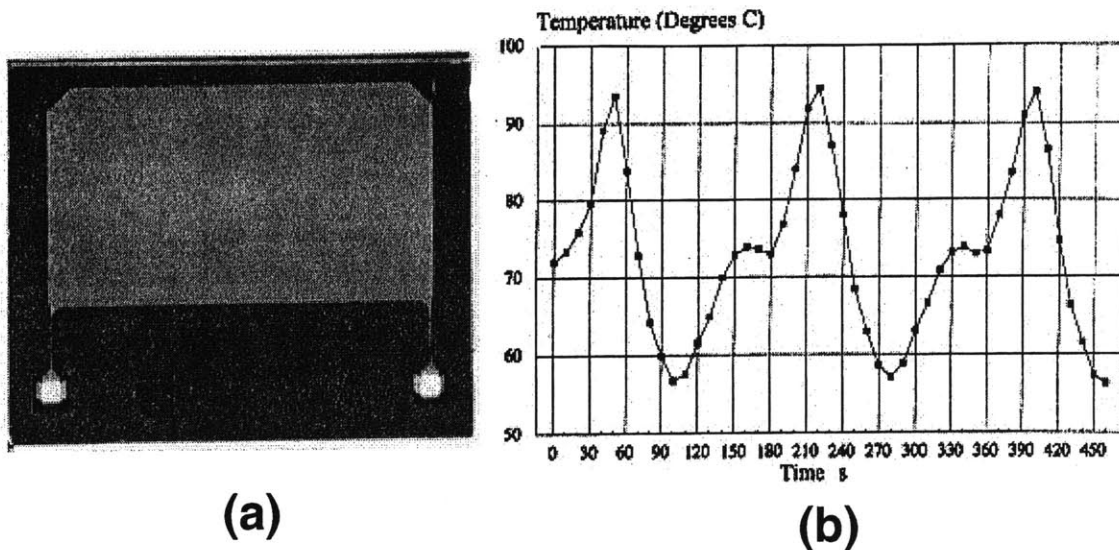
Figure 3-2: The "PCRChip": (a) the chamber; (b) temperature history for several cycles, at 3 min/cycle. From [94].

Wilding et al. tested two PCR mixes. The first consisted of 10 pg/μl (3.1×10^{-13} M) λ phage DNA, 0.3 μM each of forward and reverse primer (25 bases each defining a 500 bp target), 0.025 units/μl AmpliTaq® DNA polymerase, 50 mM KCl, 10 mM Tris-HCl (pH 8.3), 1.5 mM $MgCl_2$, 0.001% (w/v) gelatin, and 200 μM each dNTP. The second mix was identical to the first, except that the template was 10 pg/μl (9.2×10^{-15} M) Campylobacter jejuni DNA, and two different primers were used (25 bases each defining a 1.4 kb target). Thermal cycling of the λ template was as follows: an initial denature at 94°C for 1 min; followed by 35 cycles of 94°C for 15 s, 60°C for 15 s, and 72°C for 1 min; followed by a final extension of 72°C for 5 min. For the C. jejuni template, it was similar: an initial denature at 94°C for 1 min; followed by 35 cycles of 94°C for 30 s, 60°C for 30 s, 72°C for 1 min; followed by a final extension of 72°C for 5 min. Including the ramp times, total time was $\approx$3 min per cycle. Unfortunately, Wilding et al. were not able to match the yield of a
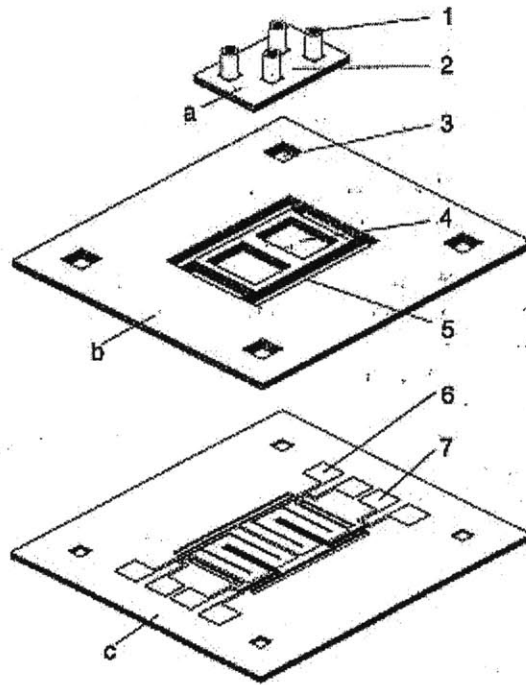
Figure 3-3: Sketch of the two-chamber PCR chip of Poser et al.: 1, inlet; 2, cover; 3, adjustment; 4, reaction chamber; 5, air chamber to provide temperature isolation; 6, thin-film heater; 7, temperature sensor; a, cover; b, topside; c, backside. From [66].

conventional PCR machine[7] in the same amount of time.

3.3.2 Poser et al.: Silicon Chamber

Poser et al. constructed a device similar to the PCRChip (see Section 3.3.1). Fig. 3-3 shows their device in its two-chamber form. They also constructed chips with one and ten chambers. Wells were etched 450 μm deep into silicon. Pyrex or silicon lids were glued on top to form 5–10 μl reaction chambers. Thin-film heaters and temperature sensors were patterned onto the opposite side of the silicon. Heating rates up to 80°C (2.5 W per chamber) and cooling rates of 40°C using a fan were

---

[7]GeneAmp™ System 9600. Applied Biosystems, formerly PE Applied Biosystems. Foster City, CA.

reported. Unfortunately, they did not find a coating for the silicon that allowed them to perform PCR successfully. They mention that polydimethylsiloxane might be a suitable coating.

3.3.3 Applied Biosystems: Silicon Chamber

Taylor et al. [14, 85] made silicon chambers similar to the PCRChip (see Section 3.3.1). They etched a 2×4 array[8] of chambers into silicon, each chamber 0.5 mm deep, 5 μl in volume, and coated with 4000 Å SiO_x for biocompatibility. Fill and vent holes for each chamber were etched on the opposite side of the silicon. A 0.5 mm thick layer of borosilicate glass was bonded on the top to seal the chambers. Heating and cooling was provided by a Peltier unit that the silicon chip rests on.

Taylor et al. [85] used a commercial PCR mix provided in the TaqMan^{TM} PCR Reagent Kit[9]. It consists of 0.2 ng/μl (1.0×10^{-16} M) human genomic DNA template, 10 mM Tris-HCl (pH 8.3), 50 mM KCl, 4.0 mM $MgCl_2$, 400 mM dUTP, 200 mM dATP, 200 mM dCTP, 200 mM dGTP, 300 nM each primer (26 base forward primer, 25 base reverse primer, defining a 297 bp target), 200 nM TaqMan^{TM} fluorescent probe, 0.01 units/μl AmpErase^{TM} uracil-N-gycosylase, and 0.10 units/μl AmpliTaq Gold^{TM} DNA polymerase. Some reagent concentrations were optimized for the silicon PCR chambers. The PCR mix contains some unusual components. dUTP is similar to dTTP in that it is a complementary base to dATP. However, it is usually found in RNA, not DNA. The TaqMan^{TM} PCR Reagent Kit mix allows reuse of the original

---

[8]In the later version tested by Chaudhari et al. [14], there is a 3×6 array of chambers, each holding 2 μl of liquid.

[9]Applied Biosytems (formerly PE Applied Biosystems). Foster City, CA.

template. AmpErase™, which is active below 55°C but above freezing, will destroy the PCR products which contain dUTP in them, but not the original template, which has dTTP instead. The PCR product can be stored and analyzed by keeping the aliquot either below freezing or above 55°C.

Taylor et al. used the following thermal schedule: an initial step of 50°C for 2 min (presumably so that AmpErase can destroy any primer-dimer or other erroneous product arising from initial assembly of the PCR mix); followed by an initial denature at 95°C for 10 minutes, which activates the AmpliTaq Gold®; then 40 cycles of 95°C for 5 s and 60°C for 10 s (annealing and extension steps are combined); and finally, the machine is held at 72°C to allow all products to reach full length. Each of the 40 cycles was 32.5 seconds, and the yield was comparable to a reaction performed on a standard Perkin-Elmer model 2400 or 9600. The reaction was 91% efficient. The Perkin-Elmer machines used the same temperature schedule, except that each of the 40 cycles was 95°C for 15 s and 60°C for 60 s, resulting in 215 s per cycle.

3.3.4 Woolley et al.: Plastic Sleeve in Silicon Heater

Woolley et al. [100] integrated a fast PCR device with rapid electrophoresis on a glass wafer (see Fig. 3-4). They etched grooves in two 1mm thick pieces of silicon and bonded them together, forming a hexagonal hole. Resistive heating elements were patterned onto the outside. The whole silicon heating assembly was epoxied onto the electrophoresis device. Polyproylene inserts were designed to insert into the hexagonal hole and hold 20 μl of PCR mix. Since the thermal mass of the
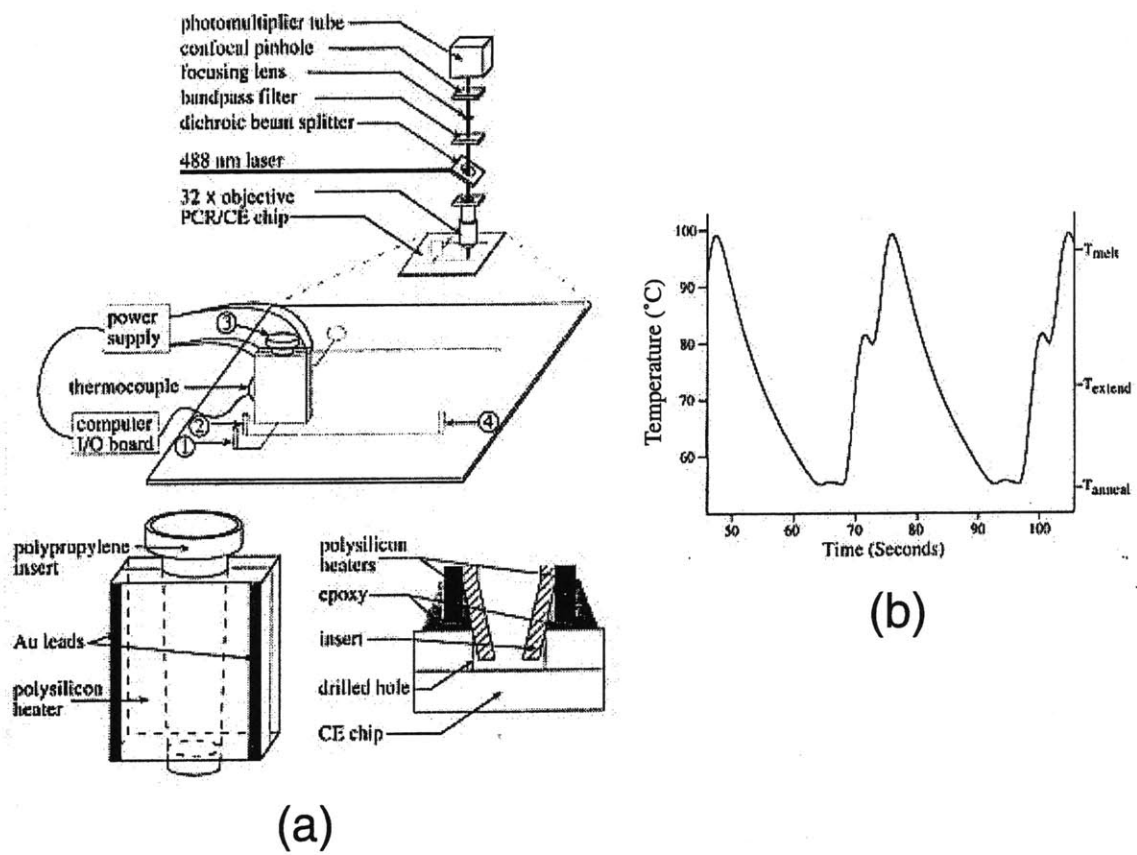
Figure 3-4: Rapid PCR integrated with electrophoresis: Woolley et al. From [100]. (a) Device schematic; (b) Temperature history sample for 15 min overall time, 30 cycles.

silicon device was small, it heated quickly and evenly at $\approx 10°C/s$. Cooling occurred passively at $\approx 2.5°C/s$.

Woolley et al. amplified both a 268 bp β-globin fragment and Salmonella DNA. In the former case, the PCR mix consisted of either 2.0×10^4 or 2.0×10^6 copies per μl $(3.3 \times 10^{-14}$ M or 3.3×10^{-12} M) of template (268 bp), 0.5 μM of each primer (target was the same as the template), 0.05 units/μl Taq, 50 mM KCl, 10 mM Tris-HCl (pH 8.3), 3 mM MgCl$_2$, 10% glycerol, and 400 μM each dNTP. The mix was identical for the Salmonella, except the template was genomic Salmonella DNA (4.6 Mb) at a concentration of 10 ng/μl (3.3×10^{-12} M), and different primers were used to define a 159 bp target.

Thermal cycling for the β-globin DNA was 30 cycles of 96°C for 2 s, 55°C for 5 s, and 72°C for 2 s. The final extension was for 30 s. The total overall time was 15 minutes. Since the template was the same as the product (268 bp), denaturing times could be kept short. The Salmonella DNA took 40 minutes total time, even though the target was only 159 bp long. It was amplified with 35 cycles of 95°C for 10 s, 56°C for 15 s, and 72°C for 20 s.

Following thermal cycling, the PCR product was injected into the detection apparatus. It was electrophoresed in a 0.75% (w/v) HEC in TAE gel containing thiazole orange fluorescent intercalating dye. A photomultiplier tube was used to detect the presence of product. No quantification was made of the yield.

Much work has been done on Woolley's original device to take it out of the laboratory and into the field. The MATCI (Miniature Analytical Thermal Cycling Instrument) [29, 59, 60] added optical windows to the silicon heater structures to im-
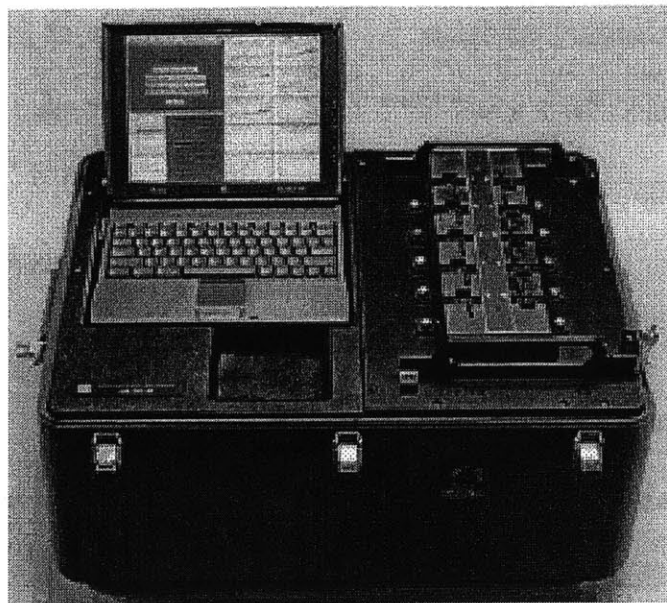
Figure 3-5: The Advanced Nucleic Acid Analyzer (ANAA): 10 rapid thermal cycling units packaged into a briefcase. From [6].

plement real-time fluorescent product detection. The thermal cycler was packaged in a briefcase with a controlling computer and all necessary hardware. While the MATCI featured a single cycler, the later ANAA (Advanced Nucleic Acid Analyzer) [5, 6] packaged 10 independently controlled units in a self-contained briefcase (see Fig. 3-5). The developers were funded by the military, and hence their PCR is of Erwinia herbicola cells, Bacillus subtilis spores, and MS2 virions, all possible biological warfare agents. Their most impressive result boasts PCR detection of bacteria in seven minutes [6]. The PCR mix in this case consists of 10 mM Tris-HCl (pH 8.3 at 25°C), 50 mM KCl, 0.4 mM each primer, 0.4 mM fluorescent TaqMan^{TM} probe, 5 mM MgCl$_2$, 0.2 mM each dNTP, 0.01 units/μl AmpliTaq® DNA polymerase, and 20 CFU/μl intact Erwinia herbicola cells[10]. For their 7 minute PCR, they used the

---

[10]CFU stands for Colony Forming Unit. One CFU is usually a single cell, though it can be a number of cells clustered near each following culturing on a Petri dish.

following thermal schedule: an initial cell lysis and denature at 96°C for 15 s, followed by cycles of 96°C for 1 s and 56°C for 1 s. Each cycle took 17 s. Product was monitored in real time, and was detected at cycle 25. The reaction was very efficient.

. These results are indeed impressive. However, they are a testimony to the detection scheme and optimization of the PCR mix and temperature schedule, rather than heating efficiency. As explained in Section 3.1.3, fluorescent detection is very sensitive. Since it can detect small amounts of product in low cycle numbers, reported efficiency is higher than if the reaction were allowed to complete more cycles. Also, although each cycle took 17 s, more than 15 s of this was transition time[11]. Heating and cooling rates for the system were 6.5°C/s and 4.3°C/s, respectively.

3.4 "Sausage Machines"

These devices are the cousins of the design presented in this work. PCR mix is pumped along a pre-heated path to perform the reaction. The cross-section of the path is small, allowing the liquid to heat and cool quickly. Since each section of the path is kept at a fixed temperature, heating depends on how fast the liquid moves and how quickly it equilibriates with the wall temperatures. The time required to heat or cool a heat block is done away with entirely. The sample or samples are put into one end of the path, and emerge from the other. Due to the small cross-section of the path, the aliquots form very elongated droplets inside the path, thus likening

---

[11]The nominal dwell time is 2 s per cycle: 1 s at 96°C and 1 s at 56°C. However, the authors measured the time lag of the aliquot temperature behind the silicon heater temperature, and noted it was significant relative to the dwell times.
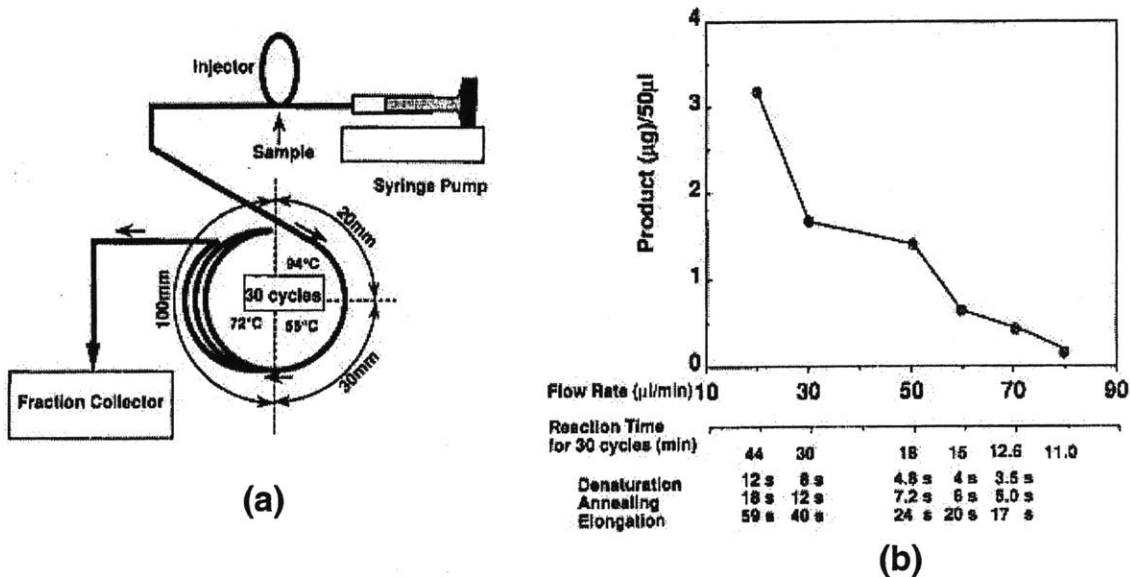
Figure 3-6: Nakano's flow-in-capillary PCR reactor: (a) device schematic; (b) results. From [57].

them to sausages and the apparatuses to "sausage machines."

3.4.1   Nakano et al.: Flow-in-Capillary PCR

Nakano et al. [57] created the device shown in Fig. 3-6. A 0.5 mm I.D., 1.5 mm O.D., 5 m long Teflon tube is looped thirty times through three different temperature oil baths, corresponding to thirty cycles of the three PCR steps. The length of tube in each loop in a given oil bath is proportional to the time that the particular step is in a cycle. This fixed the ratio of denature : anneal : extension times at 2:3:10. 50 μl aliquots of PCR mix are pushed through the tubing at a constant rate using a syringe pump. Each aliquot is 250 mm long, and different portions of the aliquot are in different temperature zones simultaneously. 5 μl air gaps are used to separate multiple aliquots from each other and the buffer[12] that fills the rest of the tube.

---

[12]10 mM Tris-HCl (pH 8.9), 1.5 mM MgCl$_2$, and 80 mM KCl.

The following PCR mix was used: 0.2 ng/μl (5.2 × 10^{-11} M) plasmid pNF-1 DNA

(5.8 kb), 2.8×10^{-7} M each primer (both 24 bases long defining a 1.0 kb target), 10 mM

Tris-HCl (pH 8.9), 1.5 mM MgCl$_2$, 80 mM KCl, 0.5 mg/ml bovine serum albumin,

0.1% sodium cholate, 0.1% Triton X-100, 0.2 mM each dNTP, and an unspecified

amount of Tth™ DNA Polymerase[13]. The denaturing, annealing, and extension

temperatures were 94°C, 55°C, and 72°C, respectively. The syringe pump rate was

varied to produce total PCR times from 11 to 44 minutes for 30 cycles. Yield was

determined by chromatography, and is shown in Fig. 3-6 (b).

3.4.2 Kopp et al.: Continuous-Flow PCR on a Chip

With the recent interest in performing electrophoresis on glass wafers using litho-

graphic technology developed for silicon chips[14], it is no wonder that the technology

has also been adapted to PCR. Kopp et al. [42] produced a PCR machine simi-

lar in concept to that of Nakano et al. (see Section 3.4.1). However, instead of the

aliquot flowing through a Teflon tube, it flows through a serpentine channel etched

into Corning 0211 glass (see Fig. 3-7). The channel is 40 μm deep, 90 μm wide, and

2.2 m long. It is treated with dichlorodimethylsilane to present adsorption of the

DNA polymerase, and covered with a glass plate. Both the base and cover plate are

0.55 mm thick. Three heat zones are established by three copper blocks that the

glass rests on, each containing a 5 W cartridge heater. The denaturing, annealing,

and extension temperatures are 95°C, 60°C, and 77°C, respectively. The geometry

---

[13]Tth™ is known to be slower than Taq, but is better for some applications. See [4] for details.
[14]For example, [77].
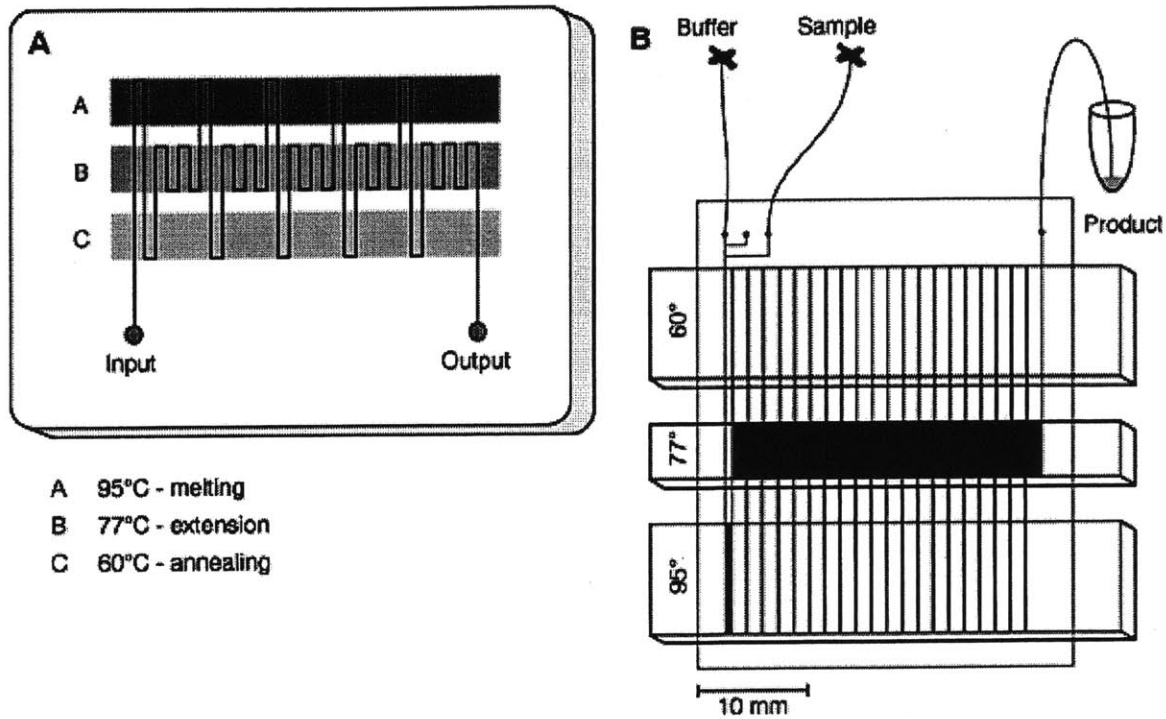
Figure 3-7: Continuous-Flow PCR on a Chip, by Kopp et al.: (a) schematic; (b) device layout. From [42].

fixes the ratio of denature : anneal : extension times at 4:4:9 and the total number of cycles at 20. The aliquot is $\approx 10~\mu l$ in volume, so it is ≈ 2.8 m long. This is longer than the channel, so different parts of the sample see different temperatures simultaneously. The rest of the channel is filled with buffer. A syringe pump is used to pump the aliquot through the channel—a pressure of 1 bar results in a total time of 4 min for 20 cycles.

Kopp et al. used the following PCR mix: 10^7 copies/μl (1.7×10^{-11} M) template (a 1 kb portion of the gyrA gene of *Neisseria gonorrhoeae*), 1 μM of each primer (18 and 19 bases long defining a 176 bp target), 0.25 units/μl Taq, 10 mM Tricine (pH 8.3), 0.01% (w/v) Tween 20, 50 mM KCl, 0.2 mM each dNTP, 1.5 mM MgCl$_2$, and 1.4 μM polyvinylpyrrolidone. The pressure in the syringe pump was varied to produce
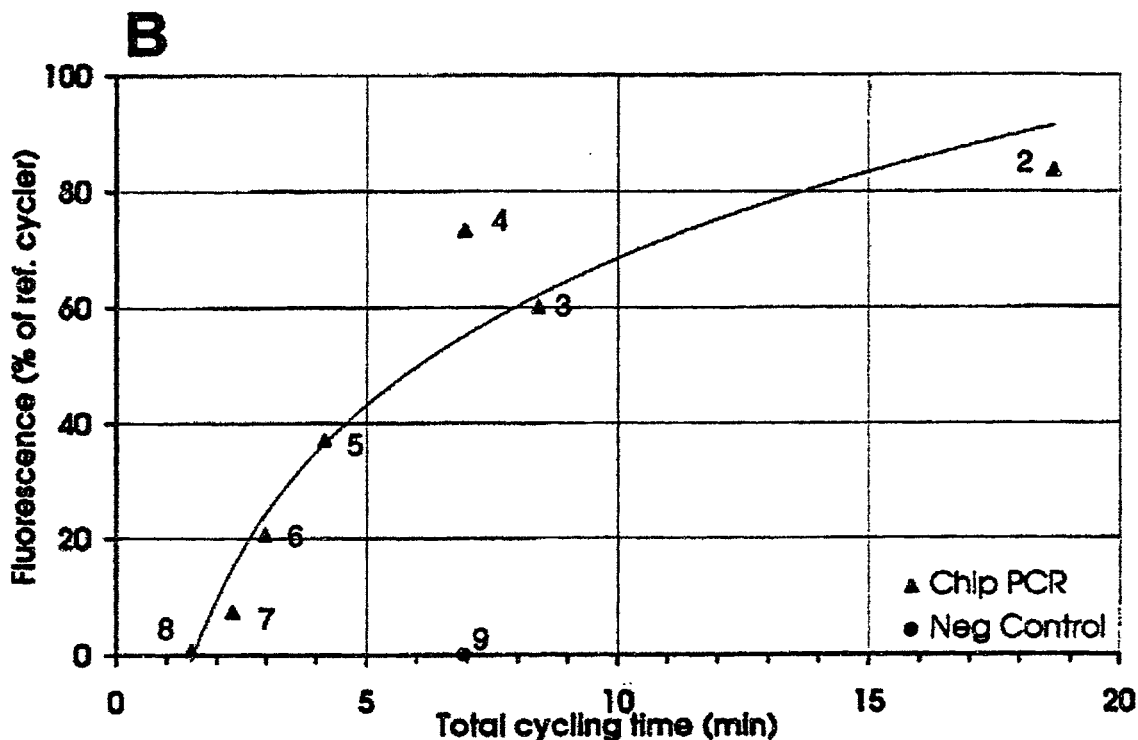
Figure 3-8: Yields for the continuous-flow PCR on a chip device by Kopp et al. From [42].

times from 2.4 to 18.7 minutes for the 20 cycles. Results are shown in Fig. 3-8.

3.5 Infrared-Mediated PCR

Oda et al. [61] investigated heating via a lamp (see Fig. 3-9). 28 μl containers contained 5–15 μl PCR mix covered with mineral oil. They were manufactured from 500μm × 5.0 mm borosilicate glass stock cut to 13 mm lengths. One end was sealed, and the interior was coated with[15] BTMSTFA to prevent adsorption of Taq onto the sidewalls. Two identical containers were placed side by side, one with the PCR mix, the other containing buffer with a thermocouple immersed in it to measure aliquot

---

[15]BTMSTFA is bis(trimethylsilyl)trifluoroacetamide.

66
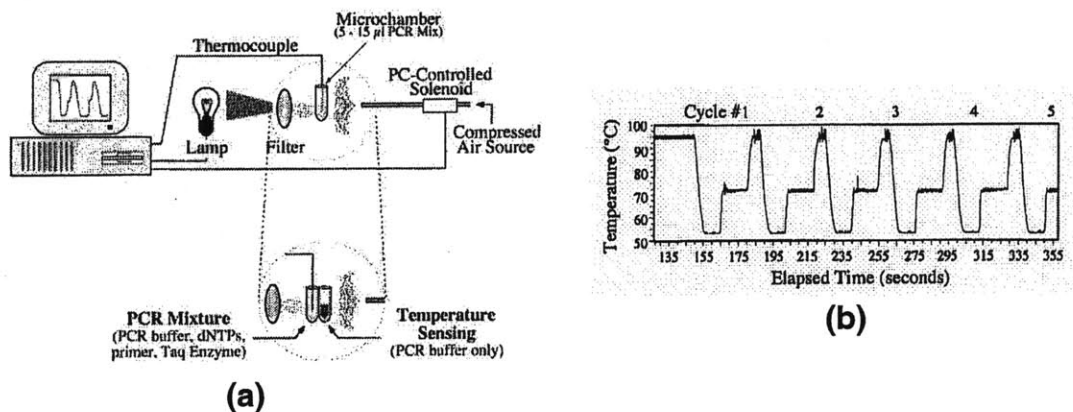
Figure 3-9: The light-heated device of Oda et al.: (a) device schematic; (b) sample temperature history. From [61].

temperature[16]. 10°C/s heating was provided by a tungsten lamp. 20°C/s cooling was accomplished by shooting compressed room temperature air at the aliquots. The system was carefully arranged to provide identical heating and cooling to the container with the PCR mix and the container with the thermocouple.

Oda et al. used the following PCR mix: 10 mM Tris-HCl (pH 8.3), 50 mM KCl, 1.5 mM $MgCl_2$, 20 μM each dNTP, 1 ng/μl each primer (0.16 μM forward and 0.17 μM reverse, defining a 216 bp target), 0.13 units/μl Taq, 0.33 ng/μl template (fragment of ah T-cell receptor β chain), and TaqStart® antibody (see Section 3.1.2). The thermal schedule was an initial 94°C, 5 min denature; followed by 30 cycles of 94°C for 30 s, 54°C for 30 s, and 72°C for 60 s; and finally an extension of 72°C for 5 min. This schedule resulted in roughly 30% yield of a commercial PCR machine[17] running the same thermal schedule. Oda et al. got the same yield but more nonspecific product using the following schedule: an initial 94°C, 150 s denature; followed by 30 cycles of 94°C for 8 s, 54°C for 8 s, and 72°C for 15 s; and finally an extension of 72°C for 150

---

[16]The authors found that the thermocouple interferes with the PCR reaction.

[17]GeneAmp 9600. Applied Biosystems (formerly PE Applied Biosystems), Foster City, CA.

s. Each of the 30 cycles took about 38 s.

3.6   Capillary Tube Resistive Thermal Cycling

Friedman and Meldrum [23] developed a PCR machine in which a capillary holding the PCR mix is heated directly via a resistive heater. They used 55 mm long, 0.84 mm O.D., 0.39 mm I.D. borosilicate glass capillaries with 5 μl internal volumes. The ends were sealed with rubber bands held in place by a custom manufactured polystyrene holder. Each capillary was coated with a 3000 Å layer of indium-tin oxide, which was used as a resistive heater. Cooling was provided by a fan. Temperature was monitored using a thermocouple.

The PCR mix used is as follows: 51 mM Tris-HCl (pH 8.3), 0.55 mg/ml bovine serum albumin, 2 mM MgCl$_2$, 0.5% sucrose, 1 mM cresol red, 4 ng/μl each primer (define a 777 bp target), 160 μM each dNTP, 0.05 units/μl Taq, and 4 ng/μl (2.0×10^{-15} M) human genomic DNA (3×10^9 bp). They used the following thermal schedule: an initial denature of 94°C for 20 s; followed by 35 cycles of 93°C for 1 s, 55°C for 1 s, and 72°C for 20 s; with a final extension of 72°C for 30 s. Although maximum heating and cooling rates of 44°C/s and 22°C/s, respectively, were mentioned, the actual PCR was performed with heating at only 5°C/s. This resulted in a total time of about 20 min, which was roughly the same as their control: an Idaho Technology air cycler running the same heat schedule. However, their yield was much less than for an air cycler.

Chapter 4

Machine Design

4.1 Introduction

This chapter describes the design of a novel capillary polymerase chain reaction machine. The primary objective was to prototype a machine with the fastest possible thermal cycling. PCR is a very commonly performed reaction, so decreasing time will increase productivity. Although the concept can be multiplexed, it is intended for the researcher analyzing a small number of samples: the machine is optimized for reaction speed rather than throughput. It is not designed to compete against machines running hundreds of samples simultaneously.

A secondary objective was to use small reaction volumes. Not only does this save on expensive PCR reagents, such as DNA polymerase and fluorescent probes, but it can also optimize upstream procedures . For example, if cell cultures are required prior to PCR, fewer cells have to be grown, decreasing culture time.

The basic concept is shown in Fig. 4-1. A $1\mu l$ drop, or "plug", of PCR sample mix
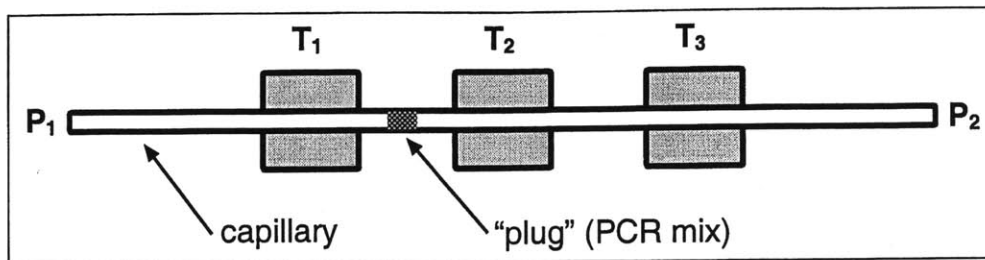
Figure 4-1: Basic capillary PCR machine concept.
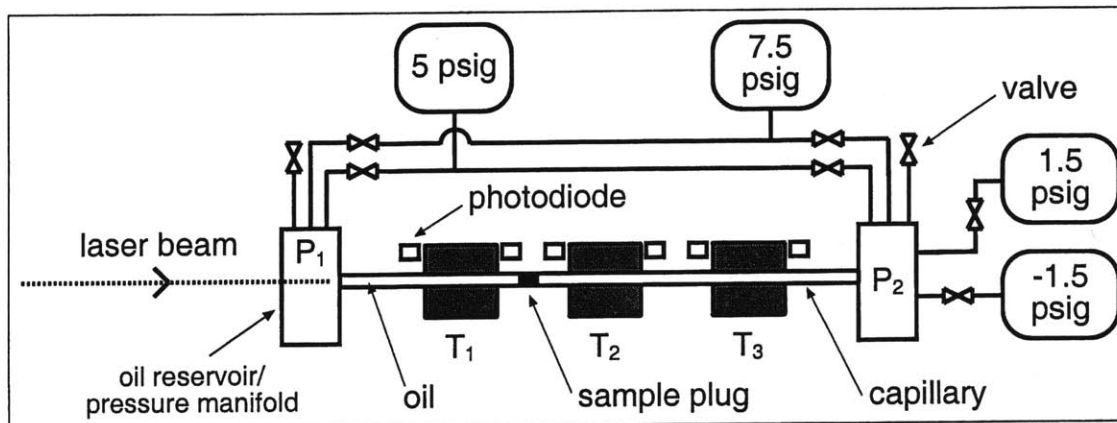
Figure 4-2: Schematic of the machine.

is placed inside of an oil-filled capillary. PCR is performed by manipulating pressures P_1 and P_2 to move the plug to heat zones at the three PCR step temperatures T_1, T_2, and T_3, established by heat blocks. Since there is one heat block for each PCR step, there is no time wasted changing a heat block temperature. The plug volume is small, and heats quickly. This satisfies the need for both high speed and low reaction volume.

4.2 Overview

Fig. 4-2 shows a schematic of the machine. To perform PCR, a 1 μl drop, or "plug", of PCR mix is loaded into a 9" long, 1 mm I.D., 1/16" O.D. Teflon tube filled with mineral oil. Each end of this tube is connected to a oil reservoir/pressure manifold
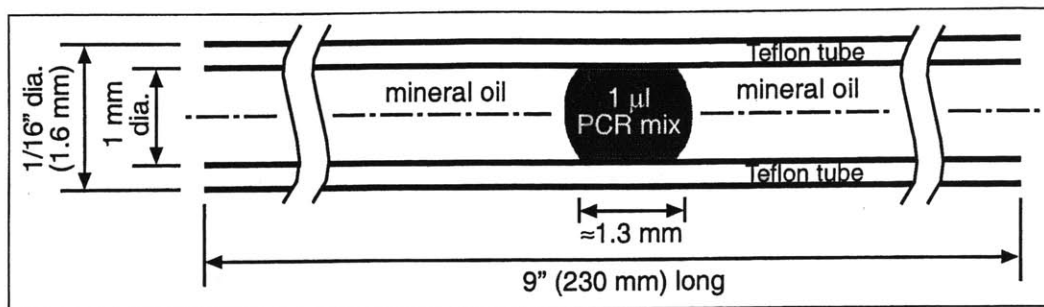
Figure 4-3: Geometry of the plug and capillary.

machined out of clear acrylic. The reservoirs are at pressures P_1 and P_2, as shown. These pressures are established by a number of different pressure air sources and computer-controlled valves. They move the sample plug between heat zones at temperatures T_1, T_2 and T_3 in an intermittent, reciprocating motion to perform PCR. A laser beam directed along the capillary scatters upon reaching the plug surface. This scatter is picked up by a series of photodiodes, and their signals are reported to the computer to locate the plug. Subsequent sections explain each of the device subsystems in greater detail.

4.3   Plug and Capillary

The arrangment of the plug and capillary is shown in Fig. 4-3. The capillary is filled with mineral oil[1]. This serves several purposes. First, it prevents the sample plug from evaporating: it is commonly used for this exact purpose in conventional PCR machines, which is why I selected it. Second, it allows the laser to waveguide down the capillary (see Section 4.6). Third, it simplifies plug motion control: compressibility and thermal expansion are negligible, and its high viscosity makes the capillary fluid

---

[1]Product #2705-01. J. T. Baker, a division of Mallinckrodt Baker, Inc. Phillipsburg, NJ.

motion dynamics overdamped[2].

The capillary is a 9" (230 mm) length of 1mm I.D., 1/16" (1.6 mm) O.D. PTFE tubing[3]. The tubing was straightened using a heat gun, then cut to length. Teflon is known to be chemically inert. It does not interfere with PCR, as proven by Nakano et al. (see Sec. 3.4.1). In fact, they found that sequential reactions could be run in the same length of Teflon tubing without cross contamination, as long as buffer was pumped through the tube between successive runs. Eventually yield decreased, presumably due to accumulation of residue, but was restored following a methanol wash of the tube. I used a new tube for every run to avoid this problem.

Teflon was also chosen because it is hydrophobic. This prevented the PCR mix from wetting the capillary. If it wetted the capillary, the plug would lose shape and be difficult to move precisely.

The tube I.D. was chosen as 1 mm as a reasonable compromise. A smaller I.D. results in faster heating, but since the plug shape is constrained (see below), plug volume can get too small to analyze. Approximating the tube inside of a heat block as having a time invariant inner wall temperature, the plug heating time is roughly the time required to heat a 1 mm diameter cylinder of water (which has similar thermal properties to the PCR mix, since the latter is an aqueous solution) solely by radial conduction via a constant temperature source at the outer radius. The dominant time constant for this reaction[4] is 0.173 (r_o^2/α_w), where[5] r_o is the cylinder radius and

---

[2]Of course, the air in the pneumatic system is compressible. This issue is dealt with separately in Chapter 9.

[3]PTFE is polytetrafluoroethylene, a form of Teflon. Part # 3132. Alltech Associates, Inc. Deerfield, IL.

[4]See, for example, [12, p. 199].

[5]Subscript comes from the fact that most of the inside of the capillary is filled with *oil*; do not

α_w is the thermal diffusivity of water. Since $r_o = 5.0 \times 10^{-4}$ m and $\alpha_w = 1.6 \times 10^{-7}$ m^2/s at ordinary PCR temperatures (see Appendix A), the time constant is 0.27 s, which is suitably fast. Heating rates are covered in much greater detail in Chapter 7.

Since the plug/oil interfacial tension is low, the possibility of the plug breakup is a serious concern. The Rayleigh instability[6] can cause the plug to break into pieces, even at low velocities, unless its aspect ratio is $< \pi$. A volume of 1 μl was chosen. Approximating the plug as a cylinder, the aspect ratio is safely 1.3 at rest. In addition, a 1 μl plug yielded enough product to be quantified using standard agarose electrophoresis.

4.4 Heating System

The hardware in all three heat blocks is identical, and is shown in Fig. 4-4. Each 0.5" (13 mm) heat zone is established by a 1/2" (13 mm) aluminum cube warmed with a cartridge heater. The cubes were cut from 1/2" (13 mm) $\times$ 1/2" (13 mm) rod. Aluminum was chosen because it has high thermal conductivity (provides even heating), is easy to machine, and is cheap. Three holes are drilled into each block to fit the capillary, heater, and thermocouple. The 10 W cartridge heater[7] is a 1/8" diameter, 1" long cylinder inserted in the block parallel to the capillary to provide even heating. The K-type thermocouple[8] is 0.010" in diameter. Both are connected to

---

confuse with *outer* radius.

[6]The Rayleigh instability, as well as other modes of plug breakup, are addressed in detail in Chapter 8.

[7]Part # CSS-01110/120 V. Omega Engineering Inc. Stamford, CT.

[8]Part # 5SC-TT-K-30-72. Omega Engineering Inc. Stamford, CT.
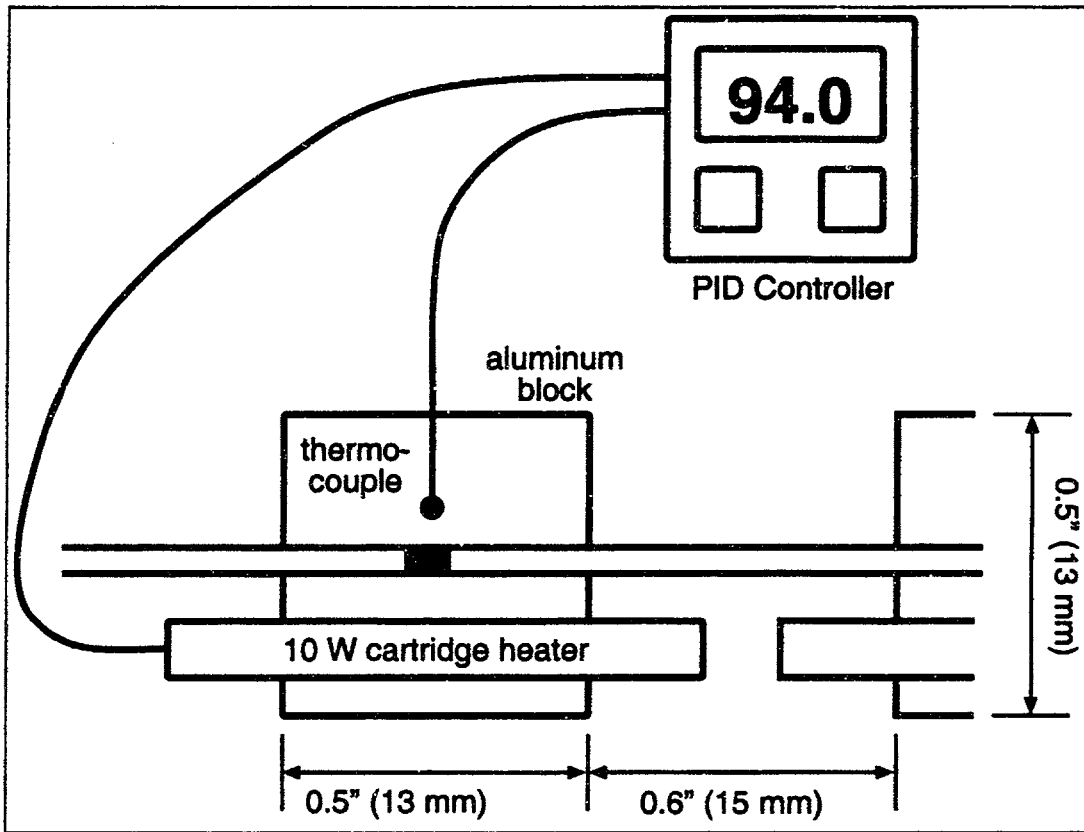
Figure 4-4: The heating system for a single heat block.

a commercial PID controller[9] with solid state relays[10] that determines the percentage of time that the heater is switched on.

The thermocouple and heater are glued into the block using silver conductive epoxy[11]. It was also used to affix the blocks to a base made out of thermally insulative (0.29 W/(m·K)) G-10 composite. There was 0.6" (15 mm) space between blocks to allow room for the photodiodes, as well as to prevent the blocks from influencing each other's temperatures.

4.5 Pneumatic Actuators

A pneumatic diagram of the pressurized air system used to move the plug is shown in Fig. 4-5. Each end of the capillary is connected to an oil reservoir/pressure manifold via an HPLC fitting[12]. The reservoirs are custom machined out of clear acrylic. Each holds ∼ 1 ml mineral oil, and is connected via 1/8" ID, 1/4" OD plastic tubing to solenoid valves[13]. Every valve can open to fill the reservoir with a different pressure air.

Both reservoirs can be set to ≈ 5 psig, ≈ 8.5 psig, or atmospheric pressure. The 5 psig pressure is the minimum pressure required during PCR to avoid plug degassing (see Section 4.5.1). The 8.5 psig pressure[14] is used at one reservoir along with 5 psig at the other to move the plug back and forth. The pressures were chosen somewhat

---

[9]Part # CN76000. Omega Engineering Inc. Stamford, CT.

[10]Part # SSR240DC10. Omega Engineering Inc. Stamford, CT.

[11]Tra-Duct 2902. Tra-Con. Medford, MA. Operating temperature range: -60°C to 110°C.

[12]HPLC stands for High Pressure Liquid Chromatography. Part # TC-2. Amersham Pharmacia Biotech, Inc. Piscataway, NJ.

[13]Part #s A141010-02 and C141014-02. Kip Incorporated. Farmington, CT.

[14]Actually, it drops to ≈ 7.5 psig during plug motion.
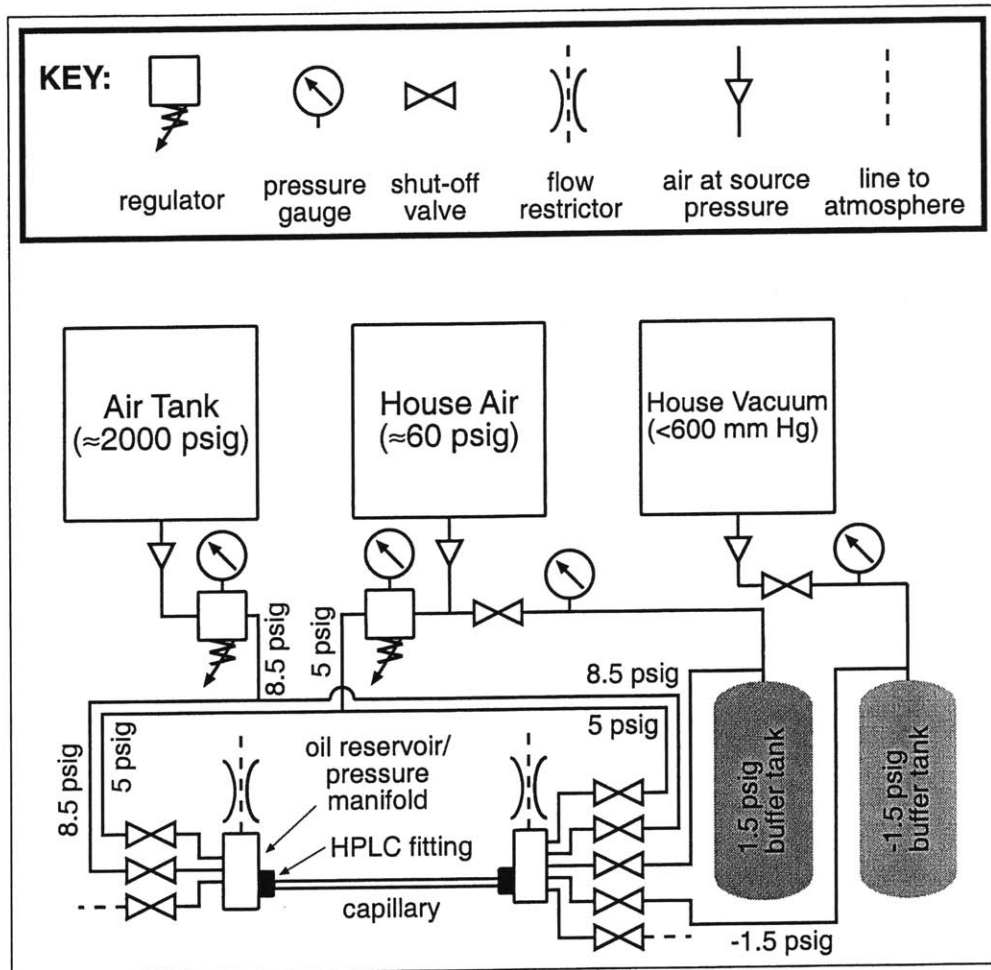
Figure 4-5: Pneumatic diagram of the actuation system.

arbitrarily, but result in reasonably low transition times ($\sim$ 1 second to move from block to block) and avoid plug breakup that results at higher speeds (see Chapter 8). Atmospheric pressure is provided so that the capillary can be inserted and removed without spraying oil out of the reservoirs. The tubing from the two 5 psig valves to the left and right reservoirs were identical in length in an effort to make their fluid resistances the same. This was also true for the tubing from the 8.5 psig and atmospheric air valves.

The right (farthest from the laser) oil reservoir also has connections to 1.5 psig and -1.5 psig air. These pressures are used to load the capillary with oil and a sample plug. The left end of the capillary is not connected to the left reservoir during these operations.

Flow restrictors connect each oil reservoir to atmosphere. The reservoir pressures cannot be lowered without them. The flow resistors are simply syringe filters. A variety of different mesh sizes were tested, and a 0.2 μm mesh[15] provided the right amount of fluid resistance: enough to allow a high pressure to bleed off when the input pressure was lowered, but not so much that the reservoir would drop to atmospheric pressure.

The building supplies both pressurized air at $\approx$ 60 psi and vacuum at < 600 mm Hg. A compressed air tank at $\approx$ 2000 psi (when freshly charged) is also used as an air source. House vacuum is routed through a shutoff valve into a 28.7 liter buffer tank. Vacuum is applied to the tank until it reaches -1.5 psig, and then the shutoff valve is closed. An indentically sized buffer tank at 1.5 psig is filled in the same way

---

[15]Acrodisc® 0.2 μm filter. Product # 4496. Pall Gelman Laboratory. Ann Arbor, MI.

using house air. House air is also routed through a regulator[16] to provide 5 psig air. The 2000 psi compressed air tank was regulated down[16] to supply 8.5 psig air. Two distinct air sources are used because it was thought that downregulating the house air to two different pressures via two closely spaced regulators might be a problem. It is not, but the arrangement was kept.

4.5.1   Preventing Sample Degassing

After mixing, the sample plug is stored at 4°C. During PCR, its temperature can reach[17] 94°C. Solubility of air in water decreases with increasing temperature, but increases with increasing pressure. If the pressure is atmospheric during both mixing and PCR, air will leave the sample plug and form bubbles in the mineral oil. This was observed experimentally. Air bubbles scatter laser light, confusing the sensor system.

To overcome this problem, I pressurized the system at 5 psi during PCR, as noted above. Let P_{min} be the minimum pressure required to keep the solubility of air in the sample plug the same as it is when it is at 4°C and atmospheric pressure. The solubility and vapor pressure information required to calculate P_{min} is shown in Table 4.1. Note that the s values listed in Table 4.1 are expressed in such a way that they are proportional to molarity.

We want to find P_{min} so that $s(94°C, P_{min})$ is the same as the value of $s(4°C, 1$ atm) listed in the table. The value of s at 94°C in the table is for a partial pressure

---

[16]Part # 2051021-000. 0–15 psig outlet pressure. B. O. C. Gases. Murray Hill, NJ.
[17]Depending on what the denaturing temperature is set at.

78

Temp.	s	Vapor pressure
4.0°C	2.632×10^{-2}	0.81984 kPa
94°C	1.110×10^{-2}	85.774 kPa

Table 4.1: Degassing calculation information. s is the volume of air (in ml) measured at 0°C and 1 atm dissolved in 1 ml of water when the total pressure (partial pressure of air + water vapor pressure) is 1 atm; values interpolated from [20, p 10-3]. Vapor pressure is the vapor pressure of water at the given temperature; values interpolated from [26, p. 638].

of

$$1 \text{ atm - } 94° \text{ C vapor pressure} = 101.35 \text{ kPa - } 85.744 \text{ kPa} = 15.606 \text{ kPa}$$

Henry's law[18] states that the solubility of gas in a liquid (expressed in molarity) is proportional to the partial pressure of that gas over the solution. Therefore,

$$(1.110 \times 10^{-2}) \left(\frac{P_{\min} - 85.744 \text{ kPa}}{15.606 \text{ kPa}} \right) = 2.632 \times 10^{-2} \tag{4.1}$$

Therefore, $P_{\min} = 122.7$ kPa (absolute) = 3.1 psig. The minimum capillary pressure was set to 5 psig to provide some margin of error.

It was experimentally observed that the mineral oil did not degas significantly in the absence of a sample plug. No air bubbles formed.

4.5.2 What Not Use a Syringe Pump?

At first glance, it seems simpler to use a syringe pump to move the plug. The assumption is that the system could run open loop, eliminating the pneumatic and

---

[18]See, for example, [11, p. 466].

sensor systems entirely. Programming motion would be trivial. Unfortunately, a sensor system is required due to the fact that the plug drifts inside of the capillary in the absence of bulk oil flow.

There are several drawbacks to using a syringe pump. When it aspirates, it creates a vacuum in the capillary which will lead to degassing. The air bubbles will interfere with the sensor system. If one becomes large enough to span the cross-section of the tube, the plug motion will be subject to a stiction effect due to the compressibility of air, and the fact that the contact angles in a stationary bubble will vary to resist motion up until the point when it is forced into motion. These effects were observed experimentally when I tried using only the ± 1.5 psig pressures to move the plug for 30 cycle PCR. Of course, degassing can be eliminated by pressurizing the system— but this would bring back the pneumatic system, albeit in simpler form. The syringe must be carefully loaded to avoid introducing air bubbles, independent of any that may arise from degassing. This is not a problem with a pneumatic system, since the surface of the oil in the reservoirs contacts the air. Syringe pumps are also more expensive. The payoff is in much greater precision, which is unimportant for this application. Due to plug drift, the current capillary PCR design requires a separate actuator for every plug. Therefore, the extra cost of using syringe pumps can be a significant factor if the system is multiplexed.
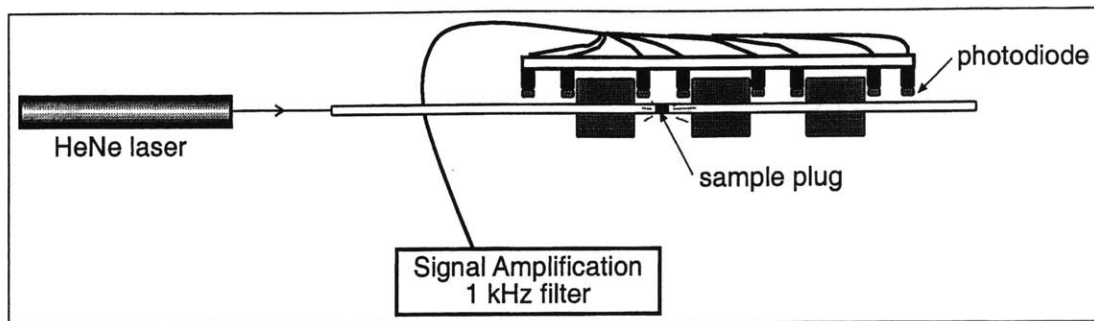
Figure 4-6: Device sensor system.

4.6 Sensor System

The control program must know *where* the plug is to know *how* to move it. Plug

location is determined via the sensor system shown in Fig. 4-6. A 20 mW HeNe laser

(632.8 nm wavelength) is directed through the clear acrylic oil reservoir/pressure

manifold into the left end of the capillary. Since the index of refraction of mineral oil

(n = 1.47. [1, p. 1173]) is higher than that of PTFE (n = 1.376. [82, p. V/40]), there

is total internal reflection as long as the angle of the laser is within

$$90° - \sin^{-1}\left(\frac{1.376}{1.47}\right) = 20°$$

of parallel to the tube wall[19]. The laser waveguides down the capillary, so the capillary

does not have to be rigorously straight. When the beam reaches the plug, it is

scattered by the curved plug/oil interface. The scatter is stronger on the right than

on the left of the plug because the laser travels from left to right.

This scatter is detected by a series of 8 photodiodes[20] which have good sensitivity

---

[19]For an explanation of total internal reflection see, for example, [27, p. 751].

[20]Part # S2386-18K. Hammamatsu Corp. Bridgewater, NJ. 0.43 A/W sensitivity at 632.8 nm
wavelength. Operating temperature: -40°C to 100°C.

to the laser light and that can withstand PCR temperatures. There are 2 photodiodes for each block, one on each side. There are an additional 2 photodiodes on the far left and far right of the heat blocks that serve as limit switches. The photodiode signals are amplified and filtered[21] before being reported to the computer.

4.7 Software

The computer[22] receives the amplified, filtered photodiode signals via an A/D card[23]. It uses these signals to determine the location of the plug. The computer commands the pneumatic system through a digital I/O card[24] that activates solid state relays[25] which switch voltage from a 28 volt DC power supply[26]. Voltage divider circuits were used to bring the voltage down to the 12 V required by the solenoid valves.

I wrote the controlling software program HPCR in C++ [27]. The user can control the pressures either manually or using a batch file. The manual option is used in conjunction with the ±1.5 psig pressures in the right reservoir to load oil and a sample plug into a capillary. The actual thermal cycling is performed using parameters specified in the batch file.

After being amplified by an inverting op-amp circuit, the photodiode signals range from roughly −4 to 0 volts. The stronger the signal, the more negative the voltage.

---

[21]Low pass filter, 1 kHz cutoff.
[22]ProLinea 4/33 (an old 80486 PC clone). Compaq Computer Corporation. Houston, TX.
[23]Part # CIO-DAS 801. Computer Boards, Inc. Mansfield, MA.
[24]Part # CIO-DIO 24. Computer Boards, Inc. Mansfield, MA.
[25](# DC05-C. Omega Engineering Engineering Inc. Stamford, CT.) and (# SSR-ODC-05. Computer Boards, Inc. Mansfield, MA.). The two parts are practically identical.
[26]Model LCS-A-28. Lambda Electronics Corp. Melville, NY. An archaic unit rescued from salvage.
[27]Turbo C++ 3.0. Part # 14MN-CPP01-30. Borland International. Scotts Valley, CA.

The range varies somewhat between individual photodiodes, since their exact placement is not precise. HPCR includes a routine to normalize the photodiode ranges. After the user manually loads a sample plug into the left capillary end, he/she connects that end to the left oil reservoir. At this point, both ends are connected to reservoirs. The user specifies a batch file. The left reservoir is pressurized to 8.5 psig, and the right to 5 psig. The plug moves to the right until the right limit switch photodiode voltage is less than[28] the value of LIMITTHRESH in the batch file. The plug is now considered to be close to the right limit switch. The pressures are interchanged, and the plug moves to the left until it the left limit switch voltage is less than LIMITTHRESH. Finally, the program opens both reservoirs to atmospheric pressure, halting the plug. During the motion, the program collects signals from all of the photodiodes. Based on the maximum and minimum voltages, it assigns each photodiode values a and b, such that the range of

$$\text{normalized photodiode signal} = b \times (\text{raw photodiode signal} + a) \qquad (4.2)$$

is the range specified by NORM_LIMITS in the batch file. NORM_LIMITS is the same for all photodiodes. The values of a and b are read into the batch file, and are used to normalize all photodiode signals whenever that batch file controls PCR.

The following terminology will be used in describing the control (see Fig. 4-7): when the reaction has completed one step (denaturing, annealing, or extension) and goes to the next, it moves from the *departure* heat block to the *destination* heat

---

[28]Recall the voltages are all negative.
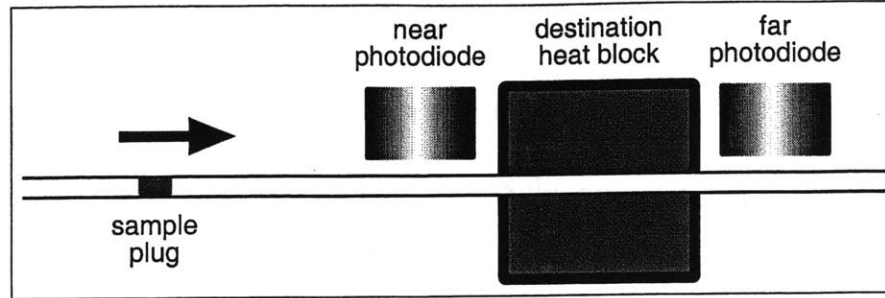
Figure 4-7: Illustration of near and far photodiodes.

block. Each heat block has two photodiodes associated with it, one placed on either side. As the plug approaches the destination block, the destination block photodiode closest to the plug is the *near* photodiode, and the one farthest from the plug is the *far* photodiode. There are also the *left* and *right* photodiodes corresponding to a particular block. This distinction is important because the laser comes in from the left side, so the scatter is stronger on the right side of the plug. However, the plug can approach a block from either the left or right side. PD_{near}, PD_{far}, PD_{left} and PD_{right} refer to the normalized (see above) near, far, left and right photodiode signals, respectively. If the plug arrives from the left, $PD_{left} = PD_{near}$ and $PD_{right} = PD_{far}$; if the plug arrives from the right, $PD_{right} = PD_{near}$ and $PD_{left} = PD_{far}$.

To perform PCR, the user loads oil and the plug into the capillary from the left end and then hooks that end up to the left reservoir, as in the normalization routine. Then, a batch file is specified which contains the cycling schedule as well as control parameters. A sample cycling schedule is shown in Fig. 4-8. The heat blocks from left to right are designated the denaturing, extension, and annealing blocks. The schedule in Fig 4-8 states that the plug moves to the right (since it is loaded in the left end) into the denature block, where it sits for 30 seconds. This is followed by 29 cycles

```
START
CYCLES    1
DENATURE  30.0
CYCLES    29
ANNEAL    5.0
EXTEND    30.0
DENATURE  5.0
CYCLES    1
ANNEAL    5.0
EXTEND    60.0
```

Figure 4-8: Sample cycling schedule in user-specified batch file.

of annealing for 5 seconds, extension for 30 seconds, and denaturation for 5 seconds. Finally, there is a 5 second annealing followed by a 60 second extension. The user uses this format to specify an arbitrary schedule of moving the plug between and waiting inside different heat blocks. HPCR starts the run by pressurizing both reservoirs to 5 psig. The program is then executed. To move the plug, 8.5 psig is applied to the reservoir that the plug moves away from.

In addition to the cycling schedule, the batch file also contains the log file name (user chosen), the temperatures and pressures used (entered by the user), and the parameters listed in Table 4.2. a and b are established using the normalization routine. NORM_LIMITS and LIMITTHRESH are chosen as the values shown in the table from the typical photodiode signal range. The rest of the parameters must be experimentally determined for a particular set of actuation pressures. The plug is positioned using simple bang-bang control. At the beginning of a move between blocks, the program knows whether the destination block is to the right or left of the departure block[29]. It starts the plug moving in that direction. Once PD_{near} < LIMITTHRESH, the progam

---

[29]It is known that the plug starts left of all of the heat blocks.

Parameter	Typical	Meaning
a	0.5	Normalizing constant, in volts. Normalized photodiode signal is (actual signal + a) × b. Different values for every photodiode.
b	1.0	Normalizing constant, in volts. Normalized photodiode signal is (actual signal + a) × b. Different values for every photodiode.
ERRORBAND (left)	0.35	If $(PD_{right} - PD_{left})$, in volts, is greater than this value, the plug is considered to be too far left of the center of the block. Is different for each block.
ERRORBAND (right)	1.0	If $(PD_{left} - PD_{right})$, in volts, is greater than this value, the plug is considered to be too far right of the center of the block. Is different for each block.
LIMITTHRESH	−2.0	Maximum limit switch photodiode signal, in volts, for the plug to be considered to be at that photodiode.
MAX_TRANSIT_TIME	3.0	Maximum amount of time, in seconds, that the plug can take travelling from block to block.
MAXDIFF	0.35	If the plug is moving toward the destination block and it is confirmed to be near via THRESHOLD, then if $|PD_{left} - PD_{right}|$ (in volts) is less than this value, the plug is considered to have arrived at the destination block. Different values for travel from each block to each other block.
MIDPOINT	0.2	The value of $(PD_{left} - PD_{right})$, in volts, at which the plug is considered to be in the middle of the block. Is different for each block.
NORM_LIMITS	−3.0, 0.0	These two voltage values specify how a and b should be chosen for each photodiode—after normalizing, the values for each photodiode fall in this range of values.
THRESHOLD	−1.5	The maximum value of PD_{near}, in volts, in which the plug is considered to be near the destination block. Different values for travel from each block to every other block.

Table 4.2: Variables specified in the user-written batch file. The "Typical" column lists typical values used for 5 psig and 8.5 psig reservoir pressures. Note that all signal voltages are negative.

checks to see if $|PD_{left} - PD_{right}| <$ MAXDIFF. When this condition is satisfied, the plug is considered to be inside of the destination block, so motion is halted by setting both reservoir pressures to 5 psig. Note that if the LIMITTHRESH proximity condition is not implemented, then $|PD_{left} - PD_{right}| <$ MAXDIFF will be prematurely satisfied because the plug starts so far from the destination block that PD_{left} and PD_{right} are at roughly the same background level. The time taken for the motion is continuously monitored. If it should exceed MAX_TRANSIT_TIME seconds, something has gone wrong, and the batch run is aborted.

Once the plug reaches the desired block, the program monitors the plug position, since it can drift. If $PD_{right} - PD_{left} >$ ERRORBAND (left), then the plug is considered to be too far to the left; if $PD_{left} - PD_{right} >$ ERRORBAND (right), then the plug is considered to be too far to the right. If the plug is too far left, it is pushed to the right until $PD_{left} - PD_{right} >$ MIDPOINT; if the plug is too far right, it is pushed to the left until $PD_{left} - PD_{right} <$ MIDPOINT. The monitoring and adjustment process continues until the step time is up. The whole procedure of moving to and waiting in the next heat block is repeated until thermal cycling is completed.

HPCR monitors the limit switch photodiode voltages during the entire run. If either falls below LIMITTHRESH, the plug is considered to be outside the blocks. Cycling is aborted, and both reservoirs are brought up to atmospheric pressure. The user can also manually abort at any time.

The monitor displays the elapsed transition, step, and total times, as well as the current stage of the cycling schedule. Times for all the transitions and steps completed are written to a log file whose name is specified in the batch file. Pressures

87

and temperatures used are copied from the batch file to the log file.

In this way, the machine performs PCR. Chapters 5 and 6 detail protocols and PCR mixes used with the machine, and yields produced.

4.8   Nomenclature

P_1, P_2 Oil reservoir/pressure manifold pressures.

PD_{far} Normalized voltage of the far photodiode.

PD_{left} Normalized voltage of the left photodiode.

PD_{near} Normalized voltage of the near photodiode.

PD_{right} Normalized voltage of the right photodiode.

r_o Inner radius of the capillary. o subscript stands for oil.

s Solubility of air in water. See Table 4.1.

T_1, T_2, T_3 Heat block temperatures.

α_w Thermal diffusivity of water.

Chapter 5

10 Cycle Experiments

5.1 Introduction

I conducted 10-cycle PCR time and temperature optimization experiments. This was
to verify that the machine works, as well as to illuminate any differences it may have
in cycling compared to a commercial heat block thermal cycler. The experiments
were designed to simulate the last 10 cycles of a 30 cycle PCR. To compensate for
the smaller number of cycles, product DNA was added to the PCR mix to equal that
after 20 cycles in a commercial machine.

5.2 PCR Mix

Table 5.1 shows the PCR mix used in the experiment.

The sterile water is distilled, filtered, and autoclaved (heated under high pressure)
to ensure the absence of contaminants and biological organisms.

10-Cycle PCR Mix Recipe

Amount	Component
37.6 μl	Sterile water
6.0 μl	λ template (1.0 ng/μl)
7.2 μl	524 bp product (84 ng/μl)
6.0 μl	λ30311F forward primer (10 pmol/μl)
6.0 μl	λ30835R reverse primer (10 pmol/μl)
16.0 μl	Purified Taq Pol mix
6.0 μl	5.0 mM each dNTP
8.4 μl	10 x buffer
6.8 μl	25 mM MgCl$_2$
100 μl	TOTAL

10-Cycle PCR Mix Concentrations

Final Concentration	Component
1.9 pM	λ template
17 nM (6 ng/μl)	524 bp product
600 nM	λ30311F forward primer
600 nM	λ30835R reverse primer
0.16 units/μl	Taq Polymerase
300 μM	each dNTP
50 mM	KCl
10 mM	Tris-HCl (pH 9.0)
2 mM	MgCl$_2$

Table 5.1: PCR mix used for the 10-cycle PCR experiments. Top chart lists the actual components used to make a 100 μl aliquot. Bottom charts lists the resulting component concentrations.

The template[1] is genomic λ phage[2] dsDNA. It is linear[3] in form, and is 48.5 kb long.

The 10-cycle experiments were intended to simulate the last 10 cycles of a 30-cycle reaction. Hence, there was 6 ng/μl of 524 bp product in the mix initially, which was the concentration found after 20 cycles in a standard heat block PCR machine[4] used as the control. The product was produced in PCR reactions in the control machine, purified via a commercial kit[5], and quantified using the standard technique of measuring the absorbance of the liquid at the 260 nm wavelength[6].

The primers were custom manufactured[7]. The forward primer λ30311F is 26 bases long. Its sequence is 5'-GGA AAA GGT CTG CGT CAA ATC CCC AG-3'. The reverse primer λ30835R is 41 bases long. Its sequence is 5'-CGT CGA TGA CAT TTG CCG TAG CGT ACT GAA GAA GCA CCG CG-3'. Together they define a 524 bp product.

The Taq mix is purifed from a commercial Taq source[8]. The commercial Taq is stored in a mix that contains Triton X-100, an anionic detergent. The plug/oil surface tension must be kept high to avoid plug breakup, so the Triton was removed via centrifugal concentration. The purified mix contains 10 mM Tris-HCl (pH 9.0),

[1]Part # US78018. USB Corporation. Cleveland, OH.
[2]A type of virus.
[3]Many viral and bacterial DNA are in the form of a continuous loop, referred to as *circular* DNA. The template DNA is circular DNA that has been cut in one place into linear form using a *restriction enzyme*.
[4]Model PHC-3. Techne, Inc. Princeton, NJ.
[5]QIAquick PCR Purification Kit. Part # 28104. QIAGEN Inc. Valencia, CA.
[6]Using a Model UV-1601 spectrophotometer. Shimadzu Scientific Instruments, Inc. Columbia, MD.
[7]Life Technologies, Inc. Rockville, MD.
[8]Part # M1861. Promega Corporation. Madison, WI.

50 mM KCl, 2 mM $MgCl_2$, and an estimated 1.0 units/μl Taq in sterile water. See Section 8.4 for details.

The PCR mix has about 0.16 units/μl Taq DNA polymerase. Standard PCR mixes contain 0.025–0.1 units/μl Taq DNA polymerase. The capillary PCR device requires more Taq to compensate for Taq adsorption onto the capillary walls. Though Teflon is chemically inert, in practice it can contain a small amount of impurities. Also, the ratio of the surface that the plug sees over the course of PCR to its volume is very high. I cannot use a blocking agent such as bovine serum albumin, since it will decrease the plug/oil interfacial tension.

The dNTPs were diluted from a commercial mix[9] containing 20 mM of each of the four dNTPs.

The 10 × buffer contains 500 mM KCl and 100 mM Tris-HCl (pH 9.0). This is identical to the 10 × buffer supplied with the commercial Taq polymerase mix, except that it does not contain any Triton X-100.

The $MgCl_2$ concentration was optimized on the control PCR machine.

The concentrations of template, primers, and dNTPs used were based on PCR mixes cycled in the control machine by previous researchers[10] in the lab and are fairly standard. The concentrations of KCl and Tris-HCl, as well as the pH of the Tris-HCl, were as recommended by the Taq manufacturer.

---

[9]Part # 27-2094. Amersham Pharmacia Biotech, Inc. Piscataway, NJ.
[10]Notably Matt Footer.

5.3 Experimental Protocol

5.3.1 The Earlier PCR Device

The 10-cycle PCR experiments were perfomed on an earlier, nonpressurized version of the device. It only had the right oil reservoir/pressure vessel, which was supplied with +1.5 psig (referred to as "the pressure" in this chapter), −1.5 psig (referred to as "the vacuum" in this chapter) and atmospheric pressures. Motion to the left and right was accomplished by opening the pressure and vacuum valves, respectively. To halt the plug, the reservoir was set to atmospheric pressure. No flow restrictors were required. The left end of the capillary was stuck through a hole drilled into a plastic cuvette[11]. I used a new cuvette for each reaction. It contained ∼1 ml of mineral oil, and was open to atmosphere. There was usually not enough time to degas for degassing to pose a problem in the 10 cycle reactions.

5.3.2 Starting the Day's Experiments

Each temperature or time optimization[12] was conducted using a single PCR mix to eliminate mix-to-mix variability. A particular optimization experiment was started by making 100 μl of the PCR mix, which was stored at 4°C when not in use. Large numbers of cuvettes with holes drilled in them, and capillaries straightened and cut into 9" lengths had been already prepared. The temperature controllers were turned on, heating the blocks within 5 minutes. The buffer tanks were set at ±1.5 psig using

---

[11]The disposable cuvettes were a commercial product used to hold spectrophotometer samples.

[12]6 in all: denaturing temperature, denaturing time, annealing temperature, annealing time, extension temperature, and extension time.

house air, house vacuum, and the shutoff valves. 1.5 ml disposable plastic centrifuge tubes (at least as many as the number of PCR runs, plus some extra) were filled with $\approx$ 0.5 ml of mineral oil each. They were used to load oil and sample plugs into the capillaries.

5.3.3 Positive Controls

To make a positive control, 10 μl of PCR mix was covered with 10μl of mineral oil (to prevent evaporation) in a standard 500 μl disposable plastic microfuge tube. The tube was cycled in the control PCR machine[13] according to the following schedule:

$$(94°C, 3 \text{ min}) \Rightarrow 10 \times [(92°C, 30 \text{ s}) \rightarrow (70°C, 45 \text{ s}) \rightarrow (72°C, 30 \text{ s})]$$

It is based on a preexisting schedule developed on the machine by a previous researcher[14] in my lab. Extension time was changed from 55 s to 30 s based on the rule of thumb of using 1 min per 1 kb target length. The annealing temperature was changed from 55°C to 70°C following an annealing temperature optimization with the control machine: annealing at 70°C produced more desired product and less nonspecific product than at 55, 60 or 65°C. This is probably due to the fact that mis-annealing can easily occur at the long annealing times and temperature transitions required by the control machine. The control samples were stored at 4°C following cycling.

---

[13] A commercial heat block thermal cycler. Model PHC-3. Techne, Inc. Princeton, NJ.
[14] Matt Footer.

5.3.4 Each PCR Run

A new capillary was used to perform every PCR reaction in my machine. One end was connected to the single oil reservoir/pressure manifold via the HPLC fitting. If it was the first run of the day, the vacuum was used to fill the reservoir with $\sim$ 1 ml oil from a 1.5 ml centrifuge tube. For subsequent runs, the pressure was used to fill the capillary with oil from in the reservoir.

A 1 μl drop of PCR mix was pipetted into one of the tubes containing 0.5 ml oil (see Section 5.3.2). The open capillary end was thrust into this tube. The vacuum was used to suck the plug, as well as enough oil to restore the level in the reservoir, into the capillary. This procedure ensured that the drop volume was $\approx$ 1 μl (sometimes small bits of drop would break off during loading) and that there were no air bubbles loaded along with the plug.

The free (left) end of the cuvette was threaded through the hole of a new cuvette. Oil was poured into the cuvette until its level was above the top of the capillary. A little extra was added: when the plug moved to the right, the oil level in the cuvette went down, but not low enough to interrupt the laser beam. The cuvette was attached to a makeshift stand. The stand was adjusted to make the capillary roughly straight, and then it was clamped onto the table. The laser, which was mounted on a manipulator, was turned on and focussed onto the end of the capillary. The manipulator allowed fine position adjustment of the beam.

The HPCR program ran a batch file to perform thermal cycling. After the cycling was done, the laser was switched off. A length of capillary containing the plug was

cut out of the machine and one end was stuck into a 1 ml syringe with an 18 gauge needle. The plug, along with some of the oil, was aspirated into a 0.5 ml disposable plastic tube. The tube was centrifuged to aggregate the contents, and stored at 4°C.

5.3.5 Negative Controls

The remaining PCR mix, which was not thermally cycled, provided the negative controls. Traditionally, negative controls are the result of cycling the mix sans template. However, there were so many reactions that produced no amplification when the cycling parameter or mix was even slightly off (expired Taq or dNTPs in the latter case) that this was deemed unnecessary.

5.3.6 Product Quantification

I used agarose gel electrophoresis, a standard molecular biology technique[15], to quantify end product. The gel is a rectangle about 1/4" thick made of a firm, Jello^{TM}-like substance containing agarose. It has a row of identically shaped dents, or *wells*, cast into one of its edges. Samples are loaded into these wells, and a voltage potential is applied across the gel. Since DNA is negatively charged, it migrates through the gel, with shorter strands migrating faster. A fluorescent intercalcating dye is used to visualize the DNA inside of the gel.

My gel consisted of 1% (w/v) agarose[16] in TBE buffer[17]. 1 g agarose powder[18] is

---

[15] See, for example, [75, Chap. 6].

[16] 1% (w/v) means 1 g in 100 ml solution.

[17] Initially, I mixed the TBE myself. Later, I diluted professionally formulated 10× TBE with sterile water.

[18] Catalog # A-6877. Sigma Chemical Company. St. Louis, MO.
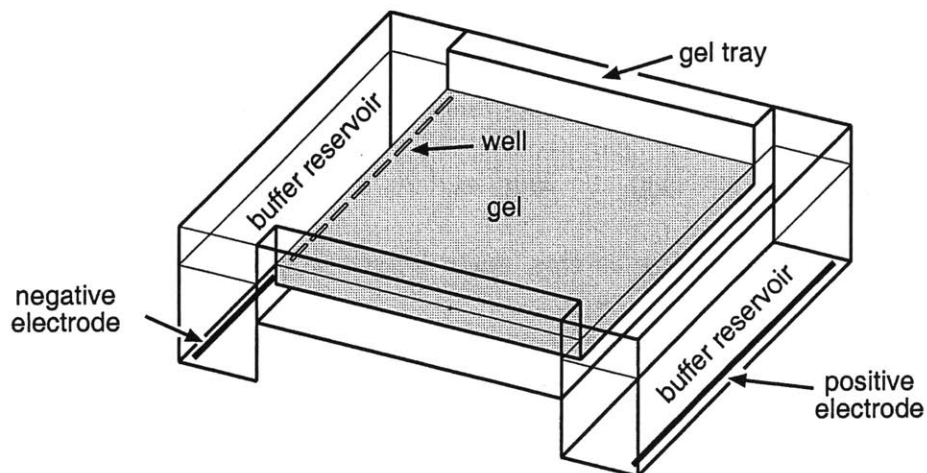
Figure 5-1: Schematic of an agarose gel inside of a gel box (agarose gel electrophoresis).

added to 100 ml TBE in a beaker. The mix is microwaved to melt the agarose, then poured into a tray in the gel box[19] to a thickness of $\approx 1/4$". In a certain orientation, the gel tray serves as a mold, and a teflon comb is used to cast the wells. Once the gel cools, the tray is moved into position for electrophoresis (see Fig. 5-1). Just enough TBE is poured into the box to cover the gel and fill the buffer reservoirs. The comb is removed.

The DNA samples are mixed with *loading buffer* prior to analysis. The loading buffer contains 0.25% (w/v) Orange-G[20] and 40% (w/v) sucrose. 5 μl loading buffer is added to 1 μl of sample. The loading buffer/sample mix is aliquoted onto parafilm, which tends to attract any residual oil, and then pipetted off of the parafilm relatively oil-free into the well. Orange-G is a dye provided to aid in sample loading (both the sample and TBE are clear). The sucrose makes the mix more dense than TBE so that it drops into the bottom of the well, rather than diffusing away. The loading

---

[19]Models B1A and B2. Owl Separation Systems. Portsmouth, NH. Also, Horizon 58. Bethesda Research Laboratories. Life Technologies, Inc. Gaithersburg, MD.

[20]Catalog # OX0185-5. EM Science. Cherry Hill, NJ.

process is repeated for every sample, each pipetted into a different well.

Commercial size and mass ladders are loaded alongside the DNA samples. The size ladder[21] contains 100, 200, 300, ... 1500, and 2072 bp DNA. When electrophoresed, the DNA separates according to size, since longer DNA migrates through the gel faster than shorter DNA. DNA of a particular size clusters together into a *band* in the gel. The size ladder bands are compared with the sample to see if the product is the correct length. To quantify sample product concentrations, they are compared against the mass ladder bands. 4 μl of mass ladder[22] contains 10, 20, 40, 80, 120, and 200 ng DNA bands. Since my DNA amounts were not this high, I used 2 μl of the mass ladder in one well, and 1 μl in another.

After loading, 100 volts are applied across the gel box electrodes for about 30 minutes. Each of the two platinum electrodes rests at the bottom of a buffer-filled reservoir at one end of the gel (see Fig. 5-1). The negative electrode is near the wells, and the positive electrode is at the opposite end. Since DNA is negatively charged, it slowly migrates through the gel, $\sim$ 2 inches/hour for the 524 bp product. All of the DNA from a single well moves along a *lane* parallel to DNA from other wells. The Orange-G migrates through the gel faster than the DNA, providing visual confirmation of electrophoresis.

Following electrophoresis, the gel is placed into a tray containing 100 ml of stain. The stain is 20 μl SYBR® Green I[23] diluted in 100 ml of TBE, according to the

---

[21]100 bp DNA Ladder. Catalog # 15628-019. Gibco BRL®. Life Technologies, Inc. Rockville, MD.

[22]Low DNA MASS™ Ladder. Catalog # 10068-013. Gibco BRL®. Life Technologies, Inc. Rockville, MD.

[23]Catalog # S-7567. Molecular Probes, Inc. Eugene, OR.

manufacturer's instructions. SYBR is a fluorescent intercalcating dye, which gets stuck inside of DNA strands. The gel is stained for $\approx$ 30 minutes on a rocker table.

The DNA bands are then visualized on a commercial CCD system[24]. The system consists of a CCD camera focussed on a UV light table, both inside of a dark box with a door. The door is opened to place the gel the UV table, and then closed. The UV light table is switched on, illuminating the SYBR-stained DNA bands. The system uses proprietary software[25] to project the CCD image onto the computer screen next to the system. There is a light aperture in front of the CCD camera, and the CCD signal can be digitally integrated. The aperature opening and integration time are adjusted to make the image as bright as possible without saturating any of the pixels, and the image is stored in memory. If some of the bands are weak, the shutter and integration time are adjusted to brighten them. In this case, some of the stronger bands are saturated, and these bands are not quantified. A second image containing the fainter bands is also stored in memory. The software is used to quantify the sample bands by linearly interpolating their fluorescence against the fluorescence of the mass ladder bands. The detection limit using this method is $\approx$ 1 ng. However, accuracy is low for samples containing < 10 ng DNA.

Figure 5-2 is an image from the commercial CCD system. It shows a SYBR-stained gel containing samples, positive and negative controls, and size and mass ladders from the 10-cycle denaturing temperature experiment, illuminated with ultraviolet light. Note that the negative control has signal due to initial product in the PCR mix (see

---

[24]Gel Doc 1000. Bio-Rad Laboratories. Hercules, CA.
[25]Molecular Analyst®/Macintosh v 2.1. Bio-Rad Laboratories. Hercules, CA.
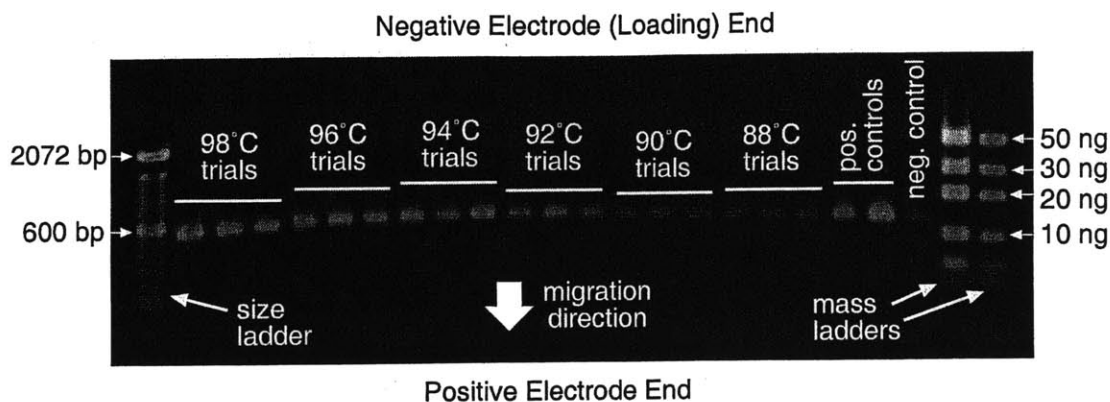
Figure 5-2: CCD image of gel used for the denaturing temperature optimization experiment.

Table 5.1). During electrophoresis, all of the bands migrate from the negative to positive electrode, as shown, with shorter DNA strands moving faster than longer DNA strands.

5.4 Experimental Results

To test the performance of the PCR machine, it was used to optimize denaturing, annealing, and extension step time and temperatures. The thermal schedule was as follows:

$$(T_D, 5 \text{ sec}) \Rightarrow 9 \times [(T_A, t_A) \to (T_E, t_E) \to (T_D, t_D)] \Rightarrow (T_A, t_A) \Rightarrow (T_E, t_E)$$

T and t are temperature and time, respectively. Subscripts D, A and E stand for denaturing, annealing, and extension, respectively. The initial denaturing time was always kept at 5 seconds to allow denaturing of the genomic 48.5 kb λ phage template DNA, which takes longer to dissociate than the 524 bp product. The other cycling

Optimization	T_D	t_D	T_A	t_A	T_E	t_E
Denaturing Temp.	88–98°C	2 sec	70°C	2 sec	72°C	30 sec
Denaturing Time	94°C	0–8 sec	70°C	2 sec	72°C	30 sec
Annealing Temp.	94°C	2 sec	54–72°C	2 sec	72°C	30 sec
Annealing Time	94°C	2 sec	56°C	0–16 sec	72°C	30 sec
Extension Temp.	94°C	2 sec	70°C	2 sec	70–80°C	30 sec
Extension Time	94°C	2 sec	70°C	2 sec	70°C	10–60 sec

Table 5.2: Thermal cycling conditions for time and temperature optimization experiments.

parameters are shown in Table 5.2.

The "default" parameters were $T_D = 94°C$, $T_A = 70°C$, $T_E = 72°C$, $t_D = t_A = 2$ seconds, and $t_E = 30$ seconds. The short denaturing and annealing times were based on Wittwer's finding that annealing and denaturing take place efficiently in < 1 second ([99]; see Section 3.2). The extension time of 30 seconds was based on the 1 min per 1 kb rule of thumb for conventional machines; it was thought that it could be reduced later. Annealing, denaturing, and extension temperatures were based on those used by the control machine (see Section 5.3.3).

The temperature of interest was varied for each temperature optimization; other conditions were their default values. The time optimization used this optimal temperature and varied the time of interest; the remaining conditions were at their default values.

To eliminate mix-to-mix variability, each of the 6 time and temperature optimization experiments was performed in a single day using a single PCR mix. The 10-cycle experiments took about 6 min 40 seconds for the default $t_D = t_A = 2$ seconds, and $t_E = 30$ seconds. This translates into 20 minutes for 30 cycles, a vast improvement on the 1–2 hours of a standard PCR machine.
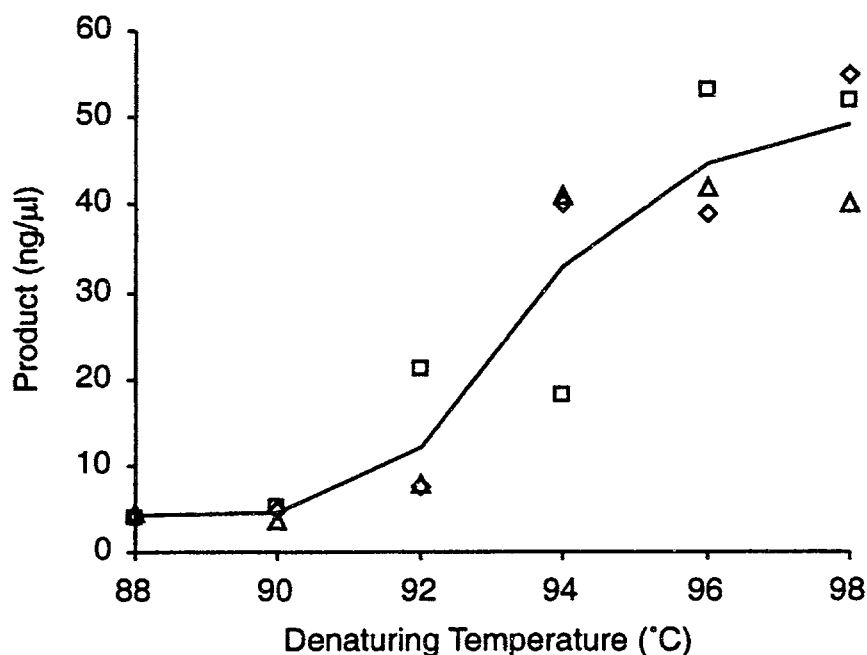
Figure 5-3: Results of the denaturing temperature optimization. T_D = 88, 90, 92, 94, 96, 98°C. t_D = 2 s. T_A = 70°C. t_A = 2 s. T_E = 72°C. t_E = 30 s. □, △, and ◇ represent 3 different trials. Positive controls: 25 and 66 ng/μl (avg: 46 ng/μl). Negative control: 3.6 ng/μl.

5.4.1 Denaturing Temperature

Figure 5-3 shows results from the denaturing temperature experiment. The highest temperature tested, 98°C, gives the best results. This is no surprise: greater temperature results in the more thorough denaturing, which produces higher yield. The yield from the capillary PCR machine was equivalent to that of the control machine at 96 and 98°C, and dropped off at lower temperatures.

The negative control product was quantified as 3.6 ng/μl, when it is known to be 6 ng/μl. The discrepancy is due to the fact that the quantification protocol loses accuracy at < 10 ng/μl. This effect will be seen throughout the results.

102
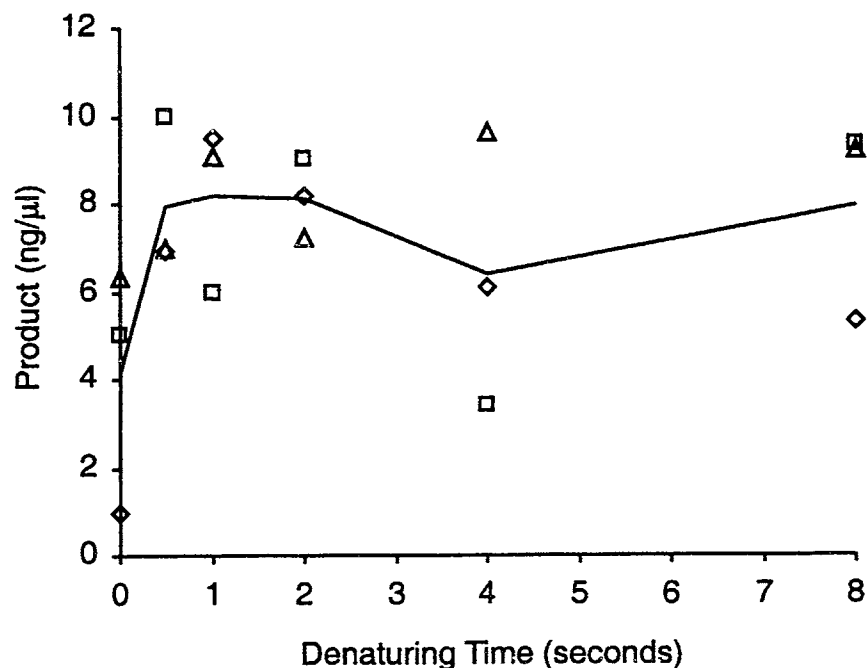
Figure 5-4: Results of the denaturing time optimization. $T_D = 94°C$. $t_D = 0, \frac{1}{2}, 1,$ 2, 4, 8 s. $T_A = 70°C$. $t_A = 2$ s. $T_E = 72°C$. $t_E = 30$ s. □, △, and ◇ represent three different trials. Positive controls: 12, 13 and 7.1 ng/μl (avg.: 11 ng/μl). Negative controls: 4.4, 2.0, and 2.9 ng/μl.

5.4.2 Denaturing Time

The denaturing time optimization was performed with the denaturing temperature at 94°C rather than 98°C . While 98°C is fine for 10 cycles, Taq activity drops rapidly as the temperature approaches 100°C, so 98°C may be unsuitable for 30 cycles. This was shown to be true in Chapter 6. Fig. 5-4 shows results for the denaturing time experiment. 0 seconds means that the plug did not have any dwell time inside of the block; however, the plug spent time inside the block to arrive at the middle and then depart, of course. More than $\frac{1}{2}$ second dwell time did not increase yield. From Table 7.5, it can be seen that it takes around 1.1–2.6 seconds for plug centerline temperature to reach 93.5°C. Since $\frac{1}{2}$ second denaturing time is sufficient,

this criteria may be too strict. Times longer than required can result in unnecessary deactivation of Taq. The positive controls (avg.: 11 ng/μl) were somewhat higher than the average capillary PCR machine value of 6–8 ng/μl at $\geq \frac{1}{2}$ seconds. This matches the denaturing temperature optimization results.

All of the yields, even for the positive control, are very low. In fact, they are barely above the negative control concentration of 6 ng/μl. However, the negative control was quantified as 3.1, rather than the expected 6 ng/μl, so there is in fact twofold to threefold amplification—still very low when compared to the denaturing temperature optimization. Since all of the trials used the same mix, the mix itself is bad due to some combination of (1) low initial Taq activity; (2) low activity recovered following centrifugal concentration of the Taq; and (3) low yield due to degradation of dNTPs.

5.4.3   Annealing Temperature

Fig. 5-5 shows annealing temperature optimization for 10 cycles. At the default annealing temperature, 70°C, the yield was a slightly less than that of the positive controls. At an average value of 9 ng/μl, is it roughly the same as that found in the denaturing time optimization, and much lower than that in the denaturing temperature optimization under the same conditions ($T_D = 94°C$, $T_A = 70°C$, $T_E = 72°C$, $t_A = t_E = 2$ seconds, $t_E = 30$ seconds).

Section 2.5.1 defines the primer melting temperature T_m and presents a number of equations to calculate it (2.2, 2.3, 2.4, 2.5 and 2.11). Section 2.5.3 states that the
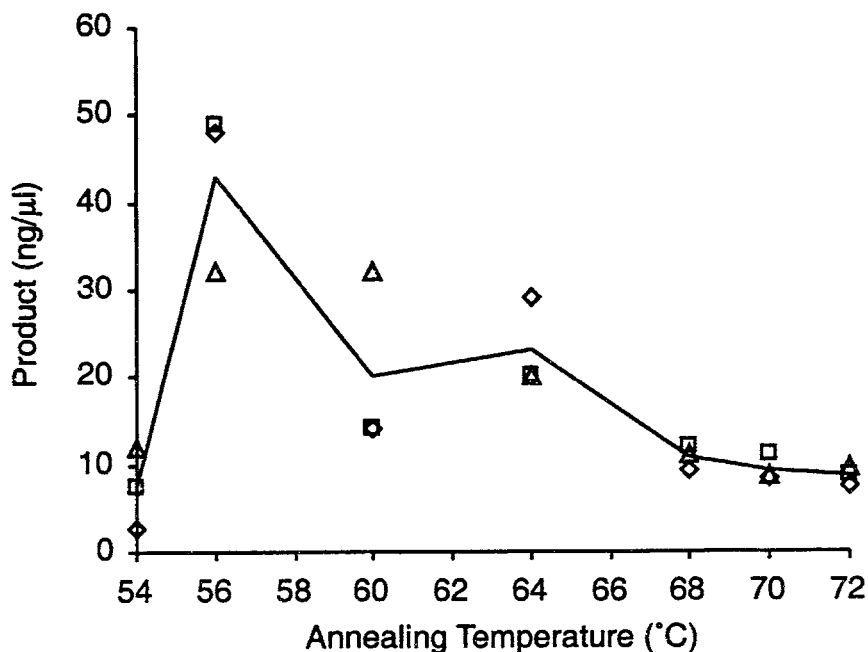
Figure 5-5: Results of the annealing temperature optimization. $T_D = 94°C$. $t_D = 2$ s. $T_A = 54, 56, 60, 64, 68, 70, 72°C$. $t_A = 2$ s. $T_E = 72°C$. $t_E = 30$ s. □, △, and ◇ represent three different trials. Positive controls: 14 and 15 ng/μl (avg. 15 ng/μl). Negative controls: 2.3 and 2.5 ng/μl (avg. 2.4 ng/μl).

optimal $T_{ANN} = T_m - 25°C$, and also presents equations to calculate T_{ANN} directly (2.12 and 2.13).

Which equations are the most reliable? (2.2, 2.3 and 2.12) are from *PCR* by Newton and Graham [58]. While the equations provide a good starting point for T_{ANN}, their origins are not referenced. There is some ambiguity between T_m and T_{ANN}: the two are expected to be within about 5°C, and (2.12) is alternately presented as an equation for T_m and an equation for T_{ANN}. Therefore, I eliminate (2.2, 2.3 and 2.12) as candidates.

Wetmur and Davidson's pioneering work in DNA hybridization [92] in 1968 remains the standard today [91]. Since this initial work, Wetmur has investigated many aspects of DNA hybridization, including its application to PCR annealing [91]. The

$\lambda 30311$F	$\lambda 30835$R	Equation
$T_m = 86°C$	$T_m = 99°C$ †	(2.11)
$T_{ANN} = 58°C$	$T_{ANN} = 63°C$	(2.13)

Table 5.3: Melting (T_m) and annealing (T_{ANN}) temperatures for the primers from the literature. †: equation may not be applicable to a primer this long.

equations he uses, (2.5 and 2.11), are credible. However, (2.5) is for long DNA, and is not as accurate for primers.

Rychlik et al. [72] did a very careful study of the optimal annealing temperature in PCR. Therefore, I feel that their equation (2.13) is reliable.

Equation (2.4) has a familiar form that is used by Wetmur [91] and Rychlik et al. [72] to find T_m for long DNA. Therefore, it may not be accurate for short primers, which are most precisely accounted for by the nearest-neighbor methods[26] incorporated into (2.11) and (2.13).

Table 5.3 shows the melting and annealing temperatures predicted by the most accurate equations, (2.11) and (2.13): Since $T_{ANN} = T_m - 25°C$, (2.11) predicts T_{ANN} = 61°C for $\lambda 30311$F and 72°C for $\lambda 30835$R, though it is questionable whether (2.11) can be applied to a primer as long as $\lambda 30835$R. The T_{ANN} value for $\lambda 30311$F is close to that found by (2.13). Therefore, theory predicts $T_{ANN} \approx 58$–$61°C$ for $\lambda 30311$F, and $\approx 63°C$ for $\lambda 30835$R.

T_{ANN} for experiment and theory match well for $\lambda 30311$F, but not as well for $\lambda 30835$R, which has a higher theoretical T_{ANN}. Why? Because if the temperature is roughly correct, annealing rate is more important than misannealing (annealing in an incorrect location) in my system. The lower the temperature, the faster the

---

[26]See Section 2.5.1.

annealing rate. I use very short annealing times, so the annealing rate must be fast. If the temperature is too low, misannealing is frequent. The machine's fast cooling also encourages misannealing. However, there is not enough time for most misannealed products to grow long enough to be extended in later cycles, either during the annealing step (at which temperature extension is very slow) or in the transitions to and from annealing. Of course, at very low temperatures, many misannealed products will arise regardless, but at 56°C , this is not yet a problem with λ30835R. Yield is high and amount of misprimed products are low for my fast temperature transitions and short annealing times, which agrees with the findings of Wittwer et al. (see Section 3.2).

Conversely, the control machine[27] had an optimal T_{ANN} of 70°C. Cooling to T_{ANN} is slow, and the required annealing time is long. Any mispriming that takes place has time to extend and produce erroneous product in later cycles. However, there is ample time to anneal even at a temperature much higher than the optimal T_{ANN}.

5.4.4 Annealing Time

Fig. 5-6 shows results for the annealing optimization experiment. There is no advantage gained by annealing > 2 seconds. From Table 7.5, we see that the time required to cool the plug to 53°C (is slightly less for 56°C) is $\approx$ 0.3–1.7 seconds. Subtracting this from the 2 second optimal annealing time (which includes temperature equilibration), we find that the optimal annealing time is $\approx$ 0.3–1.7 seconds. This matches

---

[27]See Section 5.3.3.
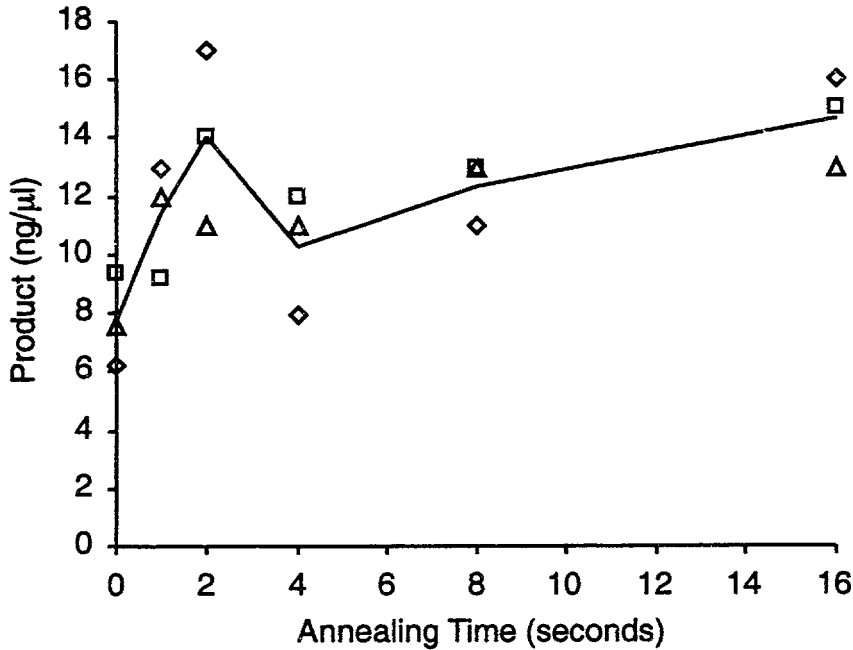
Figure 5-6: Results of the annealing time optimization. $T_D = 94°C$. $t_D = 2$ s. $T_A = 56°C$. $t_A = 0, 1, 2, 4, 8, 16$ s. $T_E = 72°C$. $t_E = 30$ s. □, △, and ◇ represent three different trials. Positive controls (2 trials): 19 and 19 ng/μl. Negative controls: 6.2 ng/μl.

Wittwer's finding (Section 3.2) that the optimal annealing time is < 1 second for rapid PCR.

We compute the theoretical time constant for annealing using equations (2.22), (2.23) and (2.25) presented by Wetmur et al.:

$$\text{annealing time constant} = (k_2 B_b)^{-1} = [(4.6 \times 10^4 M^{-1}s^{-1})B\sqrt{L}]^{-1} \qquad (5.1)$$

where k_2 is a rate constant, B is the primer molar concentration, L is primer length in bases, and $B_b = BL$. The time constant for λ30311F (26 bases) is 7.1 seconds, and for λ30835R (41 bases) it is 5.7 seconds. After one time constant, only $1/e$ of the ssDNA remains unannealed.

These times are much longer than what Wittwer et al. and I found was optimal. Why is this? First, our cooling rates may far exceed those used by Wetmur, who cooled his liquid inside of a spectrophotometer cell. Cooling rate is not accounted for by Wetmur's theory, but fast rates may affect annealing. Second, Wetmur found his rate constants using very long DNA ($\sim 10^4$ bases) with complexities N (see Section 2.5.4) $\neq L$ (the two are equal for primers). The resulting annealing time constants were in the minutes or hours, rather than seconds. In fact, when Wetmur's equations are extrapolated to short primers cooled at very rapidly, it is not so much a failure as a triumph that the results are within an order of magnitude.

5.4.5   Extension Temperature

The results for extension temperature are shown in Fig. 5-7. The optimal temperature range of Taq is that tested: 70–80°C [4]. It appears that product yield is still increasing as T_E drops below 70°C, but this may just be an artifact of the data scatter. This point was returned to in the 30 cycle experiments. The overall yield was good, and actually higher than the control machine at the optimal extension temperature.

5.4.6   Extension Time

The results of the extension temperature optimization are shown in Fig. 5-8. As expected, product drops off as time decreases. Theoretically Taq can extend[28] at 100 bases/second, so only 5.2 seconds should be required to extend the 524 bp product.

---

[28]See (2.27).
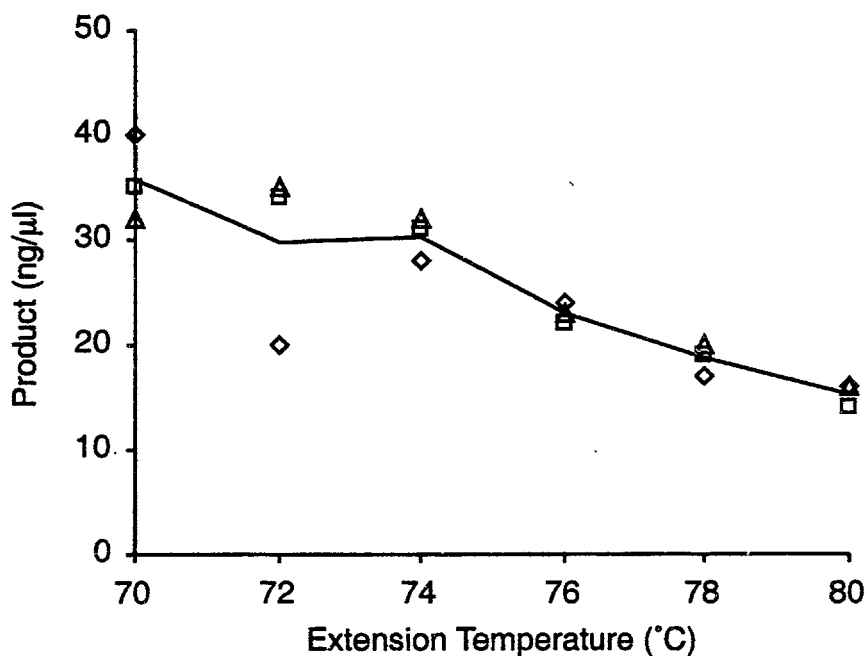
Figure 5-7: Results of the extension time optimization. $T_D = 94°C$. $t_D = 2$ s. $T_A = 70°C$. $t_A = 2$ s. $T_E = 70, 72, 74, 76, 78, 80°C$. $t_E = 30$ s. □, △, and ◇ represent three different trials. Positive controls: 18 and 24 ng/μl. Negative control: 4.8 ng/μl.
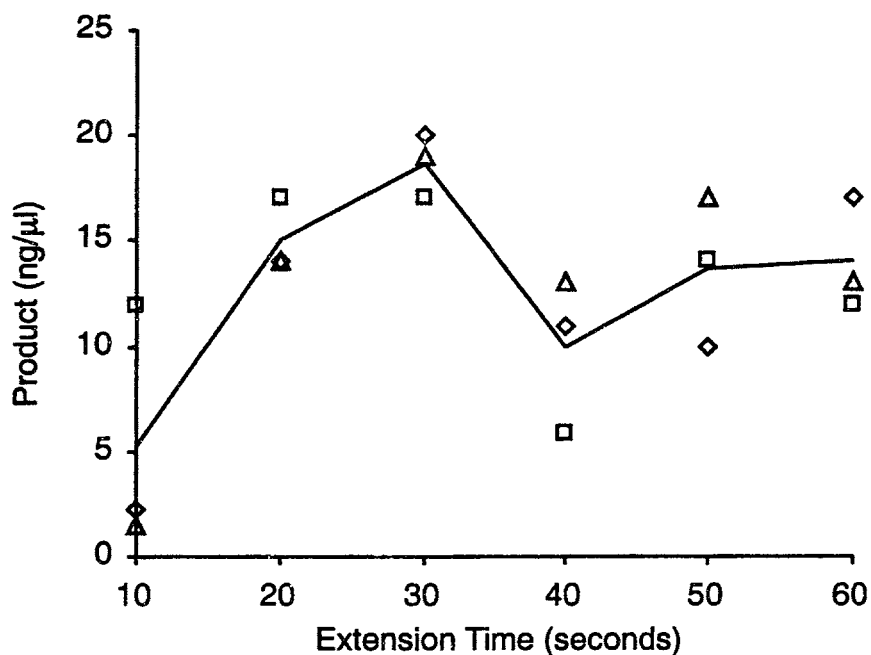
Figure 5-8: Results of the extension time optimization. $T_D = 94°C$. $t_D = 2$ s. $T_A = 70°C$. $t_A = 2$ s. $T_E = 70°C$. $t_E = 10, 20, 30, 40, 50$ and 60 s. □, △, and ◇ represent three different trials. Positive controls: 7.4 and 13 ng/μl (avg. 10 μ/l). Negative control: 3.8 ng/μl.

However, as extension time is lowered, efficiency drops. This effect is seen in many fast PCR machines[29].

There is some amplification even with only 10 seconds extension. Additionally, there seems to be no added benefit of extending longer than 30 seconds. More product was produced by the capillary PCR machine than the control. The results of this optimization are somewhat questionable, due to the low yield of both the optimization and positive controls.

5.5 Conclusion

The machine performs 10 cycles of PCR in about 400 seconds. Optimal T_D is 98°C, the highest temperature tested. However, this may result in rapid Taq decay for 30 cycles. At a standard T_D of 94°C, the most product was produced for $t_D \geq \frac{1}{2}$ seconds. 54°C $\leq T_A \leq$ 60°C was optimal for the primers used, which agrees well with theory. Optimal $t_A \geq 2$ seconds, which agrees with Wittwer's air cycler results. The optimal T_E in the 70–80°C range is 70°C, which suggest that the optimal T_E may be lower. The greater the t_E, the higher the efficiency (plateau at 30 seconds), which was as in the literature. However, product was produced for $t_E = 10$ seconds, the lowest time tested. Fluctuation in yield, including that of the positive controls, was found throughout the optimizations, suggesting that the process of removing the detergent may cause mix-to-mix variability in Taq activity.

---

[29]See Chapter 3.

5.6 Nomenclature

B Molar concentration of primer.

B_b BL.

k_2 An annealing rate constant. See Chapter 2.

L DNA length, in bases.

t_A Annealing time.

T_A Annealing temperature.

T_{ANN} Annealing temperature.

t_D Denaturing time for cycle > 1.

T_D Denaturing temperature.

t_E Extension time.

T_E Extension temperature.

T_m Primer melting temperature.

Chapter 6

30 Cycle Experiments

6.1 Introduction

After proving that 10-cycle PCR works in the capillary machine, I progressed to more realistic 30-cycle experiments. Experimental protocol was similar: unless stated otherwise, it is the same as for the 10-cycle experiments (see Chapter 5).

6.2 PCR Mix

Table 6.1 shows the PCR mix used in the experiment. Constituents are identical to those used for the 10-cycle experiments (see Section 5.2) except for the primers[1]. Their sequences are based on primers provided in a commercial PCR kit[2]. The sequence of primer 1 is 5'-GAT GAG TTC GTG TCC GTA CAA CTG-3', and the sequence

---

[1]Custom manufactured. Life Technologies, Inc. Rockville, MD.

[2]GeneAmp® PCR Reagent Kit. Part # N801-0055. Applied Biosystems (formerly Perkin-Elmer), Foster City, CA. The primers provided in this kit are both 25 bases long. The last two bases of each primer are intentionally complementary to demonstrate the primer-dimer complex. To reduce the tendency of my primers to anneal to each other, I left off the last base of each primer.

30-Cycle PCR Mix Recipe

Amount	Component
3.0 μl	λ template (1.0 pg/μl)
3.0 μl	primer 1 (10 pmol/μl)
3.0 μl	primer 2 (10 pmol/μl)
35.4 μl	Purified Taq Pol mix
3.0 μl	5.0 mM each dNTP
1.46 μl	10 $\times$ buffer
1.17 μl	25 mM MgCl$_2$
50 μl	TOTAL

30-Cycle PCR Mix Concentrations

Final Concentration	Component
1.9 fM	λ template
600 nM	primer 1
600 nM	primer 2
0.7 units/μl (3.8×10^{-8} M)	Taq Polymerase
300 μM	each dNTP
50 mM	KCl
10 mM	Tris-HCl (pH 9.0)
2 mM	MgCl$_2$

Table 6.1: PCR mix used for the 30-cycle PCR experiments. Top chart lists the components used to make a 50 μl aliquot. Bottom charts lists the resulting concentrations.

of primer 2 is 5'-GGT TAT CGA AAT CAG CCA CAG CGC-3'. They define a 500 bp product. Both primers are 24 bases long with $\approx$ 50% GC content, so they have similar melting temperatures. The primers used in the 10 cycle experiments were 26 and 41 bases long, so their melting temperatures varied considerably.

The template DNA concentration is 1/1000 that of the 10-cycle PCR mix[3]. This is toward the lower end of the range used in standard PCR mixes. I wanted to prove that the capillary PCR machine could amplify as dilute a template as a commercial thermal cycler. Of course, this resulted in lower product yields than during the 10-cycle experiment. However, the lower end product helps keep the reaction away from the primer limit. Once the product molar concentration exceeds 1/10 of the primer concentration, product reannealing starts to compete with primer annealing. Amplifying 1.9 fM template over 30 cycles with a standard 70% efficiency results in $(1.9 \text{ fM})(1.7)^{30} = 1.6 \times 10^{-8}$ M product. This is less than 1/10 of the primer concentration (6×10^{-8} M, or 20 ng/μl product), avoiding the primer limit.

The PCR mix contains about 0.7 units/μl Taq DNA polymerase. This is more than in the 10-cycle PCR mix ($\approx$ 0.16 units/μl) and a standard PCR mix (0.025–0.1 units/μl). The concentration is higher than a standard mix[4] to compensate for the adsorption of the enzyme onto the capillary walls. 30 cycles rather than 10 means that the plug sees about 3 times as much surface area, which is why the Taq concentration is higher than that used for the 10-cycle reactions. As with the 10-cycle mix, the Taq had the Triton X-100 removed via centrifugal concentration[5].

---

[3]See Section 5.2.
[4]See Section 2.3.
[5]See Sections 5.2 and 8.4.

Furthermore, since erroneous product was not a big problem in my machine[6], I decided to use as much Taq as much as possible to allow exponential amplification across all 30 cycles. Since Taq can extend[7] at 100 bases/second, it theoretically requires 5 seconds to extend the 500 base product. 30 seconds extension times were used for the 30-cycle experiments, so each new cycle can create up to $6(3.8 \times 10^{-8}$ M$) = 2.3 \times 10^{-7}$ M (38 ng/μl) new product. Of course, it is impossible to more than double the amount of existing DNA per cycle, and the Taq is not 100% efficient. Since the product resulting from the 30-cycle temperature optimizations are significantly less[8] than $2 \times 38 = 76$ ng/μl, all cycles should have exponential amplification.

6.3 Experimental Protocol

As noted at the start of this chapter, the experimental protocol was identical to that used for the 10-cycle experiments except for following details.

6.3.1 The Device

The 30-cycle experiments were conducted in the full device described in Chapter 4. I used both left and right oil reservoir/pressure manifolds. Each contained $\sim$ 1 ml of mineral oil. After loading the capillary with oil and plug using the ± 1.5 psig pressures at the right reservoir, oil was added to the left reservoir with a syringe

---

[6]Due to short annealing times and fast transitions to and from annealing. See Section 5.4.3.

[7]See (2.27).

[8]It must be significantly less to account for Taq adsorption to the capillary walls; the fact that the reaction is not 100% efficient; and the influence of the primer reannealing at 20 ng/μl, as explained previously in this section.

Figure 6-1: The Robocycler Gradient 96: the machine used for the positive controls in the 30 cycle experiments. The Robocycler has a robotic arm that moves the tubes between 4 different temperature heat blocks (denaturing, annealing, extension, and refrigerated storage). From [83].

(some oil dripped out of the reservoir after removal of the capillary following every PCR), and then the left end of the capillary was connected to the left reservoir.

6.3.2 Starting the Day's Experiments

The 30 cycle PCR experiments took a longer time to conduct than the 10 cycle experiments. Therefore, not every optimization used samples drawn from the same aliquot. Rather, each trial of each temperature optimization used a separate aliquot.

6.3.3 Positive Controls

A newer, more efficient PCR machine[9] [19] was used to perform the positive control reactions (see Fig. 6-1). The control machine has four heat blocks: one each for

---

[9]Robocycler Gradient 96. Stratagene®. La Jolla, CA.

denaturing, annealing, extension, and cold storage following PCR. Each block is at a constant temperature[10], eliminating the need to heat and cool each block (though it takes $\sim$ 30 minutes to bring the blocks to temperature once the machine is turned on). To perform PCR, a robotic arm physically moves the tubes from wells in one block to wells in another. The machine uses 0.2 ml polypropylene tubes[11] that have thin walls to reduce thermal resistance. The reaction is faster than in a standard heat block PCR machine. However, the insulating polypropylene tubes and the normal ($\sim$ 100 μl) aliquot volumes still result in times of about 1 hour for 30 cycles of PCR.

Each positive control was 10 μl of PCR mix. No oil was required to prevent evaporation since the control machine was equipped with a heater resting above the tubes that prevents condensation at the top. The following thermal schedule was used:

94°C, 8 min $\Rightarrow$ 30 × [(94°C, 30 s) $\rightarrow$ (53°C, 45 s) $\rightarrow$ (70°C, 30 s)] $\Rightarrow$ 70°C, 7 min $\Rightarrow$ 6°C, hold

The schedule was modified from that used for the 10-cycle controls[12]. The annealing temperature was optimized on the control machine. Since it has faster temperature transitions than the control machine used for the 10 cycle experiments, misannealing is not as large of a problem, so the temperature more closely approaches that predicted by theory (in the 50–60°C range). The long initial dentaure and final extension times were based on PCR protocols established by researchers in lab[13] for the same machine.

---

[10]One of the blocks can be programmed to vary its temperature linearly as much as 11°C across its length to allow temperature optimization of one of the PCR steps (usually annealing). This temperature distribution does not change over the course of the reaction.

[11]Part #s N801-0540, N801-0580 and N801-0535. Applied Biosystems. Foster City, CA.

[12]See Section 5.3.3.

[13]Notably John Newman.

A thorough initial denaturation is critical since the first cycle relies completely on the template, rather than product produced in earlier cycles; the genomic 48.5×10^3 bp template takes longer to denature than the 500 bp product[14]. 6°C is a standard holding temperature once the reaction is completed. It prevents subsequent reactions from occuring.

6.3.4 Negative Controls

Negative controls were merely uncycled PCR mix, as in the 10 cycle experiments. No negative control showed any sign of product.

6.3.5 Product Quantification

The product quantification protocol was improved for the 30 cycle experiments. A heavier (2% instead of 1% w/v) agarose gel was used along with a thin wells to produce sharper bands with less smearing. This results in more accurate quantification. Fig. 6-2 compares bands from the conventional-shaped wells used in the 10-cycle experiments and the wide, thin wells used in the 30-cycle experiments.

The instructions that come with the commercial Low DNA MASS™ ladder state the following:

> NOTE: the closer the size of the sample band relative to the band of comparable intensity in the Low DNA MASS Ladder, the more accurate the estimation will be.

Therefore, to get the best possible correlation, I quantified my product against several

---

[14]Wittwer et al. found that their template had to be boiled prior to rapid PCR in the air cycler [99].
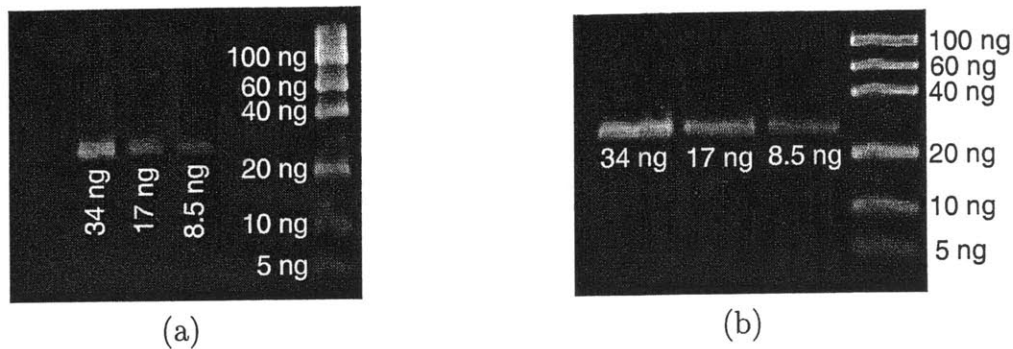
Figure 6-2: A comparison of bands: (a) the conventional bands used in the 10-cycle experiment; (b) the wide, narrow bands used in the 30-cycle experiment. 34, 17, and 8.5 ng 500 bp product, as well as a mass ladder, was loaded into the wells in both (a) and (b), as shown. Both set of bands were run on the same 2% agarose gel at 100 volts, 30 minutes. The gel was then stained for 30 minutes in SYBR Green I diluted 1:10,000 by TBE. It is not obvious from the figure, but there is significantly more smearing in the 500 bp product bands (the 34, 17, and 8.5 ng bands) in the conventional wells. The smearing is clearly visible when the image is displayed on the computer monitor.

lanes containing known concentrations[15] of the product itself, produced using the control PCR machine.

All of these measures ensure greater uniformity. Even so, quantification is only good to within about 20%. Part of this is due to nonuniformity in the UV light table within the Gel Doc 1000 itself (see Section 5.3.6).

6.4 Experimental Results

To test the performance of the PCR machine, it was used to optimize denaturing, annealing, and extension temperatures. I also intended to do a time optimization, as in the 10-cycle experiments; however, time constraints prevented its completion. The

---

[15] Quantified via the standard method of checking absorbance at 260 nm with a spectrophotometer. Model UV-1601 spectrophotometer. Shimadzu Scientific Instruments, Inc. Columbia, MD.

Optimization	T_D	T_A	T_E
Denaturing Temp.	86–96°C	53°C	70°C
Annealing Temp.	94°C	33–68°C	70°C
Extension Temp.	94°C	53°C	54–78°C

Table 6.2: Thermal cycling conditions for 30 cycle temperature optimization experiments.

thermal schedule was as follows:

$$T_D,\ 30\ \text{s} \Rightarrow 29 \times [(T_A,\ 5\ \text{s}) \to (T_E,\ 30\ \text{s}) \to (T_D,\ 5\ \text{s})] \Rightarrow T_A,\ 5\ \text{s} \Rightarrow T_E,\ 60\ \text{s}$$

T_D, T_A and T_E are the denaturing, annealing, and extension temperatures, respectively. Their values are shown in Table 6.2. The initial denaturing time was always 30 seconds to allow denaturing of the template DNA[16]. An extension time of 30 seconds was based on the rule of thumb of 1 min per 1 kb product length. The denaturing and annealing were set at 5 seconds each. Although 2 seconds were used for both in the 10-cycle optimization, it was barely enough time to reach a plateau in end product, so 5 seconds was used as a more conservative starting point. If time optimization revealed that shorter step times produced just as good results, I felt I could switch then (although I never got around to the time optimizations). A long final extension time is traditionally used in PCR protocols. As in the 10-cycle experiments, this was set to 60 seconds.

The range of annealing and extension temperatures tested were much larger than for the 10-cycle experiments. This was to ensure that a plateau existed within the range of temperatures tested. This was not the case in the 10-cycle extension tem-

---

[16]See Section 6.3.3.

perature optimization.

The "default" parameters were $T_D = 94°C$, $T_A = 53°C$, and $T_E = 70°C$. 94°C for denaturing is a standard in commercial machines. $T_A = 53°C$ was taken from the control machine T_A optimization[17]. $T_E = 70°C$ was taken from the 10 cycle T_E optimization[18].

Each trial was performed in a single day using the same PCR mix. For this reason, each temperature optimization presents a distinct curve for each trial, rather than a single curve of averaged yields as in the 10-cycle experiments.

Each 30-cycle experiment took about 24 minutes to run. This is a great improvement over the 1–2 hours required by a standard commercial heat-block PCR machine.

6.4.1 Denaturing Temperature

Figure 6-3 shows results from the denaturing temperature experiment. The results indicate that, as expected, higher temperatures deliver more product due to more thorough denaturation. At 94°C there is a plateau in product, due to the fact that more thorough denaturation is offset by decay of Taq at higher temperatures.

The yields from the control machine are generally not as high as for the capillary PCR machine at 94 and 96°C. There is one exception in which the control machine gave exceptionally high yields roughly 3 times (21 and 29 ng/μl) that of the capillary PCR machine. While this difference may seem very large, a 3-fold product difference

---

[17]See Section 6.3.3.
[18]See Section 5.4.5.
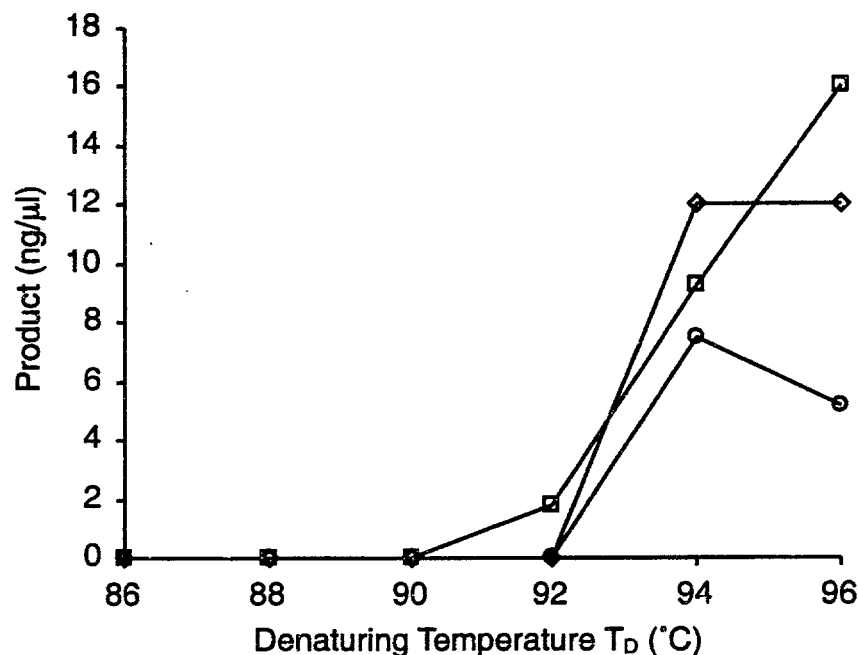
Figure 6-3: Results of the denaturing temperature optimization. T_D = 86, 88, 90, 92, 94, 96°C. T_A = 53°C. T_E = 70°C. □, ◇ and ○ represent 3 different trials. Positive controls: for ◇, 3.6 and 2.9 ng/μl; for □, 6.5 and 6.4 ng/μl; for ○, 21 and 29 ng/μl.

over the course of 30 cycles is a $3^{1/30} - 1 = 0.04$ (4%) difference in efficiency, which is actually reasonably small. This effect will be seen in the other temperature optimizations. The point is that the efficiencies of the capillary and control PCR machines are similar under the given conditions.

6.4.2 Annealing Temperature

Fig. 6-4 shows annealing temperature optimization for 30 cycles. Table 6.3 shows the theoretical melting and annealing temperatures[19]. Since $T_{ANN} = T_m - 25$°C, (2.11) predicts $T_{ANN} = 52$°C for Primer 1 and 59°C for Primer 2. Therefore, theory predicts $T_{ANN} \approx 52$–58°C for Primer 1, and $T_{ANN} \approx 59$–60°C for Primer 2. This

---

[19]See Section 5.4.3.
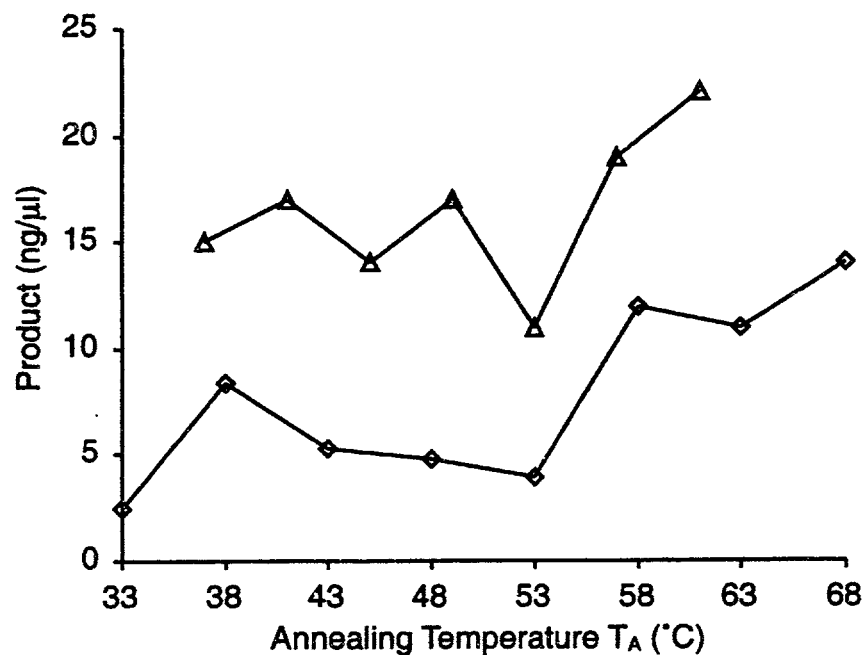
Figure 6-4: Results of the annealing temperature optimization. $T_D = 94°C$. $T_A = 37, 41, 45, 49, 53, 57$ and $61°C$ for the top curve, and $33, 38, 43, 48, 53, 58, 63, 68°C$ for the bottom curve. $T_E = 70°C$. $\triangle$, and $\diamondsuit$ represent two different trials. Positive controls: for $\triangle$, 3.6 and 2.9 ng/μl; for $\diamondsuit$, 1.7 and 1.9 ng/μl.

Primer 1	Primer 2	Equation
$T_m = 77°C$	$T_m = 84°C$	(2.11)
$T_{ANN} = 58°C$	$T_{ANN} = 60°C$	(2.13)

Table 6.3: Melting (T_m) and annealing (T_{ANN}) temperatures for the primers from the literature.

agrees reasonably well with the optimal annealing temperature found on the control machine (53°C). However, it does not seem to match well for the capillary PCR machine. In fact, it appears that the optimal annealing temperature for the capillary PCR machine is at the extension temperature!

The first possibility is that the 68°C datapoint is merely an anomaly, and that the actual peak annealing temperature is somewhere near 60°C, which matches the theory. Certainly, more data needs to be taken to confirm the optimal annealing temperature. What if this is not the case, though? There is another explanation.

It is not actually the annealing temperature that is optimized; it is the annealing *block* temperature. Ideally, the two should be the same. However, in the capillary PCR machine, the plug temperature can dip as it passes in the cool region between two heated blocks. Using the heat transfer model detailed in Chapter 7, I calculated the approximate plug temperature history as it travels from the denaturing to annealing block when the latter is at the optimal temperature[20]. The results are shown in Fig. 6-5. The minimum temperature plug temperature is between 53°C and 62°C, the all-water and all-oil minimums. The theoretical annealing temperatures for both primers fall inside this range. Therefore, I believe that the plug anneals as it travels *between* the extension and annealing blocks[21]. The total travel time from the denature to annealing block is about 2.8 seconds, so the plug spends only $\sim \frac{1}{2}$ second at temperatures optimal for annealing. However, as found by Wittwer (see Section 3.2), this is enough!

---

[20]$T_D = 94$°C, $T_A = 68$°C, and $T_E = 70$°C. This is for the highest T_A tested; any higher, and it would be $\geq T_E$.

[21]See Section 10.4.3 for suggestions on how to solve this problem.
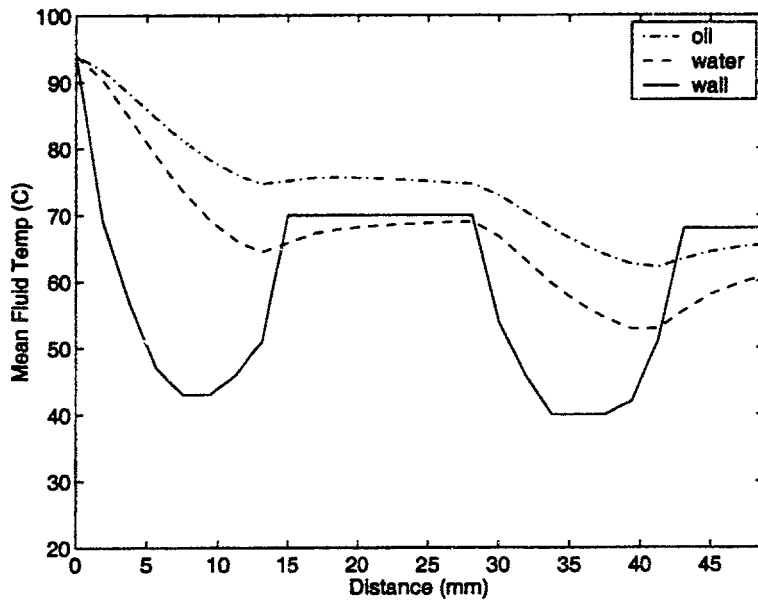
Temperature	Min.	Avg.	Max.	End
Water	53°C	67°C	94°C	61°C
Oil	62°C	74°C	94°C	65°C

Figure 6-5: Temperature as plug moves to the right (increasing distance), from denaturing to annealing block, at 0.033 m/s. Temperature is assumed to lie somewhere inbetween the temperatures shown for oil and water. $T_D = 94°C$, $T_A = 68°C$, $T_E = 70°C$.

Theory predicts an annealing time constant[22] of 7.4 seconds for each primer. My results support the idea that the hybridization theory equations are incorrect by an order of magnitude when applied to short primers[23].

If the annealing occurs between blocks, then why don't lower T_A values give as much product? First, the plug is actually *extending* efficiently inside of the annealing block at higher T_A values. Second, at high T_A values, annealing cannot occur efficiently inside of the annealing block, so the annealing time is kept short. This reduces the amount of time available for misannealed primers to extend—they fall off ssDNA at typical extension temperatures. Erroneous product is minimized and desired product is maximized.

Why don't we see this effect in the 10-cycle experiments[24]? Because in the that case, there was a lot of product to start with. Extension efficiency is not critical. At the optimal 10-cycle annealing temperature, 56°C, the product is $>$ 20 ng/μl (see Fig. 5-5). At this point[25], ssDNA reannealing starts to compete with primer annealing. To get significantly more than 20 ng/μl product, annealing has to be optimized as much as possible: it does more good to provide additional annealing time rather than additional extension time[26]. This explains the optimal T_A matching the theoretical annealing temperature for the 10-cycle experiments, but not the current 30-cycle experiments.

---

[22]After one time constant, only $1/e$ of the denatured ssDNA remains unannealed to primers. See Section 5.4.4.

[23]See Section 5.4.4.

[24]See Section 5.4.3.

[25]See Section 6.2.

[26]Although providing too much annealing time will increase erroneous products at the expense of desired products.
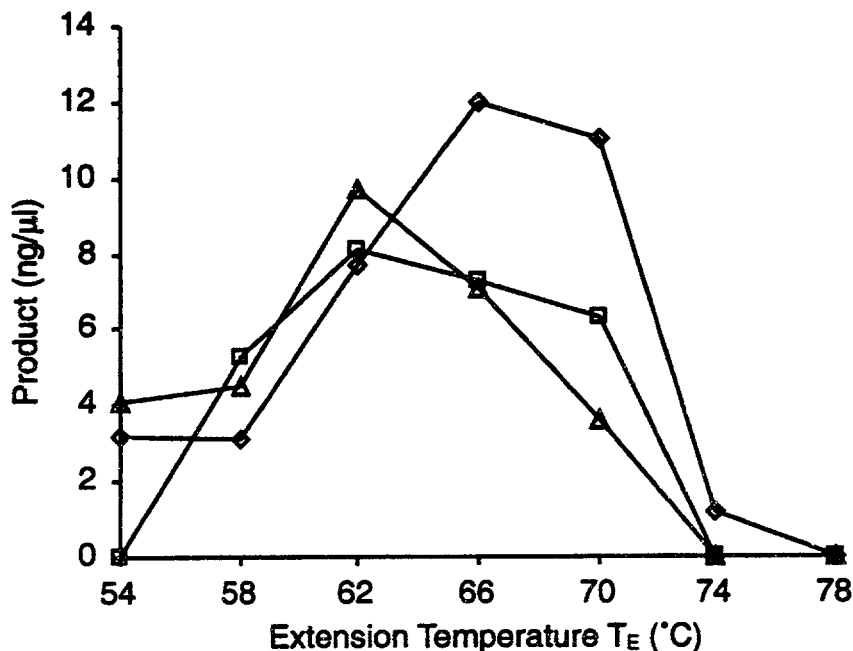
Figure 6-6: Results of the extension time optimization. $T_D = 94°C$. $T_A = 53°C$. T_E = 54, 58, 62, 66, 70, 74, 78°C. ◇, □, and △ represent three different trials. Positive controls: for ◇, 1.7 and 1.9 ng; for □, 13 and 18 ng; for △, 21 and 29 ng.

6.4.3 Extension Temperature

The results for extension temperature are shown in Fig. 6-6. Curiously, the optimal temperature seems to be around 62–68°C, rather than 70–80°C reported in the literature [4]. To test whether this was due to the unusual constituency of the PCR mix (no Triton X-100 or similar enzyme stabilizing agent, as well as an unusually high amount of DNA polymerase), I ran an extension temperature optimization on the control PCR machine. The cycling is as described in Section 6.3.3 except that the extension temperature is varied. All reactions were aliquots of the same PCR mix. The temperature gradient feature of the control machine allowed me to run 12 different extension temperatures simultaneously. Results are shown in Fig. 6-7. The figure shows some poor datapoints. For example, there is hardly any product at 64 or 72°C.
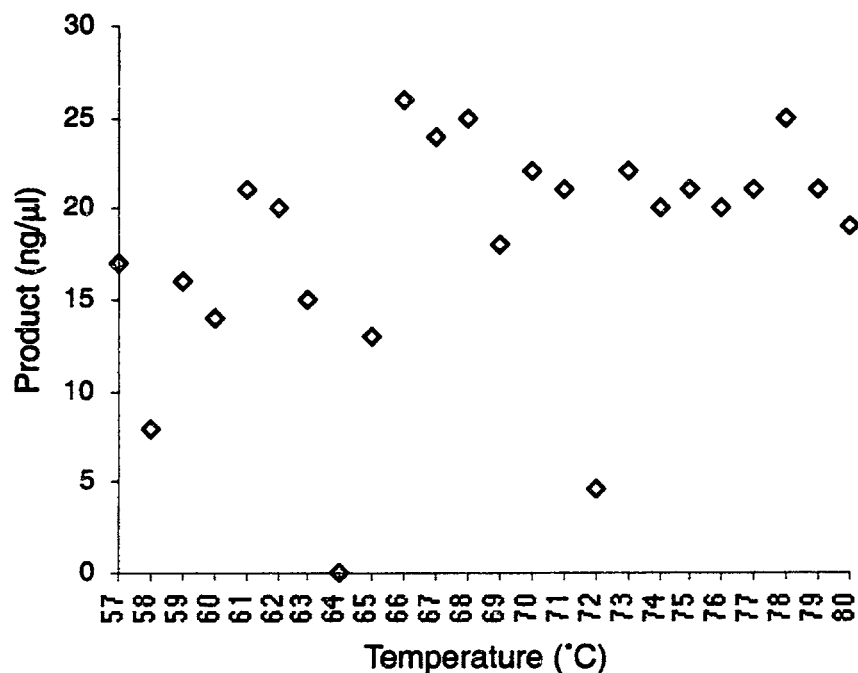
Figure 6-7: Results of extension temperature optimization for 30 cycles using the control PCR machine.

However, this is the nature of PCR: some reactions fail randomly, even though they are aliquoted from the same mixture and cycled identically to many other reactions that succeed. Discounting this anomalous data, we see that the peak is around the mid 60°C range. This is consistent with the results of Fig. 6-6, suggesting that the low optimal T_E is due to the unusual PCR mix.

The capillary PCR shows much greater sensitivity to T_E than the control machine. The control machine uses an annealing time of 45 seconds, wheras the capillary PCR machine uses only 2 seconds. The extra annealing time of the control machine also serves as additional extension time (though extension is not as efficient at 53°C), making the control machine PCR less sensitive to changes in Taq activity. In addition, Taq adsorbs to the sidewalls in the capillary PCR machine, again making PCR in the capillary machine more sensitive to changes in Taq activity.

6.5   Product Variability

There is significant variability in product between different runs, even for the same cycling conditions. For example, in Fig. 6-6, there is 3.6, 6.3, and 11 ng/μl product for 3 different trials at $T_D = 94°C$, $T_A = 53°C$, and $T_E = 70°C$. Why is this?

6.5.1   The Nature of PCR

PCR is an exponential amplification process, so a small difference in efficiency results in a large difference in product. For example, if every cycle has exponential amplification, increasing efficiency by just 5% will produce $(1.05)^{30} = 4.3$ times more product after 30 cycles.

While every effort was made to use the same PCR mix, the fact is that most trials were conducted on different days. A mix had to be formulated anew each day from frozen constituent aliquots that had to be thawed prior to use. The constituents, especially the dNTPs, can decay over time, especially with all of the freezing and thawing. This will affect the product yield.

6.5.2   Variability Due to the Mix

The mix did not have any Triton X-100 detergent. According to the manufacturer [69], this will result in deactivation of the Taq. I found that complete deactivation did not occur between the time that I removed the Triton and the time that I ran my PCR experiments. However, did (1) the absence of Triton, (2) the process[27] used to remove

---

[27]See Section 8.4.

Template DNA	Case	Taq (units/μl)	Trial (ng/μl)					Avg. (ng/μl)	Std. Dev (ng/μl)
			1	2	3	4	5		
1.9 pM	A	0.1§	88	0	84	62	83	63	37
	B	0.16†	44	11	31	69	46	40	21
	C	0.7†	86	90	91	100	‡	92	5.9
1.9 fM	D	0.1§	24	21	18	15	26	21	4.4
	E	0.16†	30	18	27	23	22	24	4.6
	F	0.7†	16	23	37	27	27	26	7.6

Table 6.4: Experiment to determine effect of centrifugal concentration and removal of Triton X-100 on product variability. All experiments of a given trial number used the same tube of Taq. For example, trial 1 of cases A, B, C, D, E and F used Taq from the same tube. §: Taq was used as supplied by the manufacturer without modification. The PCR mix also contained 0.12% Triton X-100, as recommended by the manufacturer. †: The Triton X-100 was removed from the Taq mix purchased from the manufacturer. ‡: in this instance, there was not enough Taq left to perform this case.

the Triton, as well as (3) the high concentration of Taq result in greater than normal product variability? To find out, I used the control PCR machine to compare mixes both with and without Triton. Table 6.4 shows the results. The amount of template DNA was either 1.9 pM (the concentration used in the 10-cycle experiments) or 1.9 fM (the concentration used in the 30-cycle experiments). The amount of Taq used was either 0.1 units/μl (a typical concentration in a normal reaction), 0.16 units/μl (concentration used in the 10-cycle experiments), or 0.7 units/μl (concentration used in the 30-cycle experiments). Otherwise, the mixes are identical to that described in Section 6.2.

Each trial of a given number used Taq from a given tube. For example, I took a tube of Taq and pipetted some Taq directly into aliquots for trial 1 of cases A & D. These aliquots contained the 0.12% w/v Triton X-100, as recommended by the manufacturer [69]. 20 μl of Taq from the tube was subject to centrifugal concentration

to remove the Triton X-100. The Triton-free Taq was then used to make mixes for trial 1 of cases B, C, E and F. Other than the variation of Taq, template DNA, and Triton X-100, all mixes were as described in Section 6.2. Unfortunately, there was not enough Taq left in Trial 5 to run case C. All aliquots were thermal cycled simultaneously in the control PCR machine as described in Section 6.3.3.

There is a greater difference in average product between cases A, B and C (1.9 pM template) than between cases D, E and F (1.9 fM template). The reason is that in cases D, E and F, the DNA can amplify exponentially for almost all cycles[28]. Taq is not a limiting factor for these cycles, so adding more Taq makes little difference. For cases A, B and C, there is so much initial template that the exponential limit is reached sooner. Thereafter, the amount of DNA increases linearly each cycle, and this amount is directly proportional to the amount of Taq. Also, the more Taq there is, the greater the amount of product possible before exponential amplification ceases.

Cases D and E produce very similar results. The similarity in average yield is explained above. However, I expected case E to have a higher standard deviation. Comparing cases A and B, we see that 0.1 units/μl of Taq with Triton X-100 has greater activity than the *estimated* 0.16 units/μl Taq without Triton X-100. Apparently, the absence and/or removal of the Triton reduces the activity of Taq, which is as expected. Comparing cases A and B, we again see that the standard deviation for

---

[28]In Section 6.2, I calculated that exponential amplification occurs up to the point at which there is 76 ng/μl product when there is 0.7 units/μl Taq (as in case F). In case D, there is 0.1 units/μl Taq, so exponential amplification occurs up to the point at which product is 11 ng/μl, and increases up to 5.3 ng/μl per cycle thereafter. For case E, there is 0.16 units/μl Taq, so exponential amplification occurs up to 17 ng/μl product, and increases up to 8.4 ng/μl thereafter. These numbers may be smaller for cases E and F due to Taq deactivation in the absence of Triton X-100, and lower still in the capillary PCR machine due to the Taq adsorbing to the capillary.

both is roughly the same ($\approx$50% relative of the average), suggesting again that the absence and removal of Triton does not significantly increase variation of Taq activity.

The highest concentration of Taq (0.7 units/μl) results in more product (compare case C to cases A and B) at the expense of greater variability (compare case F to cases D and E). The standard deviation is low for case C because the concentration of product is so high that the concentration of free primer 1, free primer 2, and dsDNA is about the same (all 300 nM), so ssDNA reannealing is a serious competitor to primer annealing. In short, the amount of product has pretty much hit the limit. Therefore, the standard deviation is low.

Case F is the mix used for the 30 cycle temperature optimizations. As we have shown, the absence and removal process of Triton and is not a major factor in product variability. The variability is somewhat higher than that for a standard PCR mix, and this was shown to be due to the greater amount of Taq.

6.5.3   Machine Variability

To compare product variability of the capillary PCR machine to the control machine, I analyzed 9 data points from the three temperature optimizations (T_D = 94°C, T_A = 53°C, and T_E = 70°C for all), and 10 positive controls used in these same reactions (all cycled as described in Section 6.3.3). Results are shown in Table 6.5. The slightly higher average product of the control machine is to be expected due to the longer annealing time used, since extension can take place at this temperature[29]

---

[29]See Table 2.4.

PCR Machine	No. of Datapoints	Product		
		Average	Std. Dev.	(Std. Dev.)/(Avg.)
Capillary	9	8.0 ng/μl	3.1 ng/μl	0.39
Control	10	10 ng/μl	9.5 ng/μl	0.95

Table 6.5: Comparison of capillary PCR machine and control PCR machine. See text for details.

(53°C), albeit slower than at 70°C. The lower standard deviation of the capillary PCR machine may be due to the fast annealing, which helps to prevent misannealing.

The averages for both capillary PCR machine and control machine show lower product averages and higher standard deviations (expressed as a percentage of the average product) than for the experiment detailed in Section 6.5.2. In Section 6.5.2, all of the mixes were made at the same time from the same aliquots of template, primers, dNTPs, etc. The template, primers, and dNTPs were freshly mixed from stock. This was not the case here[30], which accounts for the lower average product and greater product variability.

6.6 Conclusion

Almost 200 successful[31] 30-cycle runs were performed on the capillary PCR machine. Typical efficiencies were 74%[32] for $T_D = 94°C$, $T_A = 53°C$, and $T_E = 70°C$). Efficiency reached as high as 78%[33]. This is comparable to a standard PCR machines, which have a typical reaction efficiency of 70%[34]. However, it only takes about 24 minutes

---

[30]See Section 6.5.1.

[31]Not all data was reported in this work.

[32]Starting template concentration: 1.9 fM. End product concentration: 10 ng/μl (30 nM). 30 cycles. Efficiency = $[(30 \text{ nM})/(1.9 \text{ fM})]^{1/30} - 1 = 0.74$.

[33]See Fig. 6-4, where one datapoint is 22 ng/μl (67 nM) product. Starting template concentration: 1.9 fM. 30 cycles. Efficiency = $[(67 \text{ nM})/(1.9 \text{ fM})]^{1/30} - 1 = 0.78$.

[34]See Chapter 2.

for 30 cycles, rather than the 1–2 hours required by a commercial machine. Further time optimization is possible.

To test the machine, temperature optimization of all 3 PCR steps were performed using the PCR mix listed in Fig. 6.1. The optimal denaturing temperature is 94°C. This is a standard temperature used in commercial thermal cyclers, and is a compromise between denaturation thoroughness and loss of Taq activity, both of which increase with temperature. The optimal annealing temperature was curiously 68°C, the highest temperature tested. The theoretical optimal annealing temperature is around 58°C. The discrepancy is hypothesized to be due to the mix annealing rapidly as it travels in the cool region between the extension and annealing blocks; the annealing block just provides more extension time. The optimal extension temperature was found to be in the 60s, rather than in the 70–80°C range reported in the literature. This was due to the unusual constituency the PCR mix, which had a large concentration of Taq to compensate for sidewall adsorption and no Triton X-100 to maximize the plug/oil surface tension.

The capillary PCR machine requires a larger than normal concentration of Taq in order to compensate to loss via adsorption to the capillary walls. This results in greater mix-to-mix variability in product than would be expected using a more conventional mix[35]. However, the capillary PCR machine itself shows less sample-to-sample product variability than the control PCR thermal cycler (a commercial machine).

---

[35]See Section 10.4.7 for suggestions on how to overcome this problem.

6.7 Nomenclature

T_A Annealing temperature.

T_{ANN} Annealing temperature.

T_D Denaturing temperature.

T_E Extension temperature.

T_m Primer melting temperature.

Chapter 7

Heat Transfer Model

7.1 Introduction

Temperature cycling is performed by moving the sample plug between heat blocks.
The heat block that a plug starts at will be referred to as the *departure* heat block.
The block that the plug subsequently arrives at will be referred to as the *destination*
heat block. It is important to know the temperature history of the sample plug and
oil as they travel between these blocks for the following reasons:

1. A plug can heat or cool as it travels between blocks. This can affect temperature
   equilibration time at the destination heat block.

2. It is possible that the plug temperature can drop to the annealing temperature
   between blocks. This will influence their optimal temperatures.

3. The conditions under which the sample plug breaks into fragments are depen-
   dent on the viscosity of the oil and surface tension of the plug. These properties

0.5"　0.6"　0.5"　0.6"　0.5"

0.5"

Denature　　Extension　　Annealing
Block　　　　Block　　　　Block

Teflon capillary: 1 mm I. D. and 1/16" O. D.

Heat blocks made out of aluminum
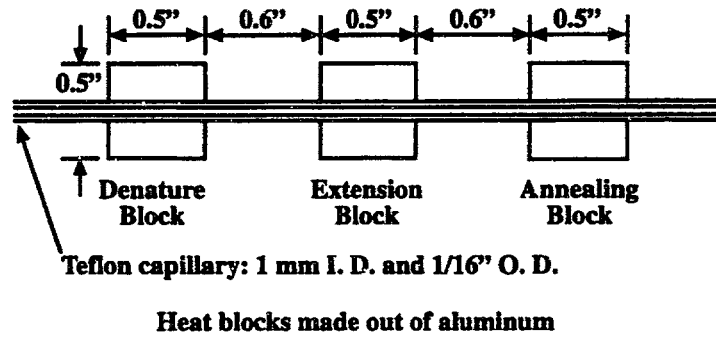
Figure 7-1: Some relevant machine dimensions used in the model.

vary with temperature.

Therefore, I developed a rudimentary model to estimate this history.

7.2 Model Development

7.2.1 Dimensions

Figure 7-1 shows some important dimensions used in the model formulation.

7.2.2 Constant Capillary Temperature

The capillary has a 1/16" outer diameter and 1 mm inner diameter. Therefore, the outer (1.2 mm^2) is roughly the same as the inner (0.8 mm^2) cross-sectional area. From Table 7.1, we see that the product of density and heat capacity of Teflon is much greater than that of mineral oil or sample plug fluid[1] in the temperature range of interest (20°C room temperature to 94°C at the hottest heat block). This suggests that as the plug moves from block to block, the fluid motion has very little effect on

---

[1]The plug fluid is assumed to have approximately the same density and heat capacity as water.

138

Material	ρc_p in J/(m³·K)
Teflon	1.1×10^6
Mineral Oil	1.8×10^6
Plug Fluid (water)	4.2×10^6

Table 7.1: Values of ρc_p for Teflon, mineral oil, and water in the 20–90°C range. Also see Appendix A.

$V = 0.030$ m/s
time = 1.9 s
$T_{\text{Teflon}} = 53°C$

If $T_{\text{in}} = 20°C$, $\Delta T_{\text{Teflon}} = -0.7°C$
$T_{\text{in}} = 94°C$, $\Delta T_{\text{Teflon}} = 0.9°C$
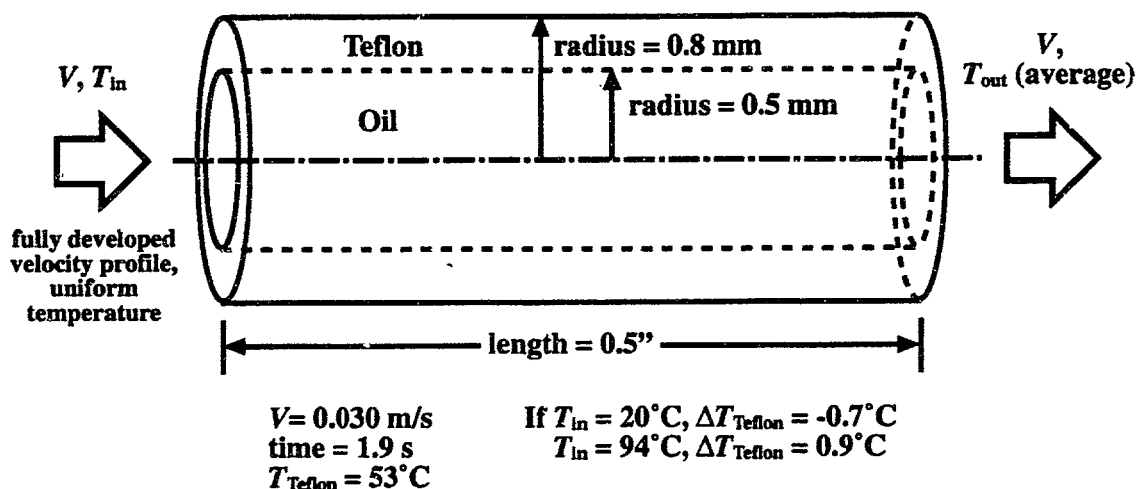
Figure 7-2: Schematic of the model used to estimate the temperature change of the capillary within the annealing block, which is 0.5" long. V is the average velocity of the oil. T_{in} is the uniform temperature (a modelling assumption) of the oil entering the capillary portion, and T_{out} is the average temperature of the fluid exiting it. T_{Teflon} is the temperature of the capillary, modelled as being uniform within the capillary region of interest.

the capillary temperature.

I used a simple model to estimate how much the temperature of the capillary inside of the annealing block changes as the plug travels from the denaturing to the annealing block (see Fig. 7-2). The annealing block was chosen rather than the denaturing or extension blocks since the plug travels about twice as far to reach the annealing block as it does to reach either of the other two blocks during PCR. There is more oil preceding the plug that can change the temperature of the capillary. The regions between the blocks were not chosen in the simple estimation since their

temperatures vary along the capillary axis, and are also not as well known.

The temperature of the capillary inside of the annealing block was taken to be 53°C, which is a typical annealing temperature[2]. The average velocity of the oil in the tube was taken to be[3] 0.030 m/s, based on experimental results. Since the plug moves a total distance of[4] 2.2 inches from the center of the denaturing block to the center of the annealing block, this corresponds to 1.9 seconds of travel[5]. The heat block is modelled as a perfect insulator, conservatively neglecting the heat input from the cartridge heater. The oil is modelled as entering the portion of the capillary inside of the annealing block at a constant temperature and with a fully developed parabolic velocity profile.

The temperature of the oil entering the annealing block cannot be cooler than room temperature (20°C) or hotter than the temperature of the denaturing heat block (94°C). The simple model[6] predicts that the average temperature of the oil exiting the annealing block is 75°C if it enters at 94°C, and 37°C if it enters at 20°C. If we take the temperature of the capillary inside of the annealing block to be uniform, we calculate that it increases 0.9°C if the oil enters at 94°C and -0.7°C if the oil enters at 20°C. This is a small change. Since the actual oil entering the block falls between 20°C and 94°C, the actual capillary temperature change will be much lower. Therefore, I decided to model the temperature of the capillary as constant.

---

[2]See Chap. 6.

[3]See Table 7.3.

[4]Each heat block is 0.5 inches long. There is a 0.6 inch distance between adjacent heat blocks.

[5]Plug acceleration and deceleration were neglected. In any event, plug acceleration to full speed takes place within 70 ms seconds, as does deceleration to a full stop. See Section 9.2.2.

[6]See Section 7.6.1.
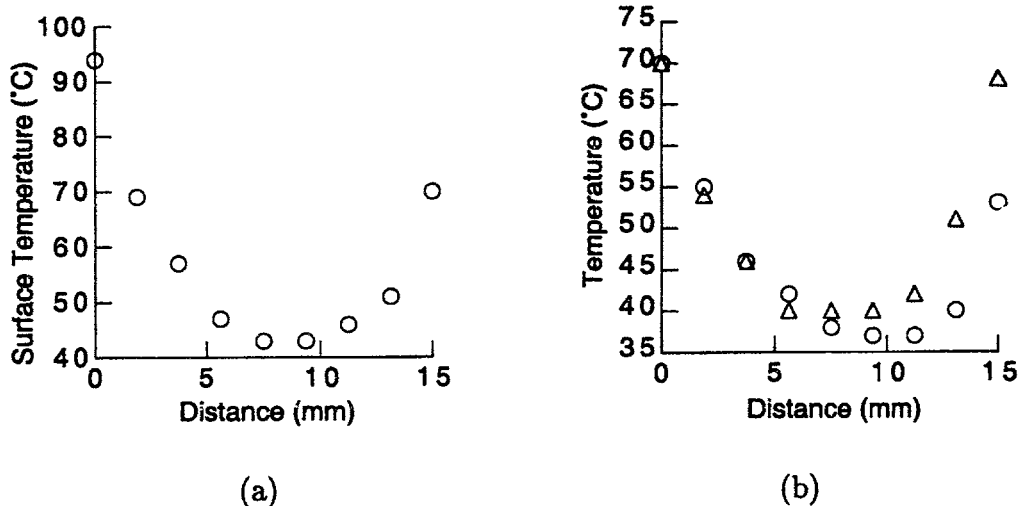
Figure 7-3: Capillary surface temperatures measured between heat blocks. (a) Between 94°C denature and 70°C extension blocks. (b) Between 70° extension and anneal blocks. △ is for anneal block at 68°C. ◯ is for anneal block at 53°C.

This simplified modelling greatly.

7.2.3 Surface Temperature Measurements

The capillary surface temperature between blocks was measured using a K-type thermocouple[7]. Results are presented in Fig. 7-3. Results for annealing block temperatures of both 53°C and 68°C are presented. These represent the typical and upper end of annealing temperatures used in my experiments. Approximating the temperature distribution as piecewise linear, the average temperature between the 94°C and 70°C blocks is 55°C; between the 70°C and 68°C blocks, 48°C; and between the 70°C and 53°C blocks, 45°C.

The thermocouple was fashioned from 36 gauge wire and was insulated along most of its length. Since (1) its size (36 gauge is 0.005" diameter) is much smaller than that

---

[7]Item # 5SC-TT-K-36-72. Omega Engineering, Inc. Stamford, CT.

of the capillary (0.063" diameter); (2) the thermocouple was insulated along most of its length (reducing its effectiveness as a fin); and (3) the thermal conductivity of Teflon is much lower than that of the thermocouple wire, it is assumed that the measurement itself did not affect the temperature readings significantly. A small amount of oil was used at the point of contact to ensure good heat transfer to the thermocouple.

Since there is very little distance (0.3 mm) between the inner and outer surfaces of the capillary, it was suspected that the two were essentially the same temperature. Heat transfer models were constructed to see if this was the case. In fact, it was.

7.2.4 Sources of Heat

Figure 7-4 is a drawing of the device near the region in which PCR occurs. Heat transfer with the capillary includes the following:

- Heat provided by the heat blocks via conduction.
- Convection to the surrounding air.
- Radiative heat provided by the laser.
- Radiative heat from the heater blocks, heaters, guard wire, base, etc.

7.2.5 The Laser

The laser is a 20 mW Helium-Neon laser (wavelength 632.8 nm). While its power output is substantial, it does not significantly heat the system. Absorption of Teflon in the 632.8 nm range is very low [82, p. 42]. Absorption in this wavelength by mineral
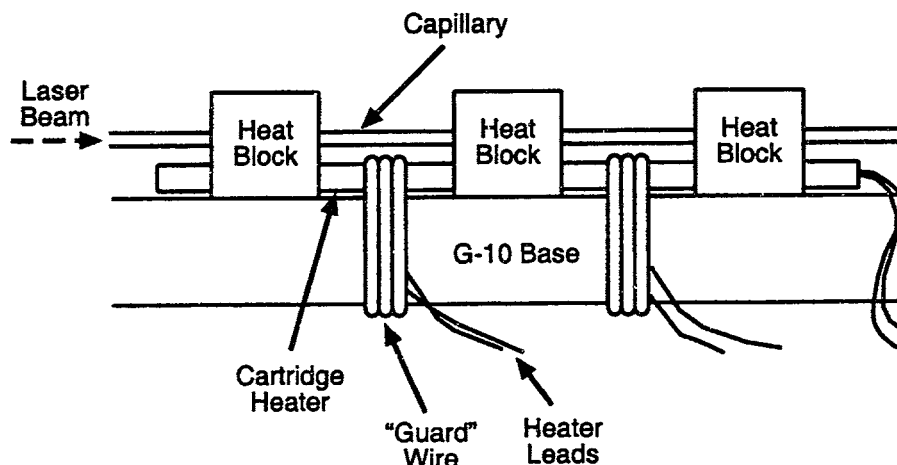
Figure 7-4: Drawing of the device in the vicinity of the heaters. The three heat blocks are epoxied onto a base of G-10 composite. Each heat block is a 1/2" cube of aluminum with holes for the capillary, cartridge heater and thermocouple. There is 0.6" spacing between blocks. Since each of the three cartridge heaters is 0.5" long, the lengths of the capillary between blocks are in close proximity to the heaters. The heater leads are very fine, so wire was wrapped around the ends of the heaters to protect them from breakage. The laser beam enters the capillary from the left, and waveguides down its length.

oil or a typical PCR mix[8] was not detectable on a commercial spectrophotometer[9].

In addition, the capillary surface temperature, as measured by a thermocouple, did

not change significantly in the presence or absence of the laser.

7.2.6 Heat Blocks

Each heat block was modelled as being at a uniform temperature. According to

Kreith and Bohn [44, p. 73], this assumption is justified if the Biot number is very

---

[8]Mix consisted of 10 mM Tris-HCl (pH 9.0 at 25°C), 50 mM KCl, 0.1% Triton X-100, 2 mM MgCl$_2$, 300 μM each of the four dNTPs, 60 pg/μl genomic λ phage DNA, 0.6 pmol/μl forward primer (24 bases), 0.6 pmol/μl reverse primer (24 bases), and 0.1 units/μl Taq DNA Polymerase.

[9]Model UV-1601. Shimadzu Scientific Instruments, Inc. Columbus, MD.

small. The Biot number is defined as

$$Bi = \frac{h_b l}{k_b} \qquad (7.1)$$

where h_b is the coefficient of convection from the heat block to the surrounding air; k_b is the coefficient of conduction inside the heat block; and l is a characteristic length of the heat block. Relations presented by King [39] were used to find h. From this reference, l is defined as follows:

$$\frac{1}{l} = \frac{1}{l_{horiz.}} + \frac{1}{l_{vert.}} \qquad (7.2)$$

where $l_{horiz.}$ and $l_{vert.}$ are the horizontal and vertical dimensions of the object in question, respectively. Since each heat block is a 1/2" cube, $l_{horiz.} = l_{vert.} = 0.5"$, and $l = 6$ mm. King's correlation, presented in Fig. 7-5, provides the Nusselt number as a function of the product of the Grashof and Prandtl numbers. The Nusselt number is

$$Nu = \frac{h_b l}{k_a} \qquad (7.3)$$

where k_a is the thermal conductivity of air. The Grashof number is

$$Gr = \frac{g \beta_a (T_b - T_\infty) l^3}{\nu_a^2} \qquad (7.4)$$
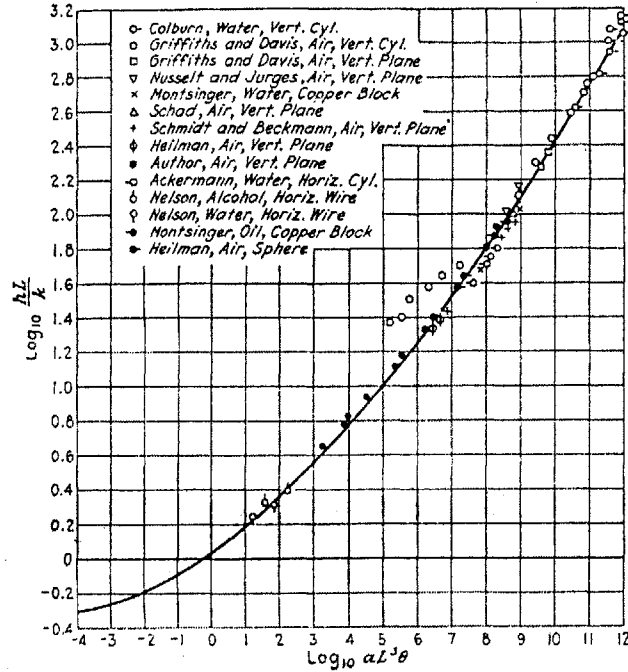
Figure 7-5: Convection data presented by King [39]. The x-axis parameter, $aL^3\theta$, is defined such that it is the product of the Grashof and Prandtl numbers, GrPr. The y-axis parameter hL/k is the same as the Nusselt number, Nu.

where g is gravitational acceleration, β_a is the coefficient of expansion of air, T_b is the surface temperature of the heat block, T_∞ is the temperature of the air far from the blocks, and ν_a is the kinematic viscosity of the air. The Prandtl number is

$$\mathrm{Pr} = \frac{\nu_a}{\alpha_a} \tag{7.5}$$

where α_a is the thermal diffusivity of air. The heat blocks typically range from 53°C (annealing block) to 94°C (denaturation block). In this range, the product[10] GrPr = 650–1100. From Fig. 7-5, Nu $\approx$ 3.5. Bi = Nu $\times (k_a/k_b) \approx 5 \times 10^{-4} \ll 1$. Therefore, the heat blocks are justifiably modelled as isothermal.

---

[10]The product GrPr is also known as the Rayleigh number, Ra.

145

Could the flow of mineral oil affect heat block temperature? Not significantly. Assuming a worst case scenario of instantaneous thermal equilibration and 20°C oil, the motion of the plug between the rightmost and leftmost block will produce a maximum heat block change[11] of 1°C. Of course, the temperature of the oil entering the heat block is actually significantly higher than 20°C, and there is constant heat input from the cartridge heaters to maintain temperature, so this calculation is an overestimation.

7.2.7 Natural Convection

The general relation presented by McAdams [49, p. 243] was used to determine the coefficient h for natural convection from the capillary to air. Fig. 7-6 shows McAdam's correlation, which is based on a wide variety of data on natural convection from horizontal cylinders to gasses and liquids. The correlation is for isothermal horizontal cylinders. However, it was assumed to apply to the present case in which the surface temperature varies axially. The cylinder surface temperature was taken to be the average surface temperature. The air properties were determined at a temperature halfway between this surface temperature and T_∞. The resulting h was applied to the entire capillary surface between two heat blocks.

Although room temperature was 20°C, the heat blocks and heaters made the air temperature in the vicinity of the capillaries higher. In essence, the capillary is within the thermal boundary layers of the blocks and heaters. Hence, T_∞, the value

---

[11]Using material properties presented in Appendix A.

146
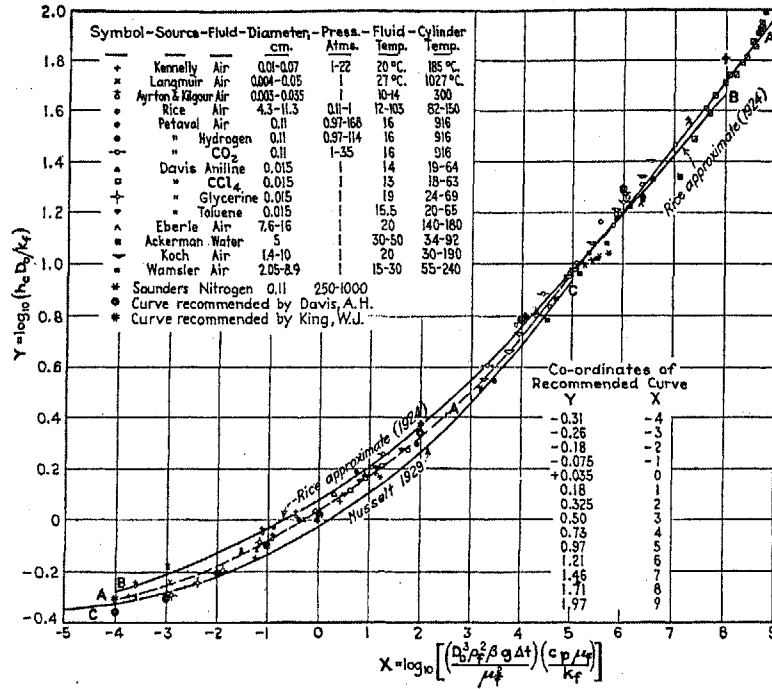
Figure 7-6: Natural convection from horizontal cylinders to gasses and liquids. From McAdams [49, p. 243]. The x-axis coordinate may be expressed as $\log_{10}(\mathrm{GrPr})$, and the y-axis coordinate may be expressed as $\log_{10}(\mathrm{Nu})$.

Heat Blocks	T_∞
94°C and 70°C	35°C
70°C and 68°C	28°C
70°C and 53°C	28°C

Table 7.2: Values of T_∞ used for calculations of natural convection from the portion of capillary between the heat blocks to air. Measured experimentally by thermocouple approximately 5 mm above the capillary surface.

of the temperature of the air "far" from the capillary (for purposes of convection calculations), was measured about 5 mm from the capillary. Results are shown in Table 7.2.

When the plug was stationary, convection in the oil was ignored, since the capillary inner diameter is small and there was no overall pressure difference across the tube. Heat flow through the oil was modelled solely via conduction.

147

7.2.8 Radiation

Radiative heating of the capillary via heat blocks, heaters, etc. is difficult to model. View factors can be difficult to calculate. The radiation sources heat different parts of the capillary to different degrees. Material absorptance and emittance values are complex functions of wavelength, and even spectrally averaged values are difficult to aquire for many materials (such as Teflon).

Since radiation was difficult to model, it was neglected in the preliminary analytical model. The subsequent finite element model incorporates radiation, modelling it as affecting the outer surface of the capillary evenly.

7.2.9 Steady State Analytical Model

As mentioned in Section 7.2.8, radiation is difficult to model. Initally, I created a simple analytical model that did not account for radiation to see if the temperature distribution was similar to that found experimentally. If the two matched well, I could use the model to estimate the temperature distribution at $r = r_o$.

The model consists of a hollow cylinder of length L, inner radius r_o (the subscript denotes oil), and outer radius r_t (the subscript denotes Teflon). From the device geometry, $r_o = 5 \times 10^{-4}$ m, $r_t = 8 \times 10^{-4}$ m, and $L = 0.015$ m. The axial and radial coordinates of the cylinder are denoted by x and r, respectively. At $x = 0$, the capillary comes into contact with a heat block at temperature T_1. At $x = L$, it comes into contact with a different heat block at temperature T_2. This was modelled via the following boundary conditions: at $x = 0$, $T = T_1$ for all r. At $x = L$, $T = T_2$ for

all r.

The cylinder is subject to a convection boundary condition at $r = r_t$. h was figured as described in Section 7.2.7.

I wanted to model the conduction in the oil. However, the requirement of temperature and heat flux continuity at $r = r_o$ is difficult to solve analytically. In the temperature range of interest (20°C room temperature to 94°C at the hottest heat block), the thermal conductivity of Teflon (0.395–0.431 W/(m·K)) is roughly three times that of oil (0.13–0.14 W/(m·K)). Therefore, in order to simplify the problem, the oil was modelled as a perfect insulator. This created a zero heat flux boundary at $r = r_o$.

The solution to this problem is derived in Section 7.4. It is:

$$T = T_\infty + \sum_{n=1}^{\infty} \frac{2r_t hkU(\lambda_n r_t)U(\lambda_n r)[(T_2 - T_\infty)\sinh(\lambda_n x) + (T_1 - T_\infty)\sinh(\lambda_n(L - x))]}{[r_t^2(\lambda_n^2 k^2 + h^2)U^2(\lambda_n r_t) - r_o^2\lambda_n^2 k^2 U^2(\lambda_n r_o)]\sinh(\lambda_n L)}$$

$$(7.6)$$

where k is the thermal conductivity of Teflon, and[12]

$$U(\lambda_n r) = J_0(\lambda_n r)Y_1(\lambda_n r_o) - J_1(\lambda_n r_o)Y_0(\lambda_n r)$$

J_0 and J_1 are the Bessel functions of the first kind of order zero and one, respectively; and Y_0 and Y_1 are the Bessel functions of the second kind of order zero and one,

---

[12]See (7.29,7.31).

149

respectively. The λ_n are values of λ which satisfy

$$k\lambda[J_1(\lambda r_t)Y_1(\lambda r_o) - J_1(\lambda r_o)Y_1(\lambda r_t)] = h[J_0(\lambda r_t)Y_1(\lambda r_o) - J_1(\lambda r_o)Y_0(\lambda r_t)]$$

From (7.6), $\overline{T}|_{r_t}$ averaged over $0 \leq x \leq L$ is

$$\overline{T}|_{r_t} = T_\infty + \sum_{n=1}^{\infty} \frac{2r_t hkQ_n[T_1 + T_2 - 2T_\infty][\cosh(\lambda_n L) - 1]}{L\lambda_n \sinh(\lambda_n L)} \tag{7.7}$$

where

$$Q_n = \frac{U^2(\lambda_n r_t)}{[r_t^2(\lambda_n^2 k^2 + h^2)U^2(\lambda_n r_t) - (r_o\lambda_n kU(\lambda_n r_o))^2]} \tag{7.8}$$

The value of T averaged over both $r_o \leq r \leq r_t$ and $0 \leq x \leq L$ is

$$\overline{T} = T_\infty + \frac{4(r_t h)^2}{(r_t^2 - r_o^2)L}(T_1 + T_2 - 2T_\infty)\sum_{n=1}^{\infty} \frac{Q_n[\cosh(\lambda_n L) - 1]}{\lambda_n^3 \sinh(\lambda_n L)} \tag{7.9}$$

Since the properties of air and Teflon vary with temperature, the temperature distribution was solved iteratively using commercial numerical software[13]. As a first guess, both $\overline{T}|_{r_t}$ and $\overline{T}$ were assumed to be the average of T_1 and T_2. The properties of air were taken at the average of $\overline{T}|_{r_t}$ and T_∞, and were used to find h. $\overline{T}$ was used to find k. h and k determined the first ten λ_n values, which were used to establish a new temperature distribution for the cylinder. The process was repeated 6 times. Convergence of $\overline{T}$ and $\overline{T}|_{r_t}$ to 6 decimal places was achieved after 3 cycles.

---

[13]MATLAB Version 5.3.0; The Mathworks, Inc., Natick, MA.

Results of the analytical model are shown in Fig. 7-7. Note that there is practically no difference between the temperatures at r_o and r_t. At first glance, the "+" and "×" symbols are so close together that they appear as a single asterisk. If the model and experimental temperature distributions were very similar, I could conclude that the temperatures at $r = r_o$ and $r = r_t$ were practically the same.

However, the model underpredicts the temperature. This is due to a combination of several factors. Use of a single Nu across the whole tube overestimates heat transfer in the middle of the capillary. There the temperature difference (as measured experimentally) between the surface and the air is small. Nu increases monotonically with GrPr (see Fig. 7-6). Pr is constant (0.71) in the temperature range of interest. Gr is proportional to the temperature difference between the capillary surface and air, so Nu and hence h should be lower in this region. In addition, the model completely neglects the contribution of radiation, as well as heat coming from the oil inside the capillary.

7.2.10 Finite Element Model

To get better matching between experimental and model surface temperatures, a finite element model was constructed using ADINA, a commercial finite element package[14]. The model consists of two concentric cylinders of length $L = 0.015$ m. The inner radius is $r_o = 5 \times 10^{-4}$ m and the outer radius is $r_t = 8 \times 10^{-4}$ m, as before.

The boundary conditions were similar to those used in the analytical model. At

---

[14]ADINA 7.3.1. ADINA R & D, Inc. Watertown, MA.

Figure 7-7: Results of the steady state analytical model. + indicates temperature at the inner radius r_o. × indicates temperature at the outer radius r_t. o is the experimentally measured surface temperature. (a) Temperature of capillary between 94°C and 70°C blocks. (b) Temperature of capillary between 70°C and 53°C blocks.

$x = 0$, the temperature is T_1 for all r. At $x = L$, the temperature is T_2 for all r.

Heat transfer within the cylinders takes place solely by conduction. The solid inner cylinder has the same thermal conductivity as oil. The hollow outer cylinder has the same thermal conductivity as Teflon. Teflon and oil thermal conductivities were based on the average experimentally determined surface temperatures (see p. 141). They are 0.41 W/(m·K) for Teflon and 0.14 W/(m·K) for oil for both the ($T_1 = 94°C$, $T_2 = 70°C$) case and the ($T_1 = 70°C$, $T_2 = 53°C$) case. Basing these values on the experimental *surface* temperatures assumes that there is not a substantial temperature difference between $r = r_o$ and $r = r_t$. As will be seen, this assumption was verified by the model. There is temperature and heat flux continuity at the interface ($r = r_o$) of the two cylinders.

At $r = r_t$, the model is subject to both convection and radiation. T_∞ for convection is based on values shown in Table 7.2. The convection coefficient h was calculated using T_∞ and the average experimental surface temperature. As with the thermal conductivities, it turned out that $h = 23$ W/(m·K) for both the ($T_1 = 94°C$, $T_2 = 70°C$) case and the ($T_1 = 70°C$, $T_2 = 53°C$) case.

ADINA allows two parameters to be specified for radiation: the emissivity of the model surface, and the temperature of the environment (assumed to be a blackbody). The emissivity was estimated as 0.9, based on values for other nonconductive materials [52, p. 77, 108]. The radiation environmental temperature was adjusted to around 60° to match the minimum surface temperature with that observed experimentally. At this point, I feel that the model heat flux at the surface is a good approximation of the actual heat flux.
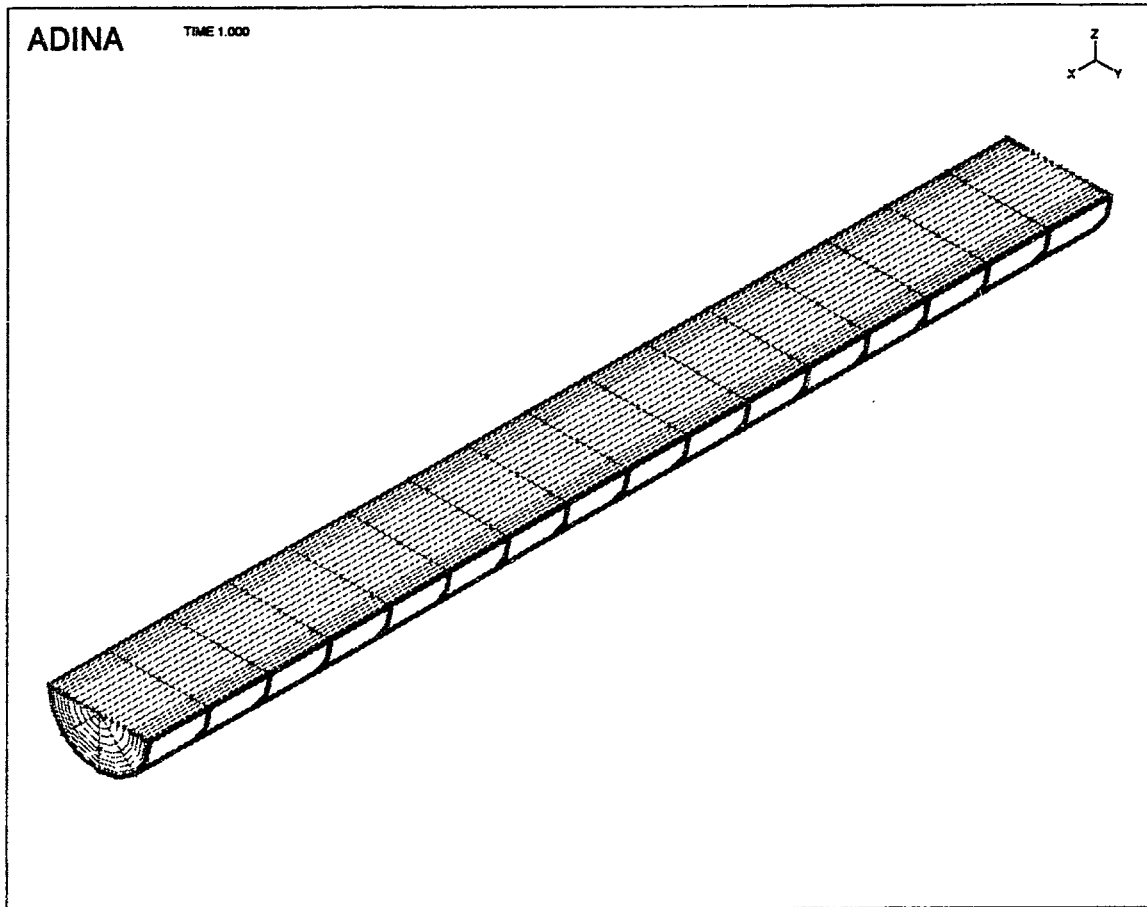
Figure 7-8: Finite element model geometry. The model is radially symmetric, so only half of the cylinder is simulated.

The model geometry is shown in Fig. 7-8. The temperature distribution is modelled as radially symmetric. In order to simplify the model, only half of the cylinders are included, with a symmetry boundary condition (zero heat flux) at the axial midplane. The two concentric half cylinders have 320 elements each. Each element has 20 nodes. The elements divide each half cylinder equally into 16 parts along the x axis, 5 parts along the r axis, and 4 parts along the θ axis. There are no temperature discontinuities across element borders, indicating that the subdivisions are sufficiently fine.

The results are shown in Fig. 7-9. While the match is not perfect, it is reasonably close. The temperature difference between $r = r_o$ and $r = r_t$ in the model is practically nonexistent. This was also the case in the analytical model. Therefore, I assumed that this temperature difference is negligible in the actual capillary.

7.2.11 Fluid Speed

To calculate the heat transfer to the sample plug when the plug is in motion, one needs to know its speed. The speed is determined by the pressures at the ends of the capillary. Each of the capillary ends is connected via a manifold to a set of solenoid valves. The solenoid valves can be opened to set each manifold to a number of different pressures. The pressures are set upstream of the valves.

For almost all of the PCR experiments, these pressures were set to 5 and 7.5 psig with regulators, resulting in ≈2.5 psi pressure difference across the capillary. However, the pressures drop somewhat along the paths from regulator to manifold. I connected a differential pressure gauge in parallel with the capillary to get a better measure of the pressure difference across the capillary. It was 2.9 psi when the fluid moved from right to left, and 2.2 psi when the fluid moved from left to right. The discrepancy is due to the different aperture sizes in the solenoid valves used.

To measure fluid velocity, the capillary was set up as it would be in a PCR run: it was filled with oil and passed through three heat blocks set at typical run temperatures (94°C, 70°C and 53°C). The right end of the capillary was coupled to the right pressure manifold, as usual. The left end was left open to atmosphere.
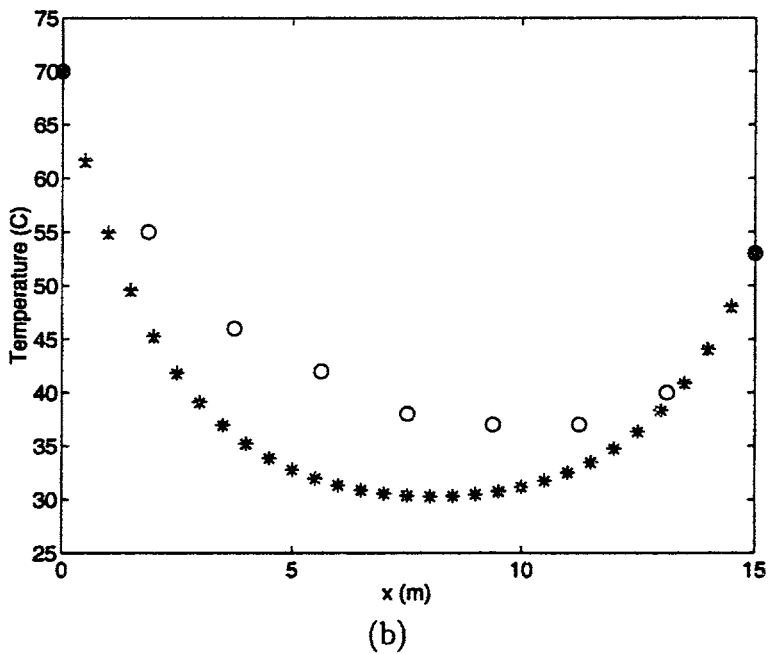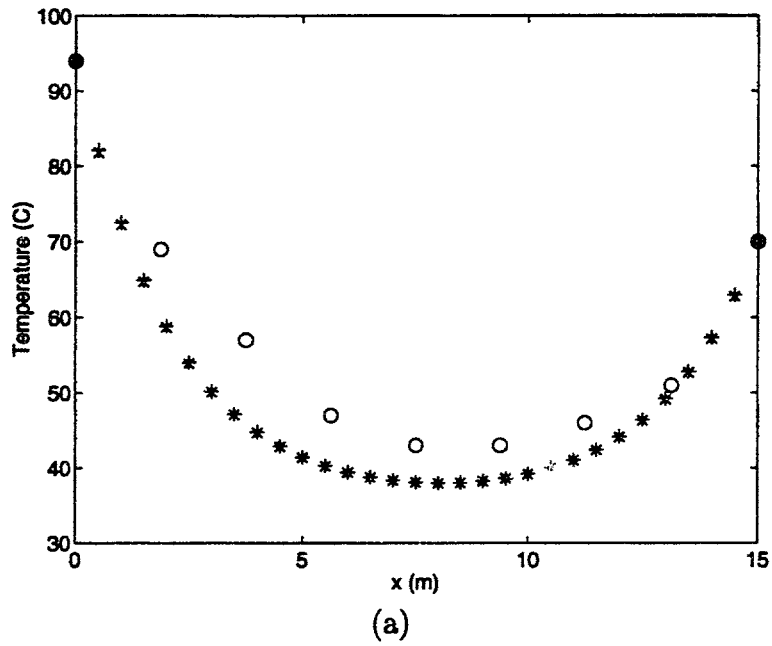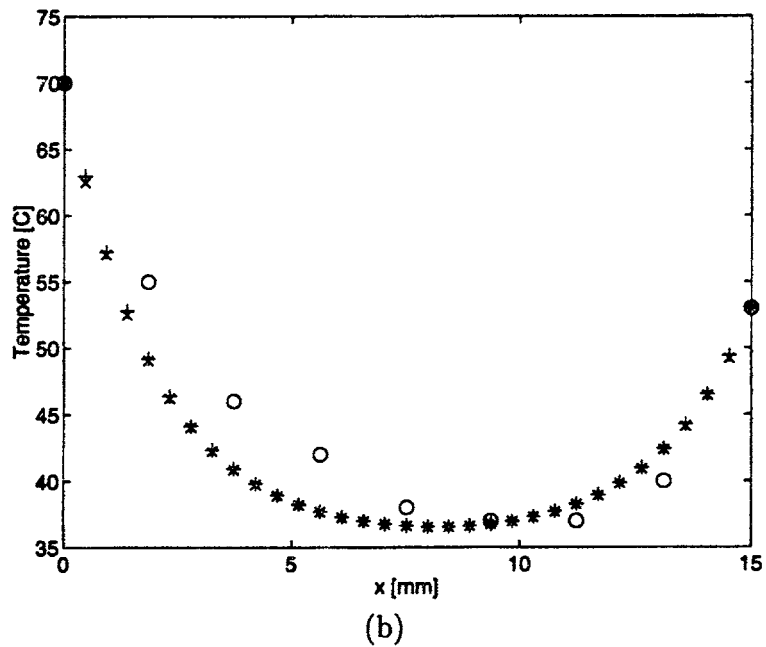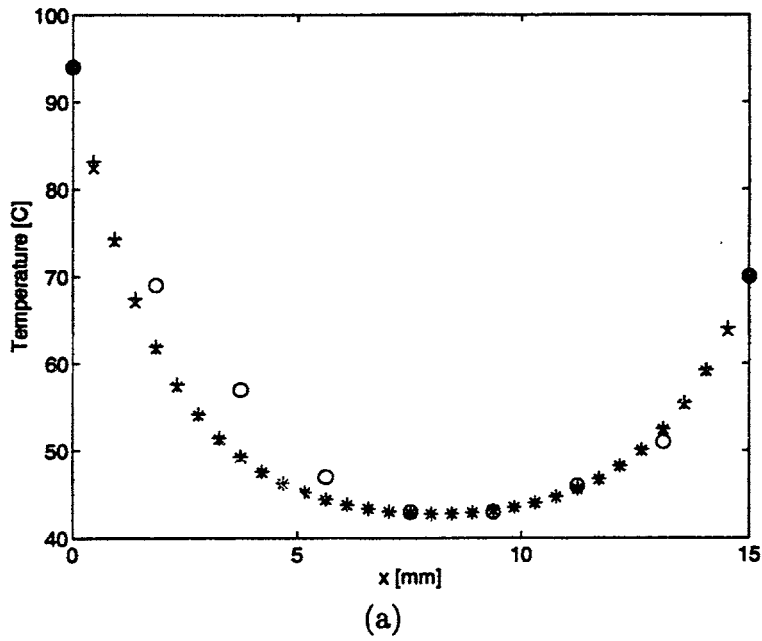
Figure 7-9: Results of the steady state finite element model. + indicates temperature at the inner radius r_o. × indicates temperature at the outer radius r_t. ○ is the experimentally measured surface temperature. (a) Temperature of capillary between 94°C and 70°C blocks. (b) Temperature of capillary between 70°C and 53°C blocks.

Oil Motion	Trials: $\Delta m/\Delta t$ (g/s)	Avg. $\Delta m/\Delta t$ (g/s)	Avg. Speed (m/s)
right to left, oil only	0.026, 0.025, 0.023, 0.025	0.025	0.037
right to left, oil with plug	0.025, 0.022, 0.020, 0.020	0.022	0.033
left to right, oil only	0.021, 0.020, 0.020	0.020	0.030
left to right, oil with plug	0.018, 0.019, 0.019, 0.016	0.018	0.027

Plug Motion	t's (s to travel 15 cm)	Avg. Speed (m/s)
right to left	0.041, 0.043, 0.044, 0.048	0.045
left to right	0.031, 0.038, 0.038, 0.041	0.037

Table 7.3: Fluid speed measurement data.

Initially, the right manifold was also open to the atmosphere. Then the manifold was pressurized to either 2.2 or 2.9 psi, depending on whether I wanted to measure left to right or right to left fluid speed. I waited about one second before taking measurements to allow the oil to reach steady state speed.

The sample plug speed was measured by using a stopwatch to record the amount of time it took to travel 15 cm. To measure oil speed, the oil was collected in a pre-weighed microfuge tube. This was performed both in the presence and absence of a sample plug. In the former case, oil was collected $\approx$10 seconds. In the latter case, it was collected $\approx$3 seconds. This produced a less accurate result, but any longer and the plug would exit the left end of the tube. Collection times were taken with a stopwatch. The collected oil was weighed. The quotient of oil mass divided by collection time was averaged over several trials. Oil velocity was determined using this average, r_o, and the density of oil.

Results are shown in Table 7.3. Oil speeds were a hair lower in the presence of the plug, but this could easily be attributable to experimental error and difference in measurement protocols, particularly given the crude nature of the velocity measurements. The plug itself moves slightly faster than the bulk flow of oil. This to

be expected since the average speed of fluid in the center is higher than that at the edges in fully developed laminar flow through a tube. This effect is widely reported in reported in slug flow literature[15].

7.2.12 Convection Model

From the results of the analytical and finite element models (Sections 7.2.9 and 7.2.10), I was confident that the temperature of the capillary did not vary appreciably from $r = r_o$ to $r = r_t$. The experimental measurements of the outer surface[16], coupled with the modelling assumption of constant capillary temperature over time[17], provided a constant inner wall temperature distribution. Coupled with a basic forced convection model, this produced a rough time-temperature history of the plug and oil.

The temperature distribution at the wall ($r = r_o$) is modelled as radially symmetric. The axial temperature distribution is based on the experimental surface measurements. I approximated the temperature between these points as linear, resulting in a piecewise linear distribution. Since the experimental measurements were taken at increments of $L/8 = 1.875$ mm, I used this as the Δx for my model. The 1/2" heat blocks were approximated as $7\Delta x = 13.125$ mm long.

The actual flow field inside and around the sample plug is very complex. To estimate the plug temperature, I assumed it fell somewhere between the temperatures of only oil and only water flow. The fluid exiting a departure block is modelled as

---

[15]See [62], for example.
[16]See Section 7.2.3.
[17]see Section 7.2.2.

being at a uniform temperature equal to that of the block.

At this point, it is useful to calculate Re for the flow. The oil is $\geq 20°C$ (room temperature) and $\leq 94°C$ (hottest heat block). Therefore, from Appendix A, we see that the range of kinematic viscosity of the oil is 9.9–204 centistokes (9.9×10^{-6} to 2.04×10^{-4} m^2/s). From Table 7.3, we see that the plug speed is slightly higher than the bulk flow speed. I modelled fluid speed as the average of the experimentally determined plug and oil speeds: 0.041 m/s for right-to-left flow, and 0.033 m/s for left-to-right flow. The fluid is assumed to start at the departure heat block and travel to the middle of the destination heat block. Acceleration of the fluid is was assumed to occur completely in the departure heat block, so its velocity is constant. The inner diameter of the capillary is 1 mm. Using the speeds, kinematic viscosities, and diameter listed above, Re is calculated as 0.16–4.1.

Since Re $\ll$ 2300, the flow is clearly laminar[18]. The velocity profile of the fluid is fully developed at a distance $\geq 0.06(2r_o)(\text{Re})$ from a capillary end[19]. Assuming that the temperature at the ends of the capillary is 20°C, this is only 24 μm. This is a ridiculously small number, due to the small Re. In any case, the region of the capillary in which PCR takes place is at least 60 mm, or 60 inner diameters, away from the capillary ends. Clearly, the velocity profile is fully developed.

It is also necessary to find the product RePr. Using Appendix A, the fluid velocities 0.041 and 0.033 m/s (see above), and a temperature range of 20–94°, RePr is calculated as 200–290 for water, and 390-600 for oil.

---

[18]See, for example, [22, p. 332].

[19]Fully developed flow criteria from [22, p. 333].

Details of the math behind the convection model are presented in Section 7.6. Briefly, I start with the differential equation expressing conservation of energy. After nondimensionalizing, it is noted that the axial conduction term is proportional to $1/(RePr)^2$. Since $RePr > 100$, axial conduction can be ignored[20]. Using the velocity profile for fully-developed laminar flow, the change in temperature due to a step change (across x) in pipe temperature is derived. This is used to find the heat flux distribution on the inside of the capillary for the piecewise linear temperature distribution. Since axial conduction is negligible, the mean fluid temperature as a function of x is derived from the heat flux distribution.

The model is realized numerically using MATLAB. The temperature of the fluid averaged over the flow path is given an initial value. The model uses this temperature to define the fluid properties. The temperature distribution is then found, and averaged to get a more accurate mean temperature. The process is repeated until the average temperature changes by less than 1°C.

7.2.13   Transient Radial Conduction

Once the plug reaches the middle of the destination block, the pressure differential across the capillary is removed, arresting plug motion. The plug resumes its original shape, filling the capillary from $r = 0$ to $r = r_o$.

Since the plug is stationary, heat transfer to the plug is considered to be completely by conduction. Axial conduction is assumed to be negligible relative to radial

---

[20]See [37, p. 128].

160

conduction[21]. The cylinder is modelled as being at a uniform initial temperature T_3 and subject to a constant T_4 at $r = r_o$.

This simple problem has long been solved. The solution presented by Carslaw and Jaeger [12] is derived in Section 7.5. The solution is[22]:

$$T = T_4 + \frac{2(T_3 - T_4)}{r_o} \sum_{n=1}^{\infty} \frac{J_0(\lambda_n r)}{\lambda_n J_1(\lambda_n r_o)} e^{-\lambda_n^2 \alpha t} \qquad (7.10)$$

where

$$J_0(\lambda_n r_o) = 0$$

I let T_3 be equal to the mean plug temperature when the plug reaches the middle of the destination block. This is determined from the convection model. The sample plug is considered to have reached the desired temperature T_4 when $T|_{r_o}$ is within 0.5°C of T_4. This is a conservative estimate. In most commercial PCR machines, the desired temperature is assumed to be reached when the device temperature is within 0.5°C of the desired temperature. However, this temperature is measured at an arbitrary location in the heat block, and there is some time lag before the temperature at the middle of the sample catches up.

The equation listed above was solved for t numerically using the first 10 λ_n on MATLAB. Actually, there was no difference in t calculated using $1 \leq n \leq 2$ and using $1 \leq n \leq 10$, since terms associated with $n > 1$ drop off quickly relative to the

---

[21]This presumption is validated in Section 7.3.
[22]See (7.59) and (7.66).

161
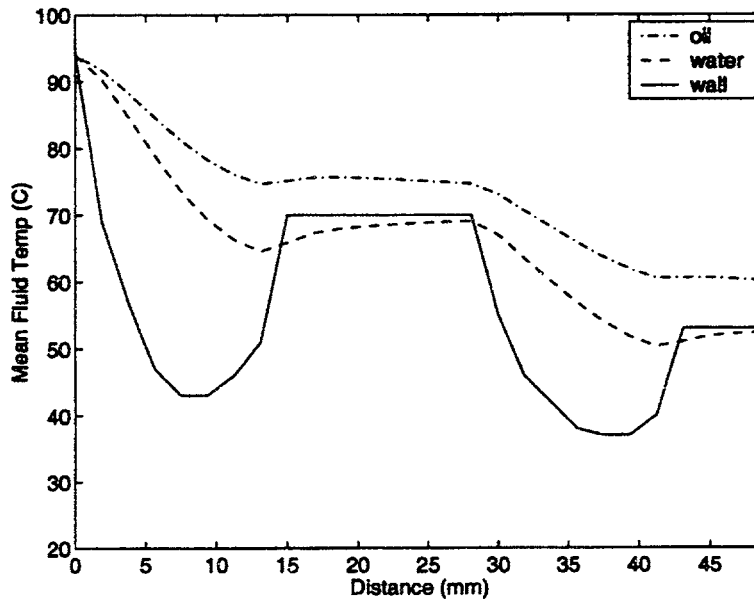
Figure 7-10: Temperature as plug moves to the right (increasing x), from denaturation to annealing block, at 0.033 m/s. Temperature of the plug is assumed to lie somewhere inbetween the temperatures shown for oil and water. Temperatures of the denaturation, extension, and annealing blocks are 94°C, 70°C, and 53°C respectively.

$n = 1$ term as time progresses. This confirms that T approximated using only the $1 \leq n \leq 10$ terms is sufficient.

7.3 Results

This section presents results for typical heat block temperatures of 94°C, 70°C, and 53°C for denaturation, extension, and annealing, respectively. As reported in Section 7.2.11, the fluid speed was taken as 0.033 m/s from left to right (denature to annealing), and 0.041 m/s from right to left (annealing to extension, and extension to denaturation). Figs. 7-10, 7-11, and 7-12 show the temperatures of oil and water as a function of x. As explained in Section 7.2.12, the plug temperature is assumed to lie inbetween the water and oil temperatures.
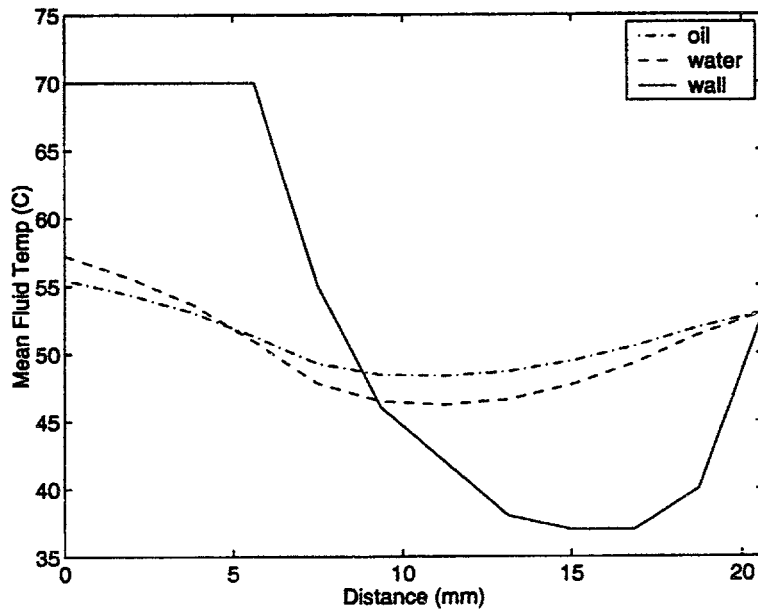
Figure 7-11: Temperature as plug moves to the left (decreasing x), from annealing to extension block, at 0.041 m/s. Temperature of the plug is assumed to lie somewhere inbetween the temperatures shown for oil and water. Temperatures of the denaturation, extension, and annealing blocks are 94°C, 70°C, and 53°C, respectively.
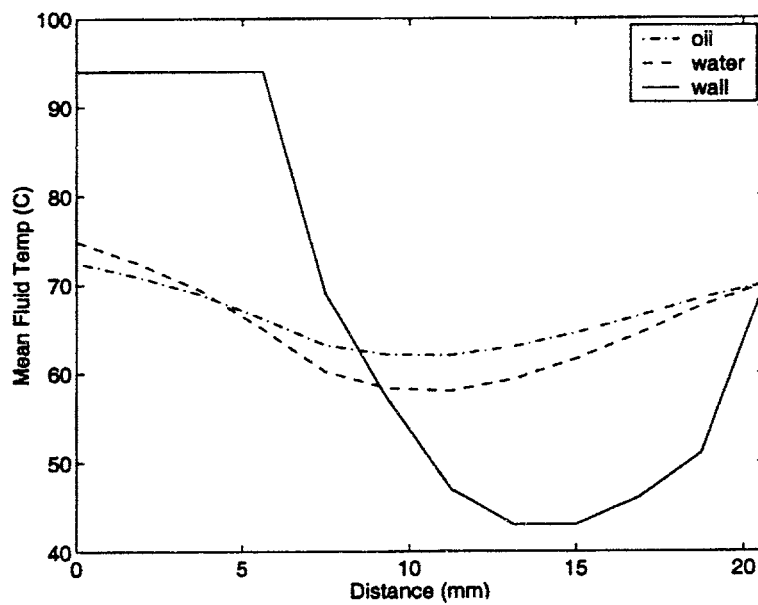
Figure 7-12: Temperature as plug moves to the left (decreasing x), from extension to denaturation block, at 0.041 m/s. Temperature of the plug is assumed to lie somewhere inbetween the temperatures shown for oil and water. Temperatures of the denaturation, extension, and annealing blocks are 94°C, 70°C, and 53°C, respectively.

Fluid motion through these blocks:	Water Temp. (°C)				Oil Temp. (°C)			
	Min.	Avg.	Max.	End	Min.	Avg.	Max.	End
From 94°C, through 70°C, to 53°C	50	66	94	52	60	73	94	60
From 53°C to 70°C	46	50	57	57	48	51	55	55
From 70°C to 94°C	58	65	75	75	62	66	72	72

Table 7.4: Temperature maximum, minimum, average, and ending values for the simulations in Figs. 7-10, 7-11, 7-12.

First, let us examine Fig. 7-10. Since the capillary temperature dips markedly between heat blocks, the fluid temperature drops quickly as in these regions. Since the diffusivity of water in the temperature range of interest ($\approx 1.6 \times 10^{-7}$ m^2/s) is higher than that of oil ($\approx 7.4 \times 10^{-8}$ m^2/s), it has a faster temperature response.

Although the fluid temperature drops between blocks, it rises slightly just before entering a heat block. This is somewhat counterintuitive, since the mean temperature of the fluid is still higher than the wall temperature. However, the temperature of the fluid *at* the wall is constrained to be the temperature *of* the wall. When the wall temperature rises rapidly, the mean temperature of the fluid will also tend to slightly increase. Of course, there is an overall drop in the fluid temperature as it travels between blocks.

Because of the cooler regions between heat blocks, the minimum fluid temperatures do not occur at the coolest 53°C annealing block, but instead between blocks. Table 7.4 reports the minimum, maximum, average, and end temperatures of the water and oil temperature curves shown in Figs. 7-10, 7-11, and 7-12. For water moving from the 94°C denaturing block to the 53°C annealing block, the minimum temperature is 50°C, although the final temperature is 52°C. For oil, these two temperatures are the same: 60°C, although this temperature is reached both outside and inside

164

the annealing block. The fact that the minimum temperature occurs between blocks is not pronounced in this case. However, annealing can occur between the extension and annealing blocks if the annealing block temperature is raised. This is covered in greater detail elsewhere in this work.

Now we turn our attention to Figs. 7-11 and 7-12. They are very similar in appearance. Note that the fluid is moving to the left (decreasing x) in each figure. The fluid temperature again dips in the colder region between heat blocks. However, the drop is not as dramatic as in Fig. 7-10 since (1) the initial plug temperature is closer to the temperature between the heat blocks, and (2) the plug is moving to a hotter heat block. The temperature dips in these cases are not important, as the plug mix has already annealed—either in the annealing block or in the temperature dip right before it reaches that block.

We see from the figures that the axial temperature gradient of the fluid once it enters a heat block is small. To get an order of magnitude estimate of the ratio of axial to radial conduction, I calculated $\Delta T/\Delta x \sim dT/dx$. ΔT was the difference between the two simulation fluid temperatures (let's call them T_5 and T_6) at the ends of the middle Δx of the heat block, where the plug is assumed to end up in. As previously mentioned, $\Delta x = L/8$. For $\Delta T/\Delta r \sim dT/dr$, I took ΔT to be the difference between the heat block (wall) temperature and the average of the T_5 and T_6. Δr is r_o, the capillary radius. I calculated these crude estimations for both the water and oil simulation data, and arrived at a ratio of $\Delta T/\Delta r$ to $\Delta T/\Delta x$ of about 50 for water and 100 for oil in all three motions presented in Figs. 7-10, 7-11, 7-12. While this is admittedly a very rough estimate, since the ratio is $\gg 1$, I assume that

Fluid motion through these blocks:	Water Time	Oil Time
From 94°C, through 70°C, to 53°C	0.3 s	0.8 s
From 53°C to 70°C	1.0 s	1.0 s
From 70°C to 94°C	1.1 s	1.1 s

Table 7.5: Temperature equilibration times required for the plug (modelled as water) at mean (modelled as uniform) temperature listed as the "end" temperature in Table 7.4 (using the all-water and all-oil models, respectively) to reach the destination heat block temperature. It is considered to have reached this temperature when its centerline $(r = r_o)$ temperature is within 0.5°C of the heat block temperature.

radial conduction dominates axial conduction for stationary plug heating.

Table 7.5 presents the plug equilibration times. The method described in Section 7.2.13 was used. When the plug stops moving, it shortens to fill the entire capillary cross-section. Therefore, I used the thermal diffusivity α of water in the equilibration calculations are based on that of water. As can be seen, the times required are on the order of 1 second. The advantage of the present capillary PCR machine lies in these brief equilibration times.

7.4   Steady State Analytical Model

7.4.1   Setting up the Problem

Let x be the axial coordinate of the tube, and r the radial coordinate. Hence, the model of the temperature between blocks is as follows: a hollow cylinder of dimensions $0 \leq x \leq L$ and $r_o \leq r \leq r_t$, where L is the distance between heat blocks, r_o is the inner ("oil") radius of the capillary, and r_t is the outer ("Teflon") radius of the capillary.

166

Within these boundaries, the conduction equation applies:

$$\frac{\partial^2 T}{\partial r^2} + \frac{1}{r}\frac{\partial T}{\partial r} + \frac{\partial^2 T}{\partial x^2} = 0 \qquad (7.11)$$

where T is temperature. The boundary conditions are as follows:

$$T = T_1 \quad \text{at } x = 0 \quad \text{for all r} \qquad (7.12)$$

$$T = T_2 \quad \text{at } x = L \quad \text{for all r} \qquad (7.13)$$

$$-k\frac{\partial T}{\partial r} = h(T - T_\infty) \quad \text{at } r = r_t \quad \text{for all } x \qquad (7.14)$$

$$\frac{\partial T}{\partial r} = 0 \quad \text{at } r = r_o \quad \text{for all } x \qquad (7.15)$$

where h is the coefficient of convection to the surrounding air, and T_∞ is the air temperature at infinity, i.e., room temperature, taken to be 20°C. Boundary condition (7.15) arises from the simplification of the oil as a perfect insulator.

I used the general method presented by Carslaw and Jaeger's classic work, "Conduction of Heat in Solids" [12] to solve this problem. Apply separation of variables to (7.11). Let

$$T = T_\infty + AR(r)X(x) \qquad (7.16)$$

where $R(r)$ is only a function of r, $X(x)$ is only a function of x, and A is a constant.

Therefore, from (7.11) and (7.16):

$$\frac{d^2R}{dr^2}X + \frac{1}{r}\frac{dR}{dr}X + R\frac{d^2X}{dx^2} = 0$$

Since R is only a function of r and X is only a function of x,

$$\frac{R''}{R} + \frac{1}{r}\frac{R'}{R} = -\frac{X''}{X} = -\lambda^2 \tag{7.17}$$

where R' is dR/dr, R'' is d^2R/dr^2, X'' is d^2X/dx^2, and λ is a constant. Therefore,

$$R'' + \frac{1}{r}R' + \lambda^2 R = 0 \tag{7.18}$$

and

$$X'' - \lambda^2 X = 0 \tag{7.19}$$

Hence, from (7.16, 7.18 and 7.19),

$$T = T_\infty + A(J_0(\lambda r) + BY_0(\lambda r))(e^{\lambda x} + Ce^{-\lambda x}) \tag{7.20}$$

where A, B, and C are constants. J_0 is the Bessel function[23] of order zero. Y_0 is the Bessel function of the second kind of order zero. Both are linearly independent solutions of (7.18).

---

[23]For a description of Bessel functions, see, for example, [76].

To solve the problem, split it into two different parts whose solutions are added to produce the final solution. Both parts I and II are subject to the convection boundary condition at $r = r_t$ (7.14) and the adiabatic condition at $r = r_o$ (7.15). The boundary conditions (7.12, 7.13) are split as follows:

$$\text{Part I:} \quad T = T_\infty \text{ at } x = 0 \quad \text{for all } r \tag{7.21}$$

$$T = T_2 \text{ at } x = L \quad \text{for all } r \tag{7.22}$$

$$\text{Part II:} \quad T = T_1 \text{ at } x = 0 \quad \text{for all } r \tag{7.23}$$

$$T = T_\infty \text{ at } x = L \quad \text{for all } r \tag{7.24}$$

7.4.2   Start on Part I

Let us first solve for part I. From equations (7.20, 7.21), we see that

$$C = -1 \tag{7.25}$$

Applying (7.14) to (7.20) and simplifying,

$$k\lambda[J_1(\lambda r_t) + BY_1(\lambda r_t)] = h[J_0(\lambda r_t) + BY_0(\lambda r_t)] \tag{7.26}$$

Here I have used the identities[24] $\frac{dJ_0(z)}{dz} = -J_1(z)$ and $\frac{dY_0(z)}{dz} = -Y_1(z)$.

---

[24]See, for example, [12, page 489].

169

Applying (7.15) to (7.20) and simplifying,

$$\lambda[J_1(\lambda r_o) + BY_1(\lambda r_o)] = 0 \qquad (7.27)$$

Since[25] $Y_0(0) = -\infty$, we cannot choose $\lambda = 0$ to satisfy (7.27). Therefore, from (7.27),

$$B = -J_1(\lambda r_o)/Y_1(\lambda r_o) \qquad (7.28)$$

Using (7.28) in (7.26),

$$k\lambda[J_1(\lambda r_t)Y_1(\lambda r_o) - J_1(\lambda r_o)Y_1(\lambda r_t)] = h[J_0(\lambda r_t)Y_1(\lambda r_o) - J_1(\lambda r_o)Y_0(\lambda r_t)] \qquad (7.29)$$

λ must satisfy (7.29).

Using (7.25) and (7.28) in (7.20),

$$T = T_\infty + \frac{A}{Y_1(\lambda r_o)}U(\lambda r)(e^{\lambda x} - e^{-\lambda x}) \qquad (7.30)$$

where λ satisfies (7.29) and

$$U(\lambda r) = J_0(\lambda r)Y_1(\lambda r_o) - J_1(\lambda r_o)Y_0(\lambda r) \qquad (7.31)$$

Only one boundary condition remains to be satisfied: Eq. (7.22). Since $U(\lambda r)$

---

[25]See, for example, [63, page 391].

varies with r, (7.22) is satisfied using an infinite series solution:

$$T = T_\infty + \sum_{n=1}^{\infty} \frac{A_n}{Y_1(\lambda_n r_o)} U(\lambda_n r)(e^{\lambda_n x} - e^{-\lambda_n x}) \tag{7.32}$$

7.4.3 Digression: Some Integrals

To solve for (7.22), we must first find the values of some integrals. Let α and β be two different values of λ. Let $U_\alpha = U(\alpha r)$ and $U_\beta = U(\beta r)$. Since $U(\lambda r)$ satisfies (7.18),

$$\frac{d^2 U_\alpha}{dr^2} + \frac{1}{r}\frac{dU_\alpha}{dr} + \alpha^2 U_\alpha = 0 \tag{7.33}$$

$$\frac{d^2 U_\beta}{dr^2} + \frac{1}{r}\frac{dU_\beta}{dr} + \beta^2 U_\beta = 0 \tag{7.34}$$

Taking Eqn. (7.33) $\times r U_\beta -$ (7.34) $\times r U_\alpha$ and integrating from r_o to r_t,

$$
\begin{aligned}
(\beta^2 - \alpha^2) \int_{r_o}^{r_t} r U_\alpha U_\beta dr &= \int_{r_o}^{r_t} \left[-r U_\alpha \frac{d^2 U_\beta}{dr^2} - U_\alpha \frac{dU_\beta}{dr} + r U_\beta \frac{d^2 U_\alpha}{dr^2} + U_\beta \frac{dU_\alpha}{dr} \right] dr \\
&= \int_{r_o}^{r_t} \left[-U_\alpha \frac{d}{dr}\left(r\frac{dU_\beta}{dr}\right) + U_\beta \frac{d}{dr}\left(r\frac{dU_\alpha}{dr}\right) \right] dr \\
&= -U_\alpha r \frac{dU_\beta}{dr}\Big|_{r_o}^{r_t} + \int_{r_o}^{r_t} r\frac{dU_\alpha}{dr}\frac{dU_\beta}{dr} dr \\
&\quad + U_\beta r \frac{dU_\alpha}{dr}\Big|_{r_o}^{r_t} - \int_{r_o}^{r_t} r\frac{dU_\alpha}{dr}\frac{dU_\beta}{dr} dr \\
&= r\left(U_\beta \frac{dU_\alpha}{dr} - U_\alpha \frac{dU_\beta}{dr}\right)\Big|_{r_o}^{r_t} \tag{7.35}
\end{aligned}
$$

171

From the convection boundary equation (7.14) and (7.30),

$$-k \left. \frac{dU(\lambda r)}{dr} \right|_{r_t} = hU(\lambda r_t) \tag{7.36}$$

Therefore, at $r = r_t$,

$$r\left(U_\beta \frac{dU_\alpha}{dr} - U_\alpha \frac{dU_\beta}{dr}\right) = r_t\left(-\frac{h}{k}U(\beta r_t)U(\alpha r_t) + \frac{h}{k}U(\alpha r_t)U(\beta r_t)\right) = 0 \tag{7.37}$$

From the adiabatic boundary condition(7.15) and (7.30),

$$\left. \frac{dU(\lambda r)}{dr} \right|_{r_o} = 0 \tag{7.38}$$

so at $r = r_o$,

$$r\left(U_\beta \frac{dU_\alpha}{dr} - U_\alpha \frac{dU_\beta}{dr}\right) = 0 \tag{7.39}$$

If $\alpha \neq \beta$, (7.37) and (7.39) can be applied to (7.35) to yield

$$(\beta^2 - \alpha^2)\int_{r_o}^{r_t} rU_\alpha U_\beta dr = 0 \tag{7.40}$$

What about the case in which $\alpha = \beta$?

Substituting $J_0(\lambda r) + BY_0(\lambda r) = U(\lambda r)/Y_1(\lambda r_o)$ for R in (7.18) (also see (7.32))

and multiplying by $2r^2 \frac{dU(\lambda r)}{dr}$,

$$2r^2 \frac{dU(\lambda r)}{dr} \frac{d^2U(\lambda r)}{dr^2} + 2r \left(\frac{dU(\lambda r)}{dr} \right)^2 + 2\lambda^2 r^2 \frac{dU(\lambda r)}{dr} U(\lambda r) = 0$$

$$\frac{d}{dr} \left[r \frac{dU(\lambda r)}{dr} \right]^2 + \lambda^2 r^2 \frac{d(U(\lambda r))^2}{dr} = 0$$

$$\left[r \frac{dU(\lambda r)}{dr} \right]^2 \Bigg|_{r_o}^{r_t} + \lambda^2 \int_{r_o}^{r_t} r^2 \frac{d(U(\lambda r))^2}{dr} = 0$$

$$\left[r \frac{dU(\lambda r)}{dr} \right]^2 \Bigg|_{r_o}^{r_t} + \lambda^2 r^2 U^2(\lambda r) \big|_{r_o}^{r_t} - 2\lambda^2 \int_{r_o}^{r_t} r U^2(\lambda r) dr = 0$$

$$\int_{r_o}^{r_t} r U^2(\lambda r) dr = \left[\frac{1}{2} r^2 U^2(\lambda r) + \frac{r^2}{2\lambda^2} \left(\frac{dU(\lambda r)}{dr} \right)^2 \right] \Bigg|_{r_o}^{r_t} \tag{7.41}$$

Using (7.36) and(7.38) in (7.41),

$$\int_{r_o}^{r_t} r U^2(\lambda r) dr = \frac{1}{2} \left[r_t^2 \left(1 + \frac{h^2}{\lambda^2 k^2} \right) U^2(\lambda r_t) - r_o^2 U^2(\lambda r_o) \right] \tag{7.42}$$

The difference between (7.40) and (7.42) is that (7.40) applies to two different λ, α and β (with $\alpha \neq \beta$), whereas (7.42) is for a single λ.

We also need to find the value of one more integral. From (7.18), again using the

fact that $R(r) = U(\lambda r)/Y_1(\lambda r_o)$,

$$\frac{d^2 U(\lambda r)}{dr^2} + \frac{1}{r}\frac{dU(\lambda r)}{dr} + \lambda^2 U(\lambda r) = 0$$

$$\frac{d}{dr}\left(r\frac{dU(\lambda r)}{dr}\right) + \lambda^2 r U(\lambda r) = 0$$

$$\int_{r_o}^{r_t} rU(\lambda r)dr = \left.-\frac{r}{\lambda^2}\frac{dU(\lambda r)}{dr}\right|_{r_o}^{r_t}$$

$$= \frac{r_t h}{\lambda^2 k}U(\lambda r_t) \qquad (7.43)$$

where (7.36) and (7.38) were used to obtain (7.43).

7.4.4 Completing Part I

Returning to (7.32) subject to the T_2 boundary condition at $x = L$ (7.22),

$$T_2 = T_\infty + \sum_{n=1}^{\infty}\frac{A_n}{Y_1(\lambda_n r_o)}U(\lambda_n r)\left(e^{\lambda_n L} - e^{-\lambda_n L}\right)$$

Multiplying both sides by $rU(\lambda r)$, integrating from r_o to r_t, and using (7.40), (7.42) and (7.43), we get

$$(T_2 - T_\infty)\left(\frac{r_t h}{\lambda_n^2 k}\right)U(\lambda_n r_t) = \frac{A_n}{Y_1(\lambda_n r_o)}\sinh(\lambda_n L)\left[r_t^2\left(1 + \frac{h^2}{\lambda_n^2 k^2}\right)U^2(\lambda_n r_t) - r_o^2 U^2(\lambda_n r_o)\right]$$

Therefore,

$$\frac{A_n}{Y_1(\lambda_n r_o)} = \frac{(T_2 - T_\infty)r_t hkU(\lambda_n r_t)}{\sinh(\lambda_n L)[r_t^2(\lambda_n^2 k^2 + h^2)U^2(\lambda_n r_t) - r_o^2\lambda_n^2 k^2 U^2(\lambda_n r_o)]} \qquad (7.44)$$

174

7.4.5 Part II

Now we shall solve Part II of the problem. From (7.20) and (7.24),

$$e^{\lambda L} + Ce^{-\lambda L} = 0$$

$$C = -e^{2\lambda L}$$

$$\text{Therefore,} \quad \left(e^{\lambda x} + Ce^{-\lambda x}\right) = -e^{\lambda L}\left(e^{\lambda(L-x)} - e^{-\lambda(L-x)}\right) \tag{7.45}$$

Since $-e^{\lambda L}$ is a constant, lump it in with A. From (7.20) and (7.45),

$$T = T_\infty + A(J_0(\lambda r) + BY_0(\lambda r))(e^{\lambda(L-x)} - e^{-\lambda(L-x)}) \tag{7.46}$$

The solution is identical to Part I, except that $(e^{\lambda(L-x)} - e^{-\lambda(L-x)})$ replaces $(e^{\lambda x} - e^{-\lambda x})$, and T_1 replaces T_2.

7.4.6 Total Solution

Therefore, from (7.32) and (7.44),

$$T = T_\infty + \sum_{n=1}^{\infty} \frac{2r_t h k U(\lambda_n r_t) U(\lambda_n r)[(T_2 - T_\infty)\sinh(\lambda_n x) + (T_1 - T_\infty)\sinh(\lambda_n(L-x))]}{[r_t^2(\lambda_n^2 k^2 + h^2)U^2(\lambda_n r_t) - r_o^2\lambda_n^2 k^2 U^2(\lambda_n r_o)]\sinh(\lambda_n L)} \tag{7.47}$$

where[26]

$$U(\lambda_n r) = J_0(\lambda_n r)Y_1(\lambda_n r_o) - J_1(\lambda_n r_o)Y_0(\lambda_n r)$$

and the various λ_n are values of λ which satisfy

$$k\lambda[J_1(\lambda r_t)Y_1(\lambda r_o) - J_1(\lambda r_o)Y_1(\lambda r_t)] = h[J_0(\lambda r_t)Y_1(\lambda r_o) - J_1(\lambda r_o)Y_0(\lambda r_t)]$$

7.4.7 Average Values

Let

$$Q_n = \frac{U^2(\lambda_n r_t)}{[r_t^2(\lambda_n^2 k^2 + h^2)U^2(\lambda_n r_t) - (r_o \lambda_n k U(\lambda_n r_o))^2]} \tag{7.48}$$

From (7.47), $T|_{r_t}$ averaged over $0 \le x \le L$ is

$$\overline{T}|_{r_t} = T_\infty + \sum_{n=1}^{\infty} \frac{2r_t h k Q_n[T_1 + T_2 - 2T_\infty][\cosh(\lambda_n L) - 1]}{L\lambda_n \sinh(\lambda_n L)} \tag{7.49}$$

The value of T averaged over both $r_o \le r \le r_t$ and $0 \le x \le L$ is

$$\overline{T} = T_\infty + \frac{4(r_t h)^2}{(r_t^2 - r_o^2)L}(T_1 + T_2 - 2T_\infty) \sum_{n=1}^{\infty} \frac{Q_n[\cosh(\lambda_n L) - 1]}{\lambda_n^3 \sinh(\lambda_n L)} \tag{7.50}$$

---

[26]See (7.29,7.31).

176

7.5 Radial Transient Conduction Model

The following problem is to be solved: a homogeneous cylinder of radius r_o, initially at uniform temperature T_3, is subjected to a temperature T_4 at $r = r_o$ at time $t = 0$. Conduction is negligible in the axial direction. The cylinder has thermal diffusivity of α_o. This section presents the solution provided by Carslaw and Jaeger ([12]).

The conduction equation for this situation is:

$$\frac{\partial^2 T}{\partial r^2} + \frac{1}{r}\frac{\partial T}{\partial r} = \frac{1}{\alpha_o}\frac{\partial T}{\partial t} \tag{7.51}$$

The boundary conditions are:

$$T = T_3 \quad \text{at } t = 0 \quad \text{for all } r \tag{7.52}$$

$$T = T_4 \quad \text{at } r = r_o \quad \text{for all } t \tag{7.53}$$

To solve this problem, apply separation of variables. Let

$$T = T_4 + AR(r)\Phi(t) \tag{7.54}$$

where A is a constant, $R(r)$ is only a function of the radius r, and $\Phi(t)$ is only a function of the time t. Therefore, from (7.51) and (7.54),

$$
\begin{aligned}
R''\Phi + \frac{1}{r}R'\Phi &= \frac{1}{\alpha}R\Phi' \\
\frac{R''}{R} + \frac{1}{r}\frac{R'}{R} &= \frac{1}{\alpha}\frac{\Phi'}{\Phi} = -\lambda^2
\end{aligned}
\tag{7.55}
$$

where R' is dR/dr, R'' is d^2R/dr^2, X' is dX/dx, and λ is a constant. Therefore,

$$R'' + \frac{1}{r}R'\Phi + \lambda^2 R = 0 \qquad (7.56)$$

$$\Phi' + \alpha\lambda^2\Phi = 0 \qquad (7.57)$$

Hence, from (7.54), (7.56) and (7.57),

$$T = T_4 + A(J_0(\lambda r) + BY_0(\lambda r))e^{-\alpha\lambda^2 t} \qquad (7.58)$$

where J_0 is the Bessel function of the first kind of order zero, and Y_0 is the Bessel function of the second kind of order zero. Since T is finite at $r = 0$, and[27] Y_0 is $-\infty$ at 0, $B = 0$.

Plugging the T_4 boundary condition at r_o (7.53) into (7.58),

$$AJ_0(\lambda r_o)e^{-\lambda^2\alpha t} = 0 \quad \text{for all } t$$

$A = 0$ results in the trivial solution, so instead choose λ such that

$$J_0(\lambda r_o) = 0 \qquad (7.59)$$

There are an infinite number of λ that satisfy (7.59).

To solve the T_3 initial temperature boundary condition (7.52), we have to use an

---

[27]See, for example, [63, p. 391].

infinite series solution:

$$T = T_4 + \sum_{n=1}^{\infty} A_n J_0(\lambda_n r) e^{-\lambda_n^2 \alpha t} \tag{7.60}$$

To get A_n values, we need to first get the value of several integrals. Let α and β be two different values of λ. Let $J_\alpha = J_0(\alpha r)$ and $J_\beta = J_0(\beta r)$. We follow the same procedure as in Section 7.4, substituting J_α for U_α, J_β for U_β, r_o for r_t and 0 for r_o. Therefore, (7.35) becomes

$$(\beta^2 - \alpha^2) \int_0^{r_o} r J_\alpha J_\beta dr = r_o \left(J_\beta \frac{dJ_\alpha}{dr} - J_\alpha \frac{dJ_\beta}{dr} \right)\bigg|_{r_o} \tag{7.61}$$

From (7.59), $J_0(\lambda r_o) = 0$. Using this in (7.61), we get

$$\int_0^{r_o} r J_\alpha J_\beta dr = 0 \tag{7.62}$$

Similarly, (7.41) becomes

$$\int_0^{r_o} r J_0^2(\lambda r) dr = \left[\frac{1}{2} r^2 J_0^2(\lambda r) + \frac{r^2}{2\lambda^2} \left(\frac{dJ_0(\lambda r)}{dr} \right)^2 \right]\bigg|_0^{r_o} \tag{7.63}$$

Since $J_0(\lambda r) = 0$ from (7.59) and $d(J_0(z))/dz = -J_1(z)$, (7.63) becomes

$$\int_0^{r_o} r J_0^2(\lambda r) dr = \frac{1}{2} r_o^2 J_1^2(\lambda r_o) \tag{7.64}$$

The same substitutions turn (7.43) into

$$
\begin{aligned}
\int_0^{r_o} r J_0(\lambda r) dr &= \left. -\frac{r}{\lambda^2} \frac{dJ(\lambda r)}{dr} \right|_0^{r_o} \\
&= \left(\frac{r_0}{\lambda} \right) J_1(\lambda r_o)
\end{aligned}
\tag{7.65}
$$

Using the T_3 initial boundary condition (7.52) in (7.60),

$$
T_3 - T_4 = \sum_{n=1}^{\infty} A_n J_0(\lambda_n r)
$$

Multiplying both sides by $r J_0(\lambda_n r)$, and using (7.62), (7.64) and (7.65),

$$
A_n = \frac{2(T_3 - T_4)}{\lambda_n r_o J_1(\lambda_n r_o)}
$$

Therefore,

$$
T = T_4 + \frac{2(T_3 - T_4)}{r_o} \sum_{n=1}^{\infty} \frac{J_0(\lambda_n r)}{\lambda_n J_1(\lambda_n r_o)} e^{-\lambda_n^2 \alpha t}
\tag{7.66}
$$

where, from (7.59),

$$
J_0(\lambda_n r_o) = 0
$$

180

7.6 Convection Model

7.6.1 Uniform Wall Temperature

This section presents calculations for heat transfer by convection to a homogeneous fluid moving within a tube. The fluid entering the tube has fully-developed laminar flow and is at a uniform temperature T_e. The tube has a constant wall temperature T_o. The solution for this simple case is taken from [37], and its derivation is required for the more complex case used in my model which has axial temperature variation.

The energy equation for this flow is as follows:

$$-\frac{\alpha_f}{r}\frac{\partial}{\partial r}\left(r\frac{\partial T}{\partial r}\right) - \alpha_f\frac{\partial^2 T}{\partial x^2} + u\frac{\partial T}{\partial x} = 0 \qquad (7.67)$$

where α_f is the thermal diffusivity of the fluid, and u is the velocity. Let us define the following nondimensional variables:

$$\hat{T} = \frac{T - T_o}{T_e - T_o} \qquad \hat{r} = \frac{r}{r_o} \qquad \hat{u} = \frac{u}{V} \qquad \hat{x} = \frac{x}{(\mathrm{Re})(\mathrm{Pr})(r_o)} = \frac{x\alpha_f}{2Vr_o^2} \qquad (7.68)$$

V is the average fluid velocity; Re is the Reynolds number, $2Vr_o/\nu_f$; Pr is the Prandtl number, ν_f/α_f; and ν_f is the fluid kinematic viscosity.

Using (7.68) to nondimensionalize the energy equation (7.67), we get

$$-\frac{\partial^2 \hat{T}}{\partial \hat{r}^2} - \frac{1}{\hat{r}}\frac{\partial \hat{T}}{\partial \hat{r}} - \frac{1}{(\mathrm{Re}\cdot\mathrm{Pr})^2}\frac{\partial^2 \hat{T}}{\partial \hat{x}^2} + \frac{\hat{u}}{2}\frac{\partial \hat{T}}{\partial \hat{x}} = 0 \qquad (7.69)$$

If the product $\mathrm{Re}\cdot\mathrm{Pr} > 10$, axial conduction can be ignored [37]. For the rest of

181

the derivation, we assume that this is the case. Therefore, (7.69) becomes

$$-\frac{\partial^2 \hat{T}}{\partial \hat{r}^2} - \frac{1}{\hat{r}}\frac{\partial \hat{T}}{\partial \hat{r}} + \frac{\hat{u}}{2}\frac{\partial \hat{T}}{\partial \hat{x}} = 0 \qquad (7.70)$$

Since the velocity is fully developed Poiseuille flow[28],

$$u = 2V\left(1 - \frac{r^2}{r_o^2}\right) \qquad (7.71)$$

or, in nondimensional terms,

$$\hat{u} = 2(1 - \hat{r}^2) \qquad (7.72)$$

Using (7.72), (7.70) becomes

$$\frac{\partial^2 \hat{T}}{\partial \hat{r}^2} + \frac{1}{\hat{r}}\frac{\partial \hat{T}}{\partial \hat{r}} = (1 - \hat{r}^2)\frac{\partial \hat{T}}{\partial \hat{x}} \qquad (7.73)$$

Boundary conditions for this equation are as follows:

$$\hat{T}|_{\hat{x}=0} \;=\; 1 \qquad \text{for all } \hat{r} \qquad \text{(Fluid enters at } T = T_e) \qquad (7.74)$$

$$\hat{T}|_{\hat{r}=1} \;=\; 0 \qquad \text{for all } \hat{x} \qquad (T = T_o \text{ at tube wall}) \qquad (7.75)$$

$$\left.\frac{\partial \hat{T}}{\partial \hat{r}}\right|_{\hat{r}=0} \;=\; 0 \qquad \text{for all } \hat{x} \qquad \text{(Radial symmetry)} \qquad (7.76)$$

---

[28]For a derviation of this standard velocity distribution, see for example, [21, page 289].

Use separation of variables to solve for (7.73). Assume that

$$\hat{T} = D\hat{R}(\hat{r})\hat{X}(\hat{x}) \tag{7.77}$$

Where D is a constant. Substituting (7.77) into (7.73), we get

$$\frac{\partial^2 \hat{R}}{\partial \hat{r}^2}\hat{X} + \frac{1}{\hat{r}}\frac{\partial \hat{R}}{\partial \hat{r}}\hat{X} = (1 - \hat{r}^2)\hat{R}\frac{\partial X}{\partial \hat{x}} \tag{7.78}$$

Since $\hat{R}$ is only a function of $\hat{r}$, and $\hat{X}$ is only a function of $\hat{x}$,

$$\frac{1}{(1 - \hat{r}^2)}\frac{\hat{R}''}{\hat{R}} + \frac{1}{\hat{r}(1 - \hat{r}^2)}\frac{\hat{R}'}{\hat{R}} = \frac{\hat{X}'}{\hat{X}} = -\lambda^2 \tag{7.79}$$

where λ is a constant, $\hat{R}'$ is $\partial\hat{R}/\partial\hat{r}$, $\hat{R}''$ is $\partial^2\hat{R}/\partial\hat{r}^2$, and $\hat{X}''$ is $\partial^2\hat{X}/\partial\hat{x}^2$. This results in the following two equations:

$$\hat{X}' + \lambda^2\hat{X} = 0 \tag{7.80}$$

$$\hat{R}'' + \frac{1}{\hat{r}}\hat{R}' + \lambda^2(1 - \hat{r}^2)\hat{R} = 0 \tag{7.81}$$

(7.80) is solved by

$$\hat{X} = \exp(-\lambda^2\hat{x})$$

To solve for the boundary condition at the wall (7.74), an infinite series is required,

183

so (7.77) becomes

$$\hat{T} = \sum_{n=0}^{\infty} D_n \hat{R}_n(\hat{r}) \exp(-\lambda^2 \hat{x}) \tag{7.82}$$

$\hat{R}$ is not so easily found. Fortunately, equation 7.81 has been studied extensively, and is known as the Graetz Problem [79], or an equation of the Sturm-Liouville type [37].

Let $T_m(x)$ be the mean temperature of the liquid at x. To find T_m, we use an energy balance with the control volume being defined by the fluid in the tube from 0 to $\hat{x}$. At $\hat{x}$, the heat flux q from the tube wall into the fluid, per unit area, is:

$$
\begin{aligned}
q &= k_f \left. \frac{\partial T}{\partial r} \right|_{r=r_o} \\
&= k_f \frac{(T_e - T_o)}{r_o} \left. \frac{\partial \hat{T}}{\partial \hat{r}} \right|_{\hat{r}=1} \\
&= \frac{2 k_f (T_o - T_e)}{r_o} \sum_{n=0}^{\infty} -\frac{1}{2} D_n \hat{R}'(1) \exp(-\lambda_n^2 \hat{x}) \\
&= \frac{2 k_f (T_o - T_e)}{r_o} \sum_{n=0}^{\infty} G_n \exp(-\lambda_n^2 \hat{x})
\end{aligned}
\tag{7.83}
$$

where k_f is the thermal conductivity of the fluid. (7.83) was arrived at using (7.82). For convenience, G_n is defined as

$$G_n = -\frac{1}{2} D_n \hat{R}'_n(1) \tag{7.84}$$

Values of λ_n and G_n for $n = 0$ to 4 were calculated by Lipkis [79], and are presented in Table 7.6. Doing an energy balance on the fluid from 0 to $\hat{x}$, we get

184

n	λ_n	G_n
0	2.7043644	0.74879
1	6.679032	0.54424
2	10.67338	0.46288
3	14.67108	0.41518
4	18.66987	0.38237

Table 7.6: Values of λ_n and G_n presented in [79]. For $n > 2$, $\lambda_n \approx 4n + \frac{8}{3}$, and $G_n \approx 1.01276\lambda_n^{-\frac{1}{3}}$.

$$\rho_f c_f V \pi r_o^2 (T_m - T_e) = \int_0^x 2\pi r_o q \, dx$$

$$\frac{1}{2}\rho_f c_f V r_o (T_m - T_e) = \int_0^x q \, dx \tag{7.85}$$

where ρ_f is the fluid density, and c_f is the specific heat at constant pressure of the fluid. Using (7.83) in (7.85),

$$\frac{1}{2}\rho_f c_f V r_o (T_m - T_e) = 2k_f \mathrm{Re} \cdot \mathrm{Pr}(T_o - T_e) \sum_{n=0}^{\infty} G_n \int_0^{\hat{x}} \exp(-\lambda_n^2 \hat{x}) d\hat{x}$$

$$= 4V r_o c_f \rho_f (T_o - T_e) \sum_{n=0}^{\infty} -\frac{G_n}{\lambda_n^2} \exp(-\lambda_n^2 \hat{x})\bigg|_0^{\hat{x}}$$

$$\frac{1}{8}(1 - \hat{T}_m) = \sum_{n=0}^{\infty} \frac{G_n}{\lambda_n^2}[1 - \exp(-\lambda_n^2 \hat{x})] \tag{7.86}$$

Where

$$\hat{T}_m = \frac{T_m - T_o}{T_e - T_o} \tag{7.87}$$

185

As $x \to \infty$, $T_m \to T_o$. Therefore, as $\hat{x} \to \infty$, $\hat{T}_m \to 0$, so from (7.86),

$$\sum_{n=0}^{\infty} \frac{G_n}{\lambda_n^2} = \frac{1}{8} \tag{7.88}$$

Plugging (7.88) into (7.86), we arrive at

$$\hat{T}_m = 8 \sum_{n=0}^{\infty} \frac{G_n}{\lambda_n^2} \exp(-\lambda_n^2 \hat{x}) \tag{7.89}$$

7.6.2 Axially Varying Wall Temperature

In this subsection, we will extend the results of Section 7.6.1 to the case of a wall with a piecewise linear axial temperature distribution. Otherwise, the case is identical to that in Section 7.6.1: radially symmetric, with fully developed fluid velocity profile and uniform temperature at the fluid entrance. Again, we model the case in which axial conduction is negligible.

We model the tube as a series of infinitesimal constant-temperature steps. The case of a single step, in which the tube wall temperature T_o is constant and different from the uniform fluid entrance temperature T_e, was presented in Section 7.6.1. From (7.68),

$$\hat{T}(\hat{x}, \hat{r}) = \frac{T - T_o}{T_e - T_o}$$

If the temperature change were to occur at $\hat{x} = \xi$ rather than $\hat{x} = 0$,

$$\hat{T}(\hat{x} - \xi, \hat{r}) = \frac{T - T_o}{T_e - T_o}$$

For an infinitesimal step of constant wall temperature T_o,

$$\hat{T}(\hat{x} - \xi, \hat{r}) = \frac{dT - dT_o}{-dT_o}$$

Rearranging:

$$dT = [1 - \hat{T}(\hat{x} - \xi, \hat{r})]dT_o$$

Therefore,

$$
\begin{aligned}
T - T_e &= \int_{\xi=0}^{\xi=\hat{x}} [1 - \hat{T}(\hat{x} - \xi, \hat{r})]dT_o \\
&= \int_0^{\hat{x}} [1 - \hat{T}(\hat{x} - \xi, \hat{r})]\frac{dT_o}{d\xi}d\xi
\end{aligned}
\qquad (7.90)
$$

Find q, the heat flux per unit area from the tube wall into the fluid:

$$
\begin{aligned}
q(\hat{x}) &= k_f \left. \left(\frac{\partial T}{\partial r} \right) \right|_{r=r_o} \\
&= \frac{k_f}{r_o} \left. \left(\frac{\partial T}{\partial \hat{r}} \right) \right|_{\hat{r}=1} \\
&= -\frac{k_f}{r_o} \int_0^{\hat{x}} \left. \left(\frac{\partial \hat{T}(\hat{x}-\xi, \hat{r})}{\partial \hat{r}} \right) \right|_{\hat{r}=1} \left(\frac{dT_o(r_o)}{d\xi} \right) d\xi \quad &(7.91) \\
&= -\frac{k_f}{r_o} \sum_{n=0}^{\infty} -2G_n \int_0^{\hat{x}} \exp[-\lambda_n^2(\hat{x}-\xi)] \frac{dT_o(r_o)}{d\xi} d\xi \quad &(7.92) \\
&= \frac{2k_f}{r_o} \sum_{n=0}^{\infty} G_n \int_o^{\hat{x}} \exp[-\lambda^2(\hat{x}-\xi)] \frac{dT_o(r_o)}{d\xi} d\xi \quad &(7.93)
\end{aligned}
$$

(7.91) was arrived at using (7.90). (7.92) was arrived at using (7.82) and (7.84).

7.6.3 Piecewise Linear Wall Temperature

The piecewise linear axial temperature distribution is as follows. Each piece covers an axial distance of $\Delta \hat{x}$. $\hat{x} = m\Delta \hat{x}$. Therefore, up to $\hat{x}$, there are m pieces. Each piece, indexed by i, spans $\Delta \hat{x}(i-1) \leq \xi \leq i\Delta \hat{x}$. Its slope, $\partial T_o/\partial \xi$, is S_i. Fig. 7-13 illustrates the piecewise axial temperature distribution for $m = 4$.

At $\xi = 0, T = T_e$, the fluid entrance temperature. This is an important distinction. If the $T_o \neq T_e$ at $\xi = 0$, then there need to be additional $[1 - \hat{T}(\hat{x} - \xi, \hat{r})]\Delta T_o$ terms present in (7.93) to account for $T_o - T_e$, as well as any other steps in wall temperature [37, page 141].

From the piecewise linear distribution, we have the $\partial T_o/\partial \xi$ values: the S_i's. Even though T_m will be only found at discrete values of $\hat{x}$, q must be defined continuously
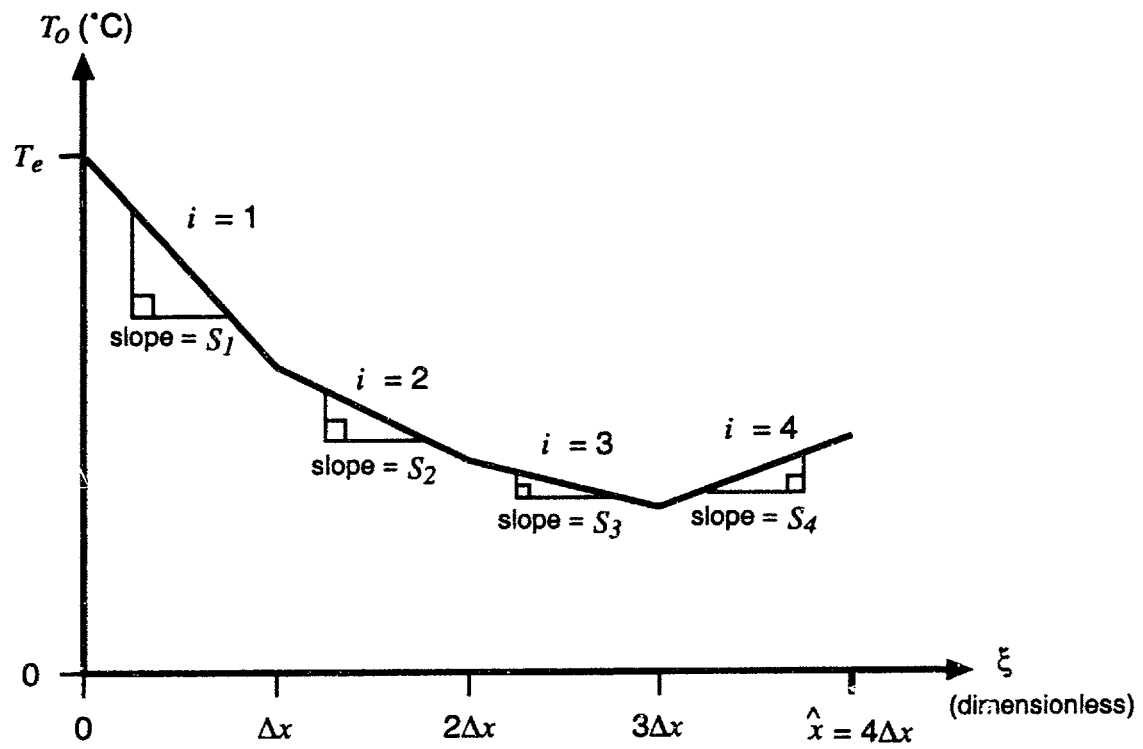
Figure 7-13: Piecewise linear wall temperature distribution for m = 4. Note that at $\xi = 0$, $T_o = T_e$.

from $0 \leq \xi \leq \hat{x}$ in order to be integrable. Continuing from (7.93),

$$
\begin{aligned}
q(\hat{x}) &= \frac{2k_f}{r_o} \sum_{n=0}^{\infty} G_n \int_o^{\hat{x}} \exp[-\lambda_n^2(\hat{x} - \xi)] \left(\frac{\partial T_o}{\partial \xi}\right) d\xi \\
&= \frac{2k_f}{r_o} \sum_{n=0}^{\infty} \frac{G_n}{\lambda_n^2} \left\{ S_m \exp[-\lambda_n^2(\hat{x} - \xi)]\Big|_{(m-1)\Delta\hat{x}}^{\hat{x}} + \sum_{i=1}^{m-1} S_i \exp[-\lambda_n^2(\hat{x} - \xi)]\Big|_{(i-1)\Delta\hat{x}}^{i\Delta\hat{x}} \right\} \\
&= \frac{2k_f}{r_o} \sum_{n=0}^{\infty} \frac{G_n}{\lambda_n^2} \left\{ S_m(1 - \exp[-\lambda_n^2(\hat{x} - (m-1)\Delta\hat{x})]) \right. \\
&\qquad \left. + \sum_{i=1}^{m-1} S_i(\exp[-\lambda_n^2(\hat{x} - i\Delta\hat{x})] - \exp[-\lambda_n^2(\hat{x} - (i-1)\Delta\hat{x})]) \right\} \\
&= \frac{2k_f}{r_o} \sum_{n=0}^{\infty} \frac{G_n}{\lambda_n^2} \left\{ S_m \left(1 - \left(\frac{1}{F_n}\right) \exp[-\lambda_n^2(\hat{x} - m\Delta\hat{x})] \right) \right. \\
&\qquad \left. + \sum_{i=1}^{m-1} S_i \left(1 - \frac{1}{F_n}\right) \exp[-\lambda_n^2(\hat{x} - i\Delta\hat{x})] \right\}
\end{aligned}
\tag{7.94}
$$

where

$$
F_n = \exp(\lambda_n^2 \Delta\hat{x}) \tag{7.95}
$$

To find $T_m(\hat{x})$, we use an energy balance on the tube from 0 to $\hat{x}$. From (7.85),

$$
\begin{aligned}
\frac{1}{2}\rho_f c_f V r_o (T_m - T_e) &= \int_0^x q\,dx \\
T_m - T_e &= \frac{4r_o}{k_f} \int_0^{\hat{x}} q\,d\hat{x}
\end{aligned}
\tag{7.96}
$$

where the definition of the $\hat{x}$ (7.68) was used to arrive at (7.96). Using the expression

for q from (7.94) in (7.96),

$$
\begin{aligned}
T_m - T_e &= \frac{4r_o}{k_f} \int_0^{\hat{x}} q\,d\hat{x} \\
&= \frac{4r_o}{k_f} \sum_{j=1}^{m} \int_{(j-1)\Delta\hat{x}}^{j\Delta\hat{x}} q\,d\hat{x} \\
&= 8 \sum_{j=1}^{m} \sum_{n=0}^{\infty} \frac{G_n}{\lambda_n^2} \left\{ S_j(\hat{x}) + \frac{S_j}{F_n\lambda_n^2} \exp[-\lambda_n^2(\hat{x} - j\Delta\hat{x})] \right. \\
&\qquad \left. \left. - \sum_{i=1}^{j-1} \frac{S_i}{\lambda_n^2} \left(1 - \frac{1}{F_n}\right) \exp[-\lambda_n^2(\hat{x} - i\Delta\hat{x})] \right\} \right|_{(j-1)\Delta\hat{x}}^{j\Delta\hat{x}} \\
&= 8 \sum_{j=1}^{m} \sum_{n=0}^{\infty} \frac{G_n}{\lambda_n^2} \left\{ S_j\Delta\hat{x} + \frac{S_j}{F_n\lambda_n^2}(1 - F_n) \right. \\
&\qquad \left. + \sum_{i=1}^{j-1} \frac{S_i}{\lambda_n^2} \left(\frac{1}{F_n} - 1\right)(1 - F_n)\exp[-\lambda_n^2(j - i)\Delta\hat{x}] \right\} \\
&= \sum_{j=1}^{m} \left\{ S_j\Delta\hat{x} + \sum_{n=0}^{\infty} \left[8\frac{S_j G_n}{F_n\lambda_n^4}(1 - F_n) \right. \right. \\
&\qquad \left. \left. + \sum_{i=1}^{j-1} 8\frac{S_i G_n}{\lambda_n^4} \left(\frac{1}{F_n} - 1\right)(1 - F_n)\exp(-\lambda_n^2(j - i)\Delta\hat{x}) \right] \right\} \quad (7.97)
\end{aligned}
$$

7.7 Nomenclature

A Constant used in T equation. See (7.20).

B Constant used in T equation. See (7.20).

Bi   The Biot number. $h_b l/k_b$. See (7.1).

C Constant used in T equation. See (7.20).

c_f Specific heat at constant pressure of the fluid.

D Constant used in T equation. See (7.77).

F_n $\exp(\lambda_n^2\Delta\hat{x})$. See (7.95).

g Gravitational acceleration.

Gr   The Grashof number. $g\beta_a(T_b - T_\infty)l^3/\nu^2$. See (7.4).

h Coefficient of convection from the capillary to surrounding air.

h_b Coefficient of convection from the heat block to surrounding air.

i Index number. See, for example, (7.94).

J_0 Bessel function of order zero.

J_1 Bessel function of order one.

k Thermal conductivity of teflon.

k_a Thermal conductivity of air.

k_b Thermal conductivity of the heat block.

k_f Thermal conductivity of the fluid.

L Distance between heat blocks.

l Characteristic length. See (7.2).

$l_{\text{horiz.}}$ Heater block horizontal dimension. See (7.2).

$l_{\text{vert.}}$ Heater block vertical dimension. See (7.2).

m Number of pieces in piecewise linear approximation of T from 0 to x.

Pr   Prandtl number. $\text{Pr} = \nu/\alpha$.

q Heat flux per unit area at tube wall, from tube wall to fluid.

Q_n $U^2(\lambda_n r_t)/[r_t^2(\lambda_n^2 k^2 + h^2)U^2(\lambda_n r_t) - (r_o \lambda_n k U(\lambda_n r_o))^2]$. See (7.48, 7.49, 7.50).

r Radial coordinate of the model.

$\hat{r}$ Normalized r. $\hat{r} = r/r_o$. See (7.68).

r_o	Capillary inner radius (the o stands for "oil").
r_t	Capillary outer radius (the t stands for "Teflon").
$R(r)$	Function of r used in T. See (7.16).
$\hat{R}(\hat{r})$	Function of $\hat{r}$ used in $\hat{T}$. See (7.77).
Ra	Rayleigh number. Ra $=$ Gr $\times$ Pr.
Re	Reynolds number. Re $= 2Vr_o/\nu_f$.
S_i	Slope $\partial T_o/\partial \hat{x}$ at piece i of piecewise linear wall temperature. See page 188.
T	Temperature.
$\hat{T}$	Normalized temperature. $\hat{T} = (T - T_o)/(T_e - T_o)$. See (7.68).
$\overline{T}$	T averaged over $0 \le x \le L$ and $r_o \le r \le r_t$. See (7.50).
T_∞	Room temperature, taken to be 20°C .
T_1	Boundary condition temperature. See (7.12).
T_2	Boundary condition temperature. See (7.13).
T_3	Boundary condition temperature. See (7.52).
T_4	Boundary condition temperature. See (7.53).
T_5	Temperature at one end of the middle Δx inside a heat block. See p. 165.
T_6	Temperature at one end of the middle Δx inside a heat block. See p. 165.
T_b	Surface temperature of the heat block.
T_e	Uniform temperature of the fluid entering the tube.

T_{in} Uniform temperature of oil entering the annealing block in the model in Section 7.2.2.

T_m Mean fluid temperature. See page 184.

T_o Tube wall temperature.

T_{out} Average temperature of oil exiting the annealing block in the model in Section 7.2.2.

$\overline{T}|_{r_t}$ T at $r = r_t$ averaged over $0 \leq x \leq L$. See (7.49).

T_{Teflon} Temperature of the portion of the capillary inside the annealing block in the model in Section 7.2.2.

u Fluid velocity.

$\hat{u}$ Normalized fluid velocity. $\hat{u} = u/V$. See (7.68).

U_α $U(\alpha r)$.

U_β $U(\beta r)$.

$U(\lambda r)$ $J_0(\lambda r)Y_1(\lambda r_o) - J_1(\lambda r_o)Y_0(\lambda r)$. See (7.31).

V Average fluid velocity.

x Axial coordinate of the model.

$\hat{x}$.   Normalized x. $\hat{x} = x/[(\text{Re})(\text{Pr})(r_o)]$. See (7.68).

$X(x)$ Function of x used in T. See (7.16).

$\hat{X}(\hat{x})$ Function of $\hat{x}$ used in $\hat{T}$. See (7.77).

Y_0 Bessel function of the second kind of order zero.

Y_1 Bessel function of the second kind of order one.

α Possible value for λ used to determine the values of some integrals.

α_a	Thermal diffusivity of air.
α_f	Fluid thermal diffusivity.
α_o	Oil thermal diffusivity.
β	Possible value for λ used to determine the values of some integrals. $\beta \neq \alpha$.
β_a	Coefficient of thermal expansion of air.
ΔT_{Teflon}	Change in T_{Teflon} in the model in Section 7.2.2.
Δx	Increment at which experimental surface temperatures are taken, and at which the convection model is split.
λ	A constant linking radial and axial conduction. See (7.17).
ν_a	Kinematic viscosity of air.
ν_f	Fluid kinematic viscosity.
ρ_f	Fluid density.
$\Phi(t)$	Function of time used in T. See (7.54).

Chapter 8

Plug Breakup

8.1 Introduction

One unique aspect of the present design is that the sample drop (sometimes referred to as the plug) moves inside of an oil-filled capillary. If the surface tension is not strong enough to hold the plug together, it will break into smaller droplets. This will confuse the sensor system; the machine cannot handle multiple plugs. Therefore, it is important to quantify this design limitation.

There are two basic failure modes (see Fig. 8-1). If the plug is too large relative to the capillary and there is even a thin layer of oil between the plug and the capillary wall, it will break into pieces via the *Rayleigh instability*. This is discussed in Section 8.2. It is solely a matter of plug shape. To keep this from happening, I chose a plug volume of 1 μl for the 1 mm I.D. capillary.

Even if the plug is small enough to avoid the Rayleigh instability, if it moves fast enough, the surface tension will not be able to keep it intact. This is a more
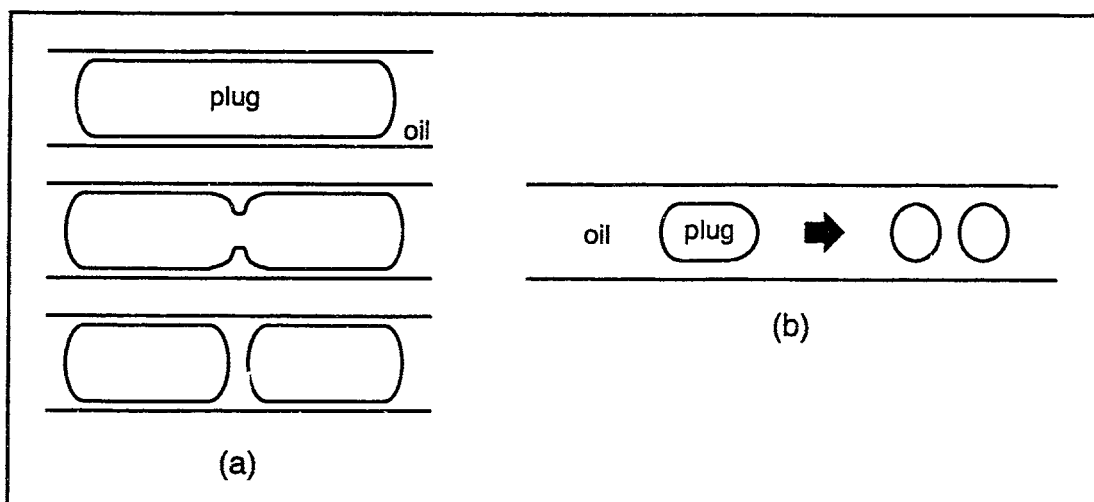
Figure 8-1: The sample plug breaks into smaller fragments if (a) the plug is too large, or (2) the velocity is too high.

complicated problem addressed in Section 8.3. An operating capillary number of $Ca \leq 0.2$ is recommended for this system to prevent breakup, based on experimental data.

In order to move the plug as fast as possible, Triton X-100 detergent present in the commercial Taq mix was removed via centrifugal concentration. This is described in Section 8.4. The resulting Taq mix was used to make the PCR mix. Section 8.5 describes the procedure used to approximate the surface tension of this mix (about 40 dyne/cm at 20°C).

8.2 Breakup Due to Excessive Plug Size

If the plug is long enough and there is even a thin layer of oil at its sides, the oil will impinge on the plug and break it into pieces. This will occur even if the plug is moving

very slowly or is stationary[1]. Lord Rayleigh analyzed this situation mathematically in 1878 in his classic work *On the Instability of Jets* [71]. He modelled an infinite liquid column immersed in a second immiscible liquid. If the column is subject to a sinusoidal disturbance of a given wavelength or greater, the surface area will decrease, causing the column to pinch off into a series of droplets. This is called the Rayleigh instability.

8.2.1 Rayleigh's Analysis

Consider an infinite cylinder of fluid with radius r_{Rayleigh} subject to a small sinusoidal disturbance of amplitude α and wavelength $\lambda_{\text{Rayleigh}}$:

$$r_{\text{Rayleigh}} = \overline{r}_{\text{Rayleigh}} + \alpha \cos\left(\frac{2\pi x}{\lambda_{\text{Rayleigh}}}\right) \tag{8.1}$$

where x is the axial coordinate, and $\overline{r}_{\text{Rayleigh}}$ is the average r_{Rayleigh}. The average surface area per unit length is

$$\hat{A} = 2\pi \overline{r}_{\text{Rayleigh}} + 2\pi^3 \, \overline{r}_{\text{Rayleigh}} \left(\frac{\alpha}{\lambda_{\text{Rayleigh}}}\right)^2 \tag{8.2}$$

The average volume per unit length is

$$\hat{V} = \pi (\overline{r}_{\text{Rayleigh}})^2 + \frac{\pi}{2}\alpha^2 \tag{8.3}$$

---

[1]This phenomenon has been observed many times in the literature. See, for example, [78].

198

Rearranging (8.3),

$$\bar{r}_{\text{Rayleigh}} = \sqrt{\left(\frac{\hat{V}}{\pi}\right)\left(1 - \frac{\pi\alpha^2}{2\hat{V}}\right)} \qquad (8.4)$$

Plugging (8.4) into (8.2) and approximating for vanishing α,

$$\hat{A} = 2\sqrt{\pi\hat{V}} + \frac{\pi\alpha^2}{2\bar{r}_{\text{Rayleigh}}}\left[\left(\frac{2\pi\bar{r}_{\text{Rayleigh}}}{\lambda_{\text{Rayleigh}}}\right)^2 - 1\right] \qquad (8.5)$$

If $\hat{A}_0$ is $\hat{A}$ if $\alpha = 0$, then

$$\hat{A} - \hat{A}_0 = \frac{\pi\alpha^2}{2\bar{r}_{\text{Rayleigh}}}\left[\left(\frac{2\pi\bar{r}_{\text{Rayleigh}}}{\lambda_{\text{Rayleigh}}}\right)^2 - 1\right] \qquad (8.6)$$

If $\hat{A} - \hat{A}_0 > 0$ for small α, then the system is stable. For this to be true,

$$\lambda_{\text{Rayleigh}} < 2\pi\bar{r}_{\text{Rayleigh}} \qquad (8.7)$$

8.2.2 Plug Volume

From (8.7), we see that the Rayleigh instability can be avoided by choosing the liquid cylinder length to be less than π times its diameter, since $\lambda_{\text{Rayleigh}}$ cannot be larger than the cylinder length. Therefore, the plug volume was chosen to be 1 μl. The capillary inner diameter is 1 mm. Approximating the shape of the stationary plug as a cylinder, the length is $4/\pi$ the diameter.

At slightly higher velocities, the plug elongates and assumes a different shape. At

199

these velocities, breakup is not governed merely by initial plug geometry.

8.3   Breakup Due to Excessive Speed

When plug speed is high enough, viscous and inertial forces can overcome the surface tension holding the plug together. This is true even if its dimensions make it safe from the Rayleigh instability.

8.3.1   Problem Definition

A homogenous drop moves at uniform velocity in a cylinder filled with a second homogeneous, immiscible fluid. The drop volume is 1 μl. The cylinder radius r_{tube} is 5.0×10^{-4} m. Due to the small dimensions of the problem, gravity is ignored. This assumption will be justified later. For simplicity, the model is axisymmetric.

Fig. 8-2 illustrates the problem as well as many of the relevant variables. r and x are the radial and axial coordinates. The fluid is split up into two regimes: the fluid inside of the drop, denoted by subscript d (which stands for drop), and the fluid outside of the drop (mineral oil), denoted by subscript f (which stands for fluid). The velocity vectors are $\vec{v}_d$ and $\vec{v}_f$; the absolute viscosities μ_d and μ_f; the pressures p_d and p_f; and the stress tensors $\vec{\sigma}_d$ and $\vec{\sigma}_f$. The position vector for a point inside of the drop is $\vec{x}_d$. $\hat{n}$ is a unit vector normal on the plug surface pointing away from the plug. γ is the surface tension at the plug/oil interface. Q is the bulk flow rate. $\bar{v}$ is the average bulk velocity, such that $\bar{v} = Q/(\pi r_{tube}^2)$.

If the plug has surfactant, it must be accounted for. If the drop is stationary, the
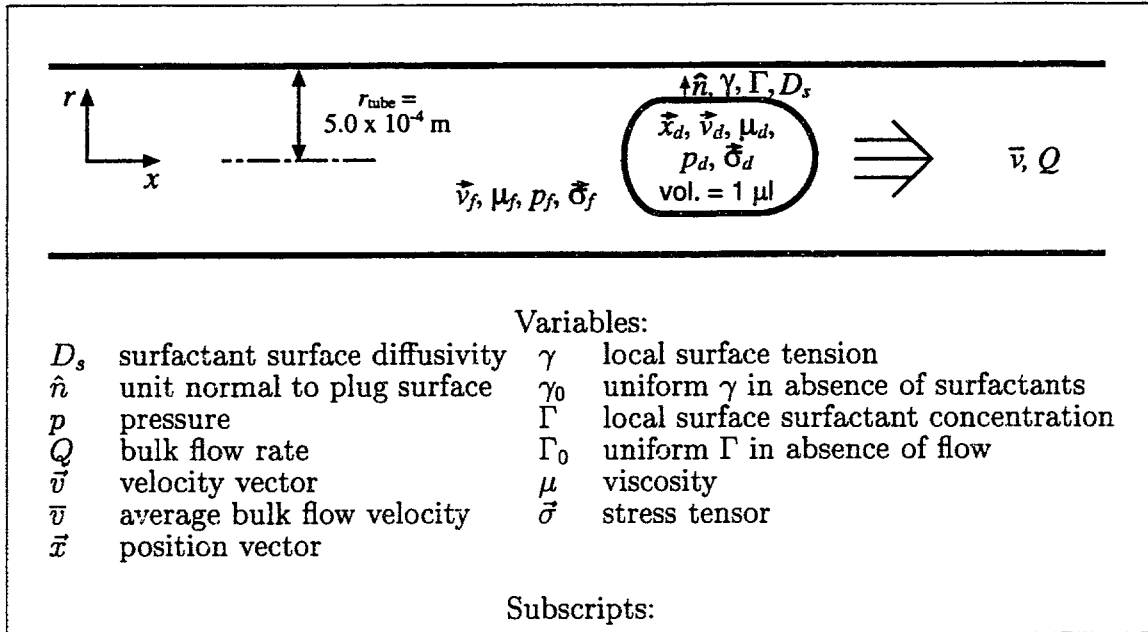
Figure 8-2: Schematic of the problem.

surfactant will eventually assume a uniform surface concentration Γ_0. When the plug

moves, the concentration varies across the surface, and the plug shape and surface

area also change. The local surfactant concentration is Γ. D_s is the diffusivity of the

surfactant at the surface, assuming that it is confined to the surface.

Table 8.1 lists the governing equations for this problem[2]. Gravity can be ignored

in the Navier-Stokes equations because the ratio of gravitational to surface tension

forces, represented by the Bond number Bo, is small:

$$\text{Bo} = \frac{\Delta \rho g r_{\text{tube}}}{\gamma} = \frac{(1000 \text{ kg/m}^3 - 855 \text{ kg/m}^3)(9.8 \text{ m/s}^2)(5.0 \times 10^{-4} \text{ m})^2}{17 \times 10^{-3} \text{ N/m}} = 0.021$$

$$(8.8)$$

Bo usually is proportional to ρ; it is the difference in density here since the density

---

[2]See, for example, [86].

201

STANDARD FORM	NONDIMENSIONAL FORM
Conservation of mass	
$\nabla \cdot \vec{v}_d = 0$ $\nabla \cdot \vec{v}_f = 0$	$\hat{\nabla} \cdot \hat{v}_d = 0$ $\hat{\nabla} \cdot \hat{v}_f = 0$
Navier-Stokes (neglect gravity)	
$\rho_d \frac{D\vec{v}_d}{Dt} = -\nabla p_d + \mu_d \nabla^2 \vec{v}_d$ $\rho_f \frac{D\vec{v}_f}{Dt} = -\nabla p_f + \mu_f \nabla^2 \vec{v}_f$	$\frac{1}{2}\frac{\rho_d}{\rho_f}\text{Re}\,\frac{\hat{D}\hat{v}_d}{\hat{D}t} = -\hat{\nabla}\hat{p}_d + \frac{\mu_d}{\mu_f}\left(\hat{\nabla}^2\hat{v}_d\right)$ $\frac{1}{2}\text{Re}\,\frac{\hat{D}\hat{v}_f}{\hat{D}t} = -\hat{\nabla}\hat{p}_f + \hat{\nabla}^2\hat{v}_f$
Effect of surfactant on surface tension	
$\gamma = \gamma_0 - \Gamma RT$	$\hat{\gamma} = 1 - \beta\hat{\Gamma}$
Surfactant convection/diffusion on plug surface	
$\frac{d\Gamma}{dt} + \nabla_s \cdot (\vec{v}_s\Gamma - D_s\nabla_s\Gamma)$ $+ \Gamma(\nabla_s \cdot \hat{n})(\vec{v}_f \cdot \hat{n}) = 0$	$\frac{d\hat{\Gamma}}{dt} + \hat{\nabla}_s \cdot \left(\hat{v}_s\hat{\Gamma} - \frac{1}{\text{Pe}}\hat{\nabla}_s\hat{\Gamma}\right)$ $+ \hat{\Gamma}(\hat{\nabla}_s \cdot \hat{n})(\hat{v}_f \cdot \hat{n}) = 0$
Boundary condition: no slip at the capillary wall	
$\vec{v}_f = \vec{0}$ at $r = r_{\text{tube}}$	$\hat{v}_f = \vec{0}$ at $\hat{r} = 1$
Boundary condition: velocity continuity at the plug surface	
$\vec{v}_d = \vec{v}_f$ at plug surface	$\hat{v}_d = \hat{v}_f$ at plug surface
Boundary condition: Stress balance at the plug surface	
$(\vec{\sigma}_f - \vec{\sigma}_d) \cdot \hat{n} = \gamma(\nabla \cdot \hat{n})\hat{n}$ at plug surface	$\text{Ca}(\hat{\sigma}_f - \hat{\sigma}_d) \cdot \hat{n} = (\hat{\nabla} \cdot \hat{n})\hat{n}$ at plug surface
Kinematic constraint at plug surface:	
$\frac{d(\vec{x}_d)}{dt} \cdot \hat{n} = \vec{v}_f \cdot \hat{n}$ at plug surface	$\frac{d(\hat{x}_d)}{dt} \cdot \hat{n} = \hat{v}_f \cdot \hat{n}$ at plug surface
Boundary condition: approaches laminar pipe flow far from plug	
$\vec{v}_f = \frac{2Q}{\pi r_{\text{tube}}^4}(r_{\text{tube}}^2 - r^2)\hat{i}_x$ at $|x| \to \infty$	$\hat{v}_f = 2(1 - \hat{r}^2)\hat{i}_z$ at $|\hat{x}| \to \infty$

Dimensionless Variables

$\hat{r} = r/r_{\text{tube}}$ $\hat{x} = \vec{x}/r_{\text{tube}}$ $\hat{p} = (pr_{\text{tube}})/(\mu_f\bar{v})$ $\hat{\gamma} = \gamma/\gamma_0$

$\hat{v} = \vec{v}/\bar{v}$ $\hat{\sigma} = (\vec{\sigma}r_{\text{tube}})/(\mu_f\bar{v})$ $\hat{\Gamma} = \Gamma/\Gamma_0$

Table 8.1: Governing equations, in standard and dimensionless forms. $\hat{i}_x$ is a x unit vector. $\nabla_s = \nabla - (\hat{n} \cdot \nabla)\hat{n}$ is the surface gradient operator. $\vec{v}_s = \vec{v}_f - (\hat{n} \cdot \vec{v}_f)\hat{n}$ is the plug surface velocity. R is the universal gas constant. T is the absolute temperature.

202

Name	Symbol	Definition
Capillary number	Ca	$(\mu_f \bar{v})/\gamma$
Reynolds number	Re	$(2\rho_f \bar{v} r_{\text{tube}})/(\mu_f)$
Viscosity ratio	κ	μ_d/μ_f
Density ratio	ϱ	ρ_d/ρ_f
Radius ratio	λ	$r_{d,\text{undeformed}}/r_{\text{tube}}$
Sensitivity to surface tension	β	$(\Gamma_0 RT)/\gamma_0$
Péclet number	Pe	$(\bar{v} r_{\text{tube}})/D_s$

Table 8.2: Dimensionless parameters determining plug breakup. R is the universal gas constant. T is the absolute temperature.

of the two liquids are of the same order. The density of the plug is taken to be the same as that of water. The γ value is based on data in Fig. 8-7: the lowest γ in the temperature range of interest (20°C room temperature to 94°C at the hottest heat block).

To find the relevant dimensionless quantities, we nondimensionalize the governing equations. Choose r_{tube} as the length scale; $\bar{v}$ as the velocity scale; $r_{\text{tube}}/\bar{v}$ as the time scale; $\mu_f \bar{v}/r_{\text{tube}}$ as the pressure scale; γ_0 as the surface tension scale; and Γ_0 as the surfactant concentration scale. Table 8.1 lists the nondimensionalized variables and equations. Note that the $\hat{\nabla}$, $\hat{\nabla}^2$, and $\hat{D}/\hat{D}\hat{t}$ operators are also nondimensional. We see that the relevant dimensionless variables are Ca, Re, β, Pe, $\kappa = \mu_d/\mu_f$, and $\varrho = \rho_d/\rho_f$. Of course, the plug size relative to the capillary matters. This is designated by the quantity $\lambda = r_{d,\text{undeformed}}/r_{\text{tube}}$. $r_{d,\text{undeformed}}$ is the radius of a sphere with the same volume as the drop:

$$r_{d,\text{undeformed}} = \sqrt[3]{\frac{3(\text{drop volume})}{4\pi}} \tag{8.9}$$

Table 8.2 lists the dimensionless parameters determining plug breakup.
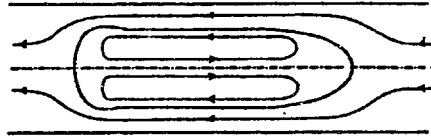
Figure 8-3: Flow, relative to the plug. From [67]. Plug is moving to the right. In the reference, the plug is pointed downward, and moves under the action of gravity; however, the flow lines are still applicable to slow pressure-induced flow.

Since Ca is proportional to $\bar{v}$, breakup conditions in the literature is usually specified in terms of a critical Ca, which we will designate Ca_c, above which breakup occurs. Re is also proportional to $\bar{v}$, but most of the cases studied in the literature have negligible Re. From Table 8.2, we see that

$$Ca_c = Ca_c(Re, \beta, Pe, \kappa, \varrho, \lambda)$$ (8.10)

Unfortunately, there is no simple equation relating these quantities. A few values of Ca_c exist in the literature for very specific cases.

8.3.2 Literature

A fluid plug moving through a capillary filled with a second immiscible liquid has the internal flow pattern shown in Fig. 8-3. At Ca_c, the drop shape is unstable. The surrounding fluid impinges upon the rear of the drop (see Fig. 8-4). This accumulation continues, leading to plug breakup.

Olbricht and Kung [62] examined equilibrium plug shapes for a range of λ, κ, and Ca, all the way up to plug breakup. The plug was a blend of Dow-Corning DC200 fluids, carefully mixed to produce the correct viscosity for the particular experiment.

204
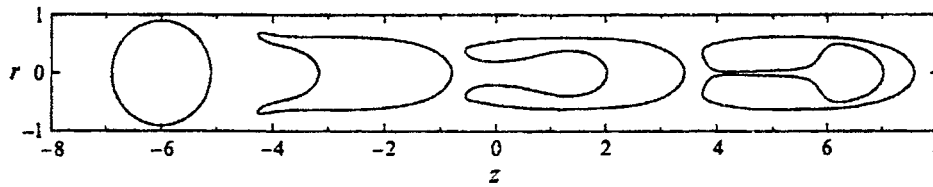
Figure 8-4: Initiation of breakup at high Ca for an initially spherical plug. From [86]. $\lambda = 0.9$, $\kappa = 0.1$, and Ca $= 1.0$. Plug motion is to the right. The surrounding fluid enters the rear of the drop and accumulates. This process continues until plug breakup.

Viscosity ratio κ	Dimensionless drop size λ								
	1.13	0.95	0.83	0.70	0.66	0.62	0.56	0.49	0.39
0.0013	4.08	4.08	4.82	5.50	>7.0				
0.0022	4.24	4.24	4.74	5.47	>5.7				
0.011	3.51	3.51	3.81	4.24	4.98	>5.7			
0.021	3.20	3.20	3.56	3.97	4.59	>5.7			
0.030	3.14	3.14	3.51	3.81	4.06	4.24	5.23	>5.7	
0.047	2.71	2.71	2.89	3.38	3.51	3.81	4.24	>5.7	
0.056	2.38	2.38	2.58	3.12	3.40	3.51	>6.4		
0.156	1.97	1.97	2.28	2.52	2.71	2.71	3.14	>5.7	
0.235	1.97	1.97	1.97	2.28	2.52	2.71	2.71	3.14	>5.7
0.469	1.85	1.85	1.97	2.28	2.52	2.89	3.14	4.24	>5.7
1.09	1.85	1.85	1.97	2.28	2.71	2.89	3.00	4.24	>5.7
1.75	1.85	1.85	1.97	2.28	2.71	2.89	3.00	4.24	>5.7
3.66	1.83	1.86	1.95	2.31	2.82	2.91	3.06	4.?8	>5.7

Table 8.3: Ca_c values found by Olbricht and Kung [62] for low Re and no surfactants. Ca_c does not change with λ for $\lambda > 0.83$.

The fluid surrounding it was either corn syrup or castor oil. To eliminate the effect of gravity, they made sure that $\varrho = 1$. The liquids were very clean, with no surfactants. They kept Re < 0.1 to eliminate the effect of inertia. The plug was observed to move faster than $\bar{v}$, which was what was predicted in earlier theoretical work. Olbricht and Kung photographed the process shown in Fig. 8-4. They also found Ca_c for different λ and κ, which is presented in Table 8.3.

There are a number of numerical simulations of a liquid drop moving within an

immiscible fluid in a capillary (for example, [8, 18, 35, 48, 67, 86, 87]). They examine low Re (Stokes) flow in which the acceleration terms in the Navier-Stokes equations are negligible. As seen in Table 8.1, if the model has Re = 0, then ϱ does not matter, since only the product ϱ Re appears in the equations of motion. Most of the simulations neglect gravitational and surfactant effects.

Martinez and Udell [48] were the first to numerically simulate Stokes flow of a fluid plug moving in an immiscible fluid within a capillary. They modelled the plug as inviscid ($\mu_d = 0$). Although they simulated Ca as high as 10, they suggested that their results could indicate breakup at Ca $\approx$ 1.

Pozrikidis [67], and later Jinnan and Maldarelli [35] improved on Martinez and Udell's model by accounting for plug viscosity. However, their studies were limited to the case of $\mu_d = \mu_f$. They investigated a train of plugs in a capillary. There was no mention of breakup criteria.

Tsai and Miksis [86] add an additional dimension by allowing for $\kappa \neq 1$. They studied a single plug in a capillary, rather than a train of plugs. They also carry their investigation to Ca values high enough for a steady-state drop shape not to exist. At this point, breakup eventually occurs as the surrounding fluid penetrates the trailing edge of the drop. Unfortunately, only two breakup conditions are listed in the paper: ($\lambda = 0.9$, $\kappa = 0.1$, Ca = 1.0) and ($\lambda = 1.2$, $\kappa = 0.1$, Ca = 2.0). Ca_c values found by Tsai and Miksis were somewhat lower than that found by Olbricht and Kung experimentally.

Coulliette and Pozrikidis [18] simulate a neutrally buoyant drop in an immiscible fluid within a capillary. As in Pozrikidis' early study, $\mu_d = \mu_f$, and a train of plugs is

206

modelled . However, they do relax the axial symmetry constraint present. For $\kappa = 1$, $\lambda = 0.7$, they present the following equation:

$$\mathrm{Ca}_c \cdot \lambda = 0.25 \left(\frac{r_{\text{tube}}}{r_{\text{tube}} + \delta r_0} \right) \qquad (8.11)$$

where δr_0 is the initial distance of the plug centroid from the capillary axis. Unfortunately, (8.11) only applies to a train of equally spaced drops, where the spacing is $2\, r_{\text{tube}}$. Under these conditions, Coulliette and Pozrikidis found that the effect of the drops on each other is significant.

Borhan and Mao [8] as well as the second study of Tsai and Miksis [87] used the two surfactant equations listed in Table 8.1 to model the effect of surfactants. They modelled insoluble surfactants that were confined the the surface of the plug.

Borhan and Mao [8] studied the following ranges of parameters: $0.01 \leq \mathrm{Pe} \leq 100$, $0 \leq \beta \leq 1$, $0.50 \leq \lambda \leq 1.30$, $0.05 \leq \mathrm{Ca} \leq 0.75$, and $0.19 \leq \kappa \leq 10.0$. They found that the greater λ, the greater the surfactant dilution. This is because a large drop deforms and increases its surface area more than a smaller drop. For large Pe, the effect of surfactant diffusion is small relative to the convective effect of the flow at the surface. In this case is little relative motion of the plug surface relative to the plug as a whole, due to Marangoni stresses. Unfortunately, Borhan and Mao do not say much about breakup. Their only comment is that for $\lambda = 0.726$, $\kappa = 1.0$, $\mathrm{Ca} = 0.75$, and $\beta = 0.5$, the plug was only stable for $\mathrm{Pe} \leq 0.1$.

In their second study, Tsai and Miksis [87] found similar results to Borhan and Mao. They only present the case of $\lambda = 0.9$, $\kappa = 0.1$, and listed two breakup

conditions: (1) Ca = 0.4, β = 0.75, Pe = 1; and (2) Ca = 1, β = 0.5, and 0.1 < Pe < 10. They found that increasing β or Pe will decrease Ca_c. Also, the mere presence of surfactant decreases Ca_c: even if two otherwise identical drops have the same γ, but one of them has surfactant and the other does not, the one with surfactant will have a lower Ca_c. This can be seen from comparing the results with their earlier study of drops without surfactants [86] (see above).

Milliken and Leal [51] modelled drops with soluble surfactants in uniaxial extensional flow. The surfactant was located both on the interfacial surface and in the fluid surrounding the drop, and was free to diffuse between the two. They found that the resulting behavior was between that of a drop with insoluble surfactant (in which the surfactant was confined to the plug surface) and that of a drop with uniform surfactant distribution. While our flow is different, and the surfactant is present inside rather than outside of the drop, we expect the same general qualitative results.

8.3.3 Room Temperature Experiment

To get an initial estimate of Ca_c for my system, I first ran an experiment with the entire system at 20°C. This made temperature-dependent properties easy to evaluate. Also, $\bar{v}$ was slower than it would be in the actual PCR system due to higher μ_f, so $\bar{v}$ was easier to measure. I used the actual PCR mix described in Table 8.6, and increased $\bar{v}$ up to plug breakup to determine Ca_c.

To find $\bar{v}$, the pressure across the capillary at (actually, just under) breakup was

Property	Value
$\bar{v}$	0.067 m/s
γ	4.08×10^{-2} N/m
$\kappa = \mu_d/\mu_f$	0.0057
$\lambda = r_{d,undeformed}/r_{tube}$	1.2
μ_f	0.174 kg/(m·s)
ρ_f	855 kg/m^3
r_{tube}	5.0×10^{-4} m
$Ca = (\bar{v} \cdot \mu_f)/\gamma$	0.29
$Re = (2 \, \rho_f \bar{v} r_{tube}/\mu_f)$	0.33

Table 8.4: Selected quantities at breakup for 20°C experiment. Material properties are from Appendix A. γ is from Fig. 8-7.

measured with a differential pressure gauge[3]. This pressure difference was duplicated with one end of the capillary at atmosphere. Oil was collected from this end in preweighed microfuge tubes for $\approx$ 8 seconds for each of 3 trials. The quotient of collected oil mass to collection time was averaged and used with the oil density to get $\bar{v} = 0.067$ m/s.

Table 8.4 lists some properties at plug breakup. For $\lambda > 0.83$ and $0.0022 < \kappa < 0.011$, Olbricht and Kung predict $3.51 < Ca_c < 4.24$ (see Table 8.3). This is much larger than my value of 0.29. There are several possible reasons for this, which are discussed in Section 8.3.5.

8.3.4 Heated Blocks Experiment

I repeated the Ca_c experiment for realistic conditions under which the denaturing, extension, and annealing blocks were 94°C, 70°C, and 53°C, respectively. Ca_c is more difficult to calculate in this instance since the sample plug moves through a range of

---

[3]Magnehelic 2230. Dwyer Instruments, Inc., Michigan City, IN.

different temperatures, and the speed is higher.

I ran three trials. In two trials, I reached the Δp limit of ≈ 19 psi across the 9"
capillary without breakup. In one trial, $\Delta p = 13$ psi just before breakup. This was
for motion from right to left, which was faster than left to right, due to a difference in
air resistance of the solenoids supplying the pressurized air to the two capillary ends.

Unfortunately, the oil was moving too fast to estimate $\bar{v}$ by the oil collection
method used in Section 8.3.3. Instead, I defined an average oil viscosity $\bar{\mu}_f$, such that
the bulk flow rate corresponds to laminar flow in a capillary with the same r_{tube} and
dp_f/dx but uniform viscosity $\bar{\mu}_f$:

$$\bar{v} = -\frac{r_{\text{tube}}^2}{8\bar{\mu}_f}\left(\frac{dp_f}{dx}\right) \tag{8.12}$$

I approximated $\bar{\mu}_f$ as 7.0×10^{-2} kg/(m·s), the value found via oil collection at Δp's of
2.2 psi and 2.9 psi. Given this $\bar{\mu}_f$, the radius $r_{\text{tube}} = 5 \times 10^{-4}$ m, and $dp_f/dx \approx \Delta p/\Delta x$
$= (-13\text{ psi})/(9")$, (8.12) is used to estimate $\bar{v}$ as 0.18 m/s.

μ_f and γ both decrease with increasing temperature. γ is not nearly as tempera-
ture dependent, however. Therefore, the highest Ca, and most likely breakup, occurs
when the plug temperature is lowest. I used the heat transfer model described in
Chapter 7 to determine the lowest temperature. Since the velocity is fairly high for
this system, the temperature does not change much during travel. The plug speed
is slightly higher than $\bar{v}$, but as a model simplification the two are taken to be the
same. The lowest temperature experienced by the plug is as it travels from the anneal
(53°C) block to denature (94°C) block, between the anneal and extension blocks. See
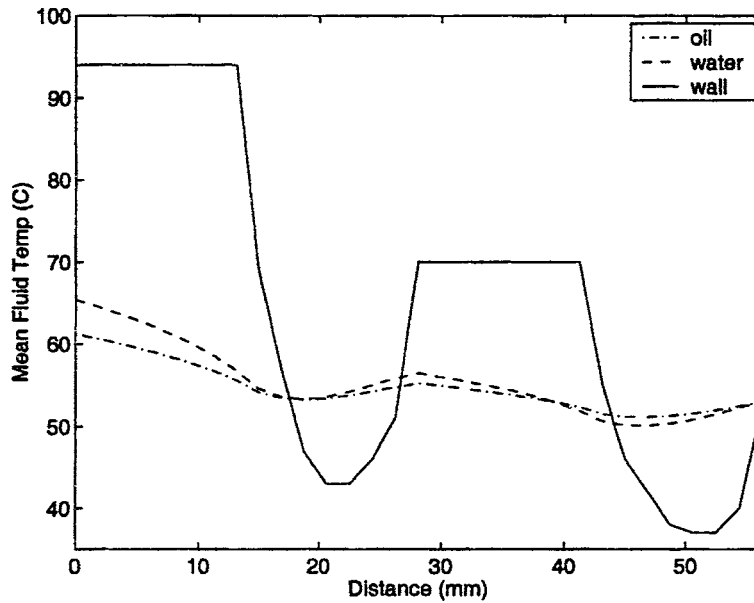
Figure 8-5: Simulation of the temperature history of the plug and the oil in its immediate vicinity. The plug temperature is between the only oil and only water curves. Heat transfer model details are found in Chapter 7. Plug is moving from right to left (decreasing distance) at a velocity of 0.18 m/s.

Fig. 8-5. The minimum temperatures for the all-water and all-oil simulations are 50°C and 51°C, respectively. They occur at the same x. These minimum temperatures are very close to the annealing block temperature as well as each other. This is because $\bar{v}$ is too high for much heat transfer to take place before the plug reaches the denature block. Since the plug is between the all-oil and all-water simulation temperatures, I take it to be 50°C.

Table 8.5 shows some quantities calculated at 50°C and just under breakup $\bar{v}$. At $\kappa = 0.013$, $\lambda > 0.83$, Olbricht and Kung predict $Ca_c = 3.5$ (see Table 8.3). This is much larger than the 0.24 found experimentally for my system. Reasons for this discrepancy are discussed in Section 8.3.5.

211

Property	Value
$\bar{v}$	0.18 m/s
γ	3.12×10^{-2} N/m
$\kappa = \mu_d/\mu_f$	0.013
$\lambda = r_{d,\text{undeformed}}/r_{\text{tube}}$	1.2
μ_f	0.0415 kg/(m·s)
ρ_f	855 kg/m^3
r_{tube}	5.0×10^{-4} m
$\text{Ca} = (\bar{v} \cdot \mu_f)/\gamma$	0.24
$\text{Re} = (2\,\rho_f \bar{v} r_{\text{tube}}/\mu_f)$	3.7

Table 8.5: Selected quantities at breakup assuming breakup at 50°C. Material properties are from Appendix A. γ is from Fig. 8-7.

8.3.5 Ca$_c$ Discrepancy

In Sections 8.3.3 and 8.3.4, we found Ca$_c$ values of 0.29 and 0.24 respectively. This is much lower than the values obtained by Olbricht and Kung (approximately 4 and 3.5, respectively) for their low Re, surfactant-free experiments [62]. From (8.10), we see that Ca$_c$ is a function of six dependent variables: Re, β, Pe, κ, ϱ, and λ. We will examine which of these variables can account for the discrepancy, as well as discussing additional causes of difference.

λ :

$\lambda = 1.2$ is a constant, and is accounted for by Olbricht and Kung, so it cannot account for the Ca$_c$ discrepancy.

κ :

κ is accounted for the Olbricht and Kung. However, κ was only calculated for at the minimum temperature in Sections 8.3.3 and 8.3.4. It was assumed that μ_f affects Ca$_c$

212
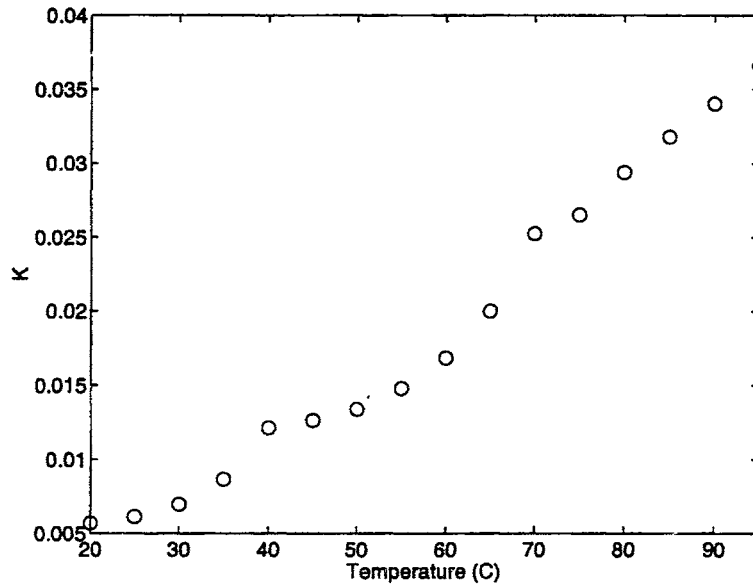
Figure 8-6: $\kappa = \mu_d/\mu_f$. μ_d and μ_f were based on values in Appendix A, and were linearly interpolated between datapoints.

more than κ, since Ca_c is proportional to μ_f. $\kappa = \mu_d/\mu_f$ changes with temperature (see Fig. 8-6). In PCR, plug temperature typically ranges from 45–94°C, so the κ range is 0.013–0.04. From Table 8.3 we see that Ca_c for $\lambda = 1.2$ does not change much in this range. Therefore, I assume that κ does not significantly affect Ca_c, and cannot account for the (greater than tenfold) Ca_c discrepancy.

ϱ :

$\varrho = \rho_d/\rho_f = (1000 \text{ kg/m}^3)/(855 \text{ kg/m}^3) = 1.17$. Olbricht and Kung used $\varrho = 1$, so the Bond number Bo $= 0$. Since $\varrho \approx 1$ and the Bo $= 0.021$ (see (8.8)), I do not expect my ϱ to cause Ca_c to deviate much from Olbricht and Kung's results.

213

β and Pe:

β and Pe play a role in systems with surfactants. I removed the Triton X-100 from my plug mix (see Section 8.4), but other constituents could possibly act as surfactants, such as the Taq itself. Based on the results of Tsai and Miksis ([87]; see Section 8.3.2), Ca_c is lower than it would be without surfactants, and their presence accounts for some of the discrepancy. However, since I cannot find D_s, I do not know Pe $= \overline{v}r_{tube}/D_s$, so I cannot further quantify the effect of surfactants using information from the literature.

Re:

In Section 8.3.4, I calculated Re $= 3.7$ at the minimum temperature (50°C), assuming that this is where breakup occurs. This assumption is based on the fact that Ca is proportional to μ_f, which is highest at this lowest temperature. At the highest temperature, 94°C, ν_f is 9.80×10^{-6} m^2/s, so Re is 18. If Ca_c drops steeply as Re goes from 3.7 to 18, breakup may occur when the plug is at the highest (94°C) rather than lowest (50°C) temperature. In any case, Re > 1, so kinetic effects are significant, and can account for some of the Ca_c discrepancy.

Additional Possible Causes:

There are several other influences which can account for Ca_c that are not covered by any of the six dependent variables listed above.

First, the γ found by the faux PCR mix may be off significantly. BSA and ATP may not have the same effect on γ as Taq and the four dNTPs. γ may have been

214

overestimated, resulting in a lower calculated than actual Ca_c.

Olbricht and Kung take care to accelerate their drops slowly to eliminate the influence of acceleration on Ca_c. In the capillary PCR system, the plug is accelerated and decelerated as fast as the actuators allow. The plug speed was too high to observe whether breakup was due to acceleration, deceleration, or the entrainment effect at constant $\bar{v}$ described Olbricht and Kung. This can definitely result in a lower apparent Ca_c. In fact, I may require a more complicated breakup criteria than just Ca_c.

$\bar{v}$ at breakup has significant variation from trial to trial. In the Ca_c experiments with the heat blocks at 94°C, 70°C, and 53°C (Section 8.3.4), 1 of the trials had the plug intact up $\Delta p = 13$ psi across the capillary, whereas the other 2 trials had the plug intact to $\Delta p \geq 20$ psi. I based Ca_c on the lowest $\bar{v}$, not the highest, and this definitely contributes to the discrepancy in Ca_c. Drop initial conditions seem to play a large role in determining breakup, and acceleration and deceleration may not be exactly the same at each application.

In addition, the breakup mode reported in the literature in Section 8.3.2 may not be applicable at all to the capillary PCR machine. In the literature, breakup occurs when the nonsteady drop shape allows the surrounding fluid to enter the interior of the drop, and so much fluid enters the drop that it splits into pieces. Oil was observed to enter the drop in the 20°C experiments, but the travel time was too short for enough oil to enter the plug to break it up. Instead, once the plug was stopped, it resumed its intact stationary shape. Unfortunately, in the more realistic experiment with the 94°C, 70°C, and 53°C blocks, the plug was moving too fast to see if this occurred.

Volume	Constituent
35.4 μl	Taq mix
1.46 μl	10× buffer mix
1.17 μl	25 mM MgCl$_2$
3 μl	λ DNA template (1 pg/μl)
3 μl	PE1 primer (10 pmol/μl)
3 μl	PE2 primer (10 pmol/μl)
3 μl	5 mM dNTPs
50 μl	TOTAL

Table 8.6: 30 cycle PCR mix. The Taq mix is described in the text. The 10× buffer is 500 mM KCl, 100 mM Tris-HCl (pH 9.0 at 25°C).

Given all these factors, it is difficult to determine a precise breakup criterion. Keeping Ca $\leq$ 0.2 should be safe. This is assuming the the plug acceleration and deceleration is no higher than that imposed in the current system (which are roughly quantified in another chapter).

8.4 Removing the Detergent

The PCR mix used in the 30 cycle experiments is shown in Table 8.6. Since it was important to have γ as high as possible, I tried to remove the Triton X-100 from the mix, since it is a nonionic surfactant. While it is necessary to stabilize the protein during storage, it was experimentally determined that Taq remains active immediately after its removal.

To remove the Triton, I used centrifugal concentration devices[4] with 50 kDa cutoff membranes. Prior to usage, I passivated the devices with 1% powdered milk in distilled water according to manufacturer's instructions. This was to prevent the

---

[4] Centricon-50. Millipore Corporation, Bedford, MA.

Property	Value	Reference
Critical Micelle Concentration	0.24 mM	[31, p. 1882]
Molecular Weight	625	[81, p. 1882]
Specific Gravity (25°C)	1.0595	[95, p. 971]

Table 8.7: Selected properties of Triton X-100.

Taq from sticking to the walls of the devices themselves. I diluted with 20 μl of Promega[5] Taq solution with 2 ml dilution buffer. The Taq solution consists of 5U/μl Taq enzyme, 50 mM Tris-HCl (pH 8.0 at 25°C), 100 mM NaCl, 0.1 mM EDTA, 1 mM DTT, 50% glycerol, and 1% Triton X-100 [69]. The glycerol and Triton X-100 are liquids, so they are expressed in volume fractions. The dilution buffer consists of 50 mM KCl, 10 mM Tris-HCl (pH 9.0 at 25°C), and 2 mM $MgCl_2$.

Triton X-100 has the properties listed in Table 8.7. Diluting 20 μl of Promega Taq with 2 mL of the buffer results in a Triton concentration of:

$$(1\%) \left(\frac{20 \times 10^{-6} \text{ l}}{2 \times 10^{-3} \text{ l}} \right) \left(\frac{1.0595 \times 10^3 \text{ g}}{1} \right) \left(\frac{\text{mole}}{625 \text{ g}} \right) = 0.17 \text{ mM} \qquad (8.13)$$

This is below the critical micelle concentration, so the Triton X-100 exists in the solution as individual particles. The solution is placed in a concentrator and spun. The 625 Da Triton molecules pass through the 50 kDa cutoff membrane, but not the 94 kDa Taq. Since 0.17 mM is close to the critical micelle concentration of 0.24 mM, the process is repeated.

About 80 μl liquid remains after the spin. Since the liquid is largely dilution buffer, the mix shown in Table 8.6 has a KCl concentration of 50 mM, a Tris-HCl (pH 9.0 at

[5]Taq DNA Polymerase in Storage Buffer A. Catalog number M1861. Promega Corporation, Madison, WI.

Solute	Concentration	Nominal MW	% Retentate Recovery
Bovine IgG Fraction II	1 mg/ml	156,000	95
Phosphorylase B	1 mg/ml	97,400	90
Bovine Serum Albumin	1 mg/ml	67,000	95
Ovalbumin	1 mg/ml	45,000	85
α-Chymotrypsinogen	1 mg/ml	25,000	75
Cytochrome c	0.25 mg/ml	12,400	35
Protamine Sulfate	1 mg/ml	5,000–10,000	≤ 5
Vitamin B12	0.2 mg/ml	1,355	≤ 5
Riboflavin	(saturated solution)	376	≤ 5

Table 8.8: Typical retentate recovery for the Centricon-50 centrifugal concentrator device. Taken from product literature.

25°C) concentration of 10 mM, and a $MgCl_2$ concentration of 2 mM, as desired. The amount of Taq and its remaining activity is unknown. However, Taq is a thermostable protein, so I assumed no loss of activity per unit mass. The centrifugal concentrator literature lists the typical retentate recoveries shown in Table 8.8. Phosphorylase B has a molecular weight (97.4 kDa) close to that of Taq (94 kDa), and its typical recovery is 90%. Therefore, I assumed 90% recovery of Taq during each of the two spins. Hence, the end Taq concentration is about

$$\left(\frac{5 \text{ units}}{\mu l}\right)\left(\frac{20\mu l}{80\mu l}\right)(0.9)^2 = 1.0\frac{\text{units}}{\mu l} \tag{8.14}$$

Note that the protein concentrations listed in Table 8.8 are ~1 mg/ml. Since the activity of Taq is $\approx 200,000$ units/mg [68], and 100 units Taq are put into 2 ml dilution buffer, the end concentration is $\approx 2.5 \times 10^{-4}$ mg/ml. This is significantly less than 1 mg/ml. This lessens the chance of the protein aggregating (destruction of activity results) or sticking to the membrane, and is likely to result in more rather than less recovery.

8.5 Plug Surface Tension

I wanted to measure the surface tension at the sample plug/oil interface. Unfortunately, the tensiometer requires ~ 100 ml of liquid. Taq and the dNTPs are far too expensive to merely scale up the PCR mix. Therefore, I created a "faux" PCR mix designed to mimic the PCR mix shown in Table 8.6.

Bovine Serum Albumin (BSA) Fraction V was used as a substitute for Taq. From Table 8.8, we see that the molecular weight of BSA is 67 kDa, so it is roughly the same size as Taq (94 kDa). Since Taq has $\approx 200,000$ units/mg, from (8.14), we see that the Taq mix has a Taq concentration of $\approx 5 \times 10^{-3}$ g/l after centrifugal concentration. Therefore, 5×10^{-3} g/l BSA in water was used to substitute for the Taq solution.

ATP is chemically very similar to dATP. The difference is merely the substitution of a single OH group with an H group in dATP. Hence, ATP was used to substitute for dATP, as well as dCTP, dGTP, and dTTP. It was assumed that the different dNTPs had similar effects on the surface tension of the mixture. The original PCR mix calls for a solution of 5 mM of each of the four dNTPs (see Table 8.6). The faux PCR mix is made with 20 mM ATP solution instead.

The rest of the mix had the same constituency as the actual PCR mix. The recipe for the faux PCR mix is shown in Table 8.9.

Surface tension measurements for the faux PCR mix were taken using a ring tensiometer[6]. The faux PCR mix was poured into a thoroughly cleaned glass dish and covered with a layer of mineral oil. The dish was placed in a water bath to alter

---

[6]Cenco #70535 with platinum-iridium ring #6406. Mean ring circumference 5.935 cm. Cenco Instrument Corp.

the temperature. Results are shown in Fig. 8-7. As can be seen, the surface tension exhibits somewhat linear temperature behavior. The best fit formula in Fig. 8-7 is used for the surface tension in this chapter.

Volume	Constituent
35 ml	faux Taq mix
1.46 ml	10× buffer mix
1.17 ml	25 mM $MgCl_2$
3 ml	λ DNA template (1 pg/μl)
3 ml	PE1 primer (10 pmol/μl)
3 ml	PE2 primer (10 pmol/μl)
3 ml	20 mM ATP mix
50 ml	TOTAL

Table 8.9: Faux PCR mix.

30 Cycle PCR Mix Surface Tension

Best Fit Line:
Surface Tension = (47.2 - 0.32 T) dynes/cm
$R^2 = 0.9$
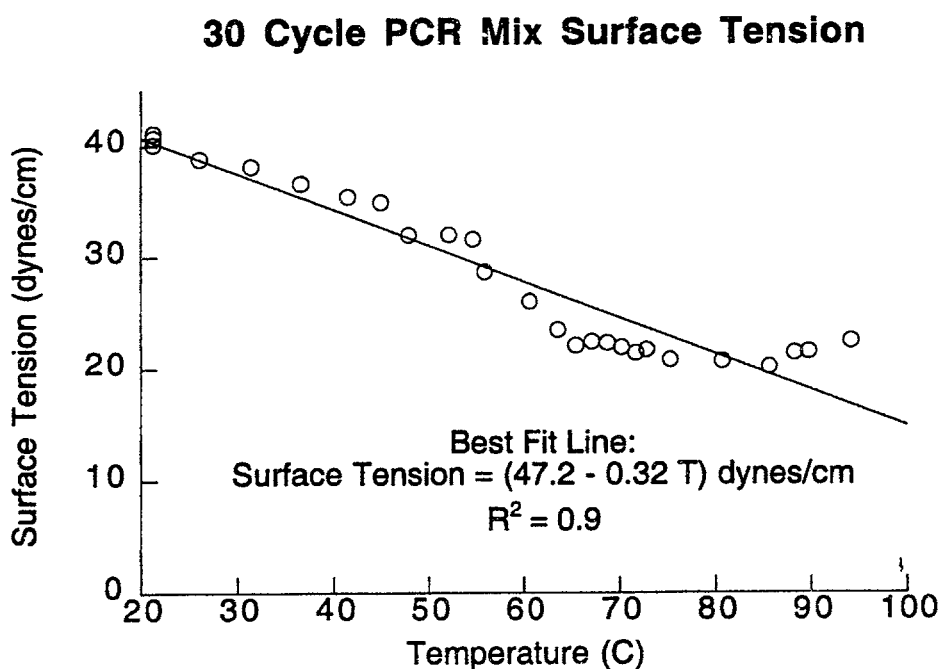
Figure 8-7: Surface tension data for faux PCR mix. T for the best fit line is temperature in °C.

8.6   Nomenclature

$\hat{A}$ Average surface area per unit length. See Eq. (8.2).

$\hat{A}_0$ $\hat{A}$ for undisturbed surface. See Eq. (8.6).

Ca   The capillary number. $\mathrm{Ca} = \bar{v} \cdot \mu_f/\gamma$.

$\mathrm{Ca_c}$ The critical capillary number. Ca at which plug breakup occurs.

D_s Surface diffusivity of surfactant.

$\hat{i}_x$ Unit normal in x direction.

$\hat{n}$ Unit normal pointing away from the plug surface. See Fig. 8-2.

p_d Pressure inside the plug.

p_f Pressure in the fluid surrounding the plug.

Pe   The Péclet number. $\mathrm{Pe} = \bar{v} \cdot r_{\mathrm{tube}}/D_s$.

Q Volume flow rate in capillary.

R The universal gas constant (1.987×10^{-3} kcal/mol·K).

Re   The Reynolds number. $\mathrm{Re} = 2r_o \bar{v}/\nu$.

r Radial coordinate of capillary.

$r_{d,\mathrm{undeformed}}$ Radius of a sphere with the same volume as the plug.

r_{Rayleigh} Radius of fluid cylinder in Rayleigh instability derivation. See

             Eq. (8.1).

$\bar{r}_{\mathrm{Rayleigh}}$ Average r_{Rayleigh}. See Eq. (8.1).

r_{tube} Inner radius of the capillary.

t Time.

T Absolute temperature.

$\bar{v}$	Average velocity of fluid in the capillary.
$\hat{V}$	Average volume per unit length. See Eq. (8.3).
$\vec{v}_d$	Velocity vector inside the plug. See Fig. 8-2.
$\vec{v}_f$	Velocity vector of fluid outside the plug. See Fig. 8-2.
$\vec{v}_s$	The surface velocity $\vec{v}_s = \vec{v}_f - (\hat{n} \cdot \vec{v}_f)\hat{n}$. See Table 8.1.
$\vec{x}_d$	Position vector of the plug surface. See Fig. 8-2.
x	Coordinate along axis of capillary, in direction of flow.
α	Disturbance amplitude. See Eq. (8.1)
β	Sensitivity of surface tension to surfactants. $\beta = \Gamma_0 RT/\gamma_0$.
γ	Surface tension.
γ_0	Surface tension in the absence of surfactants.
Γ	Local surfactant concentration.
Γ_0	Uniform surfactant concentration in the absence of flow.
κ	Viscosity ratio. $\kappa = \mu_d/\mu_f$.
λ	Radius ratio. $\lambda = r_{d,\text{undeformed}}/r_{\text{tube}}$.
$\lambda_{Rayleigh}$	Disturbance wavelength in Rayleigh instability calculation. See Eq. (8.1).
μ	Absolute viscosity.
μ_d	Absolute viscosity of the plug.
μ_f	Absolute viscosity of the fluid surrouding the plug.
$\bar{\mu}_f$	Average μ_f in the capillary.
∇_s	The surface gradient operator. $\nabla_s = \nabla - (\hat{n} \cdot \nabla)\hat{n}$. See Table 8.1.

ν	Kinematic viscosity. $\nu = \mu/\rho$.
ρ	Density.
ρ_d	Plug density.
ρ_f	Density of the fluid surrounding the plug.
ϱ	Density ratio. ρ_d/ρ_f.
σ_d	Stress tensor for the plug fluid.
σ_f	Stress tensor for the fluid surrounding the plug.

Chapter 9

Motion Control

9.1 Introduction

Chapter 8 examined the maximum speed the plug can attain before it fragments into pieces. However, at lower velocities, the speed may still be so high that the plug continually oscillates within a heat block after reaching it. This is undesirable. The solenoid valves are not designed to alternate quickly between open and closed states over many cycles. Oscillation also greatly increases the total plug displacement, and therefore the amount of Taq adsorbed onto the capillary walls.

This chapter determines the maximum velocity attainable before oscillation occurs.

9.2 Dynamics

9.2.1 Oil

There are several dynamics involved in plug motion. First is that of the mineral oil inside of the capillary. The plug velocity is slightly higher than, but directly proportional to, the bulk oil speed. The plug motion is assumed to be completely dominated by the oil, since it occupies the vast majority of the capillary. Oil velocity throughout[1] the capillary is assumed to be parallel to the capillary axis.

The problem of transient velocity distribution for axisymmetric fluid in a tube has been solved[2]. The governing equation is

$$\rho \frac{\partial u}{\partial t} - \mu \left(\frac{\partial^2 u}{\partial r^2} + \frac{1}{r} \frac{\partial u}{\partial r} \right) = -\frac{dp}{dx} \tag{9.1}$$

where ρ is oil density, $u = u(r, t)$ is oil speed, t is time, μ is oil viscosity, r is the radial coordinate, p is pressure, and x is the axial coordinate. The boundary conditions are

$$u(r, 0) = 0 \qquad\qquad u(r_{\text{tube}}, t) = 0 \tag{9.2}$$

where r_{tube} is the capillary inner radius. The solution is

$$\frac{u}{u_{\text{max}}} = 1 - \frac{r^2}{r_{\text{tube}}^2} - 8 \sum_{n=1}^{\infty} \frac{J_0(\lambda_n r / r_{\text{tube}})}{\lambda_n^3 J_1(\lambda_n)} e^{-(\lambda_n^2 \mu t)/(\rho r_{\text{tube}}^2)} \tag{9.3}$$

---

[1]Except at the entrance and exit; entrance and exit effects are assumed to be negligible since the capillary length is much greater than the capillary inner diameter.

[2]See, for example, [17, p. 189–193].

where J_0 and J_1 are the Bessel functions of order 0 and 1, respectively. The λ_n's are roots of J_0:

$$J_0(\lambda_n) = 0 \tag{9.4}$$

and $u_{\max}$ is the maximum u which occurs at $r = 0$, $t \to \infty$:

$$u_{\max} = -\frac{r_{tube}^2}{4\mu}\frac{dp}{dx} \tag{9.5}$$

We see from (9.3) that the transient component of the solution has time constants

$$\frac{\rho r_{tube}^2}{\mu \lambda_n^2} \tag{9.6}$$

The dominant time constant is associated with[3] $\lambda_1 = 2.40$. Since[4] $\rho = 855$ kg/m^3 and $\mu = 7.0 \times 10^{-2}$ kg/(m·s), the dominant time constant is 0.53 ms.

9.2.2   Valves and Pneumatics

This is very fast. However, the capillary is also connected to a pneumatic system. It takes time for the valves to open and close[5], and for the pressure to equilibriate in each oil reservoir. I felt that these dynamics were probably much slower than the oil dynamics.

---

[3]For λ values, see for example [63, p. 409].

[4]ρ was taken from Appendix A. μ was the average value established in Section 8.3.4.

[5]According to the manufacturer [40, p. 52], the typical valve response time is 6–12 ms. This is the time required for a closed valve to totally open or vice versa. Valve dynamics are reflected in the overall time constant.

To test this hypothesis, I used a VCR and CCD camera to record plug motion at 30 frames/second. The plug accelerated from stationary to steady-state speed within 2 frames. It also decelerated from steady state to a full stop within 2 frames. 2 frames is 70 ms, which is much longer than the oil time constant of[6] 0.53 ms, so the pneumatic system dynamics dominate over the oil dynamics.

I modelled the overall system dynamics as first-order. Data from the VCR was too crude to determine more than a single time constant. Since the speed reaches steady-state within 70 ms, assume that this is 3 time constants (a standard point at which a first order reaction is considered to have arrived at steady-state). Therefore, the observed time constant $\tau = 20$ ms.

9.2.3 Computer Sampling

Although the A/D card can sample up to 50 kHz, the process is much slower than that due to all the housekeeping tasks that the controlling program performs, such as updating the display and writing to the log file. I determined that the actual sampling time is about 4 ms.

---

[6]Since the opaque heat blocks had to be removed to film the plug, the experiments were conducted at room temperature. The oil also has higher μ at room temperature than during PCR, reducing the plug speed and simplifying measurements. The time constant for room-temperature mineral oil $(\mu/\rho = 2.04 \times 10^{-4}$ m^2/s) is 0.29 ms. This differs from the 0.53 ms time constant when the capillary passes through the heat blocks. However, both are $\ll 70$ ms, justifying the overall time constant measurement.

9.3 Modelling

This section presents a simple model of oscillation, which is used to determine the criteria under which it will occur.

9.3.1 Photodiode Signals

Let PD_{left} and PD_{right} be the normalized signals of the photodiodes to the immediate left and right of a heat block. Both are negative[7]. Assume that both signals have been normalized to a range of 0 (background signal) to -3 volts (maximum signal). Define $PD_{L-R} \equiv PD_{\text{left}} - PD_{\text{right}}$. Fig. 9-1a shows a typical PD_{L-R} curve as the plug moves from left to right completely through the heat block. PD_{L-R} passes over[8] the left photodiode, and largest when the plug passes over the right photodiode. PD_{left} dominates PD_{L-R} in Fig. 9-1 from a distance of about 40–60 mm. The influence of both PD_{left} and PD_{right} are strong at 60–70 mm. At 70–90 mm, PD_{L-R} is dominated by PD_{right}.

Model PD_{L-R} as linear, as shown in Fig. 9-1b. There is 18 mm distance between the signal maximum and minimum. This is the center-to-center distance between the two photodiodes (see Fig. 9-2). The actual width of each heat block is 1/2" (12.5 mm). In order to ensure that the plug is heated at the block temperature at all times, take the errorband to be 8 mm. This is a maximum value; it is often smaller in practice. The errorband is the region that the plug center must stay within. If the

---

[7]See Chapter 4 for details.
[8]Actually, when the center of the plug is just slightly to the left of the photodiode. Since the laser beam enters from the left, the scatter is stronger to the right of the plug than to the left.
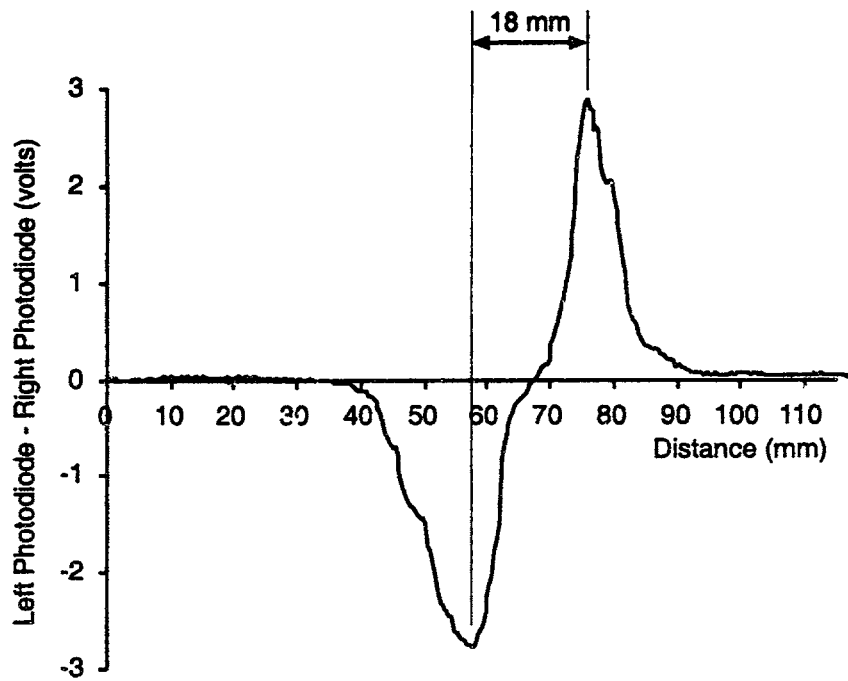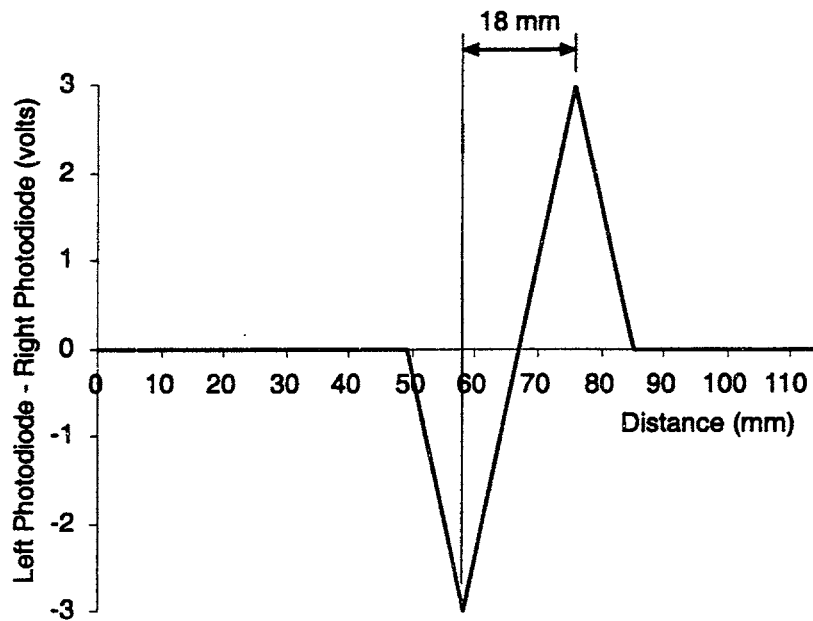
Figure 9-1: PD_{L-R} as a plug passes completely through a heat block: (a) actual sample; (b) idealized model.
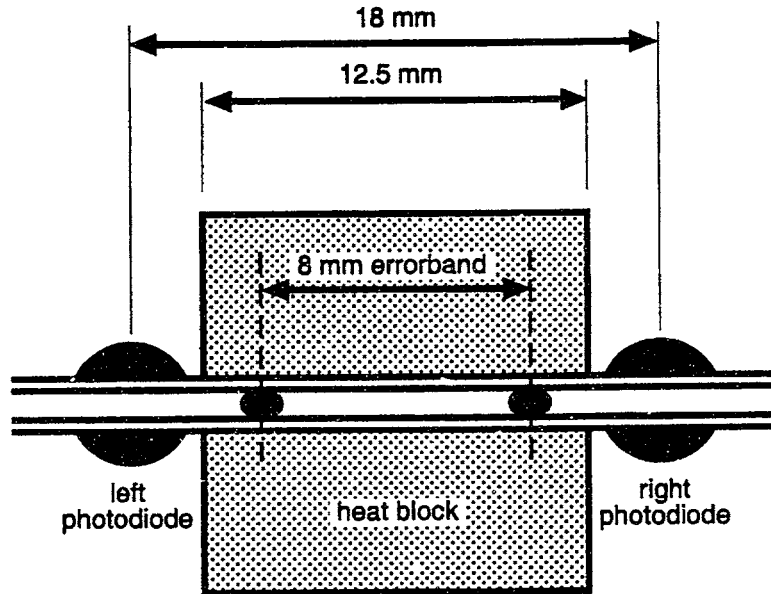
Figure 9-2: Dimensions used for the control modelling. The errorband is set at 8 mm to ensure that the plug is heated at the block temperature.

plug strays from the errorband, corrective actuation pushes it back to the middle of the block.

9.3.2 First Order Dynamics

Denote the plug velocity by v. v_{ss} is the steady-state (maximum) v. Since the motion dynamics are assumed to be first order with $\tau = 20$ ms, the relations in Table 9.1 apply. d is displacement. v is considered to have reached v_{ss} for all practical purposes when $t = 3\tau$. Therefore, when the plug is accelerating, $d(3\tau)$ in (9.9) is the distance required for the plug to reach full speed. If at time $t = 0$, $v = v_1$ and the actuation is turned off, the plug will continue to drift a distance of $d(\infty) = v_1\tau$ (see (9.12)).

Acceleration (At $t = 0$, $d = 0$ and $v = 0$. At $t \to \infty$, $v \to v_{ss}$)

$$v(t) = v_{ss}(1 - e^{-t/\tau}) \tag{9.7}$$

$$d(t) = v_{ss}(t + \tau e^{-t/\tau} - \tau) \tag{9.8}$$

$$d(3\tau) = v_{ss}\tau(2 + e^{-3}) \approx 2v_{ss}\tau \tag{9.9}$$

Deceleration (At $t = 0$, $d = 0$ and $v = v_1$. At $t \to \infty$, $v \to 0$)

$$v(t) = v_1 e^{-t/\tau} \tag{9.10}$$

$$d(t) = v_1\tau(1 - e^{-t/\tau}) \tag{9.11}$$

$$d(\infty) = v_1\tau \tag{9.12}$$

Table 9.1: Selected first-order relations.
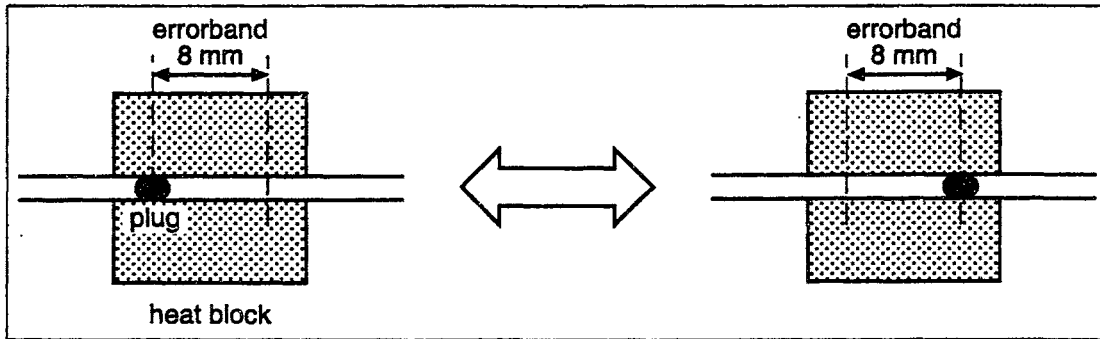
Figure 9-3: Plug oscillation.

9.3.3 Oscillation

The control scheme was presented in Section 4.7. When the plug moves outside the errorband (due to slow drift; this is observed experimentally), the control program pushes it back to the middle of the block. If the v_{ss} is high enough, the plug moves all the way to the other end of the errorband. The plug will oscillate back and forth continually, as shown in Fig. 9-3. Let t_1 be the time for the plug to move from one end of the errorband to the middle of the block. Using (9.8),

$$v_{ss}(t_1 + \tau e^{(-t_1/\tau)} - \tau) = 4 \text{ mm} \tag{9.13}$$

Let $v_1 = v(t_1)$. The plug continues to accelerate until the actuation is shut off, which can occur up to 4 ms after it passes the midpoint, due to the sampling time delay. Let $t_2 = t_1 + 4$ ms. Using (9.7), $v(t_2) = v_{ss}(1 - e^{-t_2/\tau})$. The plug will then drift a distance specified by (9.12) before coming to a halt. If the total combined distance is equal to the errorband, oscillation will occur. Using (9.8) and (9.12), we get

$$v_{ss}(t_2 + \tau e^{(-t_2/\tau)} - \tau) + v_{ss}(1 - e^{-t_2/\tau})\tau = 8 \text{ mm}$$

$$v_{ss}t_2 = 8 \text{ mm} \qquad (9.14)$$

Combining (9.13) and (9.14) and since $\tau = 20$ ms and $t_2 = t_1 + 4$ ms, we get $v_{ss} = 0.2$ m/s. Therefore,

$$v_{ss} < 0.2 \text{ m/s} \qquad (9.15)$$

To avoid oscillation. This is for the maximum errorband of 8 mm. $v < 0.2$ m/s anyway to avoid plug breakup[9].

9.4 Experiments

Table 9.2 presents the results of some experiments near the oscillation threshold. Δp is the pressure[10] applied across the end of the 9" long capillary. v_{ss} is experimental

---

[9]See Chapter 8.

[10]Due to a poor choice in valves, the pressure difference and v_{ss} is greater when the plug moves from right to left than from left to right. Δp is the lower pressure used in the left-to-right motion. This is because both left-to-right and right-to-left v_{ss} must be high enough to sustain oscillation.

233

Case No.	Δp (psi)	v_{ss} (m/s)	Errorband (volts)	Errorband (mm)	$v_{ss,max}$ (m/s)	Oscillation	$v_{ss} \geq v_{ss,max}$
1	6.5	0.09	1.0	3.0	0.07	yes	yes
2	6.5	0.09	1.35	4.1	0.1	no	no
3	6.5	0.09	1.5	4.5	0.1	no	no
4	8.5	0.1	1.35	4.1	0.1	yes	yes

Table 9.2: Comparison of experimental vs. theoretical predictions of breakup. See the text for details.

plug speed. While it is actually slightly higher than the bulk oil speed, the two are taken to be the same. The bulk oil speed was too fast to measure directly, so it was estimated[11] using the standard pipe flow equation (8.12) using the average oil viscosity $\mu = 7.0 \times 10^{-2}$ kg/(m·s) and approximating dp/dx as $\Delta p/(9")$.

The errorband used in experiments was smaller than the 8 mm maximum considered in Section 9.3. The errorband in volts is translated into mm using the linear approximation of Fig. 9-1b: 6 volts translates into 18 mm, and distances scale accordingly. The midpoint was assumed to be in the middle of the errorband voltages, and this was approximately the case. $v_{ss,max}$ is based on equations (9.13) and (9.14), substituting[12] the errorband listed for 8 mm.

The oscillation column lists whether or not continuous oscillation was experimentally observed. If the theory is correct, then oscillation can occur when $v_{ss} \geq v_{ss,max}$, and this is what was observed. $v_{ss,max}$ is an estimate good to within about 10% (approximating by comparison with the experimental data).

---

[11]See Section 8.3.4.

[12]t_1 and t_2 are not affected by the errorband. From (9.14), $v_{ss,max} = $ (errorband length)$/t_2$, where $t_2 = 42$ ms.

234

9.5 Conclusion

Continuous oscillation of the plug within a block can occur if the steady-state velocity v_{ss} is high enough. This is undesirable even if the plug stays within the heat block, since it causes undue wear on the valves and increased adsorption of Taq to the capillary walls. The plug motion dynamics were modelled simply as a 4 ms computer time delay followed by first order pneumatic/valve/oil dynamics. The time constant of the first order dynamics was determined to be ≈ 20 ms by examining plug acceleration and deceleration at 30 frames/second using a VCR and CCD camera. $v_{ss} < 0.2$ m/s to avoid oscillation if the errorband is set to a maximum value of 8 mm. The maximum allowable v_{ss} scales linearly with errorband. The theory matched observed experimental v_{ss} to within about 10%.

9.6 Nomenclature

J_0 Bessel function of order zero.

J_1 Bessel function of order one.

p Pressure.

PD_{L-R} $PD_{\text{left}} - PD_{\text{right}}$.

PD_{left} Normalized voltage signal of the photodiode to the immediate left of the heat block of interest.

PD_{right} Normalized voltage signal of the photodiode to the immediate right of the heat block of interest.

r Radial coordinate inside the capillary.

r_{tube}	Capillary inner radius.
t	Time.
t_1	Time for the plug to move from the edge of the errorband to the midpoint, if $v = 0$ at $t = 0$.
t_2	$t_1 + 4$ ms. 4 ms is the sampling time delay.
u	Local oil axial velocity.
v	Plug velocity.
v_1	v at $t = t_1$
v_{ss}	Steady-state plug velocity.
$v_{ss,max}$	v_{ss} must stay below this value to avoid oscillation.
x	Axial coordinate inside the capillary.
μ	Oil viscosity.
ρ	Oil density.
τ	Plug motion time constant (20 ms).

Chapter 10

Conclusion

10.1 Summary

I built a novel prototype capillary polymerase chain reaction machine. The purpose was to perform a single reaction as fast as possible with a reaction volume ~ 100 nl. The PCR mix is in the form of a 1 μl droplet that moves between three heat zones inside of a 9" long, 1 mm I.D. PTFE capillary filled with mineral oil via pneumatic control of the end pressures. A laser focused on one end of the capillary waveguides down its length until it hits the drop/oil interface, where it scatters. The scatter is detected by a series of 8 photodiodes which provide position feedback to a computer controlling the pneumatics. The machine can transition between one temperature step and another in $\sim$2 seconds, which includes both drop motion and temperature equilibration. It was extensively tested in both 10-cycle and 30-cycle PCR, including nearly 200 successful 30-cycle runs. The 30-cycle PCR was typically 74% (as high as 78%) efficient, and took only 23 minutes. This compares well with existing machines

237

Machine	Template (M)	Target (bp)	Time per Cycle	No. of Cycles	Y (%)	Ref.
Conventional†	5×10^{-15}	500–1000	4 min.	30	70	[13], [43]
Air Cycler	1.9×10^{-15}	536	80 s	30	≈70	[96], [98], [99]
Applied Biosystems Silicon Chambers	1.0×10^{-16}	297	32.5 s	40	91	[14, 85]
Flow in Capillary	5.2×10^{-11}	1000	88 s	30	29	[57]
PCR on a Chip	1.7×10^{-11}	176	56.1 s	20	≈70	[42]
Capillary PCR	1.9×10^{-15}	500	46 s	30	74	‡

Table 10.1: Comparison of several PCR machines. Y is efficiency (2.1). †: typical. ‡: this thesis. See text for details.

in the literature. The machine requires a modified PCR mix with high amounts of Taq to counter adsorption onto the capillary walls, and without enzyme-stabilizing Triton X-100 detergent in order to keep the drop/oil surface tension as high as possible. Even so, the plug speed must be ≤ 0.2 m/s, otherwise it will break into fragments. The control scheme also forces the speed to be ≤ 0.2 m/s.

10.2   Performance Comparison

Table 10.1 compares the performance of the present PCR machine with fast PCR machines from the literature[1]. Efficiency is defined by (2.1). A 30-cycle PCR reaction in a commercial machine is assumed to be 70% efficient, which is a typical value [13].

Much of the literature listed in Table 10.1 did not provide quantification of their product. The inventors of the air cycler [96, 98, 99] only presented photos of product bands in ethidium bromide-stained gels. The band from their 40 minute, 30-cycle reaction is almost as bright and large as that from a conventional machine they used

---

[1]See Chapter 3.

238

as a control. Neither is quantified, so I assumed that both reactions were about 70% efficient. The Applied Biosystems silicon chamber boasts an incredible 91% efficiency, with a relatively low concentration of start template and short cycle time (32.5 s/cycle). However, since they performed sensitive fluorescent product quantification during PCR, the reported efficiency is for early cycles with exponential amplification. Most of the other reactions included some cycles in which there was only linear amplification, resulting in a lower average cycle efficiency. Product from continuous-flow PCR machine developed by Kopp et al. [42] produced a band with 85% the fluorescence of a band produced by a commercial thermal cycler on an ethidium bromide-stained gel. No absolute quantification was listed, so again I assumed both the continuous-flow and control machines were ≈ 70 % efficient.

Several of the PCR machines described in Chapter 3 were not listed in Fig. 10.1 because they did not produce as much product as the commercial PCR machines they used as controls, even for identical cycling schedules. This included the PCRChip [15, 80, 93, 94], which used a conventional heat block thermal cycler as a control machine; and the infrared-mediated [61] and capillary tube resistive [23] PCR machines, both of which used a commercial air cycler as the control machine.

Some of the PCR machines listed in the literature performed the same reaction in different times. For example, 20 cycles of PCR were performed in as short as 90 seconds on Kopp et al.'s PCR chip [42]. In this case, I only listed the most efficient reactions in Table 10.1 to permit accurate comparison. Efficiency invariably decreases with time per cycle.

A notable exclusion from the chart are the silicon heater units which include

the MATCI and ANAA [5, 6, 29, 60, 100]. The reason for this is that the results are reported in terms of fluorescence, which is much more sensitive than running a gel. No absolute product quantitation is reported, so it is difficult to compare the results with those of others. In the most recent work [6], the ANAA was used to PCR initially intact cells. Product was detected within 25 cycles at 17 s/cycle, with high efficiency. However, as explained in Section 3.3.4, this is more a testimony to the sensitive fluorescent detection and PCR mix optimization than the machine, which has slow temperature transitions (all of the cycling time is literally spent in transition). The high average cycle efficiency is due to the fact that the sensitive fluorescent detection allows product to be detected in the early cycles in which all amplification is exponential.

How do my 30-cycle results compare with those in the literature? Judging from Table 10.1, pretty well. Only the Applied Biosystems chip has a faster cycle time. However, for rapid PCR, the time per cycle is dominated by extension time. Their 297 bp product is 60% as long as mine, but their time per cycle is 70% as long as mine. So for the same product, performance of my machine is expected to be similar or superior. Applied Biosystems reports greater efficiency, but this is due to their sensitive product detection that allows all cycles to have exponential amplification.

The PCR on a chip of Kopp et al. [42] successfully performed 20 cycles of PCR in a mere 90 seconds. It is doubtful that my machine could perform the same feat. However, the objective of my experiments was to get the fastest possible cycling *with no significant loss in Y*. I did not have time to perform 30-cycle time optimization. Doubtless, cycle times could be reduced. In any case, Table 10.1 indicates that for

240

comparable Y, my machine has a shorter cycle time even though my product (500 bp) is almost 3 times as long (176 bp). My PCR was performed with much less template $(5 \times 10^{-15}$ M vs. 1.7×10^{-11}M) over more cycles (30 vs. 20), which is a much more difficult reaction to perform.

While Nakano et al. report only 29% efficiency, it is not clear whether or not whether their results are inferior. They use a much smaller amount of a DNA Polymerase enzyme (Tth) that is known to be slower than Taq. Their template (1000 bp) is also twice as long as mine (500 bp).

10.3 Contributions

I was solely responsible for the design, construction, testing and analysis of a novel rapid PCR machine. It is a simple, straightforward design that incorporates hardware, software, and biology. It was extensively tested in nearly 200 successful trials. While it is not yet good enough to be a commercial product, it is very reliable. Its speed and efficiency are comparable or superior to existing rapid PCR machines.

10.4 Future Work

The following are some of the remaining system challenges.

10.4.1 Completing Time Optimizations

The 30-cycle experiments described in Chapter 6 can be completed by performing time optimization for the PCR steps, as described in Chapter 5 for 10-cycle PCR. Once the individual steps have been optimized, an optimal PCR can be performed. With any luck, it will produce as much product as the reactions listed in Chapter 6 in less time, better characterizing the time limitations of the current device.

10.4.2 Loading/Unloading

Loading and unloading are performed manually. The advantage of fast, automated PCR is lost if these procedures require a lot of operator attention. Loading in particular requires some degree of manual dexterity. Perhaps the sample can be pipetted into oil-filled well with a specially-shaped bottom (tapered?) that fixes the sample location for easy loading. Of course, loading from a well requires that either the capillary be held vertically, or (as was done in the experiment) the end tipped downward. The machine will have to be modified appropriately. Connection to the left oil reservoir following loading should also be automated. A cooled location should be added to store samples after running.

10.4.3 Eliminating Heating Irregularities

As pointed out in Chapter 7, the gap between the heat blocks allows the plug temperature to drop between blocks. This effect can be minimized by decreasing the block spacing. Currently, the size of the photodiodes limits the spacing. The spacing can be

decreased by using smaller sensors. Another option is to use fiber optic cable, which uses little space, to carry the scattered laser light to the sensors. Smaller heaters might be required.

At the limit, the capillary can be threaded through a single heat block that has a temperature gradient across its length. Instead of going from one block to another, the plug would just move to different locations inside of the block. Again, the sensor system would have to be changed. Perhaps the single block could be solid except for the capillary hole and small viewports for fiber optic cable.

10.4.4 Syringe Pump

The sensor system could be eliminated entirely by using a syringe pump rather than pneumatic actuation. To prevent degassing, the end of the capillary opposite the pump could be pressurized. However, as stated in Section 4.5.2, random plug drift requires that there is one syringe pump for every capillary. This may prove too expensive if the system is multiplexed.

10.4.5 Multiplexing

A commercial machine must have the capability of cycling multiple samples simultaneously. In the current system, this means multiple capillaries. There would only have to be three heat blocks, but each would have accomodate more capillaries. There would be more valves and sensors, and the laser beam would be split up. This would reduce the laser strength, which could be compensated for by more sensitive sensors,

a more transparent capillary, and light shielding around the apparatus.

10.4.6 Fluorescent Real-Time Product Detection

Integrating Taqman[TM] or other fluorescence-based detection[2] system into the apparatus would allow for real-time PCR detection that is faster, more sensitive, and more convenient than running the samples on a gel and staining them with an intercalating dye. This is why recent PCR literature is primarily reported using realtime fluorescent methods.

10.4.7 Dealing with the Unusual PCR Mix

The PCR mix must currently be made with a high concentration of Taq (to compensate for Taq adsorption onto the sidewalls) but no detergent (so that the sample/plug oil interface maintains high surface tension). In the PCR reactions reported in this work, I concentrated the detergent out of the manufacturer-supplied Taq solution prior to use[3]. This took about an hour. The speed advantage of the machine is lost if the detergent removal procedure must be performed every time. Perhaps it can be performed in a large batch and the resulting detergent-free Taq solution frozen. This worked over a 3-day time period, but I did not test longer time periods. Perhaps some Taq stabilizer that is not a surfactant can be found. Maybe a different capillary material or a capillary coating can be used to decrease Taq adsorption to the capillary walls, allowing the use of standard Taq concentrations. Some promising results were

---

[2]See Section 3.1.3 for a description of TaqMan[TM].
[3]See Section 8.4.

found by silanizing the PTFE capillaries[4] with dichlorodimethylsilane, but I did not have enough time to follow up on these experiments.

10.4.8 Increasing Breakup Speed

Plug breakup limits the speed of the current device, as described in Chapter 8. There is a critical capillary number Ca at which breakup occurs, which is proportional to the product of the oil bulk velocity and absolute viscosity. If we substitute a lower viscosity fluid for mineral oil, we can increase the bulk velocity. This will decrease block-to-block transit time. However, any fluid that replaces the mineral oil must (1) not interfere with the PCR reaction; (2) be immiscible with water; (3) have a higher index of refraction that the PTFE capillary; (4) have an operating temperature range compatible with PCR temperatures. If the viscosity of the fluid is significantly different than that of oil, the pneumatic pressures will have to be changed.

10.4.9 Scaling Down

Cycle times can be reduced by scaling the apparatus. Fig. 10-1 shows how components of minimum cycle time vary with apparatus size for a 500 bp product. It is assumed that the block size and distance between blocks scale with capillary inner diameter d.

One component of cycle time is the time required to heat and cool the sample plug. This was conservatively estimated by modeling the sample plug as a cylinder

---

[4]PTFE is chemically inert; however, impurities can enter the material during manufacture, which is why silanizing had some effect.
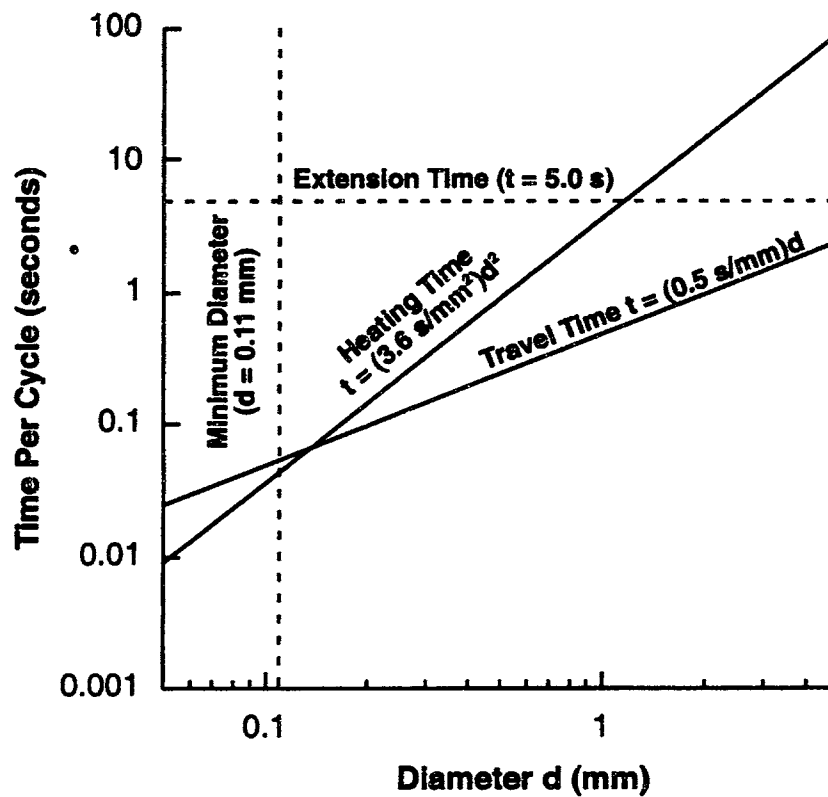
Figure 10-1: Dependence of minimum heating, travel, and extension times on capillary inner diameter d for a 500 bp product.

of water initially at uniform temperature in which heat transfer takes place solely by radial conduction. The capillary wall temperature is modelled as constant, as in Chapter 7. The greatest temperature transition[5] is between annealing and denaturing, typically 50°C and 94°C, respectively. PCR samples are considered to be at the correct temperature if they are within 0.5°C of the specified denaturing, annealing, or extension temperature. Therefore, the heating time was taken as the time for the cylinder, starting at a uniform temperature of 50°C, to reach 93.5°C along its centerline when its outer radius is exposed to a constant temperature of 94°C . To simplify the estimate, I neglected any temperature change that occurs between blocks. From the radial conduction solution presented in Section 7.2.13, the dominant time constant is $d^2/(23\alpha)$, where α is the thermal diffusivity of the plug. Assume that the faster time constants do not significantly affect the solution. Since the equilibration is first-order, it requires $-\ln[(94 - 93.5)/(94 - 50)] = 4.5$ time constants[6] for the centerline temperature to go from 50°C to 93.5°C with a steady-state temperature of 94°C. 4.5 time constants is $0.20(d^2)/\alpha$. α is taken to be the same as that of water, which is 0.16×10^{-6} m^2/s in the temperature range of the blocks. Since there are three heat steps per cycle, the heating time is $(3.6 \text{ s/mm}^2)d^2$.

Another factor to consider is the minimum transit time. If the sample plug moves too fast, it will break into pieces. In Section 8.3.4, the maximum bulk oil velocity prior to breakup was experimentally found to be ≈ 0.2 m/s, corresponding to a critical

---

[5]Other than the room temperature to initial denature transition, which is discounted since the initial denature time is much longer than subsequent denature steps.

[6]This justifies the assumption that the solution is adequately approximated using only the dominant time constant. In fact, the solution found using only the first (dominant) time constant versus the solution using the first 10 time constants are identical to within 9 decimal places.

capillary number Ca of 0.24. As a conservative estimate[7], we assumed Ca = 0.24 and $v_{\max}$ = 0.2 m/s for all d. $v_{\max}$ is the maximum plug speed and bulk oil velocity, taken to be the same (although plug speed is slightly greater). The sample plug travels 4" per cycle. Neglecting actuator dynamics, and noting that the fluid acceleration and deceleration time is very small[8] compared to travel time, the travel time is about $4"/v_{\max}$ = 0.5 seconds for the present system, in which d = 1 mm. Of course, this is at greater pressure differentials than used for the 10 and 30 cycle experiments. As the machine is scaled down, the travel distance scales with the diameter, so travel time is (0.5 s/mm)d.

For small d, PCR time is ultimately dominated by the extension time, which does not scale with size. Taq can process DNA at[9] 100 bases/second, so a 500 base DNA takes 5.0 seconds to extend.

The diameter is limited by the total number of copies of template. Less than $\approx$100 template molecules will result in unreliable PCR. Concentrations $> 5 \times 10^{-14}$ M also hurt the reaction [13]. Combining these two constraints results and keeping the same the sample plug aspect ratio, it is determined that the minimum capillary diameter is 0.11 mm.

Cycle time is comprised of the following factors: denaturing time, annealing time, extension time, travel time, and heating time. Annealing and denaturing have been

---

[7]It is conservative since the critical Ca is a function of the Reynolds number Re and Péclet number Pe. Re and Pe are proportional to d. As d decreases, Re and Pe decrease, which (as explained in Chapter 8) should permit the critical Ca to increase to the values determined experimentally by Olbricht and Kung [62]. From (8.10) and Table 8.2, we see that the other parameters that the critical Ca depends on do not change with d.

[8]See Section 9.2.1. For d = 1 mm, the time constant for acceleration and deceleration is 0.53 ms.

[9]See (2.27).

shown to take place almost instantly [99]. With good actuators, plug acceleration time is overshadowed by constant velocity travel time. Fig. 10-1 shows how the minimum times of the remaining significant factors scale with apparatus size. For a 500 bp target, cycle time is completely dominated by extension time for $d < 0.5$ mm. From this perspective, it is not worth scaling down to smaller diameters. Of course, the point of diminishing returns varies with product length.

10.5   Nomenclature

Ca   Capillary number. See Table 8.2.

d Capillary inner diameter.

Pe   Péclet number. See Table 8.2.

Re   Reynolds number. See Table 8.2.

v_{max} The maximum allowable plug velocity.

Appendix A

Material Properties

PTFE (Polytetrafluoroethylene, a.k.a. Teflon)

Property	Value
density	2.280×10^3 to 2.290×10^3 kg/m^3
heat capacity c_p	51.42 kJ/(kg $\cdot$ K) at 300 K
	59.24 kJ/(kg $\cdot$ K) at 400 K
refractive index	1.376
service temperature	-269°C to 260°C
thermal conductivity	$[4.86 \times 10^{-4}$ W/(m $\cdot$ K^2)$] \cdot T + 0.253$ W/(m $\cdot$ K)
refractive index	1.376 at 25°C

Reference: [82]

Aluminum (2024-T6)

Property	Value
Thermal conductivity	177 W/(m·K) at 300 K
	186 W/(m·K) at 400 K
Specific heat c_p	875 J/(kg·K) at 300 K
	925 J/(kg·K) at 300 K
Density	2770 kg/m^3

Reference: [30]

G-10 Composite

Property	Value	Value converted to S.I. units
Thermal conductivity	7.0×10^{-4} cal/(s·cm·°C)	0.29 W/(m·K)
Specific heat c_p	0.35–0.40 cal/(g·°C)	1300-1700 J/(kg·K)
Density	1.80 g/cm^3	1.80×10^3 kg/m^3

Reference: [33]

Mineral Oil (Product # 2705, J. T. Baker, Phillipsburg, NJ)

Property	Value	Reference
density	855 kg/m^3	[2]
heat capacity c_p	1.882 kJ/(kg · K) at 0°C	[41]
	3.263 kJ/(kg · K) at 400°C	[41]
thermal conductivity	0.14 W/(m · K) at 0°C	[41]
	0.11 W/(m · K) at 400°C	[41]
kinematic viscosity	204 centistokes at 20°C	experimental
	64.0 centistokes at 39.6°C	experimental
	19.3 centistokes at 69.6°C	experimental
	18.2 centistokes at 71.7°C	experimental
	14.2 centistokes at 79.9°C	experimental
	11.9 centistokes at 86.6°C	experimental
	9.9 centistokes at 93.6°C	experimental
refractive index	1.47 at 20°C	[1]

Kinematic viscosities were determined using cross-arm viscometers (Technical Glass Products, Dover, NJ). The heat capacity and thermal conductivity values were noted by the reference to be linear within the temperature range given.

Dry Air at Atmospheric Pressure

Temp. °C	Density kg/m^3	Coefficient of Thermal Expansion 1/K	Specific Heat c_p J/(kg·K)	Thermal Conductivity W/(m·K)	Thermal Diffusivity m^2/s	Absolute Viscosity N·s/m^2	Kinematic Viscosity m^2/s
0	1.252	3.66×10^{-3}	1011	0.0237	1.92×10^{-5}	1.7456×10^{-5}	1.39×10^{-5}
20	1.164	3.41×10^{-3}	1012	0.0251	2.20×10^{-5}	1.8240×10^{-5}	1.57×10^{-5}
40	1.092	3.19×10^{-3}	1014	0.0265	2.48×10^{-5}	1.9123×10^{-5}	1.76×10^{-5}
60	1.025	3.00×10^{-3}	1017	0.0279	2.76×10^{-5}	1.9907×10^{-5}	1.94×10^{-5}
80	0.968	2.83×10^{-3}	1019	0.0293	3.06×10^{-5}	2.0790×10^{-5}	2.15×10^{-5}
100	0.916	2.68×10^{-3}	1022	0.0307	3.36×10^{-5}	2.1673×10^{-5}	2.36×10^{-5}

Water at Saturation Temperature

Temperature °C	Density kg/m^3	Specific Heat c_p J/(kg·K)	Thermal Conductivity W/(m·K)	Diffusivity m^2/s	Absolute Viscosity N·s/m^2	Kinematic Viscosity m^2/s
0	999.9	4226	0.558	1.31×10^{-7}	1.794×10^{-3}	1.789×10^{-6}
5	1000	4206	0.568	1.35×10^{-7}	1.535×10^{-3}	1.535×10^{-6}
10	999.7	4195	0.577	1.37×10^{-7}	1.296×10^{-3}	1.300×10^{-6}
15	999.1	4187	0.585	1.41×10^{-7}	1.136×10^{-3}	1.146×10^{-6}
20	998.2	4182	0.597	1.43×10^{-7}	9.93×10^{-4}	1.006×10^{-6}
25	997.1	4178	0.606	1.46×10^{-7}	8.806×10^{-4}	8.84×10^{-7}
30	995.7	4176	0.615	1.49×10^{-7}	7.924×10^{-4}	8.05×10^{-7}
35	994.1	4175	0.624	1.50×10^{-7}	7.198×10^{-4}	7.25×10^{-7}
40	992.2	4175	0.633	1.51×10^{-7}	6.580×10^{-4}	6.58×10^{-7}
45	990.2	4176	0.640	1.55×10^{-7}	6.051×10^{-4}	6.11×10^{-7}
50	988.1	4178	0.647	1.57×10^{-7}	5.551×10^{-4}	5.56×10^{-7}
75	974.9	4190	0.671	1.64×10^{-7}	3.766×10^{-4}	3.66×10^{-7}
100	958.4	4211	0.682	1.69×10^{-7}	2.775×10^{-4}	2.94×10^{-7}

Reference: [44]

Solubility of Air in Water

Temp. °C	α	Temp. °C	α	Temp. °C	α
0	29.18×10^{-3}	12	21.87×10^{-3}	24	17.38×10^{-3}
1	28.42×10^{-3}	13	21.41×10^{-3}	25	17.08×10^{-3}
2	27.69×10^{-3}	14	20.97×10^{-3}	26	16.79×10^{-3}
3	26.99×10^{-3}	15	20.55×10^{-3}	27	16.50×10^{-3}
4	26.32×10^{-3}	16	20.14×10^{-3}	28	16.21×10^{-3}
5	25.68×10^{-3}	17	19.75×10^{-3}	29	15.92×10^{-3}
6	25.06×10^{-3}	18	19.38×10^{-3}	30	15.64×10^{-3}
7	24.47×10^{-3}	19	19.02×10^{-3}	40	14.18×10^{-3}
8	23.90×10^{-3}	20	18.68×10^{-3}	50	12.97×10^{-3}
9	23.36×10^{-3}	21	18.34×10^{-3}	60	12.16×10^{-3}
10	22.84×10^{-3}	22	18.01×10^{-3}	80	11.26×10^{-3}
11	22.34×10^{-3}	23	17.69×10^{-3}	100	11.05×10^{-3}

α is the volume of gas (in mL) measured at standard conditions (0°C and 101.325 kPa) dissolved in 1 ml of water at the temperature listed and when the pressure of gas without that of water vapor is 101.325 kPa. Reference: [20]

Bibliography

[1] Aldrich 1998–1999 catalog. Aldrich Company, Milwaukee, WI.

[2] J. T. Baker. Bakerfacts system, 2000. This is automated product information provided via fax by the manufacturer, J. T. Baker (Phillipsburg, NJ).

[3] Frank Baldino, Jr., Marie-Francoise Chesselet, and Michael E. Lewis. High-resolution *in situ* hybridization histochemistry. *Methods in Enzymology*, 168:761–777, 1989.

[4] Asim K. Bej and Meena H. Mahbubani. Thermostable DNA polymerases for *in vitro* DNA amplifications. In Hugh G. Griffin and Annette H. Griffin, editors, *PCR Technology: Current Innovations*, chapter 25, pages 219–237. CRC Press, Boca Raton, FL, 1994.

[5] Phillip Belgrader, William Benett, Dean Hadley, Gary Long, Raymond Mariella, Jr., Fred Milanovich, Shanavaz Nasarabadi, William Nelson, James Richards, and Paul Stratton. Rapid pathogen detection using a microchip PCR array instrument. *Clinical Chemistry*, 44(10):2191–2194, 1998.

[6] Phillip Belgrader, William Benett, Dean Hadley, James Richards, Paul Stratton, Raymond Mariella, Jr., and Fred Milanovich. PCR detection of bacteria in seven minutes. *Science*, 284(5413):449–450, 1999.

[7] Philip N. Borer, Barbara Dengler, Ignacio Tinoco, Jr., and Olke C. Uhlenbeck. Stability of ribonucleic acid double-stranded helices. *Journal of Molecular Biology*, 86:843–853, 1974.

[8] Ali Borhan and Ching-Feng Mao. Effect of surfactants on the motion of drops through circular tubes. *Physics of Fluids A: Fluid Dynamics*, 4(12):2628–2640, December 1992.

[9] John W. Brandis, Sydney G. Edwards, and Kenneth A. Johnson. Slow rate of phosphodiester bond formation accounts for the strong bias that *Taq* DNA polymerase shows against 2',3'-dideoxynucleotide terminators. *Biochemistry*, 35:2189–2200, 1996.

[10] Kenneth J. Breslauer, Ronald Frank, Helmut Blöcker, and Luis A. Marky. Predicting DNA duplex stability from the base sequence. *Proceedings of the National Academy of Sciences USA*, 83:3746–3750, June 1986.

[11] Theodore L. Brown, H. Eugene Lemay, Jr., and Bruce E. Bursten. *Chemistry: The Central Science*. Prentice Hall, Inc., Upper Saddle River, NJ, seventh edition, 1997.

[12] H. S. Carslaw and J. C. Jaeger. *Conduction of Heat in Solids*. Oxford University Press, Inc., New York, NY, second edition, 1997. Reprint of the original second edition published in 1959.

[13] Rita S. Cha and William G. Thilly. Specificity, efficiency, and fidelity of PCR. In Carl W. Dieffenbach and Gabriela S. Dveksler, editors, *PCR Primer: A Laboratory Manual*, pages 37–51. Cold Spring Harbor Laboratory Press, Plainville, NY, 1995.

[14] Ajit M. Chaudhari, Timothy M. Woudenberg, Michael Albin, and Kenneth E. Goodson. Transient liquid crystal thermometry of microfabricated PCR vessel arrays. *Journal of Microelectromechanical Systems*, 7(4):345–355, 1998.

[15] Jing Cheng, Mann A. Schoffner, Georgi E. Hvichia, Larry J. Kricka, and Peter Wilding. Chip PCR. II. Investigation of different PCR amplification systems in microfabricated silicon-glass chips. *Nucleic Acids Research*, 24(2):380–385, 1996.

[16] Jing Cheng, Mann A. Schoffner, Keith R. Mitchelson, Larry J. Kricka, and Peter Wilding. Analysis of ligase chain reaction products amplified in a silicon-glass chip using capillary electrophoresis. *Journal of Chromatography A*, 732:151–158, 1996.

[17] V. N. Constantinescu. *Laminar Viscous Flow*. Mechanical Engineering Series. Springer-Verlag New York, Inc., New York, NY, 1995.

[18] C. Coulliette and C. Pozrikidis. Motion of an array of drops through a cylindrical tube. *Journal of Fluid Mechanics*, 358:1–28, 1998.

[19] John L. Danssaert, Robert J. Shopes, and Daniel D. Shoemaker. Thermal cycler including a temperature gradient block, October 1993. U. S. Patent #5,525,300.

[20] John A. Dean, editor. *Lange's Handbook of Chemistry*. McGraw-Hill Book Company, New York, NY, thirteenth edition, 1985.

[21] James A. Fay. *Introduction to Fluid Mechanics*. MIT Press, Cambridge, MA, 1994.

[22] Robert W. Fox and Alan T. McDonald. *Introduction to Fluid Mechanics*. John Wiley and Sons, Inc., New York, NY, 1985.

[23] Neal A. Friedman and Deirdre R. Meldrum. Capillary tube resistive thermal cycling. *Analytical Chemistry*, 70(14):2997–3002, 1998.

[24] David H. Gelfand. *Taq* DNA polymerase. In Henry A. Erlich, editor, *PCR Technology: Principles and Applications for DNA Amplification*, chapter 2, pages 17–22. Stockton Press, New York, NY, 1989.

[25] V. L. Golo and E. I Kats. Model of the splitting of DNA molecules. *JETP Letters*, 62(7):627–632, 1995.

[26] Elias P. Gyftopoulos and Gian Paolo Beretta. *Thermodynamics: Foundations and Applications*. Macmillan Publishing Company, New York, NY, 1991.

[27] David Halliday and Robert Resnick. *Fundamentals of Physics*. John Wiley and Sons, Inc., New York, NY, second edition, 1986.

[28] Pamela M. Holland, Richard D. Abramson, Robert Watson, and David H. Gelfand. Detection of specific polymerase chain reaction product by utilizing the 5' → 3' exonuclease activity of Thermus aquaticus DNA polymerase. *Biochemistry*, 88:7276–7280, 1991.

[29] M. Sofi Ibrahim, Richard S. Lofts, Peter B. Jahrling, Erik A. Henchal, Victor W. Weedn, M. Allen Northrup, and Phillip Belgrader. Real-time microchip PCR for detecting single-base differences in viral and human DNA. *Analytical Chemistry*, 70(9):2013–2017, 1998.

[30] Frank P. Incropera and David P. Dewitt. *Fundamentals of Heat and Mass Transfer*. John Wiley and Sons, New York, NY, fourth edition, 1996.

[31] Michael A. Innis and David H. Gelfand. Optimization of PCRs. In Michael A. Innis, David H. Gelfand, John J. Sninsky, and Thomas J. White, editors, *PCR Protocols: A Guide to Methods and Applications*, chapter 1, pages 3–12. Academic Press, Inc., San Diego, CA, 1990.

[32] Michael A. Innis, Kenneth B. Myambo, David H. Gelfand, and Mary Ann D. Brow. DNA sequencing with *Thermus Aquaticus* DNA polymerase and direct sequencing of polymerase chain reaction-amplified DNA. *Proceedings of the National Academy of Sciences USA*, 85:9436–9440, December 1988.

[33] Information faxed from International Paper, the manufacturer of G-10 composite, February 2000.

[34] Alec J. Jeffreys, Victoria Wilson, Rita Neumann, and John Keyte. Amplification of human minisatellites by the polymerase chain reaction: Towards DNA fingerprinting of single cells. *Nucleic Acids Research*, 16(23):10953–10970, 1988.

[35] Chen Jinnan and Charles Maldarelli. Flow of a train of deformable fluid particles in a tube. *Applied Mathematics and Mechanics (English Edition)*, 19(7):651–661, July 1998.

[36] Peter Kainz, Angela Schmiedlechner, and Hans Bernd Strack. *In vitro* amplification of DNA fragments > 10 kb. *Analytical Biochemistry*, 202:46–49, 1992.

[37] W. M. Kays and M. E. Crawford. *Convective Heat and Mass Transfer*. McGraw-Hill Series in Mechanical Engineering. McGraw-Hill, Inc., New York, NY, third edition, 1993.

[38] Phouthone Keohavong and William G. Thilly. Fidelity of DNA polymerases in DNA amplification. *Proceedings of the National Academy of Sciences USA*, 86:9253–9257, December 1989.

[39] W. J. King. The basic laws and data of heat transmission. *Mechanical Engineering*, 54:347–353, 1932.

[40] Kip 1998 catalog. Kip Incorporated. Farmington, CT.

[41] E. E. Klaus and E. J. Tewksbury. Liquid lubricants. In E. Richard Booser, editor, *CRC Handbook of Lubrication (Theory and Practice of Tribology)*, volume II: Theory and Design. CRC Press, Inc., Boca Raton, FL, 1983.

[42] Martin U. Kopp, Andrew J. de Mello, and Andreas Manz. Chemical amplification: Continuous-flow PCR on a chip. *Science*, 280:1046–1048, May 1998.

[43] Martha F. Kramer and Donald M. Coen. The polymerase chain reaction. In Frederick M. Ausubel, Roger Brent, Robert E. Kingston, David D. Moore, J. G. Seidman, John A. Smith, Kevin Struhl, Lisa M. Albright, Donald M. Coen, and Ajit Varki, editors, *Current Protocols in Molecular Biology*, volume 2, chapter 15, pages 15.0.1–15.1.9. John Wiley and Sons, Inc., New York, NY, 1998. Series editor: Virginia Benson Chanda.

[44] Frank Kreith and Mark S. Bohn. *Principles of Heat Transfer*. Harper and Row, Publishers, Inc., New York, fourth edition, 1986.

[45] Life Technologies, Inc., Rockville, MD. *GibcoBRL Custom Primers Certificate of Analysis—Supporting Information*. Revision 983TGG.

[46] Harvey Lodish, David Baltimore, Arnold Berk, S. Lawrence Zipursky, Paul Matsudaira, and James Darnell. *Molecular Cell Biology*. Scientific American Books, New York, NY, third edition, 1995.

[47] Julius Marmur. DNA strand separation, renaturation and hybridization. *Trends in Biochemical Sciences*, 19(343–346), August 1994.

[48] M. J. Martinez and K. S. Udell. Boundary integral analysis of the creeping flow of long bubbles in capillaries. *Journal of Applied Mechanics*, 56:211–217, March 1989.

[49] William H. McAdams. *Heat Transmission*. McGraw-Hill Book Company, New York, NY, second edition, 1942.

[50] Deirdre R. Meldrum, Harold T. Evensen, William H. Pence, Stephen E. Moody, David L. Cunningham, and Peter J. Wiktor. ACAPELLA-1K, a capillary-based submicroliter automated fluid handling system. *Genome Research*, 10(1):95–104, 2000.

[51] William J. Milliken and L. Gary Leal. The influence of surfactant on the deformation and breakup of a viscous drop: The effect of surfactant solubility. *Journal of Colloid and Interface Science,* 166:275–285, 1994.

[52] Michael F. Modest. *Radiative Heat Transfer*. McGraw-Hill Series in Mechanical Engineering. McGraw-Hill, Inc., New York, NY, 1993.

[53] Darren G. Monckton and Alec J. Jeffreys. Minisatellite "isoallele" discrimination in pseudohomozygotes by single molecule PCR and variant repeat mapping. *Genomics*, 11(2):465–467, 1991.

[54] Kary B. Mullis. Process for amplifying nucleic acid sequences, July 1987. U. S. Patent #4683202.

[55] Kary B. Mullis. The polymerase chain reaction: Why it works. In Henry A. Erlich, editor, *Polymerase Chain Reaction*, Current Communications in Molec-

ular Biology, pages 237–243. Cold Spring Harbor Laboratory Press, Cold Spring Harbor, NY, 1989.

[56] Kary B. Mullis, Henry A. Erlich, Norman Arnheim, Glenn T. Horn, Randall K. Saiki, and Stephen J. Scharf. Process for amplifying, detecting, and/or cloning nucleic acid sequences, July 1987. U. S. Patent #4683195.

[57] Hideo Nakano, Koji Matsuda, Masafumi Yohda, Teruyuki Nagamune, Isao Endo, and Tsuneo Yamane. High speed polymerase chain reaction in constant flow. *Bioscience, Biotechnology, and Biochemistry*, 58(2):349–352, 1994.

[58] C. R. Newton and A. Graham. *PCR*. Introduction to Biotechniques. βIOS Scientific Publishers Limited, Oxford, England, 1994.

[59] M. Allen Northrup, Bart Beeman, Bill Benett, Dean Hadley, Phoebe Landre, and Stacy Lehew. A miniature integrated nucleic acid analysis system. In Tony J. Beugelsdijk, editor, *Automation Technologies for Genome Characterization*, chapter 9, pages 189–204. John Wiley and Sons, Inc., New York, NY, 1997.

[60] M. Allen Northrup, Bill Benett, Dean Hadley, Phoebe Landre, Stacy Lehew, Jim Richards, and Paul Stratton. A miniature analytical instrument for nucleic acids based on micromachined silicon reaction chambers. *Analytical Chemistry*, 70(5):918–922, 1998.

[61] R. P. Oda, M. A. Strausbauch, A. F. R. Huhmer, N. Borson, S. R. Jurrens, J. Craighead, P. J. Wettstein, B. Eckloff, B. Kline, and J. P. Landers. Infrared-

mediated thermocycling for ultrafast polymerase chain reaction amplification of DNA. *Analytical Chemistry*, 70(20):4361–4368, 1998.

[62] W. L. Olbricht and D. M. Kung. The deformation and breakup of liquid drops in low reynolds number flow through a capillary. *Physics of Fluids A: Fluid Dynamics*, 4(7):1347–1354, July 1992.

[63] F. W. J. Olver. Bessel functions of integer order. In Milton Abramowitz and Irene A. Stegun, editors, *Handbook of Mathematical Functions with Formulas, Graphs, and Mathematical Tables*, chapter 9. Dover Publications, Inc., 1972. Ninth printing.

[64] Perkin Elmer Biosystems, Foster City, CA. *GeneAmp PCR System 9700 with MAX Mode*, February 2000. Recently introduced conventional PCR machine. On the Perkin Elmer website page http://www.pebio.com/pc/catalog2/pg31.html.

[65] Maria R. Ponce and José L. Micol. PCR amplification of long fragments. *Nucleic Acids Research*, 20(3):623, 1992.

[66] S. Poser, T. Schulz, U. Dillner, V. Baier, J. M. Köhler, D. Schimkat, G. Mayer, and A. Siebert. Chip elements for fast thermocycling. *Sensors and Actuators A: Physical*, 62:672–675, 1997.

[67] C. Pozrikidis. The buoyancy-driven motion of a train of viscous drops within a cylindrical tube. *Journal of Fluid Mechanics*, 237:627–648, 1992.

[68] Phone conversation with Promega Corporation Technical Support, March 2, 1998. Promega Corporation, Madison, WI.

[69] Promega Corporation. *Taq DNA Polymerase Usage Information*, July 1997. Part #9PIM166.

[70] William K. Purves, Gordon H. Orians, and H. Craig Heller. *Life: The Science of Biology*. Sinauer Associates, Inc., Salt Lake City, UT, fourth edition, 1995.

[71] Lord Rayleigh. On the instability of jets. *Proceedings of the London Mathematical Society*, 10:4–13, 1878.

[72] W. Rychlik, W. J. Spencer, and R. E. Rhoads. Opimization of the annealing temperature for DNA amplification *in vitro*. *Nucleic Acids Research*, 18(21):6409–6412, 1990.

[73] Randall K. Saiki. The design and optimization of the PCR. In Henry A. Erlich, editor, *PCR Technology: Principles and Applications for DNA Amplification*, chapter 1, pages 7–16. Stockton Press, New York, NY, 1989.

[74] Randall K. Saiki, Stephen Scharf, Fred Faloona, Kary B. Mullis, Glenn T. Horn, Henry A. Erlich, and Norman Arnheim. Enzymatic amplification of β-globin genomic sequences and restriction site analysis for diagnosis of sickle cell anemia. *Science*, 230:1350–1354, December 1985.

[75] J. Sambrook, E. F. Fritsch, and T. Maniatis. *In Vitro* amplification of DNA by the polymerase chain reaction. In *Molecular Cloning: A Laboratory Manual*. Cold Spring Harbor Press, Cold Spring Harbor, NY, second edition, 1989.

[76] David A. Sanchez, Richard C. Allen, Jr., and Walter T. Kyner. *Differential Equations*. Addison-Wesley Publishing Co., Reading, MA, second edition, 1988.

[77] Dieter Schmalzing, Norman Tsao, Lance Koutny, Dan Chisholm, Alok Srivastava, Aram Adourian, Lauren Linton, Paul McEwan, Paul Matsudaira, and Dan Ehrlich. Toward real-world sequencing by microdevice electrophoresis. *Genome Research*, 9:853–858, 1999.

[78] L. W. Schwartz, H. M. Princen, and A. D. Kiss. On the motion of bubbles in capillary tubes. *Journal of Fluid Mechanics*, 172:259–275, 1986.

[79] J. R. Sellars, Myron Tribus, and J. S. Klein. Heat transfer to laminar flow in a round tube or flat conduit–the Graetz problem extended. *Transactions of the ASME*, 78:441–448, 1956.

[80] Mann A. Shoffner, Jing Cheng, Georgi E. Hvichia, Larry J. Kricka, and Peter Wilding. Chip PCR. I. surface passivation of microfabricated silicon-glass chips for PCR. *Nucleic Acids Research*, 24(2):375–379, 1996.

[81] Sigma 2000–2001 catalog. Sigma-Aldrich Company, St. Louis, MO.

[82] Carleton A. Sperati. Physical constants of fluoropolymers. In J. Brandrup and E. H. Immergut, editors, *Polymer Handbook*, pages V/35–V/44. John Wiley and Sons, Inc., New York, NY, third edition, 1989.

[83] Stratagene, La Jolla, CA. *Robocycler® Gradient Temperature Cyclers*, August 2000. Product literature. On the Stratagene website page http://www.stratagene.com/instruments/robo_gradient.htm.

[84] Harold Swerdlow, Barbara J. Jones, and Carl T. Wittwer. Fully automated DNA reaction and analysis in a fluidic capillary instrument. *Analytical Chemistry*, 69(5):848–855, 1997.

[85] Theresa B. Taylor, Emily S. Winn-Deen, Enrico Picozza, Timothy W. Woudenberg, and Michael Albin. Optimization of the performance of the polymerase chain reaction in silicon-based microstructures. *Nucleic Acids Research*, 25(15):3164–3168, 1997.

[86] T. M. Tsai and Michael J. Miksis. Dynamics of a drop in a constricted capillary tube. *Journal of Fluid Mechanics*, 274:197–217, 1994.

[87] T. M. Tsai and Michael J. Miksis. The effects of surfactant on the dynamics of bubble snap-off. *Journal of Fluid Mechanics*, 337:381–410, 1997.

[88] James D. Watson, Nancy H. Hopkins, Jeffrey W. Roberts, Joan Argetsinger Steitz, and Alan M. Weiner. *Molecular Biology of the Gene*. The Benjamin/Cummings Publishing Company, Inc., Menlo Park, CA, fourth edition, 1987.

[89] James G. Wetmur. Excluded volume effects on the rate of renaturation of DNA. *Biopolymers*, 10:601–613, 1971.

[90] James G. Wetmur. Hybridization and renaturation kinetics of nucleic acids. In *Annual Review of Biophysics and Bioengineering*, volume 29, pages 337–361. Annual Reviews, Inc., Palo Alto, CA, 1976.

[91] James G. Wetmur. DNA probes: Applications of the principles of nucleic acid hybridization. *Critical Reviews in Biochemistry and Molecular Biology*, 26(3/4):227–259, 1991.

[92] James G. Wetmur and Norman Davidson. Kinetics of renaturation of DNA. *Journal of Molecular Biology*, 31:349–370, 1968.

[93] Peter Wilding, Mann A. Shoffner, Jing Cheng, Gia Hvichia, and Larry J. Kricka. Thermal cycling and surface passivation of micromachined devices for PCR. *Clinical Chemistry*, 41(9):1367–1368, 1995.

[94] Peter Wilding, Mann A. Shoffner, and Larry J. Kricka. PCR in a silicon microstructure. *Clinical Chemistry*, 40(9):1815–1818, 1994.

[95] Martha Windholz, editor. *The Merck Index*. Merck & Co., Inc, Rahway, NJ, tenth edition, 1983.

[96] C. T. Wittwer, G. C. Fillmore, and D. R. Hillyard. Automated polymerase chain reaction in capillary tubes with hot air. *Nucleic Acids Research*, 17(11):4353–4357, 1989.

[97] C. T. Wittwer, K. M. Ririe, R. V. Andrew, D. A. David, R. A. Gundry, and U. J. Balis. The LightCycler^{TM}: A microvolume multisample fluorimeter with rapid temperature control. *BioTechniques*, 22(1):176–181, 1997.

[98] Carl T. Wittwer, G. Chris Fillmore, and David J. Garling. Minimizing the time required for DNA amplification by efficient heat transfer to small samples. *Analytical Biochemistry*, 186:328–331, 1990.

[99] Carl T. Wittwer and David J. Garling. Rapid cycle DNA amplification: Time and temperature optimization. *BioTechniques*, 10(1):76–83, 1991.

[100] Adam T. Woolley, Dean Hadley, Phoebe Landre, Andrew J. deMello, Richard A. Mathies, and M. Allen Northrup. Functional integration of PCR amplification and capillary electrophoresis in a microfabricated DNA analysis device. *Analytical Chemistry*, 68:4081–4086, 1996.